The influence of riboregulation on fitness and virulence in *Neisseria meningitidis*

Der Einfluss der Riboregulation auf Fitness und Virulenz von *Neisseria meningitidis*

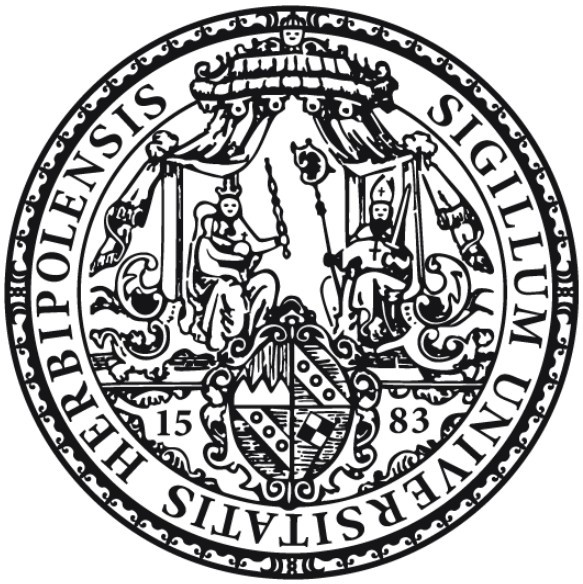

Dissertation

zur Erlangung des
naturwissenschaftlichen Doktorgrades (Dr. rer. nat.)
der Graduate School of Life Sciences (GSLS),
Bayrische Julius-Maximilians-Universität Würzburg
Sektion: Infektion und Immunität

Vorgelegt von

Saskia Corinna Bauriedl

aus Regensburg

Würzburg, 2019

Eingereicht am: 23.09.2019

Mitglieder der Promotionskommission:
Vorsitzender: Prof. Dr. med. Georg Gasteiger
Gutachter: Prof. Dr. rer. nat. Dr. med. Christoph Schoen
Gutachter: Prof. Dr. rer. nat. Jörg Vogel
Gutachter: Prof. Dr. rer. nat. Joachim Morschhäuser

Tag des Promotionskolloquiums: …….
Doktorurkunde ausgehändigt am:…..……

Eidesstattliche Erklärung

I hereby confirm that my thesis entitled ‘The influence of riboregulation on fitness and virulence in *Neisseria meningitidis*’ is the result of my own work. I did not receive any help or support from commercial consultants. All sources and/or materials applied are listet and specified in the thesis. Furthermore, I confirm that this thesis has not yet been submitted as part of another examination process neither in identical nor in similar form.

Würzburg,

……

Saskia Bauriedl

Declaration

Hiermit erkläre ich an Eides statt, die Dissertation „Einfluss der Riboregulation auf Fitness und Virulenz von *Neisseria meningitidis*“ eigenständig, d.h. insbesondere selbstständig und ohne Hilfe eines kommerziellen Promotionsberaters, angefertigt und keine anderen als die von mir angegebenen Quellen und Hilfsmittel verwendet zu haben. Ich erkläre außerdem, dass die Dissertation weder in gleicher noch in ähnlicher Form bereits in einem anderen Prüfungsverfahren vorgelegen hat.

Würzburg, den

……

Saskia Bauriedl

Contents

1. Summary

Neisseria meningitidis (*N. meningitidis*) is a human commensal that occasionally causes life-threatening infections such as bacterial meningitis and septicemia. Despite experimental evidence that the expression of small non-coding RNAs (sRNAs) as well as the RNA chaperone Hfq affect meningococcal physiology, the impact of RNA-based regulation (riboregulation) on fitness and virulence in *N. meningitidis* is only poorly understood. Therefore, this study addressed these issues using a combination of high-throughput technologies.

A differential RNA-sequencing (dRNA-seq) approach was applied to produce a single-nucleotide resolution map of the primary transcriptome of *N. meningitidis* strain 8013. The dRNA-seq analysis predicted 1,625 transcriptional start sites including 65 putative sRNAs, of which 20 were further validated by northern blot analysis. By Hfq RNA immunoprecipitation sequencing a large Hfq-centered post-transcriptional regulatory network comprising 23 sRNAs and 401 potential mRNA targets was identified. Rifampicin stability assays demonstrated that Hfq binding confers enhanced stability on its associated sRNAs. Based on these data, the interactions of two paralogous sRNAs and their cognate target mRNA *prpB* were validated *in vivo* as well as *in vitro*. Both sRNAs directly repress *prpB* encoding a methylisocitrate lyse which was previously shown to be involved in meningococcal colonization of the human nasopharynx.

Besides the well-described RNA chaperone Hfq, FinO-domain proteins have recently been recognized as a widespread family of RNA-binding proteins (RBPs) with regulatory roles in diverse bacteria. They display an intriguing bandwidth of target sites, ranging from a single RNA pair as recognized by plasmid-encoded FinO to the global RNA regulons of enterobacterial ProQ proteins. To better understand the intrinsic targeting mode of this RBP family, *in vivo* targets of the minimal ProQ protein of *N. meningitidis* were determined. *In vivo* UV crosslinking with RNA deep sequencing (UV-CLIP) identified associations of ProQ with 16 sRNAs and 166 mRNAs encoding a variety of biological functions and thus revealed ProQ as another global RBP in meningococci. It could be shown that meningococcal ProQ predominantly binds to highly structured RNA regions including DNA uptake sequences (DUS) and rho-independent transcription terminators and stabilizes many of its RNA targets as proved by rifampicin stability experiments. As expected from the large suite of ProQ-bound RNAs, *proQ* deletion globally affects both gene and protein expression in *N. meningitidis*, changing the expression levels of at least 244 mRNAs and 80 proteins.

Phenotypic analyses suggested that ProQ promotes oxidative stress tolerance and UV damage repair capacity, both of which are required for full virulence of *N. meningitidis*.

Together, this work uncovers the co-existence of two major post-transcriptional regulons, one governed by ProQ, the other by Hfq, in *N. meningitidis*. It further highlights the role of these distinct RBPs and its associated sRNAs to bacterial virulence and indicates that riboregulation is likely to contribute to the way how meningococci adapt to different host niches.

2. Zusammenfassung

Neisseria meningitidis (*N. meningitidis*) ist ein kommensal lebendes Bakterium, welches unter nicht vollständig geklärten Bedingungen auch lebensbedrohliche Infektionen im Menschen wie bakterielle Meningitis und Sepsis verursachen kann. Obwohl experimentell nachgewiesen wurde, dass die Expression kleiner, nicht kodierender RNAs (sRNAs) sowie des RNA-Chaperons Hfq in Meningokokken physiologisch relevant ist, blieb der Einfluss der RNA-basierten Genregulation (Riboregulation) auf die Fitness und Virulenz von *N. meningitidis* bisher unvollständig verstanden. Daher befasste sich diese Studie durch Kombination verschiedener Hochdurchsatz-Technologien mit dieser Fragestellung.

Es wurde differentielle RNA-Sequenzierung (dRNA-seq) angewendet, um das primäre Transkriptom des *N. meningitidis* Stamms 8013 möglichst genau zu kartieren. Die durchgeführte dRNA-seq-Analyse detektierte 1.625 Transkriptionsstartstellen (TSS) einschließlich 65 potentieller sRNAs. Durch Anwendung von Northern-Blot-Analysen konnten anschließend 20 sRNAs experimentell validiert werden. Darüber hinaus wurde durch Ko-Immunopräzipitation mit Hfq (RIP-seq) ein großes, Hfq-zentriertes, posttranskriptionelles regulatorisches Netzwerk identifiziert, welches 23 sRNAs und 401 mRNAs umfasst. Rifampicin-Stabilitätsversuche zeigten, dass durch Hfq-Bindung die Stabilität dieser sRNAs erhöht wird. Basierend auf diesen Daten konnte die Interaktion zwischen zweier Hfq-gebundener paraloger sRNAs und der *prpB* mRNA sowohl *in vivo* als auch *in vitro* bestätigt werden. Beide sRNAs reprimieren die Translation des PrpB-Gens, welches für eine Methylisocitratlyase kodiert und wahrscheinlich die Kolonisation des menschlichen Nasopharynxs durch Meningokokken begünstigt.

Neben dem ausführlich charakterisierten RNA-Chaperon Hfq wurden Proteine mit FinO-Domäne kürzlich als eine neue Familie von RNA-bindenden Proteinen (RBPs) mit regulatorischen Funktionen in verschiedenen Bakterien identifiziert. Sie weisen eine große Bandbreite regulierter Gene auf: Während das Plasmid-kodierte FinO-Protein nur ein einzelnes RNA-Paar bindet, stellt das enterobakterielle ProQ-Protein ein globales RBP dar. Um die Wirkungsweise dieser RBP-Familie besser zu verstehen, wurde *in vivo* untersucht, wie viele RNAs mit dem minimalen ProQ-Protein in *N. meningitidis* assoziiert sind. Durch Kombination von UV-Crosslinken mit RNA-Sequenzierung (UV-CLIP) konnte die Bindung von 16 sRNAs und 166 biologisch diverser mRNAs mit ProQ identifiziert werden, welches daher ebenfalls ein globales RBP in Meningokokken darstellt. Es konnte gezeigt werden, dass ProQ vorwiegend RNA-Regionen mit ausgeprägter Sekundärstruktur bindet,

darunter DNA-Aufnahmesequenzen (DUS) und Rho-unabhängige Transkriptionsterminatoren. Die ProQ-Bindung führt dabei häufig zur Stabilisation der RNAs, was durch Rifampicin-Stabilitätsexperimente nachgewiesen wurde. Wie aufgrund der großen Zahl ProQ-gebundener RNAs zu erwarten, beeinflusste die Deletion des ProQ Proteins die zelluläre Expression von mindestens 244 mRNAs und 80 Proteinen. Phänotypische Analysen deuten darauf hin, dass ProQ sowohl die Toleranz gegenüber oxidativem Stress als auch die Reparatur von DNA-Schäden reguliert, die beide für die vollständige Virulenz von *N. meningitidis* von Bedeutung sind.

Zusammenfassend beschreibt diese Arbeit die Koexistenz von zwei großen posttranskriptionellen Regulons in *N. meningitidis*, von denen eines von ProQ und das andere von Hfq kontrolliert wird. Im Rahmen dieser Arbeit wurde die Rolle beider RBPs und ihrer assoziierten sRNAs für die bakterielle Virulenz verdeutlicht und hervorgehoben, dass Riboregulation sehr wahrscheinlich dazu beiträgt, wie sich Meningokokken an verschiedene Wirtsnischen anpassen.

3. Introduction

3.1. The pathogenic commensal *Neisseria meningitidis*

Neisseria meningitidis (*N. meningitidis*) is a gram-negative diplococcus which belongs to the class of β-proteobacteria (1). As a human commensal, it colonizes the upper respiratory tract in up to 10% of the healthy population (2,3). Meningoccoci are human restricted and can be transmitted from person to person by inhalation of airbore droplets or *via* direct contact (4). Occasionally, however, *N. meningitidis* can also cause life-threatening invasive meningococcal disease (IMD)(4). Meningococci can, most likely accidentally, adhere to and pass through the pharyngeal mucosal epithelium and enter the bloodstream within less than 10 days from infection and thereby cause sepsis (1,5). Originating from the blood-stream, *N. meningitidis* can reach and adhere to the endothelial cell layer of the brain-vessels, cross the blood-brain barrier and multiply in the human cerebrospinal fluid causing acute bacterial meningitis (6). Of note, 0.01% of all colonized hosts develop meningococcal diseases (1).

The following known four virulence factors are of importance for the development of invasive meningococcal disease: (i) adhesins, (ii) polysaccharide capsule expression, (iii) ferric uptake systems and (iiii) endotoxins.

*A*dhesins such as type IV pili (Tfp) mediate adhesion, DNA uptake as well as bacterial aggregation of meningoccoci (7). Thereby, Tfp are filamentous structures which are composed of thousands of different subunits. Among these, the major subunit is encoded by the *pilE* gene. Of note, meningococci harbor one of two distinct *pilE* expression loci (8). The class I pilins possess multiple copies of silent *pilS* sequences upstream of the *pilE* gene. Thereby, pilin antigenic variation arises through homologous recombination between *pilS* cassettes and the *pilE* coding sequence (CDS) and therefore offers a mechanism of immune escape by varying antigen presentation. Contrary to that, class II *pilE* genes are highly conserved and do not undergo antigenic variation (7). Moreover, polysaccharide capsule expression, ferric uptake systems and production of endotoxins such as lipopolysaccharides (LPS) promote survival in human blood and evasion of the human immune and complement system (6).

Furthermore, *N .meningitidis* is genetically highly diverse due to its natural competence which enables the uptake of foreign DNA (9). Based on the composition of the meningococcal polysaccharide capsule, thirteen distinct serogroups can be distinguished. Yet, the majority of IMDs is caused by only six meningococcal serogroups (A, B, C, W-135, X and

Y) world-wide (10,11). Multilocus sequence typing (MLST) analysis further revealed that all pathogenic meningococci belong to a specific group of related sequence types (ST) and clonal complexes (CC) (1), called hyperinvasive lineages, suggesting that IMD is linked to the genetic background.

So far, the underlying mechanisms of divergent meningococcal virulence are not fully understood although the four described virulence factors such as the polysaccharide capsule expression were uncovered to be "necessary but not sufficient to confer full virulence" (12). Of note, no significant differences in the gene content of carriage and invasive strains were discovered which could clearly explain the differences in pathogenesis (13). Indeed, further experimental studies indicate that differences in gene expression patterns are responsible for the virulence differences among different lineages (14-16).

Taken together, these findings indicate that gene expression regulation is likely to contribute to meningococcal diversity and virulence *via* so far unknown mechanisms.

3.2. Gene regulation in *N. meningitidis*

In bacteria, the two steps of gene expression (transcription, translation) are strongly coupled in space and time and precisely regulated (17). Thereby, transcriptional gene regulation delineates processes by which bacteria regulate the conversion of DNA to RNA whereas post-transcriptional gene regulation describes processes by which cells regulate the conversion of RNA to protein. Proper gene regulation avoids wasteful consumption of energy and resources as well as the accumulation of pathway intermediates (17). In addition, a tight gene regulation is also important for the meningococcal infection process as dozens of genes were found to be differentially expressed during two key steps of meningococcal infection, more precisely, contact with human epithelial cells and human brain microvascular endothelial cells (18).

Thereby, transcriptional gene regulation is orchestrated by DNA-binding (i) alternative sigma factors, (ii) two-component systems (TCSs), and (iii) transcription factors (17).

Besides their housekeeping σ factor, which is used for the synthesis of the majority of products that are needed in all growth conditions, bacteria express a variable amount of alternative σ factors. Whereas, for example, *E. coli* possesses seven alternative sigma factors (19,20), three alternative sigma factors have been uncovered in *N. meningitidis* (RpoH (σ^{32}), RpoN (σ^{54}) and RpoE (σ^{E})) (21). Among these, only RpoE has been described in detail in meningococci as we know its genomic organization in a polycistronic operon, its

expression regulation by autoregulation and its cellular regulon comprising twelve distinct transcripts (22,23). Based on experimental studies in other pathogenic bacteria, there is raising evidence for a physiological role of RpoE in cellular stress responses and environmental changes (24,25).

TCSs consist of two central enzymatic components. They contain a histidine kinase sensing environmental stimuli and a transcriptional response regulator (26). Whereas *E. coli* possesses circa 30 TCSs (27,28), only four putative TCSs have been described for *N. meningitidis* so far (NtrY/NtrX, NarQ/NarP, NMB1606/NMB1607 and MisR/MisS) *(29,30)*. Among these, the latter has been studied most intensively uncovering a physiological role of MisR/MisS in the regulation of outer membrane structures and virulence control (30-32).

In addition, *N. meningitidis* encodes for at least 35 putative transcription factors (33) - compared to more than 200 in *E. coli* (34). For example, the meningococcal regulator Fur, encoding for a ferric uptake regulation protein, has been extensively experimentally studied. Thereby, it has been shown that Fur can regulate gene expression of putative virulence genes in response to increasing iron concentration, as present in human blood, through different mechanisms (35). In response to oxygen limitation, the meningococcal regulator FNR positively and negatively influences gene expression by binding FNR-boxes which are located in bacterial promoters (36). Another example is the carbon metabolism regulator GntR which controls meningococcal metabolism and thus important processes for the adaption to changing host environments as encountered during infection (37).
Together, transcriptional regulatory circuits are highly adapted to the individual physiological niche of each species and enable bacteria to both modify and expand their cellular functions in response to changing environmental conditions as encountered during the infection process. Of note, *N. meningitidis* possesses quite small numbers of DNA-binding transcriptional regulators raising the possibility of the existence of further important gene expression regulation mechanisms which support the meningococcal adaption to different host niches faced during infection.

3.3. RNA-mediated regulation of gene expression

Changes in gene expression can be regulated at the level of DNA by alternative sigma factors, two-component systems and transcription factors to quickly respond to changing environmental conditions as encountered during the infection process (Chapter 3.2). Moreover, regulatory RNAs have been identified to additionally modulate bacterial gene

expression. Thereby, they can both function as transcriptional gene regulators or they can act by sequestering protein (38). Most commonly, they post-transcriptionally modulate gene expression by affecting mRNA translation, mRNA stability and processing (35).

Whereas the majority of cellular RNAs consists of messenger RNAs (mRNAs) which are translated into proteins, up to 10-15% of bacterial genomes are transcribed into non-coding RNAs (ncRNAs) like ribosomal RNAs (rRNAs) and transfer RNAs (tRNAs) (39) (Figure 3-1). Some highly conserved small non-coding RNAs (sRNAs) carry out housekeeping functions, such as the ribonuclease RNase P responsible for processing of tRNAs and other RNAs, the 4.5S RNA component of the signal recognition particle (SRP) and the transfer-messenger-RNA (tmRNA), which functions as both a mRNA and tRNA to release stalled ribosomes and to tag incompletely translated proteins for degradation (40).

Further regulatory RNAs are functionally associated with the CRISPR-Cas system (clustered, regularly interspaced short palindromic repeats/CRISPR-associated proteins) of prokaryotes (41). Some *N. meningitidis* strains harbor a type II CRISPR-Cas system which seems to be associated with predominantly commensal lineages (42) (Figure 3-1). The meningococcal CRISPR/Cas locus contains a CRISPR array (crRNA array), a tracrRNA as well as genes encoding canonical Cas1, Cas2 and Cas9 proteins. Each spacer within the CRISPR array initiates transcription driven by an extended -10 box embedded within each repeat and pre-crRNAs can form a functional complex with tracrRNA and Cas9 even without 3' end processing by RNase III (42). Of note, published data provided first evidence that type II CRISPR/Cas systems might contribute to the virulence of different pathogens. For instance, deletion of *cas9*, *rnc* (encoding RNase III) and *tracrRNA* was recently found to result in reduced adhesion rates of *N. meningitidis* strain 8013 to human nasopharyngeal cells *in vitro* (43).

Another group of regulatory RNAs includes riboswitches and RNA thermometers. These molecules are *cis*-acting regulatory RNA elements which are both transcribed as a part of the 5' leaders of protein-encoding genes. Binding of small molecules such as amino acids or sugars to the 'aptamer domain' of riboswitches induces the formation of alternative secondary structures of the 'expression platform'. This conformational change can lead to the elongation or abortion of transcription or translation of the downstream open reading frame (ORF) (44). RNA thermometers regulate translation initiation of the downstream ORF as well. Contrary to riboswitches, they fold in a temperature-sensitive and not in a ligand-specific manner. A hairpin structure in the 5' leader of the mRNA occluding the ribosome

binding site (RBS) at low temperatures can melt with increasing temperature and thus enable translation initiation. Therefore, RNA thermometers are often found in the 5'untranslated regions (UTR) of virulence factors (45). In line with that, three independent RNA thermometers were identified in meningococci as part of 5' leaders of genes encoding proteins required for polysaccharide capsule biosynthesis (*cssA*) (46), negative complement regulation (*fHbp*) (47) and sialylation of LPS (*lst*) (48).

Together, the heterogeneous group of regulatory RNAs is involved in the transcriptional and post-transcriptional regulation of numerous cellular circuits by modulating the expression of e.g. housekeeping genes and virulence factors in *N. meningitidis*.

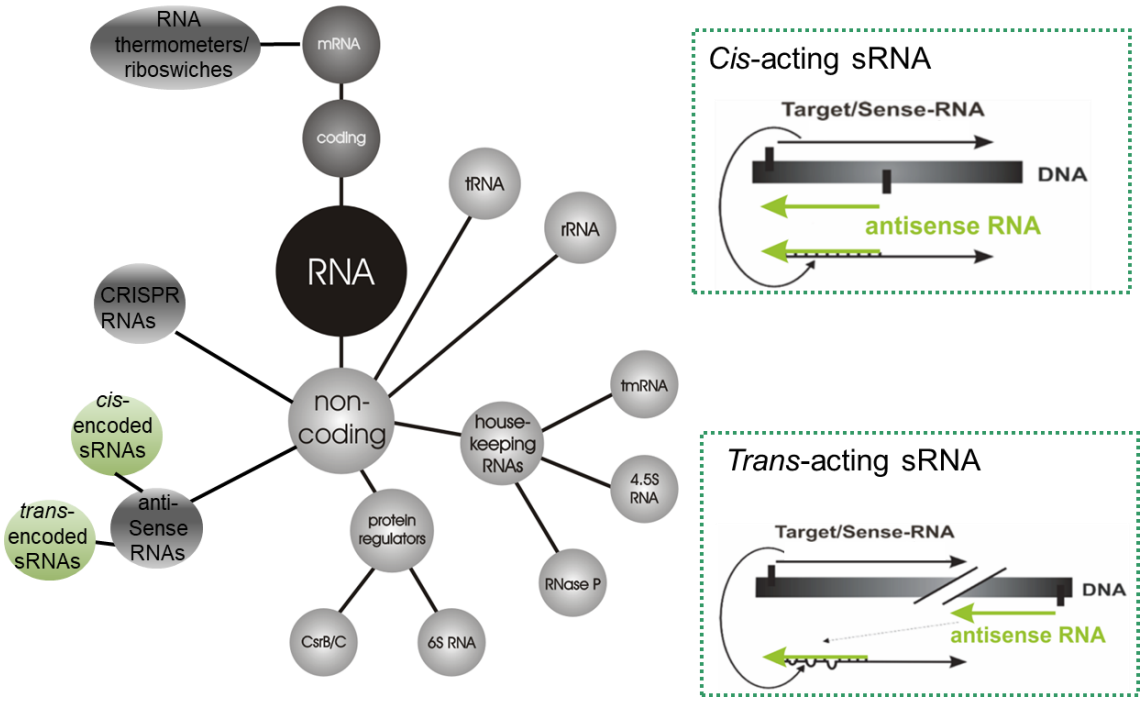

Figure 3-1 Overview of cellular RNA classes in bacteria

3.4. Base-pairing small RNAs

Another group of regulatory RNAs in bacteria consists of base-pairing small RNAs (antisense sRNAs) which can be further distinguished in *cis*-acting and *trans*-acting sRNAs (Figure 3-1). Whereas, c*is*-acting sRNAs are located in the same genetic locus on the opposite strand of their mRNA targets, t*rans*-encoded sRNAs are encoded in genomic loci which are unrelated to their target genes.

3.4.1. *Cis*-acting base-pairing sRNAs

Cis-acting sRNAs share extended regions of 75 nucleotides or more of complete complementarity with their targets. Thus, c*is*-encoded sRNAs can modulate translation as well as

mRNA stability, cause transcriptional interference or affect transcription termination (49). Due to perfectly complementary RNA-RNA interaction and the proximity of regulator and target, this regulation mechanism often occurs independently of auxiliary RNA-binding proteins (RBPs). Many *cis*-acting sRNAs are associated with transposable elements, phages and plasmids where they function to maintain the appropriate copy number of the mobile element (50).Yet, the physiological roles of the few known *cis*-encoded antisense sRNAs expressed from bacterial chromosomes are less well understood although several case studies connect the diversity of *cis*-encoded sRNAs to bacterial pathogenesis (51-53). For instance, the *cis*-encoded sRNA FasX regulates both pilus expression and adherence to promote host attachment and colonization in the human pathogen *Streptococcus pyogenes (54)*. Hitherto, only one *cis*-acting sRNA has been studied in meningococci which is complementary to the complete *pilE* CDS and 5′ UTR and might modulate antigenic variation without affecting *pil*E expression levels by unknown mechanisms (7).

3.4.2. *Trans*-acting base-pairing sRNAs

In addition, *trans*-acting RNAs are highly heterogenous regarding to their size (50-400 bp) and secondary structure and were found to act at all levels of gene expression (55,56). In the majority of studied cases, *trans*-acting sRNAs post-transcriptionally regulate their target mRNAs by carrying out direct base-pairing interactions (57) (Figure 3-1). In many gram-negative bacteria, *trans*-encoded sRNAs require RBPs such as the RNA chaperone Hfq (chapter 3.6.2) for both effective target base-pairing and intracellular stability (58). Thereby, Hfq-associated sRNAs are considered as the largest class of post-transcriptional regulators in model bacteria such as *Salmonella enterica* (59).

Typically, enterobacterial *trans*-encoded sRNAs are transcribed from a free-standing gene. Yet, *trans*-acting sRNAs can also originate from 3`ends of mRNA loci. These sRNAs either result from mRNA processing or they are transcribed from independent promotors with a terminator shared with the overlapping mRNA (59). In addition, 5′ UTR processing has been shown to result in *trans*-acting sRNA species which post-transcriptionally regulate gene expression in *Salmonella* (60). Apart from that, *cis*-acting riboswitches (chapter 3.3) have been described to be cleaved off their downstream mRNA and regulate distinct transcripts in *trans* in the gram-positive bacterium *Listeria monocytogenes* (*L. monocytogenes*) (61).

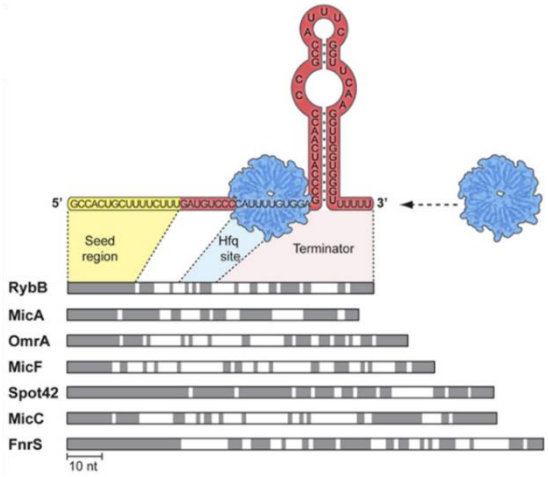

Figure 3-2: General structure of *trans*-encoded Hfq-associated sRNAs

(Top) A modular structure of a base-pairing sRNA and its contact regions with Hfq is shown. (Bottom) Seven enteric *Salmonella* sRNAs are illustrated. The most conserved regions are shaded grey illustrating that *trans*-encoded sRNAs usually feature structured 3`ends followed by a poly(U)-stretch, a short seed region for interacting with mRNA targets and a Hfq binding domain upstream of the rho-independent terminator. Indeed, the total lengths of the sRNAs vary. Figure was taken from Storz *et al.*, 2011 (14).

Recently, it has been shown that *trans*-encoded sRNAs feature a structured 3`end followed by a poly(U)-stretch which enables ρ-independent termination (Figure 3-2). Moreover, the molecule harbors domains which mediate interactions with Hfq and target mRNAs (55). In most cases, base-pairing between *trans*-acting sRNAs and their target mRNAs is single-stranded, short, imperfect and performed by conserved sequence elements referred to 'seed-pairing' (56) (Figure 3-2). The region of potential base pairing between *trans*-encoded sRNAs and target mRNAs typically is between 10–25 nucleotides long. It needs to be mentioned that in all cases where it has been examined, only some key nucleotides seemed to be essential for regulation (56). The limited complementarity enables sRNAs to target multiple transcripts with their single seed sequence. Thus, there is only little correlation between the chromosomal location of the target mRNA gene and the sRNA gene. For instance GcvB, a sRNA of *Salmonella*, interacts with more than 20 transcripts via a G/U rich element (Figure 3-2). Most of the regulated mRNAs are involved in amino acid uptake. Therefore, GcvB works similar to a protein transcription factor (chapter 3.2) by globally regulating a physiological response (62).

Trans-encoded sRNAs modulate their target mRNAs *via* several different mechanisms including negative and positive regulation. The majority of *trans*-encoded sRNAs repress protein levels through inhibiting translation initiation of their target mRNAs, leading to mRNA degradation or both. In case of translation inhibition, the sRNAs bind to the 5' UTR of mRNAs and blocks their RBS (56). In case of mRNA degradation, base pairing between the sRNA and its target mRNA is performed far upstream of the start codon of the repressed transcript. The sRNA-mRNA duplex is then quickly degraded by RNases such as RNase E (63). Besides this negative regulation, sRNAs can function as activators of bacterial gene expression. By base-pairing of the sRNA, an inhibitory secondary structure of the target mRNA gets disrupted which sequesters the RBS of this mRNA (57). It should be kept in

mind that the RNA hybrids underlying either positive or negative regulation of a participating mRNA are quite similar and therefore some sRNAs can function as both activators and repressors of distinct transcripts (64,65).

Compared to model organisms such as *E. coli* or *Salmonella*, the study of sRNAs in *N. meningitidis* is still in its infancy. Yet, using both RNA-sequencing and tiling array technology, a large number of putative *cis*- and *trans*-acting sRNAs was recently detected in *N. meningitidis* serogroup B strain MC58, indicating that sRNAs might considerably contribute to meningococcal gene expression control upon changing environmental conditions as encountered during the meningococcal infection process (37,66).
So far, only four *trans*-acting sRNAs transcribed from free-standing genes have been experimentally studied in *N. meningitidis*.
The first one is NrrF which is a Fur-regulated (chapter 3.2) sRNA that gets transcribed upon iron depletion and controls the expression of succinate dehydrogenase by destabilization of the s*dhCDAB* polycistronic RNA (67,68). In *N. gonorrhoeae*, the NrrF-dependent regulon was shown to also include genes involved in oxidative stress response and DNA metabolism, antibiotic resistance as well as amino acid biosynthesis (69).
The second sRNA is AniS which was discovered as a sRNA induced under anaerobic conditions *via* the transcriptional regulator FNR (chapter 3.2). AniS was shown to down-regulate the expression of a conserved lipoprotein of unknown function and an oligopeptidase A. Of note, this sRNA is absent in the non-pathogenic commensal *N. lactamica* (36).
Furthermore, the sRNA Bns1, which is induced upon culture of meningococci in human whole blood, responds to carbon source availability and is under control of the transcriptional regulator GntR (chapter 3.2). In line with that, deletion of Bns1 down-regulates the transcript levels of genes of the methylcitrate cycle, which enables propionic acid utilization. Of note, Bns1 knock-out mutants show attenuated virulence in an infant rat model (37,66).
The last experimentally validated sRNA is the sigma-E sRNA, which was discovered in the course of a microarray analysis investigating differentially expressed transcripts by high expression of RpoE (chapter 3.2). So far, the predicted sigma-E sRNA regulon consists of seven genes including *fur* (chapter 3.2) (23).

Together, *cis*-acting and *trans*-acting base-pairing sRNAs are numerously transcribed in *N. meningitidis* and first experimental data suggest that they are likely involved in the regulation of several cellular processes required during the course of IMD.

3.5. *Trans*-acting sRNAs that titrate proteins

Besides post-transcriptional gene regulation, *trans*-encoded sRNAs such as (i) CsrB/C and (ii) 6S RNA can also directly bind to and consequently regulate proteins.

Among the best-characterized systems of protein-targeting sRNAs are the RNA sponges of the regulatory RBP CsrA (carbon storage regulator A) in *Escherichia coli*. Known as CsrB and CsrC, these sRNAs have multiple high-affinity CsrA binding sites to efficiently sequester the CsrA protein (70). Consequently, translation of formerly repressed CsrA target mRNAs, of which many are virulence related, is inceased (71,72) (Figure 3-1). Yet, the RBP CsrA and therefore most likely its associated sRNAs CsrB/ CsrC are not conserved in *N. meningitidis*.

Rather than targeting translation, 6S RNA interacts with the housekeeping RNA polymerase holoenzyme (σ70-RNAP complex) and thereby blocks transcription of target genes (Figure 3-1). Of note, 6S RNA is ubiquitously distributed over the entire bacterial kingdom including *N. meningitidis* (73).

Together, there is indication that *trans*-acting sRNAs that titrate proteins such as 6S RNA are transcribed in *N. meningitidis* which lacks a CsrA homolog. Thus, our understanding of their physiological role is still in its infancy compared to the knowledge of these regulatory RNAs in other bacteria.

3.6. RNA binding proteins (RBPs) required for the regulatory functions of sRNAs

3.6.1. The heterologous world of RNA-binding proteins (RBPs)

RBPs occupy a central position in cellular processes as they orchestrate the fate of many bacterial RNA molecules. The class of RBPs comprises members involved in protein synthesis such as the highly conserved ribosomal proteins (74), transcription regulators like Rho promoting the release of RNA polymerase (RNAP) (75) as well as defined major RBPs that dictate the fate of sRNAs (chapter 3.4) and thereby globally regulate cellular gene expression. Of note, ribonucleases and RNA-modification proteins as well as ribonucleoprotein particles (RNPs) such as Cas proteins of the CRISPR/ Cas systems are usually not referred to as RBPs although they interact with RNA (76).

Together, bacteria express several RBPs both as regulators of distinct cellular processes such as synthesis, processing, translation, and degradation of RNA molecules as well as structural components of larger complexes e.g. the ribosome (76).

3.6.2. The RNA chaperone Hfq

The RBP Hfq is a widely conserved global RNA chaperone which is conserved among gram-negative bacteria, but is absent in many gram-positive species (58). Hfq was first described in the late 1960s as a host factor (also referred to as HF-1) of *E. coli* that unwinds phage RNA for efficient replication (77). Hfq belongs to the family of Sm and Sm-like (LSm) proteins possessing two characteristic Sm motifs. Sm and LSm proteins are RBPs that are involved in splicing as well as RNA decay in archeae and eukaryotes (78). In contrast to other members of the protein family, Hfq forms hexameric instead of heptameric complexes (Figure 3-2). Thereby, Hfq exposes four RNA-binding surfaces: The proximal surface of the ring, the distal surface of the ring, the rim and the C-terminal tail (79-81). While the proximal site preferentially interacts with uridine-rich single-stranded sequences as they can be found at sRNA 3`ends (Figure 3-2), the distal site mainly binds to A-rich sequences present in 5`UTRs of transcripts (82-84). The molecular binding mechanisms of the rim and the C-terminal tail still remain unclear (85-88). Moreover, it is not understood so far how the base pairing between sRNA and mRNA is carried out. It is possible that base pairing is enabled by changes in proximity between the two RNAs or by altered RNA structure or both (80,81). Moreover, it is not understood so far how Hfq binds preferentially mRNAs and sRNAs over more abundant RNA species such as tRNAs and rRNAs (58). It is suggested that Hfq recognizes sRNAs via their ρ-independent terminator including its 3`poly(U) tail. Yet, many protein-coding transcripts possess an equivalently structured terminator and are found to be enriched in Hfq co-immunoprecipitations (59). In *Salmonella* Hfq co-immunoprecipitations over growth showed that the sRNAs associated with Hfq varied strongly between the individual time points revealing a dynamic repatterning of Hfq regulated sRNAs at different stages of growth (59).

As Hfq functions as an RNA chaperone, it helps sRNAs to base-pair with their target mRNAs. Besides that, Hfq often protects sRNAs from endonucleolytic decay in the absence of targets mRNAs and thus stabilizes its associated sRNAs (40). Furthermore, Hfq post-transcriptionally inhibits translation of mRNAs on its own by competing with 30S ribosomes (89), decreases transcript stability by triggering polyadenylation (40,90) and impacts tRNA modification (40). In some studied cases, Hfq deploys dual regulation mechanisms

to control gene expression. In *E. coli*, Hfq binds directly to an (AAN)3 motif within the *mutS* 5′UTR promoting translation repression by restructuring the mRNA leader without any involved sRNA interaction partners. Additionally, Hfq mediates base-pairing of ArcZ sRNA with the *mutS* 5'UTR to block translation. Thereby, Hfq functions as a critical switch to increase mutation rates that have been assumed to be a response to a several cellular stresses (91).

As expected from the large suite of Hfq-associated RNAs, Hfq deletion strains in distinct bacterial pathogens exhibit pleiotropic phenotypes including severe virulence defects, reduced motility or chemotaxis defects (92).

The commensal pathogen *N. meningitidis* possesses one free-standing gene encoding for Hfq. Of note, this RBP seems to play a central role in meningococci as Hfq deletion causes diverse phenotypes. For instance, Hfq mutants feature growth defects in rich media and infection-relevant human whole blood as well as reduced stress tolerance to oxidative stress, detergents and antimicrobial peptides (93). In accordance to that, 27-107 abundant proteins were found to be deregulated in the absence of Hfq. Most deregulated proteins are involved in general metabolism whereas some proteins are related to iron metabolism and adherence to human cells such as the pilus assembly protein *pilP* (93,94). Moreover, deep sequencing of RNA co-immunoprecipitated with meningococcal Hfq expressed in *Salmonella* reveals that meningococcal Hfq can interact with *Salmonella* sRNAs such as the well-characterized sRNAs MicA, InvR and RybB (95). This finding together with the considerable amount of deregulated proteins in the Hfq deletion strain indicate that Hfq is likely to play an important role in meningococcal riboregulation.
So far, Hfq association has been described only for the meningococcal sRNA AniS (chapter 3.4.2). Thereby, northern blot analysis showed altered AniS expression levels in an Hfq overexpression as well as deletion background (36).

Together, the well-studied global RBP Hfq impacts critical steps of the meningococcal infection process as well as the meningococcal proteome, although the repertoire of direct RNA binding partners as well as molecular interactions of meningococcal Hfq and its associated sRNAs are still elusive.

3.6.3. The RNA binding protein ProQ

Despite the high degree of conservation, some base-pairing sRNAs do not require Hfq (59,96,97) and some bacteria lack Hfq (chapter 3.6.2) and/or CsrA (chapter 3.5) proteins

(98,99). As described before, *N. meningitidis* expresses Hfq but does not encode for CsrA proteins (chapter 3.5). Accordingly, there is rising evidence that so called ProQ/FinO-domain (PFAM04352) containing proteins function as RBPs in many α-, β- and γ-proteobacterial species (97,99,100).

FinO was originally described as a plasmid-encoded RNA chaperone modulating conjugation in *E. coli via* a unique antisense RNA based mechanism comprising the downregulation of the *traJ* mRNA by the antisense RNA FinP (101). Another, yet genome-encoded protein with a ProQ/FinO-domain named ProQ was identified in *E. coli* which acts as an activator of the proline transporter ProP (102).

Recently, global co-sedimentation analysis of RNAs and RNA-bound proteins followed by RNA-sequencing (Grad-seq) uncovered that the chromosome-encoded ProQ in *Salmonella* is an abundant RBP with a wide bandwidth of ligands comprising hundreds of mRNAs, structured sRNAs and many *cis*-acting sRNAs and with a global influence on cellular gene expression (97). Comparably to Hfq-associated sRNAs, ProQ-dependent sRNAs can form an RNA duplex with the ribosome-binding site of target mRNAs thus preventing mRNA translation and are therefore involved in posttranscriptional gene regulation in *E. coli* and *Salmonella* (103). As indicated by *in vivo* UV crosslinking with RNA deep sequencing (UV-CLIP-seq), the chromosome-encoded ProQ in *E. coli* and *Salmonella* binds predominantly 3' ends of mRNAs and seems to recognize its cellular targets through RNA structural motifs (104). First experiments indicate, that the binding of ProQ to cellular 3`ends of mRNAs protects these transcripts against exoribonucleolytic activity (104).

Physiologically, ProQ activity affects diverse pathways in *Salmonella* including motility and pathogenesis (105), and at least in *Enterobacteriales* this RBP is required for biofilm formation (106), oxidative stress tolerance (107,108) as well as full virulence (109).

A further chromosome-encoded ProQ/FinO-domain containing protein termed RocC was identified in *Legionella pneumophila* controlling natural transformation via a *trans*-acting sRNA. While the interaction between RocC and its associated sRNA RocR represses just four competence gene mRNAs (100), it does not affect gene expression globally as the chromosome-encoded ProQ in *S. enterica* (97,104). Consequently, whereas the target spectrum of Hfq ("targetome") usually comprises dozens to hundreds of different RNA species in most bacteria investigated so far (58,96,110), the targetome of ProQ seems to be considerably more variable.

In contrast to the hexameric Hfq protein, the ProQ/FinO-domain proteins that have been characterized so far appear to act as monomers (99). Thereby, all investigated ProQ homologous harbor a central ProQ/FinO-domain that looks like a fist with positively-charged residues on the surface enabling to bind negatively-charged RNA (111). Of note, all characterized ProQ/FinO-domain proteins additionally possess C- or N-terminal extensions: The F plasmid-encoded FinO protein harbors an N-terminal α-helical region, the chromosome-encoded ProQ protein of *E. coli* and *Salmonella* possesses a separate C-terminal domain formed by mostly β-strands while RocC has different undefined C-terminal extensions (99). Yet, the contribution of these terminal extensions to the physiological functions of ProQ/FinO-domain proteins are still elusive (99).

More recently, the crystal structure of the protein NMB1681 of *N. meningitidis* strain MC58 was solved and it was shown to have a strong similarity to the F-plasmid-encoded FinO in *E. coli* (99,111) (Figure 3-3). Yet, in contrast to FinO, NMB1681 does not possess an N-terminal α-helical region (Figure 3-3). As it also lacks C-terminal extensions, NMB1681 can be considered a minimal ProQ/FinO-domain harboring protein. Furthermore, a RNA chaperone activity of NMB1681 was demonstrated *in vitro* by RNA binding, RNA strand-exchange and RNA duplexing assays (111). However, the biological impact and repertoire of RNA interaction partners of the meningococcal ProQ protein NMB1681 are not known so far.

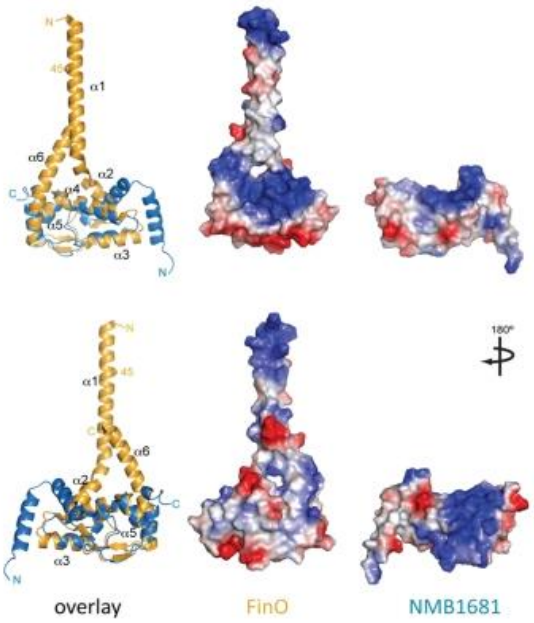

Figure 3-3. X-ray crystal structure of NMB1681 (NMV_0689) reveals structural similarity to *E. coli* FinO

The structures of FinO and NMB1681 were compared from two different orientations. A structural alignment of NMB1681 with FinO from both orientations is shown on the left side (overlay). Secondary structure elements as well as chain termini are indicated. Blue color indicates positively-charged residues. The figure was adapted from Chaulk *et al.*, 2010 (111).

Together, FinO/ProQ domain proteins represent a novel class of conserved RBPs which interact with a varying bandwidth of cellular RNA targets and are required for full virulence in some bacteria. Interestingly, *N. meningitidis* encodes a minimal ProQ/FinO-domain protein exhibiting RNA chaperone activity *in vitro*, but its cellular RNA targets as well as its physiological role are hitherto elusive.

3.7. Scope of the study

The scope of this study was (i) the genome-wide identification and functional characterization of sRNAs in *N. meningitidis* and (ii) the analysis of RBP-centered cellular regulons including their role in meningococcal infection biology.

In order to investigate the repertoire of meningococcal sRNAs, a differential RNA-sequencing approach (dRNA-seq) was used to map the boundaries of cellular transcripts at single-nucleotide resolution. Subsequently, candidate sRNAs were validated by northern blot analysis. Using a newly developed *gfp* reporter system, *in vivo* mRNA target regulation by novel sRNAs was proved. To further validate direct interaction and to map the interaction sites at single-nucleotide resolution *in vitro,* electromobility shift assays (EMSAs) as well as in-line-probing assays were performed.

To assess the direct targetome of the RNA chaperone Hfq in *N. meningitidis*, the sequencing data of a previous immunoprecipitation with Hfq (Hfq RIP-seq) experiment were re-mapped to the 8013 reference genome considering the transcript boundaries of the dRNA-seq approach. Subsequently, stabilization of selected sRNAs by Hfq was verified by northern blot analysis and rifampicin stability assays.

Using *in vivo* UV crosslinking with RNA deep sequencing (UV-CLIP-seq), *in vivo* direct RNA targets as well as RNA binding motifs of the so far uncharacterized meningococcal RBP ProQ were further determined. Based on these data, the impact of ProQ on the stability of its RNA ligands was investigated by northern blot analysis and rifampicin stability assays and direct interactions were verified by EMSA. Subsequently, the cellular ProQ regulon was investigated by RNA-sequencing (RNA-seq) and quantitative proteomics. To assess homogenicity patterns and diverse features of the ProQ-centered network and the Hfq regulon, computational comparisons were performed. In order to define the physiological roles of both RBPs, *proQ*, *hfq* as well as *proQhfq* double deletion mutants were generated and phenotypically characterized for growth deficiencies as well as in an *ex vivo* infection model.

4. Materials

4.1. Laboratory equipment

The laboratory equipment used in this study is summarized in Table 4-1.

Table 4-1 Laboratory equipment

Device	Type	Manufacturer*
10 µl pipette	Research plus, 0.5-10 µl	Eppendorf, Hamburg
100 µl pipette	Research plus, 10-100 µl	Eppendorf, Hamburg
1000 µl pipette	Research plus, 100-1000 µl	Eppendorf, Hamburg
Agarose gel electrophoresis chamber	MINI-BASIC	Cti, Idstein
Agarose gel electrophoresis chamber	Electrophoresis chamber `Maxi`	Von Kreutz, Reiskirchen
Agarose gel electrophoresis chamber	SubCell ® GT	Bio-Rad, Dreieich
Analytical balance	P-1200	Mettler-Toledo, Greifensee, CH
Analytical balance	ABT 120-5DM	Kern &Sohn, Balingen
Blotting chamber	PerfectBlue SEDEC M	Peqlab, Erlangen
Blotting chamber	PerfectBlue WEB S, M	Peqlab, Erlangen
Bunsen burner	Fireboy (electric)	Tecnorama, Zürich, Ch
Centrifuge (4 °C)	Megafuge 1.0 R	Heraeus, Hanau
Centrifuge (benchtop, 4 °C)	Mikro Rapid	Hettich, Tuttlingen
Centrifuge (benchtop, 4 °C)	5415R	Eppendorf, Hamburg
Centrifuge (benchtop, 4 °C)	5424	Eppendorf, Hamburg
Centrifuge (benchtop)	Biofuge pico	Heraeus, Hanau
Centrifuge (-Mini)	Sprout TM	Biozym, Hessisch Oldendorf
Centrifugal vacuum concentrator	SC110A	Biozym, Hessisch Oldendorf
Colony Counter	ProtoCOL	Meintrup DWS, Lähden
Diaphragm pump	Membrane vacuum pump MD 4C	Vacuubrand, Wertheim
Eraser for imaging plates	FLA	GE Healthcare, Freiburg
Gel dryer	Bio-Rad model 583	Bio-Rad, Dreieich
Heating block	VLM Q1	VLM, Bielefeld
Heating block	Eppendorf comfort	Eppendorf, Hamburg
Hight throughput sequencing	HiSEq2000	Illumina, München
Hight throughput sequencing	NextSeq 500	Illumina, München
Imaging plates cassettes	BAS 2325, 2340	Fujifilm, Minato, J
Imaging Plates	BAS-IP MS 2325, 2340	Fujifilm, Minato, J
Imaging system	Image Quant LAS 4000	GE Healthcare, Freiburg
Imaging system	ChemiDoc MP	Bio-Rad, Dreieich
Imaging System	Gel iX Imager	Intas, Göttingen
Incubator (37 °C)	Heraeus Kelvitron ® t	Heraeus, Hanau
Incubator (37 °C, 5% CO_2)	Heraeus6000	Heraeus, Hanau
Incubation hood	CERTOMAT ® H	B. Braun, Melsungen
Magnetic rack	Genesig Easy	Primerdesign, Helsinki, FI
Magnetic stirrer	IKAMAG ® RCT	IKA ®, Staufen
Membrane for nucleid acid transfer	Hybond-XL	GE Healthcare, Freiburg
Microplate reader	Infinite F200 ® PRO	TECAN, Crailsheim
Microplate reader	Multiskan ® EX	Thermo Scientific, Frankfurt

Device	Type	Manufacturer*
Microscope	Wilovert ®	WILL, Wetzlar
Mill	Retsch MM40 ball mill	RETSCH, Haan
OD_{600nm} photometer	WPA biowave	*Biochrom*, Berlin
Oven	OV5	Biometra, Göttingen
NanoLC-MS/MS analyses	Orbitrap Fusion	Thermo Scientific, Frankfurt
NanoLC-MS/MS analyses	Pico View Ion Source	New Objective, Berlin
NanoLC-MS/MS analyses	EASY-nLC 1000	Thermo Scientific, Frankfurt
Oven	UVP- HP-1000	Thermo Fisher Scientific, Waltham, US
PCR thermocycler	T3 thermocycler	Biometra, Göttingen
PCR thermocycler	MJ Mini	Bio-Rad, Dreieich
Phosphorimager	Typhoon FLA 3000	GE Healthcare, Freiburg
Pipette controller	Accu-jet ®	BRAND, Wertheim
Pipette controller	Accu-jet ®pro	BRAND, Wertheim
Protein transfer membrane	PolyScreen PVDF Transfer Membrane	PerkinElmer, Waltham, US
Power supply	EV243 Consort Power Supply	Consort, Turnhout Be
Power supply	Standard Power Pack P25	Biometra, Göttingen
Power supply	peqPOWER E250, E300	Peqlab, Erlangen
Protein gel electrophoresis	Mini-Protean	Bio-Rad, Dreieich
Semi-dry-blotter	PEGASUS S	PHASE Lübeck
Shaker	CERTOMAT ® U	B. Braun, Melsungen
Shaker	Phero Shaker	Biotec-Fischer, Reiskirchen
Spectrometer	PEQlab, ND-1000	VWR, Erlangen
Thermoshaker	Thermomixer 5436	Eppendorf, Hamburg
Ultracentrifuge	Optima L-80 XP	Beckman Coulter, Brea, US
UV crosslinker	18000	Life Technologies, Darmstadt
Vacuum concentrator	Concentrator 5301	Eppendorf, Germany
Vertical electrophoresis systems	Perfect Blue Twin S, ExW S, L	Peqlab, Erlangen
Vertical sequencing gel system	CBS SG-400-20	Thermo Fisher Scientific, Waltham, US
Vortex mixer	REAX 2000	Heidolph, Schwabach
Vortex mixer	Genie 2	Scientif industries, Bohemia, US
Waterbath	Type WB7	Memmert, Schwabing

* Unless stated otherwise, all manufacturers are from Germany.

4.2. Chemicals and consumables

Standard laboratory chemicals were purchased from AppliChem (Darmstadt), Merck (Darmstadt), Carl Roth (Karlsruhe), Difco (Heidelberg), *Roche* (Mannheim), BD (Heidelberg), Fermentas (St. Leon-Rot), Ambion/ Thermo Fisher Scientific (Schwerte), Bio-Rad (Dreieich), Life Technologies/ Invitrogen (Darmstadt), Biotium (Koeln), Hartmann Analytic (Braunschweig) and Fluka/ Sigma-Aldrich (Schnelldorf). All specific chemicals are given in Table Table 4-2.

Table 4-2 Chemicals

Reagent	Source
Alkaline hydrolysis buffer	Ambion
3-propanesulfonic acid (MOPS)	AppliChem
Ammonium persulfate (APS)	Roth
Bromphenol blue	Merck
Chloroform ultra pure	AppliChem
Coomassie Brilliant Blue R-250 Staining Solution	Bio-Rad
Crystal violet	Difco
Diethylpyrocarbonate (DEPC)	AppliChem
Dimethyl sulfoxide (DMSO)	Roth
Dithiothreitol (DTT)	Applichem
Difco Agar	BD
Ethylenediaminetetraacetic acid (EDTA)	AppliChem
Ethanole	Roth
Ethanol absolute	Applichem
Formaldehye solution, 37%	Sigma-Aldrich
Formamide, deionized	AppliChem
GelRed™	Biotium
Glycerol (99%)	Sigma-Aldrich
Glutaraldehyde	Merck
Glycine	Roth
GlycoBlue	Ambion
H_2O_2, 30%	AppliChem
Isopropanole	Roth
Lead acetate	Roth
Methanol	Roth
Nonfat dried milk powder	AppliChem
NuPAGE® LDS sample buffer	Life Technologies
Nuclease-free water	Ambion
PAGE blue staining solution	Fermentas
Paraquat	Roth
Phenol	Roth
Phenol/ chloroform/ isomylalcohol (P:C.I)	Roth
Phenol/ chloroform/ isomylalcohol (25:24:1)	AppliChem
Polyacrylamid (PAA): Rotiphorese Gel 30	Roth
Polyacrylamid (PAA): Rotiphorese Gel 40	Roth
Poly-D-lysine	Sigma-Aldrich

Reagent	Source
Rifampicin	Fluka
Roti-Hybri Quick	Roth
Simply Blue™ Safe Stain	Life technologies
Sodium dodecyl sulfate (SDS) pellets	Roth
Tetramethylethyldendiamine (TEMED)	Roth
Triton-X 100%	Roth
TRIzol Reagent	Invitrogen
Yeast RNA	Ambion
ϒ-^{32} P-ATP (222TBq (6000Ci/mmol 370 MBq (10mCi)/ml)	Hartmann Analytic
ϒ-^{32} P-UTP (222TBq (8000Ci/mmol 740 MBq (20mCi)/ml)	Hartmann Analytic
Xylene Cyanole	Sigma-Aldrich

Standard consumables were supplied from Bioline, Biozym, Dr. Maisch, Eppendorf, Fermentas, GE Healthcare, Life Technologies, New Objective, 5 Prime, *Roche*, Sarstedt, Sigma-Aldrich and Thermo Scientific. Special consumables and their sources are listed in Table 4-3.

Table 4-3 Consumables

Application	Product	Source
Agarose-gels	UltraPure™ agarose	Life Technologies, Darmstadt
Capillary columns (LC-MS/MS)	PicoFrit, 30 cmx150 µl ID	New Objective, Berlin
Porous spherical silica (LC-MS/MS)	ReproSil-Pur 120 C18-AQ, 1.9 µl	Dr. Maisch, Ammerbuch-Entringen
dNTPs (PCR reaction)	100 mM dNTP set (dATP, dCTP, dGTP, dTTP)	Sigma-Aldrich, Schnelldorf
Beads	Glass beads 0.1 mm (cell lysis)	Roth, Karlsruhe
	Protein A/G magnetic beads	Thermo Scientific, Frankfurt
Oligos (PCR reaction, northern blot)	DNA oligonucleotides	Sigma-Aldrich, Schnelldorf
Ladders	DNA HyperLadder™ 1 kb	Bioline, Luckenwalde
	PageRulerTM Prestained	Life Technologies, Darmstadt
	pUC Mix Marker 8	Fermentas, St. Leon-Rot
	RNA ladder low range	Fermentas, St. Leon-Rot
Reaction tubes	Phase Lock Gel tubes 2 ml	5 Prime, Hamburg
	LoBind tubes	Eppendorf, Hamburg
Commercial gels (LC-MS/MS)	NuPAGE® Novex® 4-12% Bis-Tris gels	Life technologies, Darmstadt
MicroSpin columns	G-25, G-50	GE Healthcare, Freiburg
Blotting		
Northern blot	Hybond-XL membrane for nucleic Acid transfer	GE Healthcare, Freiburg
Western blot	Nitrocellulose transfer membrane	GE Healthcare, Freiburg
Western blot	Pierce™ ECL Western Blotting substrate	Thermo Scientific, Frankfurt

Application	Product	Source
Antibodies		
Primary antibodies	Anti-GFP produced in mouse (working dilution: 1:3,000)	*Roche*, Mannheim
	Anti-FLAG produced in mouse (working dilution: 1:1,000)	Sigma-Aldrich, Schnell-dorf
	Anti-GroEL produced in rabbit (working dilution: 1: 10,000)	Sigma-Aldrich, Schnell-dorf
	monoclonal antibody MAbs 924	Provided by H.Claus (IHM)
Secondary antibodies	Anti-mouse; HRP-conjugated and produced in donkey (working dilu-tion: 1: 10,000)	GE Healthcare, Freiburg
	Anti-rabbit; HRP-conjugated and produced in goat (working dilution: 1: 10,000)	GE Healthcare, Freiburg
Purified Protein	*N. meningitidis* 8013 ProQ (storage in Hfq dilution buffer at -80 °C)	Provided by M. Bleck-mann (RVZ Würzburg University)
Varying Applications		
Static biofilm formation/ ELISA	96-well microtiter plate	SARSTEDT, Nürmbrecht
Cell invasion/ adhesion	24-well cell culture plates	SARSTEDT, Nürmbrecht
Cell culturing	TC Flask T75 standard	SARSTEDT, Nürmbrecht

4.3. Kits and enzymes

All kits used in this project are given in Table Table 4-4.

Table 4-4 Kits

Application	Product	Source
DNA extraction	Invisorb Spin DNA Extraction Kit	STRATEC Biomedical AG, Birkenfeld
gDNA isolation	QIAamp DNA Mini kit	Qiagen, Hilden
cDNA library preperation	NEBnext Multiplex Small RNA li-brary set for Illumina	New England Biolabs, Frankfurt
cDNA library preperation	Ribo-Zero “Bacteria”	Illumina, München
cDNA amplification (riboprobe)	MAXIScript T7 *in vitro* transcrip-tion kit	Thermo Scientific, Frankfurt
cDNA amplification (EMSA)	MEGAScript T7 *in vitro* transcription kit	Thermo Scientific, Frankfurt
PCR purification	MSB Spin PCRapace	STRATEC Biomedical AG, Bir-kenfeld
Plasmid isolation	QIAGEN Spin Miniprep Kit	Qiagen, Hilden
Plasmid isolation	QIAGEN Plasmid Midi Kit	Qiagen, Hilden

All restriction endonucleases for DNA digestion and polymerases for PCR were ordered from New England Biolabs. Enzymes for RNA-related assays were from *Roche* and Life

Technologies. For the digestion of single- or double stranded DNA, DNaseI from Thermo Scientific was used. The enzymes used in this project are given in Table 4-5.

Table 4-5 Enzymes

Application	Source
Benzonase	Sigma-Aldrich, Schnelldorf
Calf intestinal phosphatase (CIP)	New England Biolabs, Frankfurt
DNase I, RNase-free	Thermo Scientific, Schwerte
BioPrime™ Klenow enzyme	Thermo Scientific, Schwerte
Lysozyme	Roth, Karlsruhe
Polynucleotide kinase (PNK)	Fermentas, St. Leon-Rot
Restriction endonucleases	New England Biolabs, Frankfurt
RNase, DNase-free	*Roche*, Mannheim
RNase H	New England Biolabs, Frankfurt
RNase T1	Ambion/ Thermon Fisher Scientific, Schwerte
RNaseOUT™ recombinant ribonuclease inhibitor	Life Technologies, Darmstadt
T_4 DNA ligase	New England Biolabs, Frankfurt
Taq DNA polymerase	New England Biolabs, Frankfurt
Q5 ® High-Fidelity DNA polymerase	New England Biolabs, Frankfurt

4.4. Media and stock solutions

4.4.1. Bacterial growth medium for *E. coli*

LB medium was used for routine cultivation of *E. coli*. The preparation of LB medium is summarized in Table 4-6.

Table 4-6 Composition of LB

Component	Preperation
Peptone	10 g
NaCl	10 g
Yeast extract	5 g
ddH_2O	Ad 1000 ml

Medium was prepared with de-ionized water and autoclaved. Solid media were prepared by adding 1.5% (w/v) agar to the recipes given above before autoclaving. Antibiotics were added to solid and liquid media to the following final concentrations: 100 µg/ml ampicillin dissolved in sterile water, 30 µg/ml chloramphenicol dissolved in 70% ethanol, 30 µg/ml kanamycin dissolved in sterile water, 50 µg/ml erythromycin dissolved in 100% ethanol.

4.4.2. Liquid rich medium for *N. meningitidis* (GCBL^{++})

For the cultivation of *N. meningitidis, N.gonorrhoeae* liquid medium (GCBL^{++}) was used as described in Table 4-7 and Table 4-8.

Table 4-7 Composition of GCBL

Component	Preperation
Proteose Pepton	15 g
K_2HPO_4	4 g
KH_2PO_4	1 g
NaCl	1 g
ddH_2O	Ad 1000ml

Table 4-8 Supplements of GCBL

Component	Preperation
Kelloggg`s supplement I (100x)	
Glucose	40 g
Glutamine	1 g
Thiamine pyrophosphate	2 mg
ddH_2O	Ad 100 ml
Kellog`s supplement II (100x)	
Iron (III) nitrate	50 mg
ddH_2O	Ad 100 ml
Sodium bicarbonate ($NaHCO_3$)	
$NaHCO_3$	0.42 g
ddH_2O	Ad 100 ml

Medium were prepared with deionized water, autoclaved and stored at -20 °C until the day before use. 100 ml Kellog`s supplement I and 10 ml Kellog`s supplement II were prepared with deionized water, mixed, sterile filtrated and stored in aliquots at -20 °C until use. One ml of defrosted Kellog`s supplement I+II solution and 1 ml $NaHCO_3$ solution were added to 100 ml GCBL medium to obtain GCBL^{++}. Antibiotics were added to the following final concentrations to the liquid media if required: 7 µg/ml chloramphenicol dissolved in 70% ethanol, 100 µg/ml kanamycin dissolved in deionized water and 7 µg/ml erythromycin dissolved in 100% ethanol.

4.4.3. Solid medium for *N. meningitidis*

In order to cultivate *N. meningitidis* on solid media, commercial Columbia agar plates with 5% sheep blood (COS plates, Becton Dickinson) or GCB^{++} agar plates (Table 4-9) supplemented with antibiotics were used.

Table 4-9 Composition of GCB agar

Component	Preperation
Difco™ GC Medium Base (GCB)	36.25
Agar	1.25 g
ddH_2O	Ad 1000 ml

To obtain GCB^{++} agar, 1 ml Kellogg`s supplement I and II were added per 100 ml GCB agar after autoclaving. As required, antibiotics were added to the GCB^{++} agar in the following final concentrations: 7 µg/ml chloramphenicol dissolved in 70% ethanol, 100 µg/ml kanamycin dissolved in deionized water and 7 µg/ml erythromycin dissolved in 100% ethanol.

4.4.4. Liquid bacterial Chemically Defined Medium for *N. meningitidis*

The Chemically Defined Medium (CDM) was prepared as described in (112). All stock solutions were stored at room temperature except for solution 4 which has to be stored at 4 °C. The final CDM medium was prepared by adding solutions 1, 2, 3, 4, 5 and 6 to autoclaved ddH_2O (Adjust pH: 7-7.5).

Table 4-10 Composition of CDM medium

CDM	Components	Stock concentration	Final concentration
Solution 1 (40x)			
	$MgCl_2$	78 mM	1.95 mM
	$CaCl_2$	8.15 mM	0.2 mM
	Ferric citrate	6.5 mM	0.15 mM
	Dissolved in deionized H_2O, stirred at 50 °C for > 3h, pH: 7, sterile filtered		
Solution 2			
(20x)	NaCl	2 M	100 mM
	K_2SO_4	114.8 mM	5.75 mM
	K_2HPO_4	460 mM	23 mM
	NH_4Cl	360 mM	18 mM
	Dissolved in deionized H_2O, stirred at room temperature, autoclaved		
Solution 3			
(20x)	Glycin	75.6 mM	3.8 mM

CDM	Components	Stock concentration	Final concentration
	L-cystein	8.3 mM	0.4 mM
	L-arginin	14 mM	0.7 mM
	L-glutamine	80 mM	4 mM
	L-serin	95 mM	4.75 mM
	Dissolved in deionized H_2O woth few drops of NaOH, stirred at 40 °C for 1 h, sterile filtered		
Solution 4 (40x)			
	Glucose	560 mM	2.5 mM
	Dissolved in deionized H_2O, stirred at room temperature for 10 min, autoclaved		
Solution 5 (100x)			
	$NaHCO_3$	1 M	10 mM
	Dissolved in deionized H_2O, vortexed, sterile filtered		
Solution 6 (200x)			
	Proprionic acid	1 M	5 mM
	Dissolved in deionized H_2O, pH: 7.0, sterile filtered		

4.4.5. Media for growth of Detroit cells and cell culture solutions

Detroit562 cells are a human nasopharyngeal epithelial cell line. Detroit562 cells (American type Culture Collection) were grown in T75 cell culture flasks in cell culture medium $EMEM^{+++}$ at 37 °C with 5% CO_2 to 90-100% confluence and then split in two new flasks. Table 4-11 contains the composition of $EMEM^{+++}$ and Table 4-12 lists general solutions used in cell culture.

Table 4-11 Composition of $EMEM^{++}$

Component	Application	Source	Concentration
MEM Eagle (EMEM)	Standard cell culture medium	LONZA, Basel (Ch)	88%
Fetal celf serum (FCS)	Medium supplement ($EMEM^{++}$)	Thermo Fisher, Frankfurt	10%
Non-essential amino acids (NEAA)	Medium supplement ($EMEM^{++}$)	LONZA, Basel (Ch)	1%
Sodium pyruvate (NaPy)	Medium supplement ($EMEM^{++}$)	LONZA, Basel (Ch)	1%

Table 4-12 Overview of general solutions used for cell culture

Component	Application	Source
MEM Eagle (EMEM)	Standard cell culture medium	LONZA, Basel (Ch)
FCS	Medium supplement (EMEM^{++})	Thermo Fisher, Frankfurt
NEAA	Medium supplement (EMEM^{++})	LONZA, Basel (Ch)
NaPy	Medium supplement (EMEM^{++})	LONZA, Basel (Ch)
Trypsin-EDTA (0.05%)	Dissociation of cells	Thermo Fisher, Frankfurt
Gentamycin (10 mg/ml)	Antibacterial agent	Biochrom, Berlin
Saponin (20%)	Permeabilization of cells	SERVA, Heidelberg
RPMI 1640 + GlutaMAXTM-1	Cell cryopreservation	Thermo Fisher, Frankfurt
Dimethyl sulfoxide (DMSO)	Cell cryopreservation	Roth, Mannheim

For cell cryopreservation, 1x10^6 Detroit cells were resuspended in freezing media and stored in liquid nitrogen (Table 4-13).

Table 4-13 Composition of cell cryopreservation medium

Component	Preperation
RPM I 1640 + GlutaMAXTM-1	50 ml
FCS	30 ml
DMSO	20 ml

The media was stored at -80 °C.

4.5. Gels, buffers and solutions

All reagents used in this project were delivered from Carl Roth (Karlsruhe), Difco (Heidelberg), Merck (Darmstadt) and Sigma-Aldrich (Steinhein) if not indicated otherwise. For the preparation of buffers and solutions, (Aqua ad iniectabilia) ddH_2O (B. Braun) was used. For microbiological assays, 1x Phosphate-buffered saline (PBS, Table 4-22) was used in cell culture and for the application of serial dilutions.

Unless stated otherwise, all buffers and solutions were sterilized by autoclaving at 121 °C with 2 bar for 20 min.

4.5.1. Buffers and solutions for agarose gel electrophorese

TAE buffer was used for all DNA agarose gels and as running buffer (Table 4-14). The 6x agarose buffer was stored at 4 °C until use. The components of the GelRed^{TM} bath solution were mixed and agarose gels were stained for up to 45 minutes with virgous shaking.

Table 4-14 Overview of buffers for agarose gel electrophorese

	Content	Preperation
1xTAE-buffer		
	Tris-HCl, pH 8	24.2 g
	100% Acetic acid	5.71 g
	0.5 M EDTA	10 ml
	ddH_2O	Ad 1000 ml, pH to 8.3
6x DNA loading buffer		
	Saccharose	40 g
	Glycerine	30 g
	Xylencyanole	0.1 g
	Bromphenol blue	0.1 g
	ddH_2O	Ad 100 ml
GelRed™ solution/ bath	ddH_2O	150 ml
	GelRed™	15 µl

4.5.2. Buffers and solutions for hot phenol RNA preparation

For the preparation of bacterial RNA, the hot phenol method was used (5.13). Both the prepared lysis buffer and the stop solution were stored at -20 °C until use. The 30:1 mix was stored at room temperature.

Table 4-15 Composition of buffers and solutions used for hot phenol preperation

	Content	Preperation
Lysis buffer		
	Tris-HCl, 1 M, pH 8	10 ml
	0.5 M EDTA	2 ml
	Lysozyme (5 mg/ml)	1 ml
	ddH_2O	Ad 1000 ml
10% SDS		
	SDS	100 g
	ddH_2O	Ad 1000 ml
Stop solution		
	100% Ethanol	95 ml
	Phenol	5 ml
30:1 mix		
	100% Ethanol	96.5 ml
	3 M NaOAc (sodium acetate) pH 5.2	3.5 ml

4.5.3. Buffers and solutions for agarose northern blot analysis

For agarose northern blot analysis, all buffers were prepared with diethyl pyrocarbonate (DEPC)-treated water and stored at room temperature. To inhibit nucleases and to inactivate enzymes, 2 ml DEPC (Table 4-3) was added to 2 L ddH_2O, incubated overnight at 37 °C and was 2 times autoclaved. The 5xRNA loading buffer was stored at -20 °C until use. In order to prepare a formaldehyde gel for RNA electrophoresis, the agarose got dissolved in DEPC ddH_2O by heating the solution in the wicrowave over before adding prewarmed 10x MOPS buffer (60 °C) and 37% formaldehyde (room temperature).

Table 4-16 Composition of buffers and solutions used for agarose northern blot analysis

	Content	Preperation
10x 3-(N-morpholino)propanesulfonic acid (MOPS)		
	MOPS	40.5 g
	NaAc (sodium acetate)	4.1 g
	0.5 M EDTA (pH8.0)	20 ml
	10 N NaOH (sodium hydroxide)	4 ml
	DEPC ddH_2O	Ad 1000 ml
1x MOPS		
	10x MOPS	100 ml
	DEPC ddH_2O	Ad 900 ml
Formaldehyde gel for RNA electrophoresis		
	Agarose	1.2 g
	10x MOPS	10 ml
	37% Formaldehyde	3 ml
	DEPC ddH_2O	87 ml
5xRNA loading buffer		
	Formamide	3.084 ml
	Formaldehyd (37%, [v/v])	0.72 ml
	10 x MOPS	0.4 ml
	0.5 M EDTA pH 8.0	80 µl
	Glycerin 100%	2 ml
	Bromphenol blue	5 mg
	DEPC ddH_2O	3.716 ml

4.5.4. Buffers and solutions for polyacrylamide gel electrophoresis

For polyacrylamide (PAA) gel electrophoresis, 10x TBE buffer was stored at room temperature, 6% PAA gel solution at 4 °C and the formamide loading buffer (GLII) at -20 °C until use.

Table 4-17 Composition of buffers and solutions used for polyacrylamide gel electrophoresis

	Content	Concentration
10xTBE		
	Tris-base	216 g
	Boracic acid	110 g
	0.5 M EDTA, pH 8.0	80 ml
	ddH_2O	Ad 2000 ml, adjust to pH 8.3-8.5
6% PAA gel solution		
	10x TBE	100 ml
	Urea (7M)	420 g
	Rotiophorese gel 40 (19:1)	150 ml
	ddH_2O	Ad 1000 ml
Formamide loading buffer (GLII, 2x)		
	Formamide	46.821 ml
	0.5 M EDTA pH8.0	1800 µl
	Xylenecyanol	625 µl
	10% SDS	129 µl
	Bromphenol blue	625 µl

Table 4-18 Composition of PAA solution resolving gel (6%)

	Content	Preperation
6% PAA gel (20x20cm)	6% PAA gel solution	70 ml
	10% APS	700 µl
	TEMED	70 µl

4.5.5. Buffers and solutions for northern blot analysis for sRNA and mRNA detection

For northern blot analysis, the saline-sodium citrate (SSC, 20x) stock solution and all washing buffers were stored at room temperature.

Table 4-19 Composition of buffers and solutions used for polyacrylamide gel electrophoresis

	Content	Preperation
SSC (20x)		
	NaCl	175.3 g
	Sodium citrate	88.2 g
	ddH_2O	Ad 800 ml, adjust to pH 7.0 with HCl
Washing solution I		
	SSC	5x (DNA oligonucleotide); 2x (riboprobe)
	Sodium dodecyl sulfate (SDS)	0.5%
Washing solution II		
	SSC	1 x
	SDS	0.5%
Washing solution III		
	SSC	0.5
	SDS	0.5%

4.5.6. Buffers and solutions for SDS polyacrylamide gel electrophoresis (SDS-PAGE)

For SDS-PAGE, separating gels and stacking gels were always freshly prepared directly before use. The SDS running buffer was stored at room temperature, the native loading buffer at -20 °C until it was used.

Table 4-20 Composition of buffers and solutions used for SDS polyacrylamide gel electrophoresis

	Content	Preperation
SDS running buffer (10x)		
	Tris	30.275 g
	Glycin	144 g
	SDS	10 g
	ddH_2O	Ad 1000 ml
Native loading buffer		
	Glycerol 100%	75 ml
	10x TBE	7.5 ml
	Bromphenol blue	0.075 g
	ddH_2O	Fill up to 150 ml
Protein loading buffer (5x)	Tris-HCl, 1 M, pH6.8	46.95 ml
	Bromphenol blue	0.075 g
	Glycerol 100%	75 ml

	Content	Preperation
	Dithiothreitol (DTT)	11.56 g
	SDS	15 g
	ddH_2O	Fill up to 150 ml

Table 4-21 Preperation of polyacrylamide resolving gel (12%)

	Content	Preperation
Seperating gel (12%)		
	30% Acrylamide/ Bisacrylamide (37:5:1)	4 ml
	1.5 M Tris/ HCL pH 8.8	2.5 ml
	ddH_2O	3.4 ml
	10% SDS	100 µl
	10% APS	100 µl
	TEMED	10 µl
Stacking gel (12%)		
	30% Acrylamide/ Bisacrylamide (37:5:1)	0.65 ml
	1.5 M Tris/HCL pH 8.8	1.25 ml
	ddH_2O	3.05 ml
	10% SDS	505 µl
	10% Ammoniumperoxodisulfat (APS)	50 µl
	N,N,N′,N′-Tetramethylethylendia-min (TEMED)	5 µl

4.5.7. Buffers and solutions for Western Blot analysis

All prepared buffers and solutions were stored at room temperature except the developing solution A which wa kept at 4 °C. Of note, developing solution B was stored in dark.

Table 4-22 Composition of buffers and solutions used for Western blot analysis

	Content	Preperation
10xPBS		
	NaCl	80 g
	KOH	5.04 g
	NaH2PO4*1 h_2O	15.6 g
	ddH_2O	Ad 1000 ml
PBST		
	1xPBS	1 l
	Tween 20	0.5 ml

	Content	Preperation
PBST + 3% BSA		
	Bovine serum albumin (BSA)	6 g
	PBST	Ad 200 ml
10x Transfer buffer		
	Tris base	30.25 g
	Glycine	150 g
	ddH_2O	Ad 1000 ml
1x Transfer buffer		
	Methanol (MeOH)	100 ml
	10x Transfer buffer	100 ml
	ddH_2O	Ad 800 ml
Blocking solution		
	Milk powder	20 g
	PBST	Ad 200 ml
Developing solution A		
	1 M Tris-HCl pH 8.5	20 ml
	Luminol sodium salt	50 mg
	ddH_2O	180 ml
Developing solution B		
	Para-hydroxycomaric acid	55 mg
	DMSO	50 ml
Western blot developing solution		
	Developing solution A	3 ml
	Developing solution B	300 µl
	3% H_2O_2	0.9 µl

4.5.8. Buffers and solutions for ProQ CLIP-seq

All prepared buffers and solutions were stored at room temperature except the PK solution which was freshly prepared before use and stored on ice.

Table 4-23 Composition of buffers and solutions used for CLIP-seq

	Content	Preperation
NP-T buffer		
	1 M NaH_2PO_4	25 ml
	5 M NaCl	30 ml
	100% Tween-20	250 µl
	ddH_2O	Fill up to to 500 ml, Adjust to pH 8.0
NP-T buffer		

	Content	Preperation
8 M urea		
	5 M NaCl	30 ml
	1 M NaH_2PO_4	25 ml
	100% Tween-20	250 µl
	Urea	240.24 g, dissolve at 60 °C
	ddH_2O	Fill up to 500 ml
High-salt buffer		
	5 M NaCl	100 ml
	1 M NaH_2PO_4	25 ml
	100% Tween-20	250 µl
	ddH_2O	Fill up to 500 ml, Adjust to pH 8.0
	Spermidine	0.1 mM
PK buffer (2x)		
	10% SDS	5 ml
	1M Tris-HCL pH 7.9	5 ml
	0.5 M EDTA	1 ml
	ddH_2O	Fill up to 50 ml
PK buffer 9 M urea		
	10% SDS	5 ml
	1M Tris-HCL pH 7.9	5 ml
	0.5 M EDTA	1 ml
	Urea	27 g, dissolve at 60 °C
	ddH_2O	Fill up to 50 ml
PK solution (per sample)		
	Proteinase K (ThermoScientific)	20 µl
	SUPERaseIN (Life technologies)	1 µl
	PK buffer (2x)	100 µl
	ddH_2O	79 µl

4.5.9. Buffers and solutions for quantitative proteomics

The 10x Lysis buffer (stock) and 1xLysis buffer (stock) were stored at room temperature. The Lysis buffer (work solution) was prepared freshly at the day of the experiment and stored on ice in course of the experiment as the buffers contain enzymes, DTT and phenylmethylsulfonyl fluoride (PMFS).

Table 4-24 Buffers and solutions for quantitative proteomics

	Content	Preperation
10x Lysis buffer (stock)		
	1 M Tris-HCl pH7.5	20 ml
	2 M KCl	75 ml
	2 M $MgCl_2$	500 µl
	Triton X 100	2 ml
	H_2O	4 ml
1x Lysis buffer (stock)	1 M Tris-HCl pH7.5	2 ml
	2 M KCl	7.5 ml
	2 M $MgCl_2$	50 µl
	Triton X 100	200 µl
	H_2O	90 ml
Lysis buffer (work solution)		
	1x Lysis buffer (stock)	2 ml
	DTT (1 M)	2 µl
	PMFS (0.1 M)	20 µl
	DNase	40 µl
	RNase	20 µl

4.5.10. Buffer for *in vitro* transcription and 5' end labelling of RNAs

The buffer was prepared with ddH_2O and stored at room temperature.

Table 4-25 Buffer for *in vitro* transcription and 5' end labelling of RNAs

	Content	Preperation
RNA elution buffer		
	3 M Sodium acetate	333 µl
	10% SDS	100 µl
	0.5 M EDTA (pH 8)	10 mM
	ddH_2O	9.367 ml

4.5.11. Buffer and solutions for EMSAs and in-line probing

All buffers and solutions with exception of the colorless gel-loading solution were stored at -20 °C and slowly defrosted on ice directly before use. For EMSAs using one labeled RNA and one unlabeled RNA, the recipe `Native gel (RNA-RNA)` in Table 4-27 was used. For EMSAs using one labeled RNA and purified ProQ protein, the recipe `Native gel (RNA-Protein)` in Table 4-27 was used containing glycerol which enables better migration

of the protein in the gel. The gels were allowed to polymerize for at least 45 minutes at room temperature before use.

Table 4-26 Composition of buffers and solution required for EMSAs and in-line probing

	Content	Composition
5x native loading buffer		
	Glycerol	50% (v/v)
	TBE (10x)	0.5x
	Bromphenol blue	0.02% (w/v)
Structure buffer (10x)		
	Tris-HCl (pH 7)	100 mM
	KCl	1 M
	$MgCl_2$	100 mM
ProQ storage buffer		
	Structure buffer (10x)	1x
	Glycerol	1% (v/v)
	Triton-X 100	0.1%
Colorless gel-loading solution		
	Urea	10 M
	EDTA	1.5 mM
		Adjust to pH: 8.0
1x In-line probing buffer		
	Tris-HCl pH 8.3	50 mM
	$MgCl_2$	20 mM
	KCl	100 mM

Table 4-27 Preperation of native PAA gels

	Content	Preperation
Native gel (RNA_RNA)		
(20x20 cm)	40% PAA	10.5 ml
	10x TBE	3.5 ml
	H_2O	56 ml
	TEMED	70 µl
	10% APS	700 µl
Native gel (RNA_protein)		
(20x20 cm)	Glycerol	3 ml
	H_2O	45 ml

	Content	Preperation
	Roth Gel (19:1, 40%)	9 ml
	10x TBE	3 ml
	TEMED	60 µl
	10% APS	600 µl

4.5.12. Solutions for serum bactericidal assay

The veronal buffered saline (VBS)/ BSA solution (Table 4-28) was prepared with deionized water, mixed, sterile filtrated and stored in aliquots at -20 °C until use.

Table 4-28 Preperation of VBS/ BSA required for serum bactericidal assay

	Content	Composition
VBS/ BSA		
	Barbitone	0.461 g
	NaCl	4.237 g
	$MgCl_2$ x 6 H_2O	0.051 g
	$CaCl_2$ x 2 H_2O	0.011 g
	BSA	2.5 g
	ddH_2O	Ad 450 ml, adjudt pH to 7.4 with NaOH

4.6. Strains

E. coli cells were grown in 15 ml tubes at 37 °C under vigorous shaking in LB medium until reaching the required optical density at 600nm (OD_{600nm}) or overnight. The cultures were inoculated using freshly streaked-out colonies on LB-plates. Strains were stored in cryo tubes (80% Standard I nutrient broth, 20% glycerin) at -80 °C.

N. meningitidis cells were routinely grown at 37 °C in a 5% CO_2-95% air atmosphere with 95% humidity on either blood agar plates or GC plates. Freshly streaked-out colonies on solid medium were used for inoculating liquid cultures. *N. meningitidis* cells were grown in 50 ml tubes at 37 °C under vigorous shaking in $GCBL^{++}$ medium until reaching the required optical density or overnight. Their growth was monitored by measuring the OD_{600nm} using a spectral photometer. Strains (Table 4-29, Table 4-30) were stored in cryo tubes (80% Standard I nutrient broth, 20% glycerin) at -80 °C.

Table 4-29 *E. coli* strains used in this study

Strain	Genotype/ relevant characteristict	Source, reference
XL_1 blue	*Δ((mcrA)183Δ(mcrCB-hsdSMR-mrr)173 recA1 endA1 gyrA96 thi-1 hsdR17 supE44 relA1 lac F´ proAB lacIqZΔM15 Tn10 Tetr*	Stratagene
DH5α	*lacZ*(del)*M15 gyrA96 recA1 relA1 endA1 thi-1 hsdR17*	Invitrogen
Top10	*F- mcrA Δ(mrr-hsdRMSmcrBC) Φ80lacZΔM15 ΔlacX74 recA1 araD139 Δ(ara-leu)7697 galU galK rpsL endA1 nupG λ-*	Invitrogen

Table 4-30 *N. meningitidis* strains used in this study

Strain	Relevant genotypes	Resistance	Source
8013	Wild type	-	IHM strain collection
WUE2594	Wild type	-	IHM strain collection
MC58	Wild type	-	IHM strain collection
Z2491	Wild type	-	IHM strain collection
Δ*hfq*	*hfq*::*cat*, Deletion of *hfq* (NMV_1646)	Cm^R	IHM strain collection
Δ*hfq*	*hfq*::apha-1, Deletion of *hfq* (NMV_1646)	Km^R	This study
Δ*hfq*-C	*hfq*:: lctP::hfq-3xFLAG::erm::aspCD, complementation of *hfq* (NMV_1646)	Erm^R Km^R	This study
Hfq-3xFLAG	*hfq*-3xFLAG::*aphA-1* C-terminal 3xFLAG tag at native locus (NMV_1646) in 8013 background	Km^R	This study
Δ*NMnc0017*	NMnc0017::*aphA-3 Deletion of* NMnc0017	Km^R	This study
Δ*NMnc0018*	NMnc0018::*aphA-3* Deletion of NMnc0018	Km^R	This study
ΔΔ*NMnc0017/18*	NMnc0017/0018::*aphA-3* Deletion of NMnc0017 and NMnc0018	Km^R	This study
prpB::sf*gfp*	*lctP::prpB*-15th-sf*gfp::erm::aspC*	Erm^R	This study
prpB::sf*gfp*/Δ*hfq*	*lctP::prpB*-15th-sf*gfp::erm::aspC, hfq*::*cat*	Erm^R Cm^R	This study
prpB::sf*gfp*/ Δ*NMnc0017*	*lctP::prpB*-15th-sf*gfp::erm::aspC,* NMnc0017::*aphA-3*	Erm^R Km^R	This study
prpB::sf*gfp*/ Δ*NMnc0018*	*lctP::prpB*-15th-sf*gfp::erm::aspC,* NMnc0018::*aphA-3*	Erm^R Km^R	This study
prpB::sf*gfp*/ ΔΔ*NMnc0017/18*	*lctP::prpB*-15th-sf*gfp::erm::aspC,* NMnc0017/0018::*aphA-3*	Erm^R Km^R	This study
porA::sf*gfp*	*lctP::porA*-15th-sf*gfp::erm::aspC*	Erm^R	This study
porA::sf*gfp*/Δ*hfq*	*lctP::porA*-15th-sf*gfp::erm::aspC, hfq*::*cat*	Erm^R Cm^R	This study
porA::sf*gfp*/ Δ*NMnc0017*	*lctP::porA*-15th-sf*gfp::erm::aspC,* NMnc0017::*aphA-3*	Erm^R Km^R	This study
porA::sf*gfp*/ Δ*NMnc0018*	*lctP::porA*-15th-sf*gfp::erm::aspC,* NMnc0018::*aphA-3*	Erm^R Km^R	This study

Strain	Relevant genotypes	Resistance	Source
porA::sf*gfp*/ ΔΔ*NMnc0017/18*	*lctP::porA*-15th-sf*gfp::erm::aspC*, NMnc0017/0018::*aphA-3*	Erm^R Km^R	This study
Δ*proQ*	*proQ*::*cat*, Deletion of *proQ* (NMV_0689)	Cm^R	This study
Δ*proQ-C*	*proQ*::*cat*, *lctP*::*proQ*-3xFLAG::*erm*::*aspCD*, complementation of *proQ* (NMV_0689)	Erm^R Cm^R	This study
Δ*proQ*Δ*hfq*	*proQ*::*cat*, Deletion of *proQ* (NMV_0689); *hfq::aphA-3*, Deletion of *hfq (NMV_1646)*	Cm^R Km^R	This study
Δ*proQ-C*Δ*hfq*-C	*proQ*::*cat* , *hfq aphA-3* C, *lctP*::*proQ*-3xFLAG *hfq*-3xFLAG::*erm*::*aspCD*, complementation of *proQ* (NMV_0689) and *hfq* (NMV_1646)	Erm^R Cm^R Km^R	This study
ProQ-3xFLAG	*proQ*-3xFLAG::*aphA-1* C-terminal 3xFLAG tag at native locus (NMV_0689) in 8013 background	Km^R	This study
ProQ-3xFLAG/ Δ*hfq*	*proQ*-3xFLAG::*aphA-1* C-terminal 3xFLAG tag, *hfq*::*cat*	Km^R Cm^R	This study
Hfq-3xFLAG/ Δ*proQ*	*hfq*-3xFLAG::*aphA-1* C-terminal 3xFLAG tag, *proQ*::*cat*	Km^R Cm^R	This study

4.7. Plasmids

Table 4-31 Plasmids used in this study

Plasmid trivial name	Comment	Resistance	Reference
pGCC2	pGCC2 empty vector	Erm^R Km^R	Zhang *et al.*, 2013
pGG1	Plasmid (based on pZE12-luc) harbouring a non-polar *aphA-3* kanamycin resistance cassette	Km^R AmpR	Dugar *et al.*, 2016
pXG-10-SF	Plasmid for directional cloning of a target mRNA 5'UTR as N-terminal translational fusion to super-folder GFP	Cm^R	Corcoran *et al.*, 2012
pUC4K	Plasmid carrying an *aphA-1* kanamycin resistance cassette	Km^R	GE healthcare
pBluescript II SK(+)	Cloning vector	Amp^R	Invitrogene
pTnMax5	Plasmid harbouring a catGC chloramphenicol resistance cassette	Km^R,Cm^R	Kahrs *et al.*, 1995
p8013_Δ*hfq*::aph a-1	Plasmid (based on pBluescript II SK(+)) harbouring construct for generating knockout of hfq	Km^R	This study
p*hfq*-3xFLAG::*aphA-1*	Plasmid (based on pBluescript II SK(+)) harbouring construct for generating a 3xFLAG tagged version of *hfq*	Km^R	This study
pNHSB03	Plasmid (based on pXG-10) harbouring *prpB*::*sfgfp* fusion	Cm^R	This study
pNHSB03_neis	Plasmid (based on pGCC2) harbouring *prpB*::*sfgfp* fusion	Erm^R Km^R	This study
pNHL5	Plasmid (based on pXG-10) harbouring *porA*::*sfgfp* fusion	Cm^R	This study

Plasmid trivial name	Comment	Resistance	Reference
pNHL5_neis	Plasmid (based on pGCC2) harbouring *porA*::*sfgfp* fusion	Erm^R Km^R	This study
p8013_Δ*proQ*::*cat*	Plasmid (based on pBluescript II SK(+)) harbouring construct for generating knockout of *proQ*	Cm^R	This study
p*hfq*-3xFLAG::*aphA-1*	Plasmid (based on pBluescript II SK(+)) harbouring construct for generating a 3xFLAG tagged version of *hfq*	Km^R	This study
p*proq*-3xFLAG::*aphA-1*	Plasmid (based on pBluescript II SK(+)) harbouring construct for generating a 3xFLAG tagged version of *proQ*	Km^R	This study
p8013_Δ*hfq*::*aphA-1*	Plasmid (based on pBluescript II SK(+)) harbouring construct for generating knockout of *hfq*	Km^R	This study

4.8. Oligonucleotids

Table 4-32 Oligonucleotides used in this study

Name	Sequence	Purpose
	For detection of sRNAs and mRNAs	
JVO-13858	TCACTTACCGCTTGATTTATTTAA	NMnc0001
JVO-13786	TCGCTGGTTTGTACGTCCTGAAAA	NMnc0006
JVO-13282	AAACTATTAACTGACTACTCGAAC	NMnc0017
JVO-13283	GAGAAAAATCAAGCTGCATCAAGC	NMnc0018
JVO-14017	TCTGCCTGCTGTTTCCTCTTTATT	NMnc0019
JVO-14016	GAAAGCCCCCAACCTTGTTGCTCC	NMnc0024
JVO-13390	GGATATGCCGTCTGATGATGCA	NMnc0026
JVO_13412	TTCCACGTCCCAGATTCCCGCCTT	NMnc0029
JVO-13746	AGCTTGATAAAACCCGCCTTCCCC	NMnc0030
JVO-13747	TTTCAGAACAGTCTTGCAAGCCCC	NMnc0031
JVO-13780	CGGGTTCAGGGAAACGCTTTCAAT	NMnc0034
JVO_13411	CATTGTAGTTGGGTGTAACACTCT	NMnc0037
JVO-13782	CGTGCCGTTGAAGCCGAATTGTTC	NMnc0038
JVO-11436	TGCTGCTGTCCGTTGAAGTGAACC	NMnc0040
JVO-13289	ACGGCACTTGTCTTCCCCCCAAT	NMnc0041
JVO_13286	GCCGAAAAGGGAGAAACGGCAGCGG	NMnc0044
JVO-11738	CAGCAAACAAGTAATCTAGATTTC	AniS
JVO-14113	TTATTCAGCCTTTATAATACTTGGAC	Bns1
JVO-14114	GTCTGCGAAACAGACATTGCTAAA	Bns2
JVO-14150	GAGGTAAGGTAGTGTTTGCTGTTA	sRNA 0863-0864_F
JVO-14117	AAGGAGTATTGATAGATATAAAGGAC	σE sRNA
JVO-4862	ATCTTTTCAGACGGCCTTATTGTAGC	tracrRNA
JVO-4863	CGAAATGAGAAAGGGAGCTACAAC	Crispr-spacer
JVO-13920	TCATCGGCGCTGAATCGTTTCACG	5SrRNA
1313	GGAAAGTTTTAACGTGTTTG	*pnp*
1391	TTCAGTTTGGTTTCTTTGTAC	*rpmG*

1471	GCTAATAAGGTTTTCATATT	*sodC*
For detection of *prp-BC* mRNA applying a riboprobe		
JVO-14493	gttttttTAATACGACTCACTATAGG-GAGGTTAAAACGAATCAAAGAAAAA CAGCA	PCR template for riboprobe to detect *prpB*, carries T7 promoter
JVO-14494	gttttAT-GCATAAAATAAAACTACATAACACTA CAAAG	PCR template for riboprobe to detect *prpB*
For creating GFP–reporter fusion (cloned in pXG-10-SF for amplification and cloning into pGCC2)		
JVO-14494	gttttATGCATAAAATAAAAC-TACATAACACTACAAAG	*prpB* 5'UTR cloning in pXG-10-SF
JVO-14495	gttttGCTAGC CACGGCTTGGCGGAAACG	*prpB* 5'UTR cloning in pXG-10-SF
JVO-11108	gttttGCTAGCAAGCGGCAGTGCG-GACAATAC	*porA* 5'UTR cloning in pXG-10-SF
JVO-11109	gttttATGCATGTATCGGGTGTTT-GCCCGATG	*porA* 5'UTR cloning in pXG-10-SF
pZE-Cat	TGGGATATATCAACGGTGGT	Verification of inserts in pXG-10-SF
JVO-0155	CCGTATGTAGCATCACCTTC	Verification of inserts in pXG-10-SF
JVO-13362	TCGCTTAATTAACGGCGGATTTGTCCT ACT	Amplification of *prpB*-15th-sf*gfp* or *porA*-15th-sf*gfp* insert for cloning in pGCC2
pZE-Cat	TGGGATATATCAACGGTGGT	Amplification of *prpB*-15th-sf*gfp* or *porA*-15th-sf*gfp* insert for cloning in pGCC2
JVO-12665	CGAGCAATACAGCGGCAGATTTTCC	Verification of inserts in pXG-10-SF and in *N. meningitidis*
JVO-12824	CTAAACCTAAAGTGAATAGCTCACTT ATCAG	Verification of inserts in pXG-10-SF and in *N. meningitidis*
JVO-12822	GCTCGAATTCCGATCATATTCAATAA CCC	Sequencing primer to verify in-frame fusion of *lctP::prpB*-15th-sf*gfp::erm::aspC* and *lctP::porA*-15th-sf*gfp::erm::aspC* in *N. meningitidis*
For construction of sRNA deletions applying overlap PCR		
JVO-14374	GATTTCGGTTTTCCCGATAT	Overlap PCR construction of NMnc0017 deletion with *apha-3* cassette
JVO-14375	TCCTAGTTAGTCACCCGGGTAGGAAT GAATTATGCAGCTTT	Overlap PCR construction of NMnc0017 deletion with *apha-3* cassette
JVO-14376	ATTGTTTTAGTACCTGGAGGGAATAC CG GTCTGAAATATTCAATCC	Overlap PCR construction of NMnc0017 deletion with *apha-3* cassette
JVO-14377	TGCCCGCATCCCGATGAC	Overlap PCR construction of NMnc0017 deletion with *apha-3* cassette
JVO-14378	AGATGGCAAGGGACGAATC	Verification of NMnc0017 deletion
JVO-14379	TACCCAAAACATACTGTGCC	Overlap PCR construction of NMnc0018 deletion with *apha-3* cassette

JVO-14380	TCCTAGTTAGTCACCCGGGTAGGGAA TTATCCGCCGTTTC	Overlap PCR construction of NMnc0018 deletion with *apha-3* cassette
JVO-14381	ATTGTTTTAGTACCTGGAGGGAATAG ACTTGGCACACATTCAACT	Overlap PCR construction of NMnc0018 deletion with *apha-3* cassette
JVO-14382	GCTGCAATCCAAATCGGG	Overlap PCR construction of NMnc0018 deletion with *apha-3* cassette
JVO-14383	CCGCTGACTGATACACAAAA	Verification of NMnc0018 deletion
JVO-14434	ATTGTTTTAGTACCTGGAGGGAATAG GCACACATTCTATTGAATGTG	Overlap PCR construction of-NMnc0017/0018 deletion with *apha-3* cassette
HPK1	GTACCCGGGTGACTAACTAGG	Amplification of *aphA-3* cassette
HPK2	TATTCCCTCCAGGTACTAAAACA	Amplification of *aphA-3* cassette

For creating 3XFLAG tagged *proQ* (cloned in pBluescript II SK (+) vector)

JVO-13234	gttttGGATCCCCGTT-GGCACTCGGCATCGAT	Amplification of the *Bam*HI-*Eco*RI up-stream fragment to create *proQ*::3xFLAG::*aphA-1*
JVO-13235	gttttGAATTC TTACTATTTATCGTCGTCATCTTTGTA GTCGATATCATGATCTTTATAATCACC GTCATGGTCTTTGTAGTCTTCTGCTGC GGAAGATTCGGC	Amplification of the *Bam*HI-*Eco*RI up-stream fragment to create *proQ*::3xFLAG::*aphA-1*
JVO-13236	gttttGAATTCATCCCCAAACGAAAT-GCCGTC	Amplification of the *Eco*RI-*Hind*III down-stream fragment to create *proQ*::3xFLAG::*aphA-1*
JVO-13237	gttttAAGCTTCTGCTTATTCCATCA-GCCGTT	Amplification of the *Eco*RI-*Hind*III down-stream fragment to create *proQ*::3xFLAG::*aphA-1*
329	ACCATGATTACGCCAAGC	Verification of inserts in the pBluescript II vector
kb9	AATACGACTCACTATAGGGC	Verification of inserts in the pBluescript II vector
JVO-11502	GCGTCGGACTGCGCGCCGCCCCCA	Verification of *proQ*::3XFLAG::*aphA-1* in *N. meningitidis*
JVO-11603	CTGCGAAAGCGAAGACATCCGCGA	Verification of *proQ*::3XFLAG::*aphA-1* in *N. meningitidis*
JVO-13238	CCCGCAAGGCTTCCTGTCCAA	Sequencing primer to verify in in-frame fusion of *proQ*::3xFLAG::*aphA-1*

For creating and detecting of Δ*proQ and* Δ*hfq* strains (cloned in pBluescript II SK (+) vector)

1241	GCGCGCGGATCCTTCGTTGTATTCCTC TAAGAATC	*Bam*HI-*Hind*III up-stream fragment to create pNHBJ01 for Δ*proQ*
1242	GCGCGCGAAGCTTAAATCGTTGGATT CCGTCGGAGCG	*Bam*HI-*Hind*III up-stream fragment to create pNHBJ01 for Δ*proQ*
1243	GCGCGCAAGCTTATCCCCAAACGAAA TGCCGTCTGA	*Hind*III-*Xho*I downstream fragment to create pNHBJ01 for Δ*proQ*
1244	GCGCGCCTCGAGTTGATCCGCACGGC ATCAACGACA	*Hind*III-*Xho*I downstream fragment to create pNHBJ01 for Δ*proQ*
329	ACCATGATTACGCCAAGC	Verification of inserts in the pBluescript II vector
kb9	AATACGACTCACTATAGGGC	Verification of inserts in the pBluescript II vector

JVO-13303	GCGCGCAAGCTTTTGATCCGCACGGC ATCAACGACA	Verification of 8013 ProQ deletion in *N. meningitidis*
JVO-13305	CTGCGAAAGCGAAGACATCCGCGA	Verification of 8013 ProQ deletion in *N. meningitidis*
1237	GTTTTTTGGATCCCATTTGTCGCCGCC ATGAACCGCA	*BamH*I-*EcoR*I up-stream fragment to create p8013_Δ*hfq*:: *aphA-1* for Δ*hfq*
1238	GTTTTTGAATTCATTTTTAACTCCGCT ATTATGATT	*BamH*I-*EcoR*I up-stream fragment to create p8013_Δ*hfq*:: *aphA-1* for Δ*hfq*
1239	GTTTTTTGAATTCTCCGCACGAAGCAT GACGTGTCAT	*EcoR*I-*Hind*III down-stream fragment to create p8013_Δ*hfq*:: *aphA-1* for Δ*hfq*
1240	GTTTTTTAAGCTTCTGTTTGCCGTTTT CGTGTCCCGG	*EcoR*I-*Hind*III down-stream fragment to create p8013_Δ*hfq*:: *aphA-1* for Δ*hfq*
329	ACCATGATTACGCCAAGC	Verification of inserts in the pBluescript II vector
kb9	AATACGACTCACTATAGGGC	Verification of inserts in the pBluescript II vector
JVO-11502	GCGTCGGACTGCGCGCCGCCCCCA	Verification of 8013 *hfq* deletion in *N. meningitidis*
JVO-11603	CTGCGAAAGCGAAGACATCCGCGA	Verification of 8013 *hfq* deletion in *N. meningitides*

For construction of Δ*proQ* and Δhfq complementation strains applying overlap PCR

JVO_14059	ACCATCCATAGCGGCAGC	Overlap PCR construction ProQ complementation with *erm*C cassette
1395	ACGGCAACATCCGCATTTTGCTCCTTT AGCCTGCCGATGGC	Overlap PCR construction ProQ complementation with *erm*C cassette
JVO_14061	GCAAAATGCGGATGTTGCC	Overlap PCR construction ProQ complementation with *erm*C cassette
JVO_14129	TACCGAGCTCGAATTCCGATTTACTA TTTATCGTCGTCATCTTT	Overlap PCR construction ProQ complementation with *erm*C cassette
1396	AGTCTAGTGTGTTAGACTTTAATGTTG CAAAGCCGCAATCCGCTAT	Overlap PCR construction ProQ complementation with *erm*C cassette
JVO_12664	GTCCAAGACTTTCGGCACGGCTTTG	Overlap PCR construction ProQ complementation with *erm*C cassette
JVO_14059	ACCATCCATAGCGGCAGC	Overlap PCR construction Hfq complementation with *erm*C cassette
1394	CATCCACGATTCGATTTTGCTCCTTTA GCCTGCCGATGGC	Overlap PCR construction Hfq complementation with *erm*C cassette
JVO_14651	GCAAAATCGAATCGTGGATG	Overlap PCR construction Hfq complementation with *erm*C cassette
JVO_14129	TACCGAGCTCGAATTCCGATTTACTA TTTATCGTCGTCATCTTT	Overlap PCR construction Hfq complementation with *erm*C cassette
1396	AGTCTAGTGTGTTAGACTTTAATGTTG CAAAGCCGCAATCCGCTAT	Overlap PCR construction Hfq complementation with *erm*C cassette
JVO_12664	GTCCAAGACTTTCGGCACGGCTTTG	Overlap PCR construction Hfq complementation with *erm*C cassette
JVO_14059	ACCATCCATAGCGGCAGC	Overlap PCR construction ProQ and Hfq complementation with *erm*C cassette
1265	CATCCACGATTCGATTTTGCTTACTAT TTATCGTCGTCATCTTT	Overlap PCR construction ProQ and Hfq complementation with *erm*C cassette
JVO_14651	GCAAAATCGAATCGTGGATG	Overlap PCR construction ProQ and Hfq complementation with *erm*C cassette
JVO_12664	GTCCAAGACTTTCGGCACGGCTTTG	Overlap PCR construction ProQ and Hfq complementation with *erm*C cassette
JVO_14130	ATCGGAATTCGAGCTCGG	Amplification of *ermC* cassette
JVO_14153	AAACATTAAAGTCTAACACACTAG	Amplification of *erm*C cassette
JVO_14067	GTCGCGGCAATGATTTTCTT	Verification of ProQ, Hfq and ProQ/ Hfq complementation
JVO_12664	GTCCAAGACTTTCGGCACGGCTTTG	Verification of ProQ, Hfq and ProQ/ Hfq complementation

For creating templates for *in vitro* transcribed RNAs for EMSAs and in-line probing assay

JVO-14444	gttttttTAATACGACTCAC-TATAGGGAGGGTTAGCTGGTTCGAGTAGTC	*in vitro* transcription of NMnc0017, carries T7 promoter
JVO-14445	AAAAAAATGCACACATTCAATAGAAT	*in vitro* transcription of NMnc0017
JVO-14446	gttttttTAATACGACTCAC-TATAGGGAGGGTCGAGTTGCTTGATGCAG	*in vitro* transcription of NMnc0018, carries T7 promoter
JVO- 14447	AAAAAAATGCACACATCCAGTTGA	*in vitro* transcription of NMnc0018
JVO-14539	gttttttTAATACGACTCACTATAGGGAG-GAAAATAAAACTACATAACACTACAAAG	*in vitro* transcription of *prpB* 5'-UTR carries T7 promoter
JVO-14495	gttttGCTAGC CACGGCTTGGCGGAAACG	*in vitro* transcription of *prpB* 5'-UTR
1418	gttttttTAATACGACTCACTATAGGGAG-GATGAAATCTAGATTACTTGTTTG	PCR template for *in vitro* transcription of AniS; carries T7 promotor
1419	AAAAAAAAGGGGTGGCGG	PCR template for *in vitro* transcription of AniS
1420	gttttttTAATACGACTCACTATAGGGAG-GACAAGTCCAAGTATTATAAAG	PCR template for *in vitro* transcription of Bns1, carries T7 promotor
1421	AAAAAAGCAGATATATTCGG	PCR template for *in vitro* transcription of Bns1
1422	gttttttTAATACGACTCACTATAGGGAG-GATGCAAGAGCTTTTTCAGGA	PCR template for *in vitro* transcription of NMnc0006, carries T7 promotor
1423	AAAAAGACAAAAGCACCCAATAA	PCR template for *in vitro* transcription of NMnc0006
1424	gttttttTAATACGACTCAC-TATAGGGAGGCAACCCAAACCATTTTTTTGCG	PCR template for *in vitro* transcription of NMnc0034, carries T7 promotor
1425	AAATCCAATCAAAAAAGCGTGA	PCR template for *in vitro* transcription of NMnc0034
1426	gttttttTAATACGACTCAC-TATAGGGAGGGGTCATATCCGCGCCGCGTA	PCR template for *in vitro* transcription of NMnc0041, carries T7 promotor
1427	AACAAAAGAATGCCGTCCGAACG	PCR template for *in vitro* transcription of NMnc0041
1428	gttttttTAATACGACTCAC-TATAGGGAGGTGGAATTGCTTTCAGCGTCCG	PCR template for *in vitro* transcription of *pnp*, carries T7 promotor
1429	GGTGTGGTTGCCGTATTG	PCR template for *in vitro* transcription of *pnp*
1463	gttttttTAATACGACTCACTATAGGGAGGGTTGCCCGCAAACACGTAGT	PCR template for *in vitro* transcription of *rpmG*, carries T7 promotor
1480	GATAAAAATAAAAAAGCCTCCGAAC	PCR template for *in vitro* transcription of *rpmG*
1478	gttttttTAATACGACTCACTATAGGGAGGCTTGGCGGTGGCGGCCCAC	PCR template for *in vitro* transcription of *sodC*, carries T7 promotor
1479	ATATCTAGCAAAAAAGTGCGGTCA	PCR template for *in vitro* transcription of *sodC*

5. Methods

5.1. Cultivation of bacteria

E. coli were cultivated overnight on solid LB agar plates (Table 4-6) in an incubator at 37 °C or in LB media (Table 4-6) at 37 °C at 220 rpm shaking at 200 rpm. For growth of recombinant clones both the solid and liquid medium was supplemented with appropriate antibiotics (100 µg/ml ampicillin, 30 µg/ml chloramphenicol, 250 µg/ml erythromycin, 30 µg/ml kanamycin).

All *N. meningitidis* strains used were either grown on Columbia sheep blood (COS) agar plates or on GCB^{++} agar plates (Table 4-7) with appropriate antibiotics (7 µg/ml erythromycin, 100 µg/ml kanamycin, 7 µg/ml chloramphenicol or 5 µg/ml) at 37 °C in a 5% CO_2 humidified atmosphere overnight. For liquid cultures, *N. meningitidis* grown as solid cultures overnight were harvested and a starter culture was inoculated to a final optical density (OD_{600nm}) of 1.0 in 5 ml $GCBL^{++}$ liquid medium (Table 4-7, Table 4-8) in 50ml Falcon-tubes. After one hour the starter culture was used to inoculate $GCBL^{++}$ medium to a final OD_{600nm} of 0.15. Bacteria were either grown in 50 ml Falcon-tubes at 37 °C at 220 rpm without added CO_2 for total RNA isolation (chapter 5.13) or in 96-well microtiter plates to measure bacterial growth. Growth in 96-well microtiter plates was monitored using the Infinite F 200 Pro instrument (Table 4-1) at 37 °C with 3 mm amplitude shaking.

5.2. Determination of the optical density at 600nm

1 ml of the bacterial suspension was pipetted in a cuvette and the absorption at 600 nm (OD_{600nm}) was measured with a photometer (WPA biowave, Table 4-1) against the blank medium. Thereby, the bacterial suspension was adjusted to the desired optical density if appropriate. In order to calculate the cell number, an OD_{600nm} 1.0 is equivalent to approximately $1x10^9$ cells/ml for *N. meningitidis* and to approximately $2x10^8$ cells/ml for *E. coli*.

5.3. Preperation of chemically compentent *E. coli* cells

A 15 ml starter culture in LB medium (Table 4-6) was inoculated with a single colony from DH5α, Top10 or XL-1 Blue MRF' cells (Table 4-29) grown on solid media overnight and grown overnight at 37 °C. 25 ml LB medium (Table 4-6) were inoculated with 1 ml starter culture and incubated at 37 °C in a shaker (Thermomixer 5436, Table 4-1). Once reaching an OD_{600nm} of 0.5-0.7, the cells were cooled down for 10-20 minutes on ice. Subsequently,

cells were pelleted in precooled tubes by centrifugation at 4 °C for 5 minutes at 4000 rpm. The pellet was chilled on ice for 1 minute, then resuspended and washed twice with 10 ml of ice cold 80 mM $MgCl_2$/20 mM $CaCl_2$ (Table 4-13) by centrifuging at 4 °C for 5 minutes at 4000 rpm. The pellet was resuspended in 800 µl of 100 mM $CaCl_2$/20% glycerol, and aliquots of 100 µl were shock frozen in liquid nitrogen and stored at -80 °C until use.

5.4. Transformation of *E. coli*

A 100 µl aliquot of chemically competent *E. coli* DH5α or *E. coli* XL-1 Blue MRF' (Table 4-29) was thawed slowly on ice. The ligation reaction was carefully mixed with the bacteria and chilled on ice for approximately 30 minutes. The cells were incubated at 42 °C for 90 seconds prior to cooling them down on ice for 2 minutes. Subsequently, 800 µl LB medium (Table 4-6) was added and the cells were incubated for 1 h at 37 °C at 200 rpm. Then, bacteria were plated on LB agar plates supplemented with the appropriate antibiotic(s) and incubated overnight at 37 °C.

5.5. Transformation of *N. meningitidis*

The strain to be transformed was grown overnight on COS agar plates at 37 °C with 5% CO_2 in an incubator. A 5ml $GCBL^{++}$ (Table 4-7, Table 4-8) starter culture was inoculated with the bacteria grown overnight on solid media and incubated for 1 h at 37 °C at 200 rpm. Next, bacterial suspensions were adjusted to an OD_{600nm} 0.15 in a final volume of 1 ml $GCBL^{++}$. For the transformation, 600 ng – 1.5 µg of the DNA (plasmids or PCR products), were added to the culture and incubated for 5 to 6 hours at 37 °C and 200 rpm. Subsequently, bacteria were pelleted at 5000 rpm for 3 minutes at room temperature and plated on GCB^{++} agar plates supplemented with the required antibiotic for selection of transformants. The plates were incubated overnight at 37 °C with 5% CO_2.

5.6. Preperation of meningococcal genomic DNA

Meningococcal genomic DNA was isolated with the QIAamp DNA Mini Kit (Table 4-4) with some modification of the manufacturer's protocol. Bacteria were streaked onto two COS agar plates and grown overnight at 37 °C with 5% CO_2 in an incubator (Heraeus 6000, Table 4-1). Next day, the entire bacterial material was harvested with a cotton swab and

resuspended in 1.25 ml PBS (Table 4-12). Then, the bacterial suspension was centrifuged for 5 minutes at 8000 rpm and the pellets were resuspened in 180 µl ATL buffer of the QIAamp DNA Mini Kit with 20 µl Proteinase K (20 mg/ml). Subsequently, the suspensions were incubated at 56 °C for 2-3 hours and vortexed every thirty minutes. Afterwards, the tubes were mixed with 80 µl RNase A (5 mg/ml) and vortexed 10 times. 200 µl AL buffer of the QIAamp DNA Mini Kit was added, the tubes were vortexed 10 times and incubated for 10 minutes at 70 °C. After adding 200 µl ethanol to the suspensions, the samples were vortexed 10 times and centrifuged shortly. The whole material was pipetted onto a QIAamp spin column and was centrifuged for 1 minute at 8000 rpm. The column was transferred into a fresh tube, 500 µl AW1 buffer was added and centrifuged for 1 minute at 8000 rpm, the flow-through was discarded and the column was washed with 500 µl AW2 buffer of the QIAamp DNA Mini Kit 3 minutes at 13000 rpm. Afterwards, the column was dried with a 1 min centrifugation step at 13000 rpm and then transferred into a fresh 2 ml microcentrifuge tube. To elute the DNA, 100 µl H_2O was applied to the column, incubated at room temperature for at least one minute and then centrifuged for 1 minute at 8000 rpm. Concentration and purity of the DNA was measured using a spectrophotometer (PEQlab, ND-1000, Table 4-1) and stored at 4 °C.

5.7. Preperation of plasmid DNA

For the isolation of plasmid DNA the QIAprep Spin Miniprep Kit or the Qiagen Plasmid Midi Kit were used (Table 4-4). To elute the DNA, 20-50 µl H_2O was applied to the column, incubated at room temperature for at least one minute and then centrifuged for 1 minute at 13000 rpm. Concentration and purity of the plasmid DNA was measured using a spectrophotometer (PEQlab, ND-1000, Table 4-1) and stored at 4 °C.

5.8. Polymerase chain reaction (PCR)

PCRs were used to amplify specific DNA fragments and to screen for correct clones after transformation. Q5® High-Fidelity DNA polymerase (NEB, Frankfurt) was used for cloning purposes and to generate DNA templates for *in vitro* transcription of RNAs because of its proof reading activity. Taq DNA polymerase (NEB, Frankfurt) was used for colony PCRs (Table 5-2). Generally, 100 ng genomic or plasmid DNA was used as template DNA. To screen for transformants, a colony was picked and directly rubbed into the PCR mix.

PCR was performed in modification of the manufacturer's protocol as given in Table 5-1.

Table 5-1 PCR protocol for Taq DNA polymerase

Component	25µl reaction	Final concentration
10x ThermoPol reaction buffer	2.5 µl	1x
20 mM dNTPs	0.25 µl	200 µM
25µM forward primer	0.5 µl	0.5 µM
25µM reverse primer	0.5 µl	0.5 µM
Template DNA	variable	<1 µg
Taq DNA polymerase	0.25 µl	0.05 U/ µl
ddH_2O	Add to 25 µl	

PCR reactions were quickly transferred to a thermocycler (Thermomixer 5436) preheated to the denaturing temperature (95 °C). The standard PCR program is given in Table 5-2.

Table 5-2 PCR program for Taq polymerase

Step	Temperature	Time
(1) Initial denaturation	95 °C	30 seconds (5`for lysates)
(2) Denaturation	95 °C	30 seconds
(3) Annealing	45-70 °C	30 seconds
(4) Extension	68 °C	1 minute/ kb
(5) Final extension	68 °C	5 minutes
(6) Hold/ Cooling	4 °C	∞
(7)	30-40 cycles of steps 2 to 4	

The standard reaction used for Q5® High-Fidelity DNA polymerase is shown in Table 5-3.

Table 5-3 PCR protocol for Q5® DNA polymerase

Component	25µl reaction	Final concentration
5x Q5 reaction buffer	10 µl	1x
20 mM dNTPs	0.5 µl	200 µM
25µM forward primer	1 µl	0.5 µM
25µM reverse primer	1 µl	0.5 µM
Template DNA	variable	<1 µg
Q5® High-Fidelity DNA polymerase	0.5 µl	0.02 U/ µl
ddH_2O	Add to 25 µl	

The PCR cycling scheme used for Q5® High-Fidelity DNA polymerase is given in Table 5-4 and the PCR cycling scheme applied for overlap PCR reactions is given in Table 5-5.

Table 5-4 PCR program for Q5® High-Fidelity DNA polymerase

Step	Temperature	Time
(1) Initial denaturation	98 °C	30 seconds
(2) Denaturation	98 °C	30 seconds
(3) Annealing	50-72 °C	30 seconds
(4) Extension	72 °C	30 seconds/ kb
(5) Final extension	72 °C	2 minutes
(6) Hold/ Cooling	4 °C	∞
(7)	30 cycles of steps 2 to 4	

Table 5-5 PCR program for overlapping PCRs for Q5® High-Fidelity DNA polymerase

Step	Temperature	Time
(1) Initial denaturation	98 °C	1 minute
(2) Primer annealing	61 °C	1 minute
(3) Initial annealing	72 °C	10 minutes
(4) Initial Denaturation	98 °C	1 minute
(5) Denaturation	98 °C	15 seconds
(6) Annealing	50-72 °C	30 seconds
(7) Extension	72 °C	30 seconds/ kb
(8) Final extension	72 °C	10 minutes
(9) Hold/ Cooling	4 °C	∞
	40 cycles of the steps 5 to 7	

The annealing temperatures (Ta) of both Taq-Polymerase and Q5® High-Fidelity DNA polymerase were calculated by using the Tm Calculator (http://tmcalculator.neb.com/#!/) from NEB (Frankfurt).

5.9. Agarose gel electrophoresis of DNA

PCR products were electrophoretically separated in an agarose gel with TAE buffer (chapter 4.4) using agarose concentrations between 1% and 2% (w/v), depending on the size of the DNA fragment. The mixture of agarose and buffer was heated in a microwave oven (Table 4-1), cooled down at room temperature, prestained with GelRedTM (Table 4-3) (e.g. 5 µl stock solution added to 50 ml of gel solution) and poured into a gel chamber. Five µl of the length standard 'Hyper Ladder I' (Table 4-3) were used as standard molecular weight marker while DNA samples were diluted to a 1X concentration with 6X DNA loading

buffer/dye (Table 4-3). DNA samples were separated at 170 V in 1X TAE buffer for approximately 30 min. DNA fragments were visualized with the Chemi Doc MP System (Bio-Rad) (at 302 nm or 312 nm). Afterwards, PCR products were either purified using the Stratec INVISISORB Purification Kit (Table 4-4) or were extracted from the gel with the Stratec Gel Extraction Kit (Table 4-4).

5.10. Sequencing of PCR products and plasmids

Sequencing reactions were prepared in a final volume of 10 µl in ddH_2O and included 25 µM of the respective primer and either 20-80 ng of PCR fragments or 200-400 ng of plasmids. Sequencing reactions were set up in a 1.5 ml tube and sent to GATC (Köln, Germany) for sequencing.

5.11. Cloning procedure: digestion of DNA, gel extraction and ligation

DNA digestion was performed with restriction endonucleases purchased from New England BioLab. For cloning purposes, plasmids or purified PCR products were enzymatically digested using different restriction endonucleases which are listed in Table 4-5. Enzymatic digestions were performed at 37 °C without shaking for one to two hours as described in Table 5-6.

Table 5-6 Standard restriction digest

Component	50 µl reaction
Restriction Enzyme	10 U
DNA	1 µg
10x NEBuffer	5 µl
Total Reaction volume	50 µl
ddH_2O	Add to 50 µl

Digested DNA fragments were purified using the MSB Spin PCRapace Kit (Table 4-4). Digested plasmid DNA was separated using agarose gel electrophoresis (chapters 4.5.1 and 5.9) and the separated band was sliced out of the gel. DNA was extracted from the gel pieces using the Invisorb Spin DNA Extraction Kit (Table 4-4) according to the manufacturer's instructions.

Table 5-7 Standard ligation protocol (T4 DNA ligase)

Component	20 µl reaction
10x T4 DNA Ligase Buffer	2 µl
Plasmid DNA	50 ng
Insert DNA	variable
T4 DNA ligase	1 µl
ddH_2O	Add to 20 µl

Ligation reactions were set up as described in Table 5-7 with purified digested DNA fragments, linearized plasmids and T4 DNA ligase. Generally, a molar ratio of 1:5 plasmid to insert was used in standard ligation reaction. Subsequently, ligation reactions were performed at 16 °C overnight in a thermocycler. Next day, the ligation was used for chemical transformation using compentent cells (5.4) or were stored at -20 °C until use.

5.12. Mutant construction

The Integrated Genome Browser (chapter 5.33, (113)) was used to control the binding of all designed primers and probes. Serial Cloner 2.6 (chapter 5.33, Serial basic) was used to design the cloning vectors and to carry out DNA alignments.

5.12.1. Construction of a *proQ* deletion strain

The *proQ* gene (NMV_0698) was deleted from 8013 strain by replacing the coding sequence by the insertion of the chloramphenicol resistance cassette *catGC* (Table 4-31). First, p8013_Δ*proQ*::cat plasmid was constructed in competent *E. coli* cells (chapter 5.3). Upstream and downstream flanking regions of the ProQ gene were amplified by PCR (Table 5-3) from chromosomal DNA using primer pairs 1241/ 1242 and 1243/1244, respectively. The resulting upstream flanking region was digested with *BamH*I and *Hind*III while the flanking downstream region was digested with *Hind*III and *Xho*I. The *catGC* cassette was generated by digestion of pTnMax5 (Table 4-31) with *Hind*III. The predigested upstream and downstream flanking regions and the *catGC* cassette were cloned into the *BamH*I and *Xho*I predigested pBluescript II SK (+) vector (Table 4-31) to yield the p8013_Δ*proQ*::*cat* plasmid (p8013_Δ*proQ*::*cat*) (Figure 5-1). The plasmid was checked by colony PCR with primer pair kb9 and 329. The plasmid was used for transformation in *N. meningitidis* 8013 cells (chapter 5.5). Chloramphenicol-resistant clones were checked by PCR using gDNA and JVO_13303/-13305, resulting in strain Δ*proQ*. Additionally, the

phfq-3xFLAG::*aphA-1* plasmid of the IHM strain collection (Table 4-30) was used for transformation of the Δ*proQ* strain in order to generate a Hfq-3xFLAG/Δ*proQ* strain.

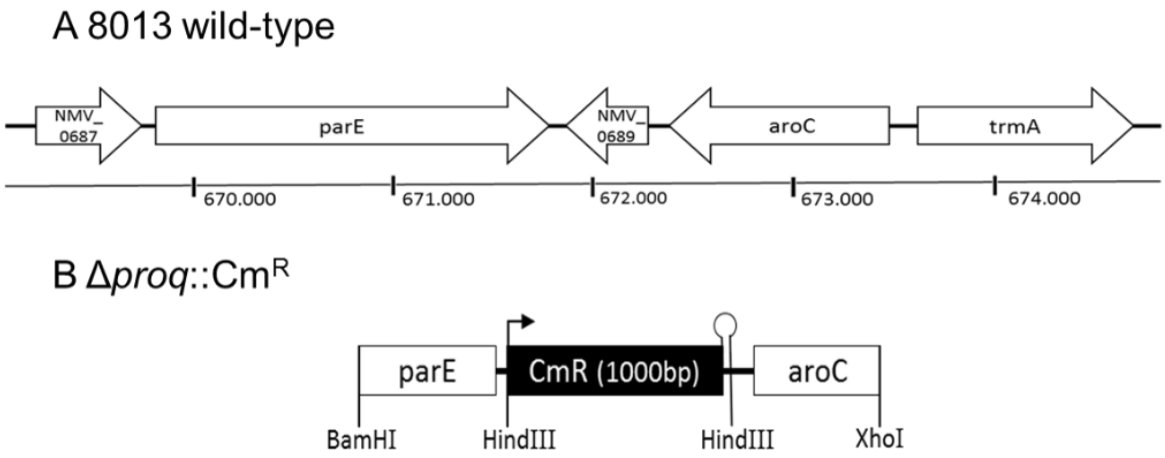

Figure 5-1 Schematic representation of the *proQ* deletion strategy

(A) Representation of the *N. menigitidis* wild-type ProQ locus. The CDSs are indicated by arrows, the numbers below represent the nucleotide positions of the genes in the *N. meningitidis* 8013 genome. (B) Representation of the chloramphenicol resistance-cassette and the homologous flanking regions including restriction sites of plasmid p8013_Δ*proQ*::*cat* used for *proQ* deletion in *N. meningitidis* 8013.

5.12.2. Construction of *hfq* and *proQhfq* deletion mutants

In order to knock out the *hfq* gene in strain 8013, the *hfq* gene was deleted by the insertion of the kanamycin resistance cassette *aphA-1*. First, p8013_Δ*hfq*::*aphA-1* plasmid (Table 4-31) was constructed in *E. coli* Top10 cells (chapter 5.3). Upstream and downstream flanking regions of the *hfq* gene were amplified by PCR (Table 5-3) from chromosomal DNA using primer pairs 1237/1238 and 1239/1240, respectively. Then, the upstream flanking region was digested with *BamH*I and *EcoR*I while the downstream flanking region was digested with *EcoR*I and *Hind*III. The *aphA-1* cassette was generated by digestion of pUC4K with *EcoR*I (Table 4-31). The predigested upstream and downstream flanking regions and *aphA-1* cassette were cloned into the *BamH*I and *Hind*III predigested pBluescript II SK (+) vector (Table 4-31). to yield the p8013_Δ*hfq*::*aphA1* plasmid (Figure 5-2). The plasmid was checked by colony PCR using the primers kb9 and 329. The plasmid was used for transformation (chapter 5.5) of *N. meningitidis* 8013 wild-type and Δ*proQ* cells to obtain the double knockout strain Δ*proQ*Δ*hfq*. Positive kanamycin-resistant clones were checked by PCR on gDNA using JVO_11603/JVO_11502, resulting, in strain Δ*hfq* and Δ*proQ*Δ*hfq*.

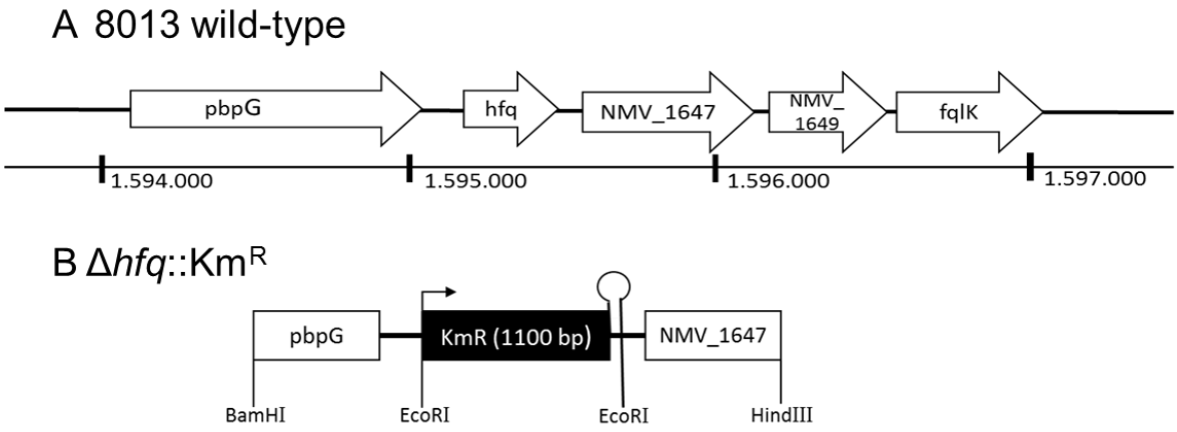

Figure 5-2 Schematic representation of the *hfq* deletion strategy

(A) Representation of the *N. menigitidis* wild-type Hfq locus. The CDSs are indicated by arrows, the numbers below represent the nucleotide positions of the genes in the *N. meningitidis* 8013 genome. (B) Representation of the kanamycin resistance-cassette and homologous flanking regions including restriction sites of plasmid p8013_Δ*hfq*::*aphA-1* used for *hfq* deletion in *N. meningitidis* 8013.

5.12.3. Construction of *N. meningitidis* complementation strains by overlap PCR

All *N. meningitidis* complementation strains are listed in Table 4-30 and were constructed by overlap PCR (Table 5-5). The strains were generated by transformation of the obtained overlap PCR products into the *lctP* and *aspC* locus of strain 8013 (Figure 5-3), respectively. All PCR products carried a fragment encoding the target gene::3xFLAG including its native promotor and an erythromycin resistance cassette. The PCR products were flanked by ~500 bp of homologous sequences of the *in trans* complementation locus situated in the intergenic region between NMV_1884 and NMV_1885. As an example, for the complementation of Δ*proQ*, the *proQ* complementation construct was generated by overlap PCR (Table 5-5) as followed: A PCR fragment of 500 bp upstream of the intergenic region of NMV_1884/_1885 using upstream region primers (JVO_14059/-1395) and a second PCR fragment of ~300bp downstream of the intergenic region of NMV_1884/-1885 using downstream region primers (1396/JVO_12664) were amplified from chromosomal DNA of strain 8013 wild-type. A PCR fragment of *proQ*::3xFLAG including its native promotor was amplified using the target gene primers JV_14061/-14129 from chromosomal DNA of *proQ*::3xFLAG. The resistance cassette was amplified from plasmid pgcc2 (Table 4-31) uing primers 14130/14153 (Ery^R).

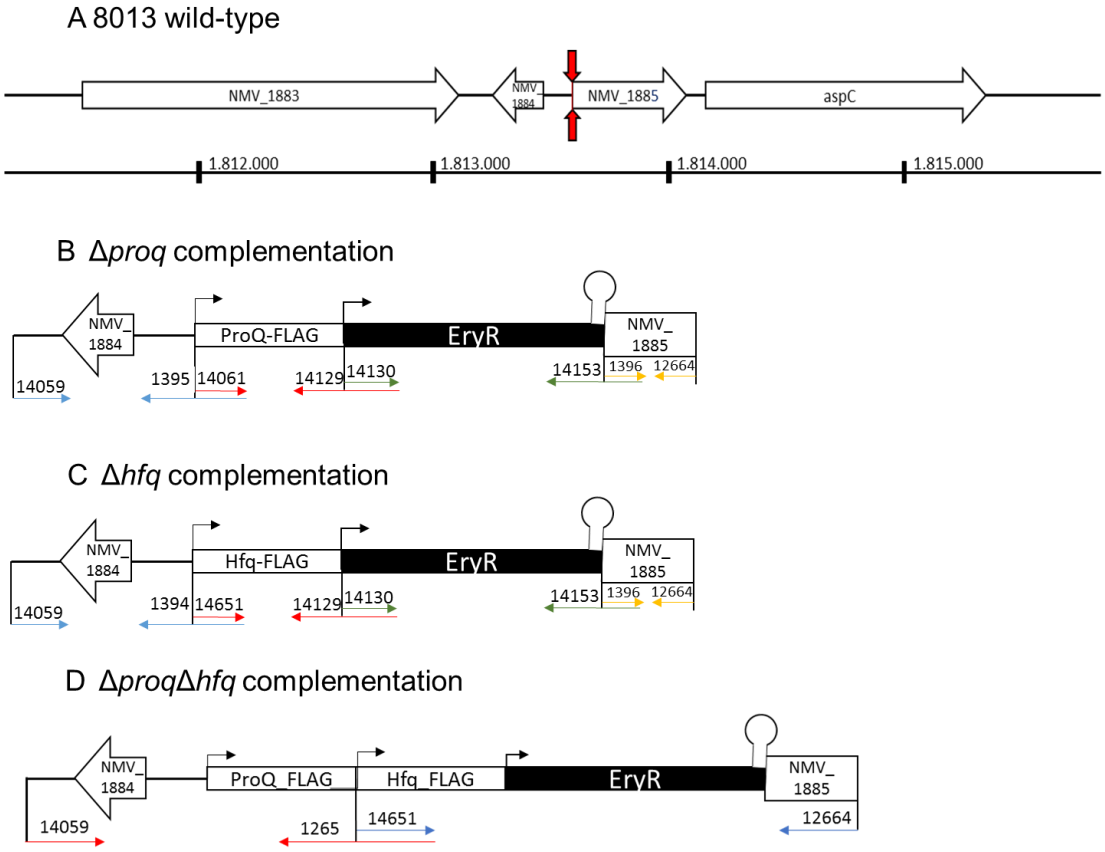

Figure 5-3 Schematic representation of the Δ*proQ* and Δ*hfq* complementation strategy

(A) Representation of the *N. menigitidis* wild-type complementation locus. The CDSs are indicated by arrows, the numbers below represent the nucleotide positions of the genes in the *N. meningitidis* 8013 genome. The red arrows indicate the integration site of the complemented genes (B) Representation of the erythromycin resistance cassette and homologous flanking regions including primers used for Δ*hfq* complementation in *N. meningitidis* 8013. (C) Representation of the erythromycin resistance cassette and homologous flanking regions including primers used for Δ*proQ* complementation in *N. meningitidis* 8013. (D) Representation of the erythromycin resistance cassette and homologous flanking regions including primers used for Δ*proQ*Δ*hfq* complementation in *N. meningitidis* 8013.

The 5’ ends of the antisense upstream region primer 1395, the antisense target gene primer JVO_14129 and sense downstream region primer 1396 contained ~25 bp of sequence homologous to the sense or antisense primer of the nearby fragment. All four PCR products were purified and then added together in a ratio of 50:50:50:50 ng to a 50 µl Q5 polymerase PCR reaction with sense and antisense primers (JVO-14059/-12664) at a final concentration of 0.06 µM. Overlap PCR was performed according to Table 5-5. Knockout strains were transformed with purified PCR fragment and transformants were isolated by selction on erythromycin. All complementation strains were verified by PCR using JVO_14067/-12664 which bind outside of the region used for cloning. Complementation strains for Δ*hfq* and Δ*proQ*Δ*hfq* were constructed similarly (Table 4-32) (Figure 5-3).

5.12.4. Construction of *N. meningitidis* sRNA mutants by overlap PCR

All *N. meningitidis* sRNA deletion strains are summarized in Table 4-30 and were constructed by overlap PCR (Figure 5-4). All PCR products carried a *aphA-3* kanamycin resistance cassette (Table 4-31) flanked by ~500 bp of homologous sequence up- and downstream of the resistance cassette. The kanamycin resistance cassettes (Kan^R) were amplified from plasmid pGG1 (Table 4-31) using primers HPK1/HPK2. As an example, for the deletion of NMnc0017, the Δ*nmnc0017* deletion construct was generated by overlap PCR (Table 5-5) as followed. A PCR fragment of 500 bp upstream of NMnc0017 transcriptional start site was amplified from genomic DNA of strain 8013 using the primers JVO14374/-14375. Secondly, a ~500bp PCR fragment downstream of NMnc0017 was amplified using primers JVO-14376/-14377. The 5' ends of JVO-14375 and JVO-14376 contained ~25 bp of sequence homologous to the sense or antisense primer (HPK1/HPK2), respectively, which were used to amplify the resistance cassette. The three purified PCR products were added together in a ratio of 50:50:50 ng to a 50 µl Q5 polymerase PCR reaction (chapter 5.8) with the primers JVO-14374/-14377. Overlap PCR was performed with the conditions described in Table 5-5. Wild-type strain was transformed with purified PCR fragment and transformants were isolated by selction on kanamycin. The deletion strain Δ*nm*nc0017 was verified by PCR using JVO-14377/-14378 which bind outside of the region used for cloning. Deletion mutants for NMnc0018::KanR and NMnc0017/-N0018::Kan^R were constructed similarly (Table 4-32) (Figure 5-4).

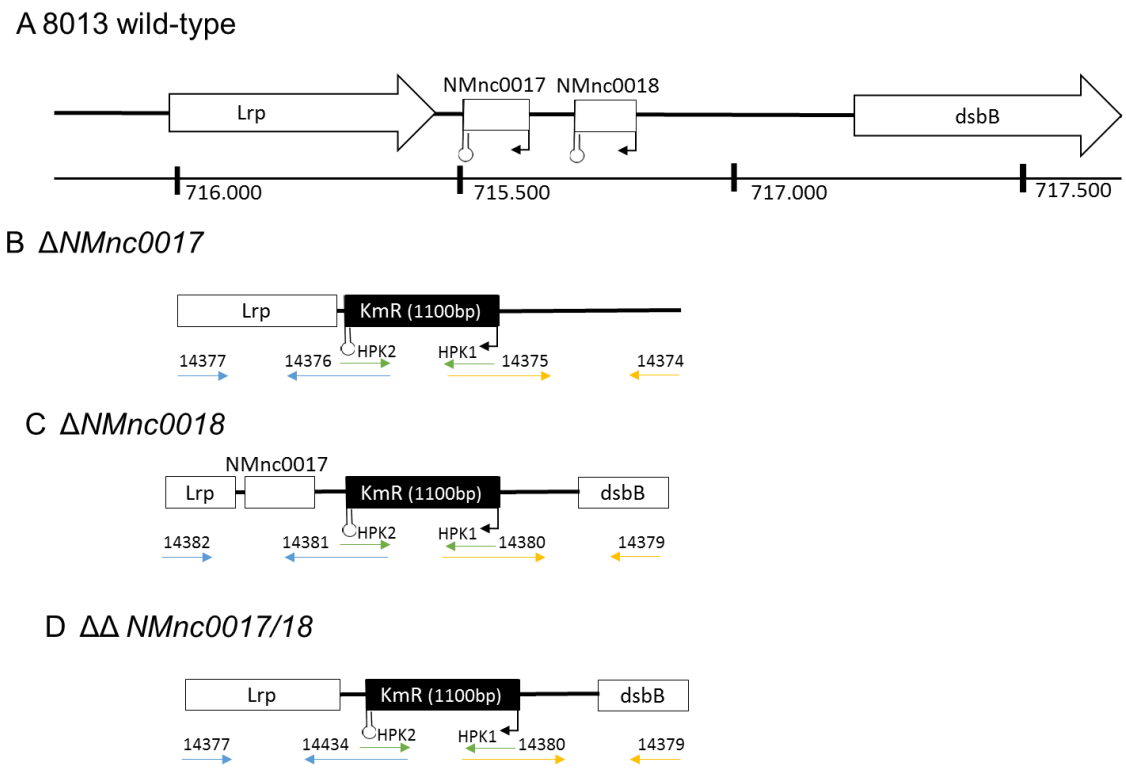

Figure 5-4 Schematic representation of the Δ*NMnc0017* and Δ*NMnc0018* cloning strategy

(A) Representation of the *N. menigitidis* wild-type locus. The CDSs are indicated by arrows, the numbers below represent the nucleotide positions of the genes in the *N. meningitidis* 8013 genome. The black arrows indicate the transcriptional start sites of the sRNAs. (B) Representation of the kanamycin resistance cassette and homologous flanking regions including primers used for *NMnc0017* deletion in *N. meningitidis* 8013. (C) Representation of the kanamycin reistance cassette and homologous flanking regions including primers used for *NMnc0018* deletion in *N. meningitidis* 8013. (D) Representation of the kanamycin resistance cassette and homologous flanking regions including primers used for *NMnc0017 and NMnc0018* deletion in *N. meningitidis* 8013.

5.12.5. Construction of a 3xFLAG tagged ProQ strain

To construct a ProQ::3xFLAG-tagged strain, a plasmid (3xFLAG::*aphA-1*) containing the 3xFLAG and the *aphA-1* cassette flanked by 500 nt up- and downstream of the *proQ* stop codon was cloned into *E. coli* (Figure 5-5). First, 500 nt upstream of the *proQ* stop codon were amplified by PCR (Table 5-3) from chromosomal DNA (chapter 5.6) of 8013 with primers JVO_13234 and JVO_13235 containing the 3xFLAG sequence at its 3`end. The resulting PCR product was digested with *BamH*I and *EcoR*I. Secondly, the downstream region of the *proQ* gene was amplified by PCR from chromosomal DNA of strain 8013 with primers JVO_13236 and JVO_13237 followed by digestion with *EcoR*I and *Hind*III. Next, the pUC4K plasmid (Table 4-31) was digested with *EcoR*I to obtain the *aphA-1* kanamycin resistance cassette. Both fragments and the *aphA-1* cassette were cloned into the pBluescript II SK (+) vector predigested with *Bam*HI and *Hind*III. The generated pproQ-3xFLAG::*aphA-1* plasmid was checked by colony PCR (Table 5-1) with primer pair kb9

and 329. This plasmid was then used for transformation of the 8013 wild-type and 8013 Δ*hfq*::Cm mutant strains to generate a ProQ-3xFLAG strain and a ProQ-3xFLAG/Δ*hfq* strain. Transformants were verified by colony PCR on gDNA using JVO_11502/-11603 and in-frame fusion of ProQ::3xFLAG by sequencing with JVO-13238, respectively.

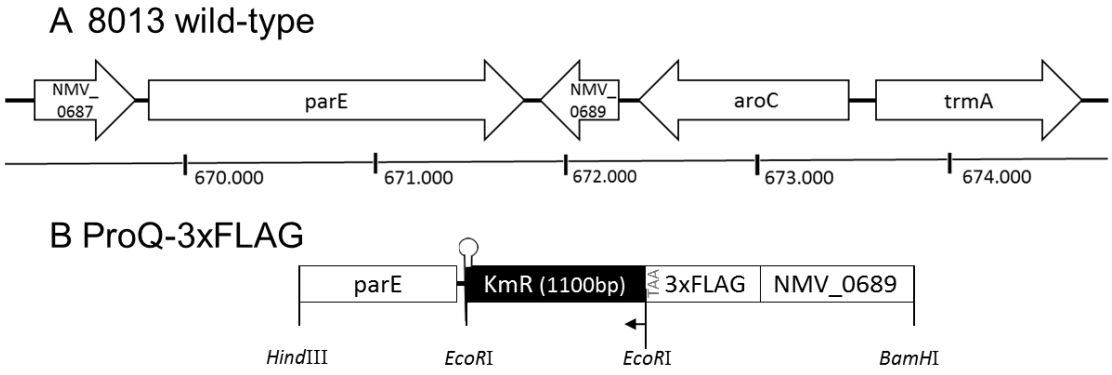

Figure 5-5 Schematic representation of the cloning strategy for constructing a ProQ-3xFLAG strain

(A) Representation of the *N. menigitidis* wild-type ProQ (NMV_0689) locus. The CDSs are indicated by arrows, the numbers below represent the nucleotide positions of the genes in the *N. meningitidis* 8013 genome. (B) Representation of the kanamycin resistance cassette and homologous flanking regions including restriction sites of plasmid pproQ-3xFLAG::*aphA-1* used for *ProQ FLAG-tagging* in *N. meningitidis* 8013.

5.12.6. Cloning of translational reporter fusions to sfGFP.

In order to construct a translational reporter fusion, we fused the 5'UTR and 15 aminoacids of the N-terminal coding region of the *prpB* gene and the *porA* gene (expression control as *porA* is a housekeeping gene), respectively, to *sfGFP* amplified from pXG-10-SF plasmid (114). These reporter fusions were transformed together with the Erm^R resistance (42) cassette into the *lctP*/*aspC* locus of *N. meningitidis* 8013 using the pGCC2 plasmid (Table 4-31) as a shuttle vector (Figure 5-6). The inserts (*prpB*, *porA*) were amplified by PCR from chromosomal DNA with primer pairs JVO14494/JVO14495 and JVO11108/JVO11109, respectively. The generated PCR fragments were digested with *Nsi*I/*Nhe*I, purified (chapter 5.11) and cloned into NsiI/*Nhe*I-predigested pXG-10-SF plasmid (Table 4-31) resulting in pNHSB03 (*prpB*-15th-*sfgfp*) and pNHL5 (*porA*-15th-*sfgfp*). The plasmid pGCC2 was digested with *Aat*II/*Pac*I and ligated to *Aat*II/*Pac*I-digested PCR products amplified from pNHSB03 (*prpB*-15th-*sfgfp*) and pNHL5 (*porA*-15th-*sfgfp*) with primer pairs JVO13362/pZE-Cat. As the pGCC2 plasmid contains homologous regions to the meningococcal *lctP*/*aspC* locus, the resulting plasmids pNHSB03-neisseria (*prpB*-15th-sfgfp) and pNHL5_neisseria (*porA*-15th-*sfgfp*) were used for transformation of several *N.*

meningitidis strains (8013 wt, Δ*hfq*, Δ*NMnc0017*, Δ*NMnc0018*, ΔΔ*NMnc0017/18*). Transformants were selected on erythromycin containing GC plates (chapter 4.4.3). The correct double homologous recombination event was verified by colony PCR JVO12665/-12824 and in-frame fusion of *lctP*::*prpB*-15th-*sfgfp*::*erm*::*aspC* and *lctP*::*porA*-15th-*sfgfp*::*erm*::*aspC* by sequencing with JV012822/-0155, respectively

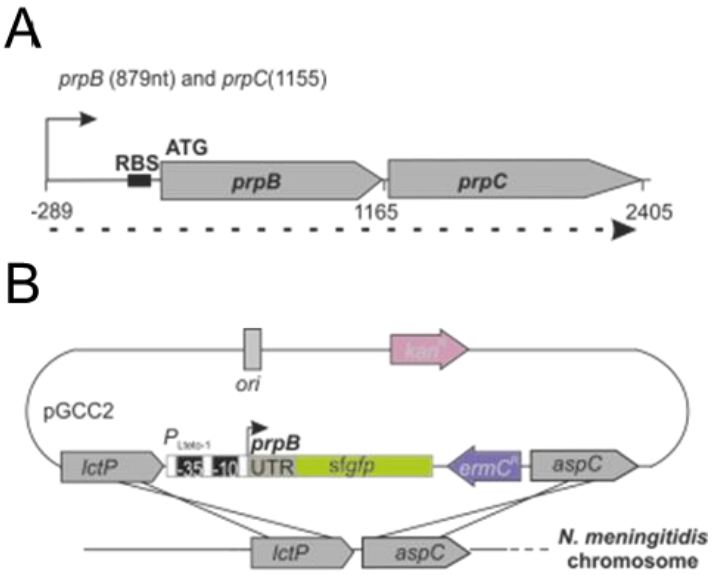

Figure 5-6 Schematic representation of the cloning strategy of the translational reporter fusions to sfGFP

(A) Representation of the *N. menigitidis* wild-type *prpB* locus. The CDSs are indicated by arrows, the numbers below represent the nucleotide positions of the genes in the *N. meningitidis* 8013 genome. (B) Representation of the erythromycin resistance cassette and homologous flanking regions of plasmid pNHSB05 used for translational reporter fusion of prpB to sfGFP in *N. meningitidis* 8013. The figure was adapted from Heidrich *et al.*, 2017 (117).

5.13. Total RNA isolation with the hot phenol method

Bacterial pellets stored at -80 °C were suspended in 600 µl 0.5 mg/ml lysozyme in TE buffer (Table 4-15). 60 µl of 10% SDS (Table 4-15) were added and mixed by inversion. An incubation at 64 °C for 1-2 min followed. Next, 66 µl of 3 M sodium acetate (pH 5.2) were added. After mixing by inversion 750 µl phenol were added. The suspension was mixed again by inversion and and incubated at 64 °C for 6 min. The reaction mixture was then put on ice. After centrifugation at 13,000 rpm and 4 °C for 15 min, the aqueous layer was transferred to a new tube and 750 µl chloroform were added. A centrifugation at 13,000 rpm and 4 °C followed. Next, the aqueous layer was transferred to one or two new tubes and 1.4 ml 30:1 mix (Table 4-15) were added. An incubation for 3-12 h at -80 °C followed to precipitate the RNA. After the precipitation the RNA was pelleted by centrifugation at 13,000 rpm and 4 °C for 30 min. The ethanol was removed carefully and the RNA pellet was dried using a SpeedVac system (Table 4-1) at low temperature for 10 min. 100 µl DEPC water was added and the RNA was solubilised by incubation at 800-1000 rpm and 65 °C for 5 min. The RNA was stored at -80 °C until a *DN*ase digestion (chapter 5.14) was performed to remove any residual DNA.

5.14. DNase digestion

For DNase digestion, the RNA samples stored at -80 °C were incubated at 65 °C for 5 min and further 5 min on ice. Then 20 µg RNA were diluted in 81 µl DEPC water and 19 µl mastermix were added to each sample as described in Table 5-8.

Table 5-8 Composition of DNase digestion mastermix

Component	19 µl Mastermix
10x DNase reaction Buffer	10 µl
RNase Out (40U/ml)	1 µl
DNase I (1U/ µl)	8 µl

The samples were incubated at 37 °C for 45 min. DNase was removed by phenol-chloroform extraction (115). The pellets were then dissolved in 40 µl DEPC water and incubated at 65° C for 5 min. The concentration of the RNA was measured using a spectrophotometer (PEQlab, ND-1000, Table 4-1).

5.15. RNA gel electrophoresis

To check the integrity of the isolated RNA, 0.15-1.5 µg of the solubilised RNA was mixed with GLII loading buffer (Table 4-17) and separated on a 1% TBE (Table 4-17) agarose gel at 5 V/cm , which was either prestained with GelRed™ or stained in GelRed™ solution (Table 4-14) afterwards.

5.16. Northern blot analysis for sRNA detection

For northern blot analysis, 5 µg of isolated total RNA was denatured in an equal volume of formamide loading buffer (Table 4-17), boiled at 95 °C for 5 min and run on a 6% denaturing polyacrylamide gel (Table 4-18) in 1x TBE (Table 4-17) at 300 V. For application as a size marker, a pUC8 DNA ladder (Table 4-3) was radioactively labeled by incubating the reaction mix given below for 1 h at 37 °C, followed by column purification using Microspin G50-columns (Table 4-3) according to the manufacturer`s instructions:

Table 5-9 pUC8 DNA ladder labelling reaction

Component	20 µl Mastermix
pUC 8 Mix Marker (0.5 µg/µl)	1 µl
10x Kinase Buffer (PNK Buffer B)	2 µl
Polynucleotidkinase (PNK)	1 µl
[γ-32P] ATP	3 µl
H_2O	13 µl

After electrophoresis, the RNA was electroblotted onto a Nylon N+ membrane for 1.15 h at 50 V. The transfer was performed in a Bio-Rad blotting chamber (Table 4-1) in 1x TBE buffer (Table 4-17) at 4 °C. The membranes were dried and UV-crosslinked before prehybridization for 1 h at 42 °C in 15 ml RotiHybriQuick (Table 4-1). Hybridization with radioactively labeled [γ-^{32}P] ATP-labeled DNA probes (chapter 5.18) was performed overnight at 42 °C, using the same hybridization buffer. Following the hybridization, the membranes were washed in 50 ml 5x SSC, 50 ml 1x SSC and 50 ml 0,1x SSC (Table 4-19). All washing steps were performed at 42 °C for at least 15 min. Hybridization with radioactively labeled ^{32}P-UTP -labeled riboprobes (chapter 5.18) was performed overnight at 65 °C, using the same hybridization buffer. Following the hybridization, the membranes were washed in 50 ml 2x SSC, 50 ml 1x SSC and 50 ml 0,1x SS (Table 4-19). All washing steps were performed at 65 °C for at least 15 min, respectively. To detect signals, the membranes were exposed to PhosphorImager screens overnight. Afterwards the blots were visualized using a PhosphorImager (Typhoon FLA 3000, Table 4-1) and quantified with ImageQuant Tools from AIDA software (Table 5 11).

5.17. Agarose northern blot for mRNA detection

To analyze mRNA expression, 10 µg total RNA dissolved in 24 µl H_2O were mixed with 6 µl 5xRNA loading buffer (Table 4-16), incubated at 65 °C for 5 minutes and cooled down on ice for 5 minutes (Table 4-16). If necessary, the same was done for the RNA molecular weight marker puc8 (chapter 5.16). RNA samples were separated in 1.2% formaldehyde gel (Table 4-16) for 5 – 6 hours in 1x MOPS running buffer (Table 4-16) at 80 V. Afterwards, the gel was incubated for 10 - 20 minutes in DEPC H_2O. Subsequently, the gel was stained in a GelRed™ bath (Table 4-14) for 30 minutes to assess RNA quality. Afterwards, the gel was equilibrated in 10xSSC (Table 4-19) for 30 minutes. Then, the seperated RNA was transferred from the gel onto Hybond-XL membranes (Table 4-3) by capillary transfer

using 10xSSC as transfer buffer overnight. The next day, the membrane was neutralized by incubation in 10x SSC for 5 minutes. The membrane was placed on a fresh sheet of dry blotting paper and the RNA was fixed via UV light (UV crosslinker 1800, Life technologies, Table 4-1) to the membrane. A thirty minutes pre-hybridization step in RotiHybriQuick was followed by an overnight hybridization in RotiHybriQuick (Table 4-2) with radioactively-labeled probes (chapters 5.18, 0). Hybridization with radioactively labeled [γ-^{32}P] ATP-labeled DNA probes (chapter 5.18) was performed overnight at 42 °C, using the same hybridization buffer. Following the hybridization, the membranes were washed in 50 ml 5x SSC, 50 ml 1x SSC and 50 ml 0,1x SSC (Table 4-19). All washing steps were performed at 42 °C for at least 15 min. Hybridization with radioactively labeled ^{32}P-UTP -labeled riboprobes (5.18) was performed overnight at 65 °C, using the same hybridization buffer. Following the hybridization, the membranes were washed in 50 ml 2x SSC, 50 ml 1x SSC and 50 ml 0,1x SS (Table 4-19). All washing steps were performed at 65 °C for at least 15 min, respectively. Signals were visualized on a Phosphorimager (Typhoon FLA 3000, Table 4-1).

5.18. Generation of radiolabelled DNA oligonucleotides for RNA detection

For labelling, 1 pmol of the oligonucleotide (Table 4.8) was incubated for 1 h at 37 °C in a 20 µl reaction volume as described in Table 5-10. Unincorporated nucleotides were removed using Microspin G-25 Columns (Table 4-3) according to the manufacturer`s instructions.

Table 5-10 Composition of the mastermix for radioactive labelling

Component	20 µl Mastermix
Primer (40 pmol/µl)	4 µl
10x Kinase Buffer (PNK Buffer A)	2 µl
PNK	1 µl
[γ-32P] ATP	4 µl
H_2O	9 µl

5.19. Generation of radiolabelled RNA transcripts (riboprobes) for RNA detection

DNA templates for T7 *in vitro* transcription of riboprobes were amplified by PCR from template *N. meningitidis* strain 8013 genomic DNA using primer sets summarized in Table 4-32. *In vitro* transcription was performed with the MAXIscript kit (Table 4-4) using 200 ng of template PCR product in the presence of 25 µCi α-^{32}P-UTP at 37 °C for 1 h following DNase I digestion (chapter 5.14) according to the manufacturer`s instructions. The riboprobes were purified using a MicroSpin G50 column (Table 4-3) according to the manufacturer`s instructions.

5.20. Rifampicin stability assay

For the determination of the RNA half-life, a 50 ml meningococcal culture was grown at 37 °C and vigorous shaking in GCBL^{++} (Table 4-7, Table 4-8) until an OD_{600nm} of either 0.5 or 2.0 was reached (chapter 5.1). Then, 8 ml of the culture was transferred to a separate flask as a control. Rifampicin (Table 4-2), dissolved in DMSO, was added to the remaining culture (final concentration 500 µg/ml) and samples (8 ml each) were taken from the culture at certain time points (0, 2, 4, 8, 16, 32 min) and immediately mixed with 1.5 ml stop solution (Table 4-15). The samples were snap frozen in liquid nitrogen and stored at -80 °C until use. After thawing of the samples on ice, total RNA was isolated using the hot phenol method (chapter 5.13) and subjected to northern blot analysis (chapter 5.17).

5.21. Differential RNA-sequencing

Collecting the bacterial samples for differential RNA-sequencing (dRNA-seq) of *N. meningitidis* strain 8013 was done by N. Heidrich. For dRNA-seq, liquid cultures of *N. meningitidis* 8013 wild-type were grown to OD_{600nm}=0.5 and OD_{600nm}=1.5, respectively, in GCBL^{++} medium as described in chapter 5.1. All cultures were centrifuged for 30 min at 13.000 rpm and 4 °C, stop solution (Table 4-15) was added to the resulting pellets prior to snap-freezing in liquid ni-trogen. Samples were stored at −80 °C until RNA preparation with hot phenol (chapter 5.13). cDNA libraries of dRNAseq samples were constructed by vertis Biotechnology AG, Germany (http://www.vertis-biotech.com/), as described previously for eukaryotic microRNA (116), but omitting the RNA size-fractionation step prior to cDNA synthesis. Then, cDNA libraries were pooled and sequenced using an Illumina

HiSEq2000 machine in the single-read mode. The resulting Illumina reads in FASTQ format were trimmed with a cut-off phred score of 20 using the program fastq_quality_trimmer from FASTX toolkit version 0.10.1(http://hannonlab.cshl.edu/fastx_toolkit/) and mapped to the reference genome *N. meningitidis* 8013 (NC_017501.1) by L. Li as described more detailed in (117).

5.22. ProQ UV-CLIP-sequencing

ProQ UV-CLIP-sequencing was performed in cooperation with N. Heidrich. For each biological replicate, *N. meningitidis* strain 8013 expressing 3×FLAG-tagged ProQ protein (chapter 5.12.5) was grown in $GCBL^{++}$ (Table 4-7, Table 4-8) in the presence of kanamycin until an OD_{600nm} of 2.0. As a negative control, the 8013 wild-type strain was grown until an OD_{600nm} of 2.0 as well. For each strain cells equivalent to an OD_{600nm} of 200 were collected and subjected to CLIP-seq as described in (57). Half of the culture was directly placed in a 22 × 22 cm plastic tray and irradiated with UV light at 800 mJ/cm^2 at 254nm (Table 4-1). Cells were pelleted in 50 ml fractions by centrifugation for 40 min at 6,000 g and 4 °C and resuspended in 800 µl NP-T buffer (Table 4-23). The resuspended pellets were mixed with 1 ml glass beads (Table 4-3). Afterwards, cells were lysed at 30 Hz (Retsch, Table 4-1) for 10 min and centrifuged for 15 min at 13 000 rpm and 4 °C. Cell lysates were transferred into new tubes and centrifuged for 15 min at 13000 rpm and 4 °C. To enrich the generated covalent bonds, the cleared lysates were mixed with one volume of NP-T buffer with 8 M urea (Table 4-23), incubated for 5 min at 65 °C in a thermomixer (Table 4-1) at 900 rpm shaking prior to storing on ice for 2 min. Lysates were transferred into 50 ml falcon tubes and diluted 10 x in NP-T buffer (Table 4-23). For immunoprecipitation of ProQ-RNA complexes, 30 µl of anti-FLAG magnetic beads (50% bead suspension, Table 4-3) were washed three times with 800 µl NP-T buffer. Washed magnetic beads were added to the cooled lysate following rotation for 1 h at 4 °C. Afterwards, beads were resuspended in 2 ml high-salt buffer (Table 4-23), transferred into new tubes and placed into a magnetic rack (Table 4-1). Then, beads were washed with high-salt buffer again followed by two washes with 2 ml NP-T buffer. Beads were resuspended in 100 µl NP-T buffer containing 1 mM $MgCl_2$ and 2.5 U benzonase (Table 4-5) and were incubated for 10 min at 37 °C at 800 rpm shaking. After that, beads were cooled down on ice, followed by one wash with 500 µl high-salt buffer and two washes with 500 µl CIP buffer (New England Biolabs, Table 4-5). To dephosphorylate the 5’ ends of the RNA ligands, beads

were resuspended in 100 µl CIP buffer containing 10 units of calf intestinal alkaline phosphatase (CIP, Table 4-5) and incubated for 30 min at 37 °C at 800 rpm shaking. Afterwards, beads were washed once with 500 µl high-salt buffer and twice with 500 µl PNK buffer A (Fermentas, St. Leon-Rot, Table 4-5, 10x diluted in DEPC-H_2O) following resuspension of the beads in 100 µl PNK buffer A containing 1 µl T4 polynucleotide kinase (Table 4-5) and 1 µl ^{32}P-ATP. After an incubation time of 30 min at 37 °C, 10 µl 1 mM non radioactive ATP was added and samples were incubated for 5 min at 37 °C. After two washes with 1 ml NP-T buffer the beads were resuspended in 10 µl 5x protein loading buffer (Table 4-20) and incubated for 5 min at 95 °C in order to elute the labeled RNA-protein complexes from the beads. Afterwards, 15 µl of each sample was boiled for 1 min at 95 °C, cooled on ice for 5 min and loaded along with a protein marker (PageRulerTM Prestained, Table 4-3) on a 12% SDS-gel (Table 4-21). The SDS-PAGE was performed in 1xSDS running buffer (Table 4-20). Afterwards, RNA protein complexes were transferred onto a nitrocellulose membrane (Table 4-3) and exposed to a phosphorscreen for at least one hour. Signals were visualized using the laser scanner Typhoon FLA 3000 (Table 4-1). Afterwards, labeled RNA–protein complexes were cut-out from the membrane and transferred into LoBind tubes (Table 4-3) and incubated with 200 µl PK-solution (Table 4-23) for 1 h at 37 °C and 800 rpm shaking. After addition of 100 µl PK buffer with 9 M urea (Table 4-23), the samples were incubated for 1 h at 37 °C and 800 rpm shaking. Then, the supernatants were transferred into PLG tubes (Table 4-3) and RNA was extracted by adding one volume of Phenol:Chloroform:Isopropanol (P:C.I). Samples were incubated for 5 min at 30 °C at 1000 rpm and centrifuged for 12 min at 13000 rpm and 4 °C. Each aqueous phase was transferred into a new tube and precipitated with 2.5 volumes of pre-cooled 30:1 mix (Table 4-15) and 1 µl of GlycoBlue (Table 4-2) for 2 h at -20 °C. RNA was pelleted by centrifugation (30 min at 13000 rpm and 4 °C), washed with 800 µl of 80% EtOH and centrifuged again (30 min at 13000 rpm and 4 °C). Air-dried pellets were resuspended in 10 µl DEPC-H_2O at 65 °C and 800 rpm and stored at -20 °C.

UV-CLIP libraries were prepared using the NEBNext Multiplex Small RNA Library Prep Set for Illumina (#E7300, New England Biolabs, Table 4-4) according to the manufacturer's instructions.

cDNA libraries of UV-CLIP samples were pooled on an Illumina NextSeq 500 mid-output flow cell (Table 4-1) and sequenced in paired-end mode (2x75 cycles) at Vertis Biotechnology AG, Munich, Germany. Processing of sequence reads and mapping to the *N. meningitidis* 8013 genome (NCBI accession: NC_017501.1) using READemp-tion version

0.3.7 and segemhel version 0.2.0 was performed by L.Barquist following the protocol established in (104). Thereby, NCBI annotations were supplemented with sRNA and UTR boundaries defined in our dRNA-seq approach (chapter 5.21) and by computational prediction of Rho-independent terminators (117,118). Afterwards, normalization and peak calling was performed by L. Barquist according to a similar procedure to that previously described in (104).

5.23. Analysis of crosslink-specific mutations (UV-CLIP)

Analysis of crosslink-specific mutations was done by L.Barquist according to a previous approach (96). Mutated sites needed to be present in both paired reads mapping to a significant peak. Putative crosslinking induced mutations which were found in non-crosslinked samples as well were eliminated.

5.24. RNA-sequencing (RNA-seq)

For analyzing the ProQ-associated RNAome, we used RNA from three different clones considered as biological replicates for RNA-seq comparing the *N. meningitidis* 8013 wt targetome to the Δ*proQ* targetome.

N. meningitidis 8013 cells were grown in 50 ml tubes at 37 °C under vigorous shaking in $GCBL^{++}$ (Table 4-7, Table 4-8) medium and sample were collected by centrifugation for 30 min at 4 °C and 4,000 rpm at OD_{600nm} of 2.0 followed by total RNA preparation with the hot phenol method (chapter 5.13) and DNase digestion (chapter 5.14) of the isolated RNA.

cDNA libraries of RNA-seq-samples were constructed by Vertis Biotechnology AG, Munich, Germany. To deplete ribosomal transcripts, RNA-seq samples were treated with the Ribo-Zero "Bacteria" kit (Illumina, Table 4-4) followed by RNA fragmentation and adapter ligation. cDNA libraries of RNA-seq samples were pooled on an Illumina NextSeq 500 high-output flow cell (Table 4-1) and sequenced in single-read mode (1x76 cycles). The processing and trimming of the reads and read mapping to the *N. meningitidis* 8013 (NC_017501.1) reference genome was performed by T. Bischler applying segemehl version 0.2.0 (119), Cutadapt version 1.16 (120) and the pipeline READemption (119) version 0.4.5.

5.25. Differential expression analysis (RNA-seq)

The differential expression analysis of Δ*proQ* vs. wild-type samples was performed by T. Bischler *via* DESeq2 (121) version 1.22.1. Thereby, all features with $\log_2$FoldChange ≤ -1 or ≥ 1 and padj < 0.05 were considered as significantly differentially expressed.

5.26. Functional enrichment analysis

In order to identify classes of genes that are overrepresented in the set of differentially expressed protein-coding genes in the Δ*proQ* strain compared to the wild-type strain, a functional enrichment analysis based on COG classification scheme was performed (122,123) using the function "enricher" of the R package clusterProfiler (124) v3.10.1 seperately considering all regulated genes, only up-regulated genes ($\log_2$FoldChange ≥ 1) and only down-regulated genes ($\log_2$FoldChange ≤ -1) by T. Bischler.

5.27. *In vitro* transcription and 5'end labelling of RNA

For RNA *in vitro* synthesis, template DNA fragments were amplified by PCR using proof-reading Q5 polymerase and primers carrying a T7 promoter sequence (Table 4-32). The quality of the PCR products was checked by agarose gel electrophoresis (chapter 5.9). Subsequently, ~200 ng of template DNA were reverse transcribed employing the T7 MEGAscript kit (Table 4-4) according to the manufacturer's instructions overnight at 37 °C. After P:C:I extraction (P:C.I) (Table 4-2) and precipitation of the RNA by three vol. equiv. 30:1 mix (Table 4-15) overnight, the correct size and integrity of the RNA were confirmed by denaturing PAGE (chapter 5.16). Gels were stained using a GelRed™ bath (Table 4-14).

For 5' end-labelling, 20 pmol RNA were dephophorylated by CIP-treatment (10 U, Table 4-5) at 37 °C for one hour according to the manufacturer`s instructions. Afterwards a P:C:I extraction (Table 4-2) was performed and the RNA was precipitated by three volumes 30:1 mix (Table 4-15) at -20 °C overnight. Then, the RNA was 5' phosphorylated at 37 °C for one hour by 1 U PNK in the presence of 20 µCi γ-^{32}P-ATP as described in Table 5-10. Unincorporated nucleotides were removed with Microspin G-50 columns (Table 4-3) according to manufacturer`s instructions. Subsequently, the labelled RNA was separated by denaturing PAGE as described in chapter 5.16. Afterwards, the gel was exposed to imaging

plates and the radioactive signals were determined by phosphorimaging using a PhosphoImager (FLA-3000, Table 4-1). The sections of the gel containing the radioactively labeled RNA were cut out and collected in 1.5 ml Eppendorf tubes. RNA was extracted from the gel slices by incubation at 8 °C overnight in RNA elution buffer (chapter 4.5.10). Labeled RNA was purified by P:C:I extraction (P:C.I) (Table 4-2), and quantified using a spectrophotometer (PEQlab, ND-1000. Table 4-1).

5.28. Gel Mobility Shift Assays

About, ~0.04 pmol 5'-end labeled RNA (4 nM final concentration) and increasing amounts of unlabeled RNA (chapter 5.27) or purified ProQ protein (Table 4-3) were applied in 10 µl reactions. After denaturation for 1 min at 95 °C, labeled RNAs were cooled for 5 min on ice and 1 µg yeast RNA and 1 µl 10 x RNA structure buffer (Table 4-26) were added. Increasing concentrations of unlabeled RNA or purified ProQ protein were added to varying final concentrations. After incubation for 15 min at 37 °C, samples were immediately loaded after addition of 3 µl 5x native loading dye (Table 4-26) to a native 6% (vol/vol) PAA gel (Table 4-17). Gel electrophoresis was done in 0.5 x TBE buffer (Table 4-17) at 30 mA per gel for 4 hours. Afterwards, gels were dried (gel dryer Bio-Rad Model 583, Bio-Rad, Table 4-1) and analyzed using a PhosphoImager (FLA-3000, Table 4-1) and ImageQuant Tools from AIDA software (Table 5-11).

5.29. In-line probing assay

For in-line probing assays (125), ~0.4 pmol 5' end labeled sRNA were subjected in absence or presence of unlabeled target mRNA to RNase T1 (Table 4-5) treatment in 10 µl reactions as previously described (126) with minor modifications. Briefly, for RNase T1 ladders, ~0.4 pmol labeled RNA were denatured in 1x structure buffer (Table 4-26) for 1 min at 95 °C and afterwards incubated with 0.1 U/µl RNase T1 (Table 4-5) for 5 min. OH ladders were generated by the incubation of ~0.4 pmol labeled RNA in 1x alkaline hydrolysis buffer (Table 4-5) for 5 min at 95 °C. All reactions were stopped by addition of 10 µl colorless gel-loading solution (Table 4-26). Ladders were denatured 3 min at 95 °C. Approximately, ~0.4 pmol labeled sRNA (40 nM final concentration) were incubated in the absence or presence of 20 nM, 200 nM and 2 µM unlabeled mRNA leader for 40 hrs at room temperature in 1x in-line probing buffer (Table 4-26). All reactions were stopped by

adding 10 µl colorlessgel-loading solution (Table 4-26) on ice. Cleavage products and ladders were analyzed on 6% (vol/vol) PAA gels (Table 4-17, Table 4-18) under denaturing conditions at constant power of 40 W for 3 hours. Afterwards, gels were dried (gel dryer Bio-Rad Model 583, Table 4-1) and analyzed using a PhosphoImager (FLA-3000, Table 4-1) and ImageQuant Tools from AIDA software (Table 5-11).

5.30. Coomassie staining and Western Blot analysis

For Western Blot analysis, bacterial cultures with an $OD_{600nm} \approx 0.5$ were centrifuged for 3 min at 13,000 rpm and the cell pellet was resuspended in 5x protein loading buffer (Table 4-20). After denaturation for 5 min at 95 °C, 10 µl of the protein samples were run on a 12% SDS-polyacrylamide gel at 30 mA (Table 4-21). The proteins were electroblotted on activated PVDF membranes (incubation in methanol, water and transfer buffer for 15 sec, 2 min, 5 min respectively) at 100 V for 1 h. Transfer was performed using a peqlab tank transfer system (Table 4-1) in 1x transfer buffer (Table 4-22) at 4 °C. After blocking non-specific binding sites on the membranes using PBST containing 5% milk powder (Table 4-22) for 1 h at RT, the membranes were rinsed 3x with PBST and incubated with the primary antibody (Table 4-3). Primary antibody incubation was performed either one hour at room temperature or overnight at 4 °C, followed by washing the membranes three times for 10 min with PBST. Afterwards the membrane was incubated with the secondary antibody (Table 4-3) for 1 h at room temperature. Western Blots were developed using the developing solute (Table 4-22). Chemiluminescence was detected via the gel imaging system (Image Quant LAS 4000, GE Healthcare) (Table 4-1). For coomassie staining, polyacrylamide gels were stained in Coomassie Brilliant Blue R-250 Staining Solution (Table 4-2) overnight. The gels were destained by incubating in ddH_2O overnight. Pictures of the destained gels were taken with the gel documentation system Gel iX Imager (Intas) (Table 4-1).

5.31. Quantitative proteomics

For analyzing the ProQ-associated proteome, we used RNA from two different clones considered as biological replicates for quantitative proteomics comparing the *N. meningitidis* 8013 wt targetome to the Δ*proQ* targetome. For each sample, 4ml *N. meningitidis* 8013 wt and Δ*proQ* culture grown in GC broth to OD_{600nm}: 2.0 was pelleted by centrifugation at 6000 g at 4 °C for 10 min. The pellets were washed twice with 15 ml 1xPBS (Table 4-22)

in 50ml falcon tubes and once with 1 ml 1xPBS in 2 ml Eppendorf tubes. Afterwards, the pellets were lysed in 100 ul lysis buffer (Table 4-24) with 0.1-mm glass beads (Table 4-3) by 10 times vortexing the tubes for 30 sec followed by incubation on ice 10 times for 15 sec. The lysates were centrifuged for 15 min and 13.000 rpm at 4 °C and supernatants were mixed with equal amounts of 5x PL protein loading buffer (Table 4-20).

The following gel electrophoresis, in-gel digestion and NanoLC-MS/MS analysis was performed by AG Schlosser (RVZ, Würzburg). Protein precipitation was performed overnight at -20 °C with fourfold volume of acetone. Pellets were washed three times with acetone at -20 °C. Precipitated proteins were dissolved in NuPAGE® LDS sample buffer (Life Technologies, Table 4-2), reduced with 50 mM DTT at 70 °C for 10 minutes and alkylated with 120 mM Iodoacetamide at room temperature for 20 minutes. Separation was performed on NuPAGE® Novex® 4-12% Bis-Tris gels (Life Technologies, Table 4-3) with MOPS buffer according to manufacturer's instructions. Gels were washed three times for 5 min with water and stained for 45 min with Simply Blue™ Safe Stain (Life Technologies, Table 4-2). After washing with water for 2 h, each gel lane was cut into 15 slices.

The excised gel bands were destained with 30% acetonitrile in 0.1 M NH_4HCO_3 (pH 8), shrunk with 100% acetonitrile, and dried in a vacuum concentrator (Concentrator 5301, Eppendorf, Germany, Table 4-1). Digests were performed with 0.1 µg trypsin per gel band overnight at 37 °C in 0.1 M NH_4HCO_3 (pH 8). After removing the supernatant, peptides were extracted from the gel slices with 5% formic acid, and extracted peptides were pooled with the supernatant.

NanoLC-MS/MS analyses were performed on an Orbitrap Fusion (Thermo Scientific, Table 4-1) equipped with a PicoView Ion Source (New Objective, Table 4-1) and coupled to an EASY-nLC 1000 (Thermo Scientific, Table 4-1). Peptides were loaded on capillary columns (PicoFrit, 30 cm x 150 µm ID, New Objective, Table 4-3) self-packed with ReproSil-Pur 120 C18-AQ, 1.9 µm (Dr. Maisch, Table 4-3) and separated with a 30-minute linear gradient from 3% to 30% acetonitrile and 0.1% formic acid and a flow rate of 500 nl/min. Both MS and MS/MS scans were acquired in the Orbitrap analyzer with a resolution of 60,000 for MS scans and 15,000 for MS/MS scans. HCD fragmentation with 35% normalized collision energy was applied. A Top Speed data-dependent MS/MS method with a fixed cycle time of 3 seconds was used. Dynamic exclusion was applied with a repeat count of 1 and an exclusion duration of 30 seconds; singly charged precursors were excluded

from selection. Minimum signal threshold for precursor selection was set to 50,000. Predictive AGC was used with a AGC target value of 2e5 for MS scans and 5e4 for MS/MS scans. EASY-IC was used for internal calibration.

For MS data analysis, raw MS data files were analyzed with MaxQuant version 1.6.2.2 (127). Database search was performed with Andromeda, which is integrated in the utilized version of MaxQuant. The search was performed against the NCBI *N. meningitidis* strain 8013 database. Additionally, a database containing common contaminants was used. The search was performed with tryptic cleavage specificity with 3 allowed miscleavages. Protein identification was under control of the false-discovery rate (1% FDR on protein and peptide level). In addition to MaxQuant default settings, the search was performed against following variable modifications: Protein N-terminal acetylation, Gln to pyro-Glu formation (N-term. Gln) and oxidation (Met). Carbamidomethyl (Cys) was set as fixed modification. For protein quantitation, the label-free quantification (LFQ) intensities were used (128). Proteins with less than two identified razor/unique peptides were dismissed. Further data analysis was performed using R scripts developed in-house (AG Schlosser). LFQ intensities were used and missing LFQ intensities in the control samples were imputed with values close to the baseline. Data imputation was performed with values from a standard normal distribution with a mean of the 5% quantile of the combined $\log_{10}$-transformed LFQ intensities and a standard deviation of 0.1. For the identification of significantly co-immunoprecipitated proteins, mean $\log_2$ transformed protein ratios were calculated from the two replicate experiments and boxplot outliers were identified in intensity bins of at least 300 proteins. Log_2 transformed protein ratios of CoIP versus control with values outside a 1.5x (potential) or 3x (extreme) interquartile range (IQR), respectively, were considered as significantly co-immunoprecipitated.

5.32. Phenotypic characterization

5.32.1. *In vitro* growth experiments

In preparation for phenotype assays, RNA and protein preperation, *in vitro* growth experiments in GCBL^{++} (Table 4-7, Table 4-8) and CDM (Table 4-10) were performed. The bacterial cells grown overnight on solid media were resuspended in 5ml GCBL^{++} or CDM in 50 ml Falcon tubes and incubated at 200 rpm and 37 °C for 45 min for adapting to the liquid media. Next, the bacterial suspension was diluted to an $\text{OD}_{600\text{nm}}$ of 0.15 in 20ml GCBL^{++} or CDM in 50 ml Falcon tubes or 200 ml flasks, respectively. During an incubation

at 200 rpm and 37 °C for 8 h ($GCBL^{++}$) or 12 h (CDM), the OD_{600nm} was measured hourly with 1ml of the diluted bacterial suspension using a WPA biowave CO 8000 cell photometer (chapter 5.2). At 2 h, 4 h and 8 h and 12 h, the colony forming untis (CFU) were determined by plating 100 µl of serial dilutions of the bacterial cultures in PBS on COS agar plates. The chosen time points were 2 h, 4 h and 8 and 12h. All plates were incubated overnight at 37 °C with 5% CO_2. The next day the number of CFU were counted using the colony counter ProtoCOL SR (Table 4-1).

For total RNA preperation, the bacterial liquid cultures were pelleted by centrifugation at 4,000 rpm at 4 °C for 30 min following snap-freezing of the pellets in liquid nitrogen. The bacterial pellets were stores at -20 °C until they were applied to RNA preparation with the hot phenol method (chapter 5.13).

For preparation of total protein, the bacterial liquid cultures were pelleted by centrifugation at 13,000 rpm at room temperature for 3 min following resuspension in protein loading buffer (5x) (Table 4-20) to a final concentration of 0.01 OD/µl. Bacterial pellets were stored at -20 °C until they were applied to western blot analysis.

Alternatively, bacterial growth was measured fully automated using the Infinite 200 Pro plate reader (Table 4-1). The evening before the experiment, the meningococcal strains were streaked out on GC agar supplemented with antibiotics if required and incubated for 18 h at 37 °C and 5% CO_2 in an incubator. Subsequently, 10 single colonies of each strain were collected with a swab and were dabed on fresh COS agar plates following incubation for 4 h at 37 °C and 5% CO_2. Afterwards, the bacteria were absorbed with swabs and used for inoculation of 3 ml $GCBL^{++}$ medium per strain. The OD_{600nm} of each bacterial suspension was adjusted to OD_{600nm}: 0.1 by adding the required volume of $GCBL^{++}$. Subsequently, each well of a 96-well microtiter plate was filled with 200 µl of the bacterial suspensions or $GCBL^{++}$ medium as a blank. For each strain under investigation, 4 wells of the 96-well microtiter plate were implemented with bacterial suspension. Growth in 96-well microtiter plates was monitored using the Infinite 200 Pro instrument (Tecan) at 37 °C with 3 mm amplitude shaking. Optical density was monitored (absorbance at 595 ± 10 nm) every 30 min for 12 hours. For the analysis of the data, a logistic growth model was fitted to the data by non-linear regression analysis using R version 2.7.0 and the nls package to estimate the growth rate τ [1/min] and the capacity K (OD_{600nm} in the stationary phase) as described in (129)

5.32.2. Cell adhesion and invasion assay

The strain pairs 8013 WT/8013 Δ*hfq* and MC58 WT/MC58 were tested for their ability to adhere to and invade in Detroit562 cells, a human epithelial cell line. Detroit562 cells (American type Culture Collection) were grown in T75 cell culture flasks (Table 4-3) in $EMEM^{+++}$ (Table 4-11, Table 4-12) at 37 °C with 5% CO_2 to 90-100% confluence and then split in two new flasks. For the assay, cells were seeded in 24-well plates.

Before starting the experiment each well was washed with PBS (Table 4-22) prior adding 1 ml fresh $EMEM^{+++}$. The bacterial strains were suspended in 10 ml $EMEM^{+++}$ and incubated at 200 rpm and 37 °C for 30-45 min. Next, $4x10^6$ bacterial cells were added to 8 wells per tested strain. As a confluent well of a 24-well-plate is estimated to contain $4x10^5$ cells, so that the multiplicity of infection (MOI) used in this experiment was 10:1. After infection, the 24-well-plate was incubated at 37 °C with 5% CO_2 for 4 h. In the meantime, the same volume of the bacterial suspension which was added to each well was added to 1 ml PBS, and serial dilutions were plated on COS agar plates to determine the number of bacterial cells used for infection. After the infection, the medium of 4 wells per strain was removed separately, diluted in PBS and plated on COS agar plates to determine the number of bacterial cells in the supernatant. The medium of the 4 additional wells per strain was discarded. Each well was washed with 1 ml $EMEM^{+++}$. Then 1 ml of 1% Saponin (Table 4-12) was added to each of 4 wells per strain and 1 ml of 400 µg/ml gentamicin (Table 4-12) in $EMEM^{+++}$ was added to the 4 remaining wells per strain. Saponin was added to destroy the Detroit562 cells and to release all cell associated bacteria, gentamicin to kill all extracellular bacteria. The 24-well-plate was incubated at 37 °C with 5% CO_2 for 15 min. Then the Saponin was removed, diluted in PBS and 100 µl were plated in serial dilutions on COS agar. After additional 45 min of incubation, the remaining wells were washed with $EMEM^{+++}$ to remove the remaining gentamicin. Then 1 ml 1% Saponin in $EMEM^{+++}$ was added to these wells to release all invasive bacterial cells followed by incubation for 15 min at 37 °C with 5% CO_2. The number of CFU was determined by plating 100 µl of serial dilutions of the bacterial cultures in PBS on blood agar plates. All plates were incubated overnight at 37 °C with 5% CO_2. The next day the number of CFU were counted using the colony counter protoCOL SR (Table 4-1).

5.32.3. Static biofilm assay

A static microtiter plate biofilm assay was performed to compare the ability of the different strains to form biofilm. The strains were streaked on COS agar and incubated at 37 °C with

5% CO_2 for not longer than 12 h to avoid biofilm formation on the plate. The bacterial cells were suspended in 3 ml $GCBL^{++}$ (Table 4-7, Table 4-8) and this suspension was diluted to an OD_{600nm}=0.1 in 3 ml $GCBL^{++}$. For each strain, 100 µl of the bacterial suspension were added to 8 wells of a 96-well-plate. Additional 8 wells were each filled with 100 µl $GCBL^{++}$. The plate was incubated at 37 °C with 5% CO_2 for 17.5 h. Afterwards, the medium was removed from all wells prior to adding 100 µl crystal violet (Table 4-2) and incubating the plate for 10 min at room temperature to stain the biofilm. The dye was removed and each well was washed twice with 200 µl PBS (Table 4-22). Next, 100 µl 100% ethanol were added per well. An incubation of 20 min at room temperature followed. Before measuring the absorbance of the dye with a Microplate reader (Table 4-1) in each well, the suspension was mixed by pipetting. The values of 7 wells, which showed the lowest variance, were used for calculation. The cut-off was determined as three times the average of the OD_{450nm} of the wells filled with medium only.

5.32.4. Oxidative stress assay

Oxidative stress assays were performed as described in (130). In short, *N. meningitidis* cells grown in $GCBL^{++}$ (Table 4-7, Table 4-8) to OD_{600nm} of 0.5 (chapter 5.1) were diluted to an OD_{600nm} of 0.01 in $GCBL^{++}$. One ml of each bacterial dilution was exposed to 0.25 mM H_2O_2 (Table 4-2) for 15 min or 2 mM paraquat (Table 4-2) for 60 min at 37 °C with vigorous shaking prior to plating serial dilutions on 5% COS agar plates. As negative controls, 1 ml of each diluted bacterial culture was exposed to equal volumes of PBS for 15 and 60 min at 37 °C with vigorous shaking prior to plating. After incubation in 5% CO_2 at 37 °C for 20 h, the survival rates were calculated as the ratio of H_2O_2 (paraquat)-stressed survivors to the total number of cells of the negative controls. The number of colonies formed by the bacteria was counted with the colony counter ProtoCOL (Table 4-1).

5.32.5. UV radiation assay

Sensitivity to UV irradiation was measured as described in (131). In short, serial dilutions of *N. meningitidis* strains grown overnight on solid media were plated on COS agar plates and exposed to either zero or 20 J/m^2 of UV irradiation at 254nm (UV stratalinker 1800, Stratagene, Table 4-1) and incubated in 5% CO_2 at 37 °C for 20 h. The number of colonies formed by the bacteria was counted with the colony counter ProtoCOL (Table 4-1). The

survival rates were calculated as the ratio of UV-irradiated survivors to the total number of cells, in particular the bacteria exposed to zero J/m^2.

5.32.6. Serum bactericidal assay

Serum bactericidal assay were performed as described in (132). In short, *N. meningitidis* strains grown overnight on solid media were resuspended in VBS/BSA (Table 4-28) and serial dilutions were done in PBS (Table 4-22) in order to obtain bacterial concentrations of 10^6 CFU/ml. Then, 35 µl of each bacterial suspension was resuspended in either VBS/BSA (represents 0% Normal human serum (NHS), Table 4-28) or 10% NHS diluted in VBS/BSA in a final reaction volume of 350 µl. The reactions were incubated at 37 °C for 60 min and stopped by incubation on ice. Serial dilutions of the samples were plated on COS agar plates and incubated overnight at 37 °C with 5% CO_2. The number of colonies formed by the bacteria was counted with the colony counter ProtoCOL (Table 4-1). The survival rates were calculated as the ratio of 10% NHS survivors to the 0% NHS survivors. Normal human serum was collected from healthy individuals without meningococcal vaccination. Fresh blood samples were centrifuged for 5 min at 2000 g and the obtained serum was snap-frozen in liquid nitrogen and stored at –80 °C.

5.32.7. Capsule ELISA

The ELISA was performed as described in (133) using the monoclonal antibody MAbs 924 (Table 4-3) which specifically detects the *N. meningitidis* serogroup C capsule polysaccharide. In short, meningococci were grown overnight on solid media and resuspended in 1xPBS (Table 4-22) to a final OD_{600nm} of 0.15. Of each bacterial suspension, 20 µl were added to each well of a microtiter plate (Table 4-3) which had been coated with 25 ng/ml Poly-D-lysine (Table 4-2) before. The plates were dried at room temperature for at least 2 hours prior to fixing the bacteria with 100 µl/well PBS–0.05% glutaraldehyde (Table 4-2) for 10 min at room temperature. After washing of the wells with PBS for three times, non-specific binding sites were blocked by incubation of the wells with PBS–1% BSA for 1 h at 37 °C (150 µl/ well) following three wash steps with PBS. The binding of the primary antibody (Table 4-3) was performed for 1 h in 1% BSA/PBS (20 µl/well; antibody dilution 1:4000 in 1% BSA/PBS) at 37 °C. After three wash steps with PBS, incubation with the secondary peroxidase-conjugated anti-mouse antibody (Table 4-3) was performed for 1 h

in 1% BSA/PBS (20 µl/well; antibody dilution 1:2500 in 1% BSA/PBS) at 37 °C. Photometric measurement was performed at OD_{414nm} with the ELISA reader Multiskan® EX (Thermo Scientific, Table 4-1).

5.33. Computational analyses

For presentation and analysis of experimental data Microsoft Excel 2016, Microsoft PowerPoint 2016, ImageJ (134) and CorelDRAW X8 were used.

BlastN searches (http://www.ncbi.nlm.nih.gov/sutils/ genom_table.cgi, (135)) were used to get information for sequence alignments as well as the molecular cloning procedures of the following genome sequences (accession numbers are given in parentheses): *N. meningitidis* 8013 (NC_017501), *N. meningitidis* MC58 (NC_003112), *N. meningitidis* M22718 (NZ_CP016627), *N. meningitidis* α14 (NC_013016), *N. meningitidis* Z2491 (NC_003116), *N. meningitidis* 331401 (NZ_CP012694), *N. meningitidis* WUE2594 (NC_017512), *N. gonorrhoeae* MS11 (NC_022240*), N. lactamica* 020-06 (NC_014752).

Sequence alignments were created using MultAlin (Table 5-11). The Integrated Genome Browser (IGB, Table 5-11) and the Serial Cloner 2.6 (Table 5-11) were used to construct and visualize plasmids or DNA sequences, respectively. Transcription start sites were predicted with the TSSpredator with the "more strict" parameter setting (Table 5-11). Normalized wiggle files of the global data sets mentioned in this study have been deposited in the National Center for Biotechnology Information's Gene expression omnibus (GEO) (136) via the GEO accession number GSE85252 (dRNA-seq, Hfq RIP-seq) and GSE129868 (ProQ UV-CLIP, ProQ RNA-seq) and can be visualized with the Integrated Genome Browser. The ProQ peak sequences of the UV-CLIP-seq approach (chapter 5.22) (log_2 f.c.>2, adj. p-value<0.05) were used for sequence motif identification with the MEME program (Table 5-11) with all parameters set at default values with the exception of `Motif search on the given strand only` and `sequence length limitation of 6 to 20 nucleotides`. Venn-diagrams were drawed to indicate the overlap and the discrepancies between distinct data sets. Thereby, venn diagrams were generated by VENNY (Table 5-11). RNA secondary structure predictions were performed with mfold (Table 5-11) and sRNA/ mRNA duplex predictions were done with RNAhybrid (Table 5-11) with all parameters set at default values. CopraRNA (Table 5-11) was used as a tool for sRNA target prediction. As input, at least six homologous nucleotide sequences from at least six distinct *neisseriales* species (NC_017501, NC_003112, NZ_CP016627, NC_013016, NC_003116,

NZ_CP012694, NC_017512, NC_022240, NC_014752) were used with all parameters set at default values. Operon predictions were based on the DOOR database (137), domain predictions were done with Rfam (138), statistical analyses were conducted by C. Schoen using R (139) and terminator prediction with RNIE were performed by L. Barquist as described in (117). Table 5-11 provides an overview of software programs used in this study.

Table 5-11 Software programs applied in this study

Program	Application	Developer/ Source
Excel 2016	Spreadsheet analysis and statistics	Microsoft
Word 2016	Creating this thesis	Microsoft
PowerPoint 2016	Creating illustrations	Microsoft
CorelDRAW X8	Creating illustrations and graphical figures	Corel Corporation
Serial Cloner 2.6	DNA sequence analysis	Serial basic
Integrated Genome Browser (IGB)	Genome browsing and DNA sequence analysis	Freese *et al.,* 2016 (113)
mfold	RNA secondary structure prediction	Zuker *et al.,* 2003 (140)
RNAhybrid	Prediction of sRNA/target duplexes	Rehmsmeier *et al.,* 2004 (141)
CopraRNA	sRNA target prediction	Wright *et al.,* 2014 (142)
VENNY	Construction of venn diagrams	Bioinformatics for Genomics and Proteomics
AIDA software	Quantification of blot bands	Raytest, Germany
MultAlin	Sequence alignments and analysis	Corpet 1988 (143)
TSSpredator	Transcriptional start site prediction	Dugar *et al.,* 2013 (144)
MEME	RNA binding motif prediction	Bailey *et al.,* 2015 (145)
RNIE	Terminator prediction	Gardner *et al.,* 2011 (118)

6. Results

6.1. The primary transcriptome of *N. meningitidis* strain 8013

In order to analyze the primary transcriptome of *N. meningitidis* serogroup C strain 8013 (146), RNA from the mid logarithmic (OD_{600nm} of 0.5) and late logarithmic growth phase (OD_{600nm} of 1.5) was isolated. The RNA was subjected to dRNA-seq library preparation for primary transcriptome analysis. Of note, the dRNA-seq approach enables the differentiation between primary transcripts which are characterized by 5'-PPP ends and processed transcripts which exhibit 5'-P ends by the use of the enzyme terminator exonuclease (TEX). The terminator exonuclease enriches RNA samples for primary transcripts as it only degrades 5'-P ends. Therefore, each total RNA sample from these technical replicates were used for the preparation of two cDNA libraries, either being specifically enriched for primary transcripts by TEX treatment or covering all transcripts such as processing products by being left untreated. Afterwards, a precise annotation of transcriptional start sites (TSS) could be done with the TSS predator pipeline (chapter 5.33) based on a characteristic enrichment pattern in the +TEX libraries relative to the -TEX libraries. The TSS predator automatically assigned five different classes of TSSs based on the location relative to existing gene annotation: primary TSS (pTSS; main transcription start of a transcriptional unit), secondary TSS (sTSS; alternative start with lower expression level), internal TSS (iTSS; start within a gene), antisense TSS (aTSS; transcript start antisense to a gene ±100 nt), and orphan TSS (oTSS; requiring a distance of ≥300 nt relative to existing gene annotations).

In total, 1,625 TSSs were identified under both growth conditions including 706 pTSSs, 62 sTSSs, 286 iTSSs, 633 aTSSs and 135 oTSSs (Figure 6-1). Interestingly, the comparative dRNA–seq data showed that the majority of TSSs are detected in both investigated growth phases.

The *N. meningitidis* 8013 genome encodes for 2,126 annotated CDSs including 1,918 protein encoding genes. Of these, 1,011 proteins are organized in 379 multi-gene operons as predicted by the DOOR algorithm (137). The majority out of the 706 pTSSs were detected for protein coding sequences, with 382 pTSSs detected for free-standing genes and 240 pTSSs detected for multi gene operons. Among those 240 operon associated pTSSs, 187 pTSSs were detected in front of the first gene in the operon, while the remaining 53 pTSSs are derived from internal genes of operons and suggest a different composition of these

operons than predicted. For instance, one pTSS was found inside the operon *pilHIJKX* indicating that these pilus genes are translated from two rather than one polycistronic mRNA (data not shown). Of note, 573 out of 1913 protein coding genes of *N. meningitidis* 8013 possess at least one aTSS (Figure 6-2). Among those genes, 236 have a pTSS identified by dRNA-seq.

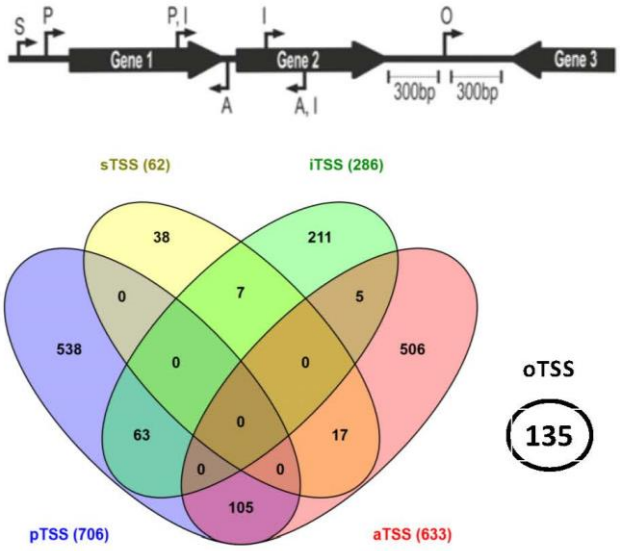

Figure 6-1 TSS mapping based on a dRNA-seq approach

(Top) TSS classifications based on genomic localization and expression strength: primary (P), secondary (S), internal (I), antisense (A), or orphan (O) TSS. (Bottom) The Venn-diagram indicates the overlap and the discrepancies of the 1,625 genome-wide TSSs identified in *N. meningitidis* strain 8013 by dRNA-seq according to their genomic context.

The 768 primary and secondary TSSs were used to examine the length distribution of 5' UTRs in *N. meningitidis* strain 8013. Thereby, 5'UTRs with a minimal length of 0 nt, a median length of 55 nt and a maximal length of 294 nt were detected (Figure 6-3 A). Of note, 24 genes exhibited 5'UTRs shorter than 10 nt and therefore it is possible that these genes might possess alternative ORFs as recently annotated. Additionally, for 706 coding sequences rho-independent terminators were predicted (118). Thereby, 3'UTRs with a minimal length of 8 nt, a median length of 65 nt and a maximal length of 492 nt were detected (Figure 6-3 B).

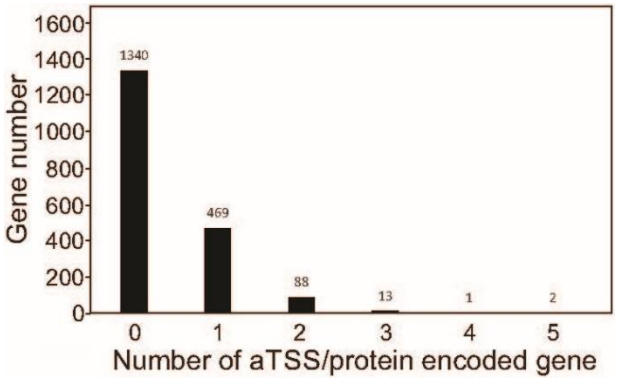

Figure 6-2 Distribution of aTSSs detected in our dRNA-seq approach

The histogram shows the number of antisense TSSs per protein coding gene annotated in the *N. meningitidis* 8013 genome.

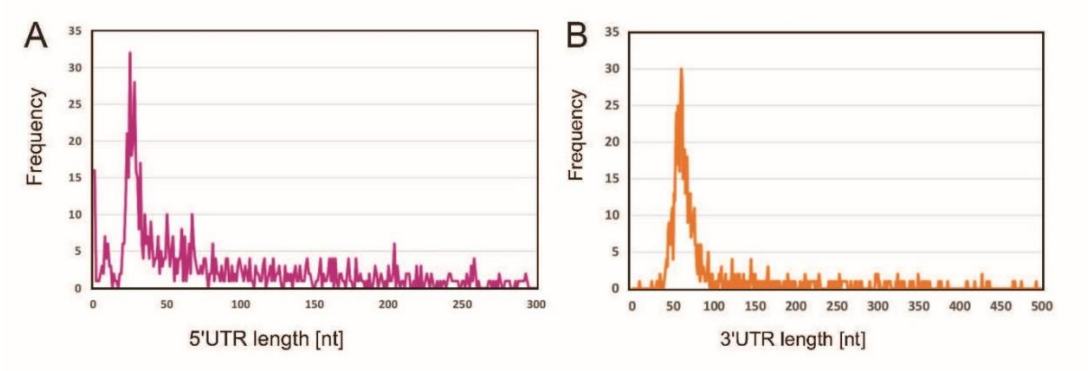

Figure 6-3 UTR length distribution based on dRNA-seq data from two growth phases and promotor predictions

dRNA-seq data of *N. meningitidis* strain 8013 were obtained from two growth phases (OD_{600nm} 0.5 and 1.5) in rich medium ($GCBL^{++}$, Table 4-7, Table 4-8). (A) 5'UTR length distribution of mRNAs. Each 5'UTR was plotted as the frequency of the distances between pTSS or sTSS to the start codon. The average 5'UTR length is 81 nt (95% CI: 5.3). (B) 3'UTR length distribution of mRNAs. Each 3'UTR was plotted as the frequency of the distances between *in silico* predicted rho-independent terminators to the stop codon. The average 3'UTR length is 97 nt (95% CI: 6.1).

The accuracy of the performed dRNA-seq approach is illustrated by the iron-responsive regulator *fur* (chapter 3.2) which was previously described to be transcribed from two independent promoters in *N. meningitidis* (147). Detection of a primary TSS and a secondary TSS confirm both the location of both promoters and their activity at late logarithmic growth phase (Figure 6-4).

Taken together, 1,625 genome-wide TSSs could be identified in *N. meningitidis* strain 8013 applying a dRNA-seq approach. Based on these data, the genome-wide distribution of 5'UTRs and 3'UTRs in this meningococcal strain was analyzed which was afterwards used as a base for determining binding site preferences of the RBPs Hfq (chapter 6.3) and ProQ (chapter 6.5.4).

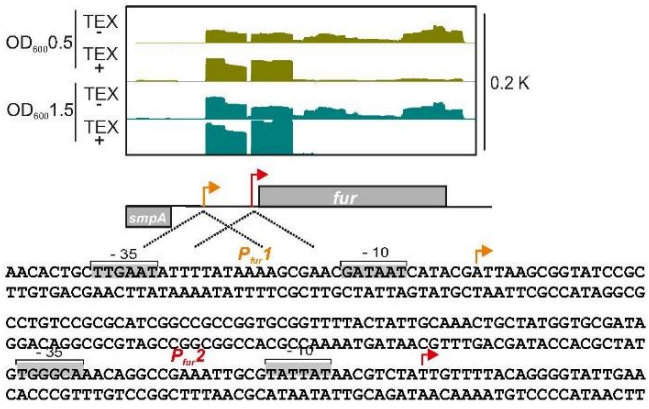

Figure 6-4 Validation of dRNA-seq data

(Top) Screenshot of dRNA-seq data from mid logarithmic (OD_{600nm} 0.5) and late logarithmic growth-phase (OD_{600nm} 1.5) at the *fur* locus. The data were visualized with the IGB (chapter 5.33) (Bottom) Red and orange arrows denote a pTSS and sTSS according to our dRNA-seq data and confirm transcription initiation at the *fur* locus as indicated by primer extension experiments in . The *smpA*- *fur* IGR with marked -10 and-35 boxes at $P_{fur}1$ and $P_{fur}2$ is indicated as described in Delany *et al*., 2003 (147).

6.2. The repertoire of meningococcal sRNAs

6.2.1. Identification and verification of sRNAs in *N. meningitidis* strain 8013

Besides UTR length determination, the dRNA-seq approach allowed the prediction of non-coding RNAs. In particular, the class of orphan TSSs was considered as a hotspot for the prediction of sRNAs derived from intergenic regions and the class of antisense TSSs as the primary source of *cis*-encoded base-pairing RNAs. In addition, regulatory RNAs derived from 3'UTRs as well as 5'UTRs of mRNAs could be detected by visual inspection of the dRNA-seq cDNA libraries in a genome browser (chapter 5.33).

In total, 45 novel sRNA candidates and a TSS and thus expression of 20 sRNAs described in the literature could be detected (Table 6-1). This compendium of 65 regulatory RNAs comprises housekeeping RNAs, riboswitches, previously described base-pairing sRNAs and novel sRNAs (Table 6-1). Of the 45 novel sRNAs, 22 are canonical intergenic sRNAs which are transcribed from their own promoters and possess ρ-independent terminators. Five of them have a extended -10 box σ^{70}- promoter, another five a canonical σ^{70}-promoter, whereas no promoter motif could be identified for the remaining 12 sRNA candidates (117).

Table 6-1: Repertoire of sRNAs of different *N. meningitidis* strains

RNA classes*	8013	MC58	WUE2594	Z2491
Housekeeping RNAs (n = 4)	6S RNA	6S RNA	6S RNA	6S RNA
	RNaseP	RNaseP	RNaseP	RNaseP
	tmRNA	tmRNA	tmRNA	tmRNA
	SRP	SRP	SRP	SRP
Riboswitches (n = 2)	preQ riboswitch	preQ riboswitch	preQ riboswitch	preQ riboswitch
	Tpp riboswitch	Tpp riboswitch	Tpp riboswitch	Tpp riboswitch
Previously published base-pairing RNAs (n = 7)	AniS [36] *	AniS [36]	AniS [36]	AniS [36]
	NrrF [67]	NrrF [67]	NrrF [67]	NrrF [67]
	Bns1[66] *	Bns1 [66]	Bns1 [66]	Bns1 [66]
	Bns2 [66]	Bns2 [66]	Bns2 [66]	Bns2 [66]
	σ^EsRNA[23] *	σ^EsRNA [23]	σ^EsRNA [23]	σ^EsRNA [23]
	0863-0864_F [148] *	0863-0864_F [148]	0863-0864_F [148]	0863-0864_F [148]
	tracrRNA [42]	-	tracrRNA [42]	tracrRNA [42]
sRNAs of this study (n =45)	crRNAs (n = 7 of n =25)	-	crRNAs (n = 22)	crRNAs (n =16)
	NMnc001 *	NMnc001	NMnc001	NMnc001
	NMnc002	NMnc002	NMnc002	NMnc002
	NMnc003	NMnc003	NMnc003	NMnc003
	NMnc004	-	-	-
	NMnc005	-	-	-
	NMnc006 *	-	-	-
	NMnc007	NMnc007	NMnc007	NMnc007
	NMnc008	NMnc008	NMnc008	NMnc008

RNA classes*	8013	MC58	WUE2594	Z2491
	NMnc009	NMnc009	NMnc009	NMnc009
	NMnc010	NMnc010	NMnc010	NMnc010
	NMnc011	NMnc011	NMnc011	NMnc011
	NMnc012	NMnc012	NMnc012	NMnc012
	NMnc013	NMnc013	NMnc013	NMnc013
	NMnc014	-	-	-
	NMnc015	NMnc015	NMnc015	NMnc015
	NMnc016	NMnc016	NMnc016	NMnc016
	NMnc017 *	NMnc017	NMnc017	NMnc017
	NMnc018 *	NMnc018	NMnc018	NMnc018
	NMnc019 *	NMnc019	NMnc019	NMnc019
	NMnc020	NMnc020	NMnc020	NMnc020
	NMnc021	NMnc021	NMnc021	NMnc021
	NMnc022	NMnc022	NMnc022	NMnc022
	NMnc023	NMnc023	NMnc023	NMnc023
	NMnc024 *	-	-	-
	NMnc025	NMnc025	NMnc025	NMnc025
	NMnc026 *	NMnc026	NMnc026	NMnc026
	NMnc027	NMnc027	NMnc027	NMnc027
	NMnc028	NMnc028	NMnc028	NMnc028
	NMnc029 *	NMnc029	NMnc029	NMnc029
	NMnc030 *	-	-	-
	NMnc031 *	NMnc031	-	-
	NMnc032	NMnc032	NMnc032	NMnc032
	NMnc033	NMnc033	NMnc033	NMnc033
	NMnc034 *	NMnc034	NMnc034	-
	NMnc035	NMnc035	NMnc035	NMnc035
	NMnc036	NMnc036	NMnc036	NMnc036
	NMnc037 *	NMnc037	NMnc037	NMnc037
	NMnc038 *	NMnc038	NMnc038	NMnc038
	NMnc039	NMnc039	NMnc039	NMnc039
	NMnc040 *	-	NMnc040	NMnc040
	NMnc041 *	NMnc041	NMnc041	NMnc041
	NMnc042	NMnc042	-	-
	NMnc043	NMnc043	NMnc043	NMnc043
	NMnc044 *	NMnc044	NMnc044	NMnc044
	NMnc045	NMnc045	NMnc045	NMnc045
Reference genome	(Rusniok *et al*., 2009)	(Tettelin *et al.*, 2000)	(Schoen *et al.*, 2011)	(Parkhill *et al.*, 2000)

Number of ORFs according to NCBI annotation (Februar 2016). Previously published sRNAs can be found in (23,36,42,66,67,148), n°-number, - sRNAs which are absent in *N. meningitidis* strains WUE2594, MC58 or Z2491 (Identity values below 40%), *: validated sRNAs by northern blot analysis (Figure 6-5). Conservation analyses of sRNAs were done with BLAST searches.

Subsequently, the expression of 16 novel sRNA candidates and four known conserved sRNAs serving as positive controls (AniS (36), Bns1 (37), sRNA 0863–0864_F (37) and σE sRNA (23)) could be validated by northern blot analysis using a *N. meningitidis* 8013 wild-type and a Δ*hfq* strain (chapter 5.12.2, Table 6-1, Figure 6-5).

Thereby, the expression of six novel sRNAs transcribed from their own promoters from intergenic regions could be verified (NMnc0017, NMnc0018, NMnc0030, NMnc0029, NMnc0006 and NMnc0040). Of note, NMnc0017 and NMnc0018 are ~90 nt paralogous sRNAs which share 80% of identical residues and are transcribed from the same intergenic region between the gene *dsbB* encoding for a disulfide bond formation protein and the gene *lrp* encoding for a leucine-responsive regulatory protein. The expression levels of the sRNAs NMnc0017/18 are decreased in the *hfq* deletion strain, suggesting that Hfq is required for their stability (Figure 6-5).

Additionally, the expression of two 5'-UTR derived ncRNAs transcribed from their own promoters (NMnc0013 and NMnc0037) could be confirmed. By screening both sRNAs with the Rfam database (138), NMnc0013 could be identified as a member of the glycine riboswitch family, which forms an on-switch when bound to glycine (149). As NMnc0013 is stabilized by Hfq (Figure 6-5), it might function in parallel as a *trans*-acting sRNA.

Likewise, the expression of two out of four predicted *cis* encoded antisense RNAs (NMnc0019, NMnc0024) could be validated. NMnc0019 is transcribed from the opposite strand of NMV_1107 exhibiting high homology to infection bacteriophage resistance proteins (IPR011664) which provide phage protection by the abortion of infection (150) Due to the fact that NMnc0019 is stabilized by Hfq (Figure 6-5), it might act in parallel as a *trans*-acting sRNA. NMnc0024 is transcribed from the opposite strand of NMV_0836 encoding an OsmC/Ohr family protein (IPR003718) that has been described to be involved in oxidative stress response in *E. coli* (151).

The expression of seven out of 17 novel 3' UTR-derived sRNAs could be detected that were further sub-divided into sRNAs that are derived from processing of longer mRNA transcripts (NMnc0026, NMnc0034, NMnc0038, NMnc0041, NMnc001) and sRNAs that possess their own promoters (NMnc0031/0044). Of note, the majority of these 3'UTR derived sRNAs accumulate intermediate processing products which could be the consequence of further coupled degradation whereby sRNAs are degraded as they base-pair with their targets. The expression levels of NMnc0001, NMnc0041 and NMnc0044 decreased in the *hfq* deletion strain, suggesting that Hfq is required for their stability.

In summary, 65 putative sRNAs could be detected in *N. meningitidis* strain 8013. Additionally, it could be shown that the absence of the RBP Hfq affects transcript-levels of several newly identified sRNAs belonging to multiple classes of regulatory RNAs.

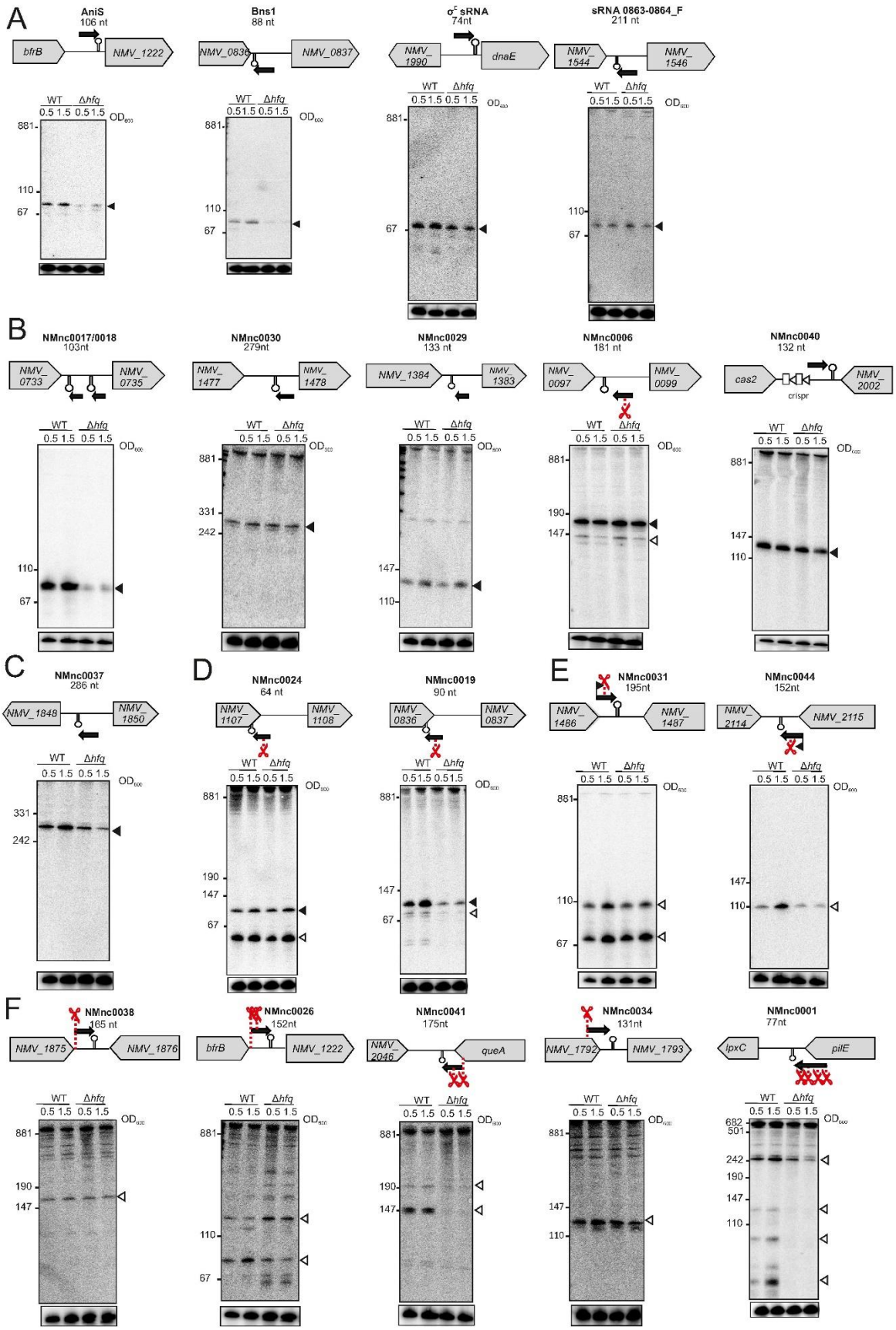

Figure 6-5 Expression analysis of 8013 sRNAs in *N. meningitidis strain* 8013

Total RNA was extracted at mid logarithmic (OD_{600nm} = 0.5) and late logarithmic (OD_{600nm} = 1.5) growth phases in $GCBL^{++}$ from *N. meningitidis* 8013 wild-type and Δ*hfq* strains and investigated by northern blot analysis using labeled DNA probes complementary to the analysed sRNAs (Table 4-32). The housekeeping 5S rRNA served as a loading control. The genomic locations of the candidate sRNAs are shown above the gel images. Genes are shown in grey, sRNAs are shown in black. Arrows and scissors label TSSs and processing sites. Filled triangles indicate bands derived from TSSs and open triangles indicate processing products. (A) sRNAs detected in course of other studies. (B) sRNAs from intergenic regions. (C) sRNAs from 5' UTRs of mRNAs. (D) *Cis*-encoded antisense sRNAs. (E) sRNAs from 3' UTRs of mRNAs. (F) sRNAs derived from transcript processing.

6.2.2. Conservation of meningococcal sRNAs

Small non-coding RNAs display a high intra-specific diversity (152) and they evolutionary turn-over in genetically diverse bacterial species like *Campylobacter jejuni* (144). Given the high genetic diversity of meningococci, the conservation levels of the novel sRNAs was assessed by BLAST searches among the four prototypical *N. meningitidis* strains MC58, WUE2594, 8013, Z2491 which belong to the three serogroups A, B and C causing the majority of IMDs worldwide (1). According to *Neisseriales* genome annotations available in the NCBI database, the sequences of 35 out of 45 newly identified sRNAs are conserved among these four strains, whereas ten sRNAs are strain-specific (Table 6-1).

Among the 16 experimentally validated sRNAs (Figure 6-5), five sRNA candidates were found to be strain-specific by BLAST searches (Table 6-1). Consequently, the expression levels of these five sRNAs were tested by northern blot analysis in *N. meningitidis* strains MC58, WUE2594, 8013, Z2491 at two different growth phases (Figure 6-6 A). As predicted by BLAST searches (Figure 6-6 B, Table 6-1), three sRNAs were only expressed in *N. meningitidis* strain 8013 (NMnc0030, NMnc0006 and NMnc0024), one sRNA was absent in serogroup A (NMnc0031) while one sRNA was absent in strain MC58 (NMnc0040) (Figure 6-6 A).

Interestingly, NMnc0040 is located next to the CRISPR-Cas locus in *N .meningitidis* strain 8013 (Figure 6-5 B). Therefore, the sequences of 71 *N. meningitidis* strains harbouring a completely sequenced genome available in the NCBI database were tested for the presence of NMnc0040 by BLAST searches. Of note, all 17 strains that possess a CRISPR/Cas locus also encode NMnc0040. On the other hand, the 54 *N. meningitidis* genomes lacking a CRISPR/Cas locus did not contain the *nmnc0040* gene in their genome (data not shown) indicating a possible association of NMnc0040 with the CRISPR-Cas system.

Furthermore, NMnc0031 is located on the island of horizontal gene transfer E (IHT-E) (153) which was recently linked to hyperinvasive meningococcal lineages (12) and might

derive from an integrated prophage that is absent in strains WUE2594 and Z2491 (117). Therefore, these findings indicate a phage-related function of NMnc0031.

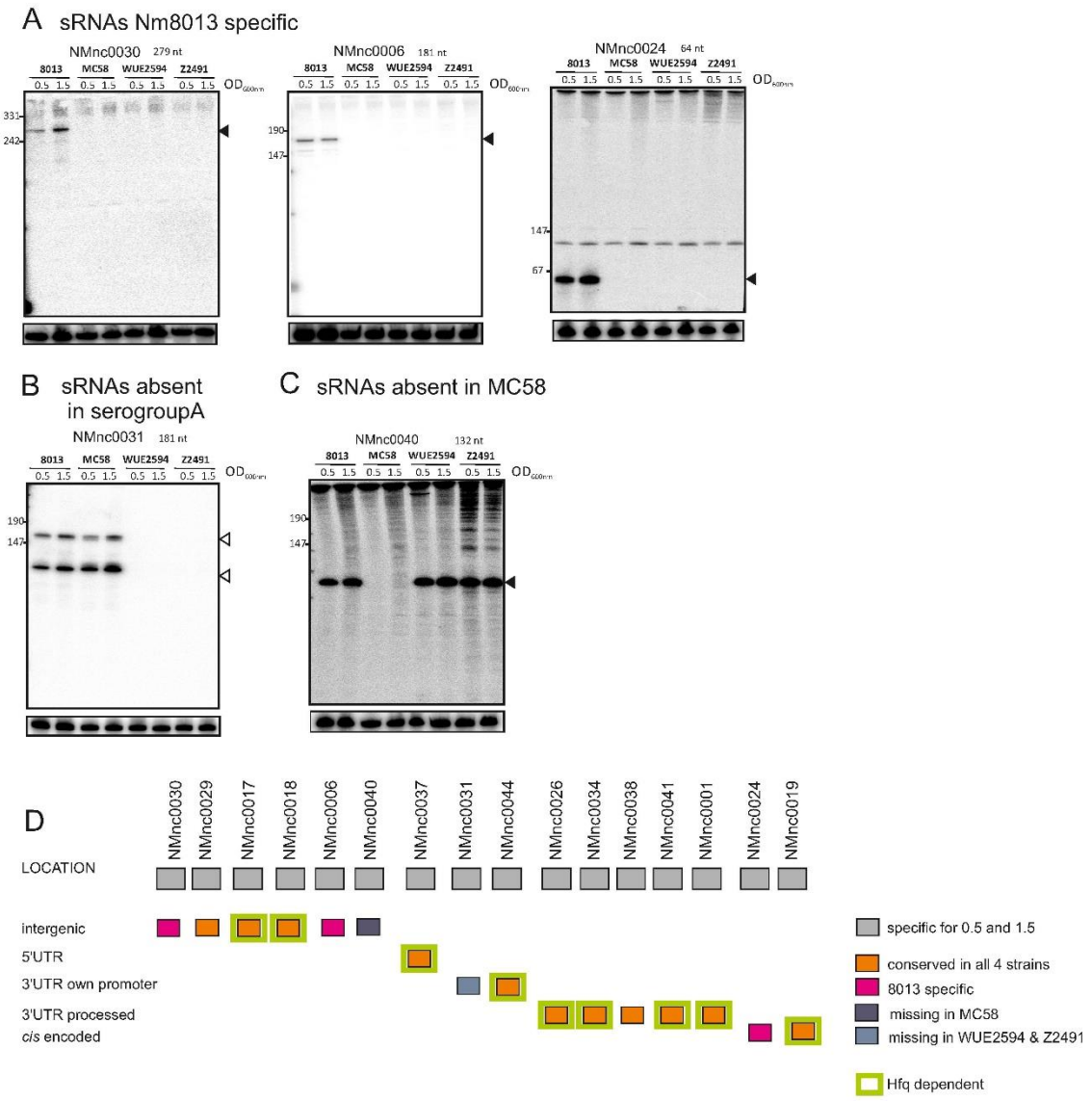

Figure 6-6 Expression analysis of candidate sRNAs in different *N. meningitidis* strains

Total RNA was extracted at mid logarithmic (OD_{600nm} = 0.5) and late logarithmic/early-stationary (OD_{600nm} = 1.5) growth phase from *N. meningitidis* strains 8013 (serogropup C), MC58 (serogroup B), WUE2594 (serogroup A) and Z2491 (serogroup A) and investigated by northern blot analysis using labeled DNA probes complementary to the sRNAs (Table 4-32). The housekeeping 5S rRNA served as a loading control. Filled triangles indicate bands derived from TSSs and open triangles indicate processing products. (A) Expression analysis of *N. meningitidis* strain 8013 specific sRNAs. (B) Expression analysis of sRNAs which are absent in the investigated *N. meningitidis* serogroup A strains (WUE2594, Z2491). (C) Expression analysis of sRNAs which are absent in *N. meningitidis* serogroup B strain MC58. (D) Graphic illustration of sequence conservation of the investigated candidate sRNAs among four meningococcal strains. Small RNAs which are absent in *N. meningitidis* strains WUE2594, MC58, Z2491 were determined based on conservation analyses by BLAST searches regarding identity values below 40% as absent.

Another biologically striking sRNA is NMnc0001which is derived as processing product from a transcript encoding the major pilin (PilE) that forms the pilus fiber of tfp and (Figure

6-5, Figure 6-7 A, B) was conserved in the four prototypical *N. meningitidis* strains MC58, WUE2594, 8013, Z2491 according to BLAST searches (Table 6-1, Figure 6-6 B). Interestingly, NMnc0001 was not expressed in strain WUE2594 (Figure 6-7 C). In the three strains in which NMnc0001 is expressed the sRNA is located within the 3'UTR of the class I *pilE* genes (chapter 3.1). Yet, in strain WUE2594 which has a class II *pilE* gene (chapter 3.1), NMnc0001 is located within a *pilS* cassette (Figure 6-7). The *pilS* cassettes and consequently NMnc0001 are not transcribed as they serve as a reservoir for antigenic variation of class I *pilE*. NMnc0001, which is only expressed if pili from class I are expressed, could therefore provide a *trans*-acting link between type IV pili variation and the regulation of different classes of genes not directly related to type IV pilus function.
Of note, a predicted mRNA target spectrum of NMnc0001 can be found in chapter 6.4.1 (Figure 6-11).

In conclusion, the dRNA-seq data indicate that sRNA conservation and expression varies between distinct strains and serogroups of *N. meningitidis* suggesting a role of these sRNAs in meningococcal genetic diversity.

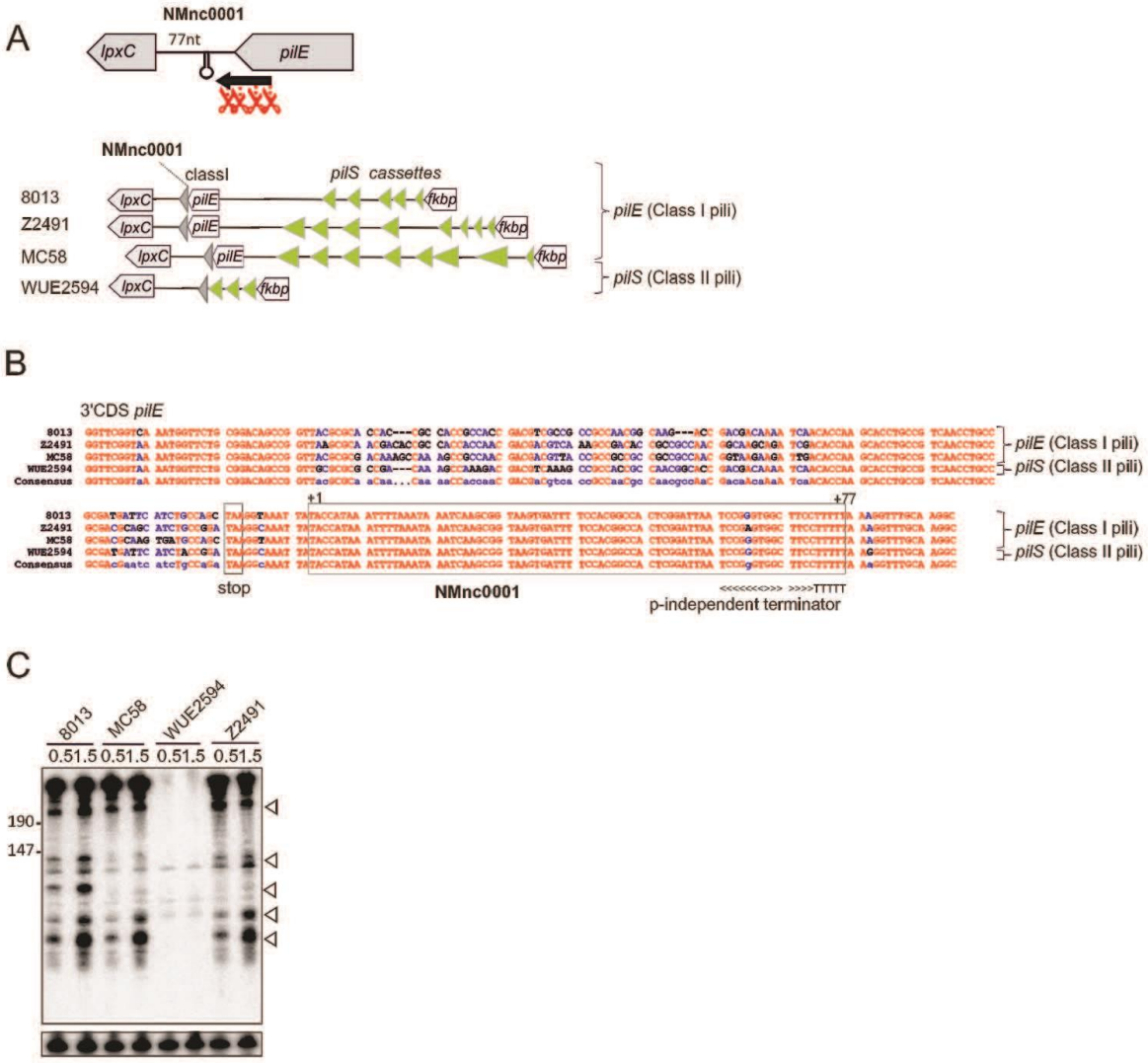

Figure 6-7 Genetic organization and expression of the sRNA NMnc0001

(A) Conservation of the putative sRNA NMnc0001 that is processed from class I *pilE* genes in different *N. meningitidis* strains. (B) Nucleotide sequence alignment of NMnc0001 from four *N. meningitidis* strains (8013 (serogroup C), MC58 (serogroup B), WUE2594 (serogroup A) and Z2491 (serogroup A)). The color of the nucleotides indicates their degree of conservation (red: highly conserved nucleotides; blue: partial conservation; black: little or no conserved nucleotides). The rho-independent terminator of the corresponding *pilE* gene is plotted below the alignement. '+1' indicates the processing site, and the NMnc0001 nucleotide sequence is boxed. (C) Total RNA from the meningococcal strains 8013, MC58, WUE2594 and Z2491 was isolated at mid logarithmic (OD_{600nm} = 0.5) and late logarithmic growth phase (OD_{600nm} = 1.5) and subjected to northern blot analysis using labelled DNA probes complementary to the sRNA NMnc0001 (Table 4-32). The 5S rRNA served as a loading control. Open triangles indicate processing products.

6.3. The repertoire of Hfq-associated RNAs in *N. meningitidis* strain 8013

Hfq is the major RNA chaperone in N. meningitidis and plays an important role in IMD (93). Therefore, in order to identify directly associated transcripts of the meningococcal Hfq protein, RNA was co-immunoprecipitated with a chromosomally FLAG epitope-

tagged Hfq protein expressed by *N. meningitidis* strain 8013 at mid logarithmic growth-phase (OD_{600nm} 0.5) in $GCBL^{++}$ medium (chapter 5.1).

In brief, cell lysates of the wild-type (control coIP) and a mutant strain expressing 3xFLAG tagged Hfq protein (Hfq coIP) were incubated with anti-FLAG antibodies and Protein A-Sepharose beads in order to extract Hfq-associated RNAs which were used for constructing cDNA libraries followed by deep-sequencing (95,154) (Figure 6-8).

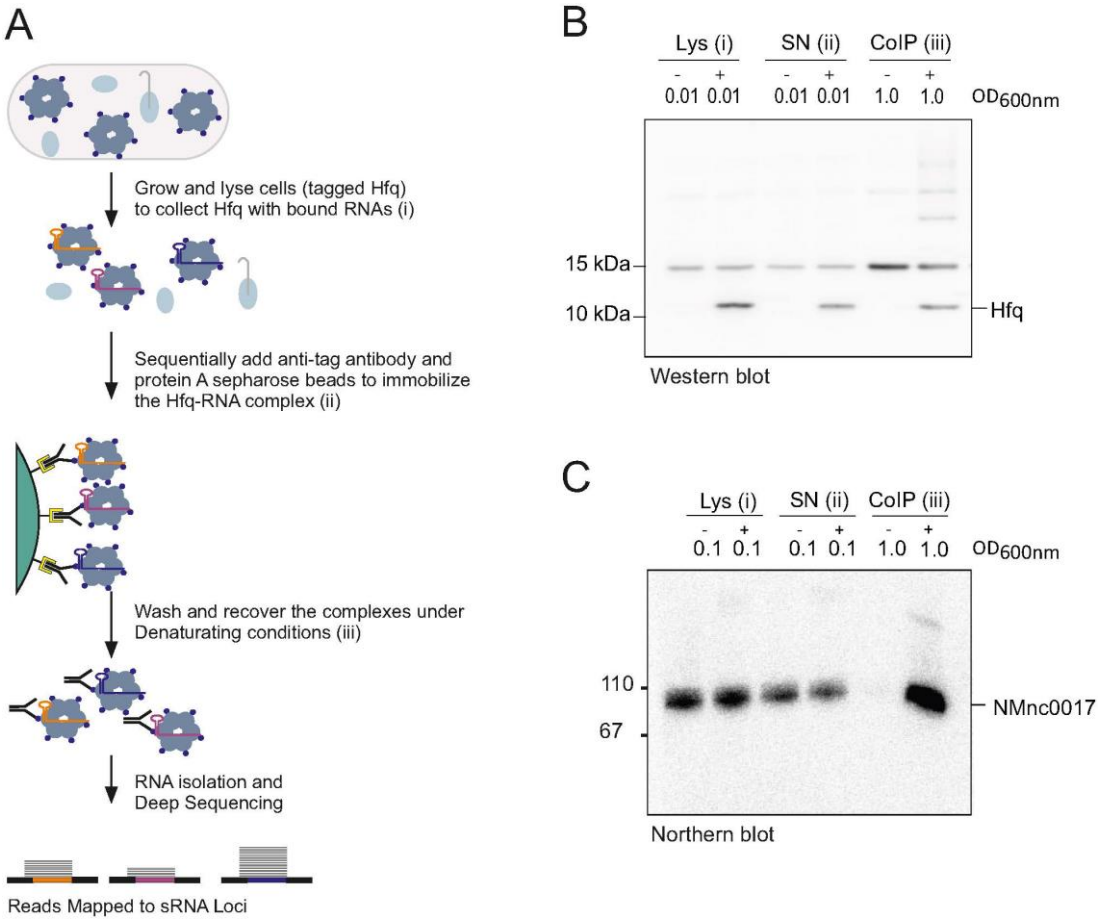

Figure 6-8 Workflow and quality controls for generating coIP samples *of N. meningitidis* 8013 wild-type and 3xFLAG-tagged Hfq strains

(A) Schematic illustration of generating coIP samples of wild-type and 3xFLAG-tagged Hfq strains grown in $GCBL^{++}$ to OD_{600nm} 0.5 corresponding to mid logarithmic growth phase. Two technical replicates were performed per experiment. The figure was adapted from (117). Western blot (B) and northern blot analyses (C) prove quality of protein and RNA samples. Lysate (Lys), supernatant (SN) and coIP samples were obtained from coIP experiments with mouse anti-FLAG anti-body (A) performed in the *N. meningitidis* 8013 wild-type (−) or 3×FLAG tagged Hfq strain (+). Western blot performed with rabbit anti-FLAG antibody (Table 4-3) and northern blot probed against NMnc0017 (Table 4-32) verified the success of the Hfq pull-downs. On the left side of the blots, size markers are denoted (in B: kDa; in C: nt).

Both the RNA co-immunoprecipitation with Hfq and cDNA sequencing (Hfq RIP-seq) as well as a rough data analysis of the cDNA-sequencing results were already done during my master thesis. Therefore, a detailed description of the experimental set-up, performed quality controls as well as mapping statistics can be looked up both in my written thesis (155) and in (117). Yet, the mapping of the recovered cDNA sequences was re-defined using a

genome annotation containing the 5'UTRs, 3'UTRs as well as putative sRNAs detected in the dRNA-seq approach (chapter 6.1). Accordingly, Hfq-binding sites in mRNAs as well as the genome-wide repertoire of Hfq-associated sRNAs could be precisely categorized.

The majority of recovered cDNA sequences mapped to sRNAs (Figure 6-9 A) confirming that Hfq is a global RBP in *N. meningitidis*. The scatter-plot in Figure 6-9 B shows the distribution of cDNA reads for sRNAs and illustrates that 19 of 45 novel sRNAs as well as four previously described sRNAs (AniS, Bns1, Bns2 and σE sRNA) are Hfq-associated sRNAs. Of note, the three most abundant sRNAs, according to the numbers of Hfq cDNA sequence reads are NMnc0017, NMnc0018 and AniS (Table 6-2). The coIP of Hfq enriched these three sRNAs by 5 - to 25 -fold, in comparison to the control.

In addition to the identification of Hfq-bound sRNAs, Hfq RIP-seq data analysis identified 401 mRNAs bound by Hfq by considering an mRNA that was represented by ≥ 10 cDNA reads to be significantly enriched (Figure 6-9 B). Of note, of the 107 proteins known to be regulated by Hfq (93,94,156), seven mRNAs (*prpB, acnB, glyA, argG, godB, ibpB* and NMV_1914) were enriched in our Hfq RIP-seq analysis. The majority (70%, 320 CDS) of the cDNAs of Hfq-bound mRNAs corresponded to CDSs and the rest (30%, 80 5'UTRs and 62 3'UTRs) corresponded to the termini of mRNAs. It is possible that Hfq binding to the termini of mRNAs controls expression of these mRNAs through control of translation initiation or modulation of mRNA decay initiating at the 3' end. Additionally, 5'UTRs of mRNAs represent classical binding sites for Hfq dependent sRNAs. Therefore, these Hfq-bound mRNAs represent good candidates for target genes post-transcriptionally regulated by sRNAs (55,56).

To assess the role of Hfq in stabilizing those sRNAs that were enriched in the Hfq coIP (Figure 6-9) and that showed descreased steady-state levels in a Δ*hfq* strain compared to the wild-type (Figure 6-5), changes in RNA half-life were tested in rifampicin stability assays for nine sRNAs (Figure 6-10).

The sRNA AniS, which has been previously described as a Hfq binding sRNA (36), served as a positive control while the Hfq-independent sRNA NMnc0006 (Figure 6-5, Figure 6-9) did not show decreases RNA half-lifes in the *hfq* deletion strain compared to the wild-type (Figure 6-10).

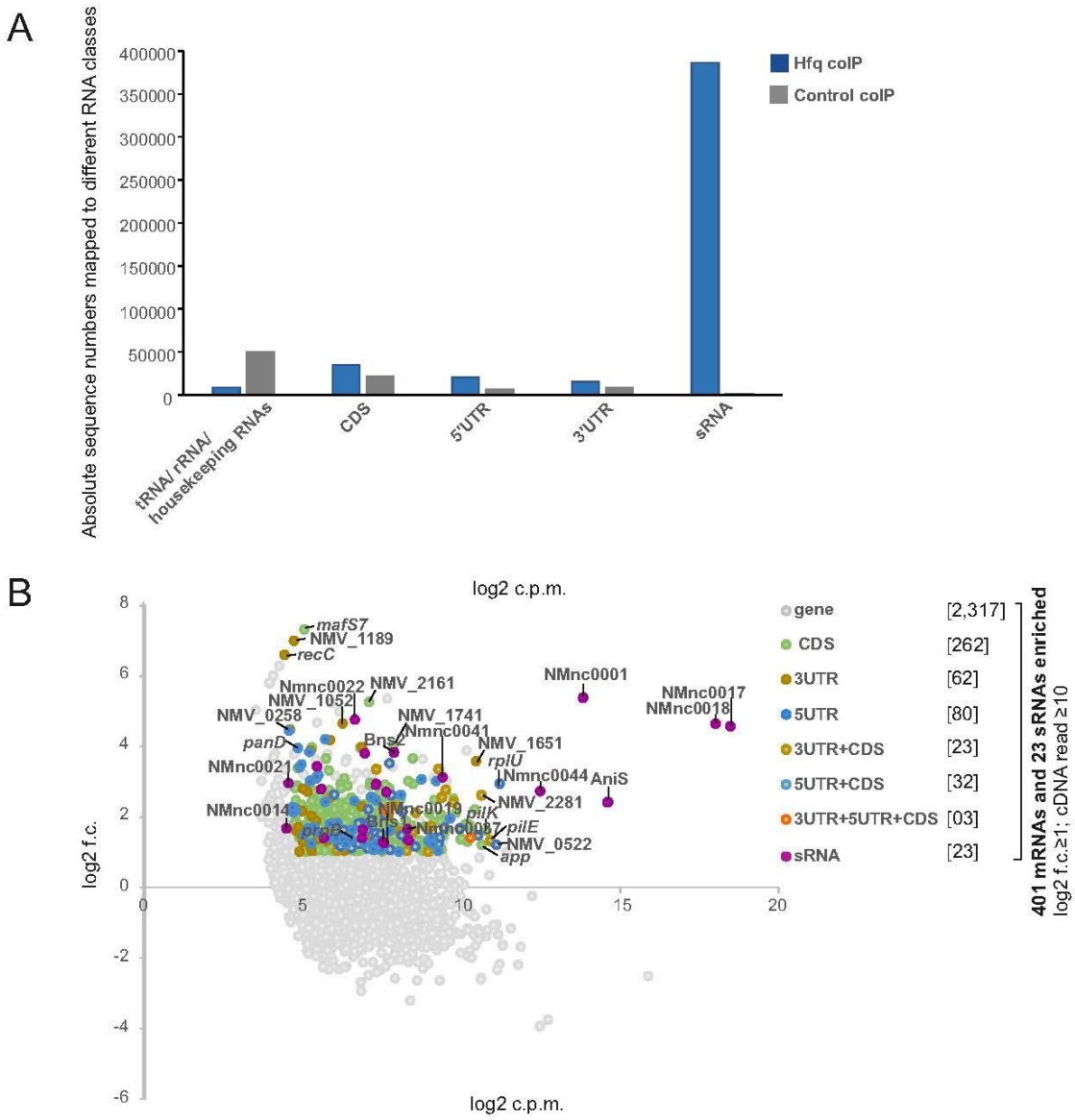

Figure 6-9 The repertoire of Hfq-associated RNAs in *N. meningitidis* strain 8013

(A) The bar diagram represents the Hfq coIP data which were experimentally generated during my master thesis and which were remapped during my PhD using annotations based on the dRNA-seq approach in *N. meningitidis* strain 8013. The bar diagram was adapted from (157) and shows the relative proportions of all analyzed sequences that unequivocally mapped to different classes of RNA sequences in the Hfq coIP and the control coIP, respectively. The analysis is based on two technical replicates. (B) Scatter-plot analysis of RNA-seq data from coIPs of Hfq-bound RNAs which was adapted from (157). The analysis is based on two technical replicates. The 23 significantly enriched (log_2 fold-change (log_2 f.c.) ≥1; cDNA read number ≥10) sRNAs and the 401 significantly enriched mRNAs and their associated RNA features (CDS, 5'UTR and 3'UTR) are indicated in color. log_2 f.c. ≥1 stands for the enrichment and log_2 counts per million reads (log_2 c.p.m) represents the abundance. The total number of each RNA feature is given in parenthesis.

Table 6-2 Hfq-binding candidates with log_2 f.c.≥1.

Class	Annotated gene [a]	Reads	log_2 f.c.	COG number [b]	Class functional category [b]	Process [b]
sRNA	NMnc0017	209162	4.6			
	NMnc0018	151733	4.6			
	AniS	12697	2.4			
	NMnc0001	8456	5.3			
	NMnc0044	2959	2.7			
	NMnc0037	140	1.6			
	NMnc0026	134	1.3			
	Bns2	133	3.8			
	σ^EsRNA	100	2.7			
	NMnc00030	83	2.9			
CDS	NMV_0360 (*rplU*)	1246	2.9			
	NMV_0522	911	1.2	COG0457	R	Poorly characterized
	NMV_1824 (*rplS*)	815	2.6			
	NMV_0019 (*pilE*)	814	1.3			
	NMV_1510 (*pilK*)	795	1.6			
	NMV_0215 (*rne*)	672	2.2			
	NMV_2184 (*app*)	658	1.2			
	NMV_2281	645	1.4	COG1741	S	Poorly characterized
	NMV_0045 (*pilC2*)	567	1.6			
	NMV_1823 (*trmD*)	562	1.8			
5'UTR	NMV_1222	12700	2.4	COG1396	K	Information storage and processing
	NMV_0360 (*rplU*)	645	3.9			
	NMV_2281	514	1.8	COG1741	S	Poorly characterized
	NMV_0522	395	3.0	COG0457	R	Poorly characterized
	NMV_1106 (*nrdA*)	377	1.9			
	NMV_1646 (*hfq*)	345	3.2			
	NMV_0309	343	2.0	COG1611	R	Poorly characterized
	NMV_1440 (*sucA*)	309	3.0			
	NMV_1803 (*rpsO*)	305	1.4			
	NMV_1593	246	3.6	COG1469	S	Poorly characterized
3'UTR	NMV_0019 (*pilE*)	8503	5.3			
	NMV_2115	2964	2.7	COG0483	G	Metabolism
	NMV_1651	769	3.5			
	NMV_2048 (*queA*)	295	3.0			
	NMV_0526	192	1.9	COG2018	R	Poorly characterized
	NMV_1509 (*pilX*)	126	1.6			
	NMV_0208	98	2.0	COG1192	D	Cell cycle control, cell division,
	NMV_0057 (*comE1*)	97	2.6			
	NMV_2146	74	3.1	COG4300	P	Inorganic ion transport, metabolism
	NMV_1220 (*bfrB*)	71	1.4			

[a] Top-10 Hfq-associated RNA features for each given class of RNA as well as biological function.
[b] Functional characterization based on the COG classification (123).

Indeed, declined RNA stabilities were found for all investigated Hfq-associated sRNAs in a Δ*hfq* strain (Figure 6-10). Among them, most drastic effects were observed for the sRNAs NMnc0017, NMnc0018, NMnc0044 and NMnc0034. For example, the RNA half-life of NMnc0017 decreased from 32 minutes in the wild-type strain to ~5 minutes in the Δ*hfq* strain. Taken together, a significant decrease in sRNA stability was observed for all investigated Hfq-associated sRNAs in Δ*hfq* compared to the isogenic wild-type strain (Wilcoxon rank sum test, $p = 0.014$).

Alltogether, a direct association of Hfq with 401 mRNAs as well as 23 putative sRNAs could be shown via RIP-seq thus confirming that Hfq is a global RBP in *N. meningitidis*.

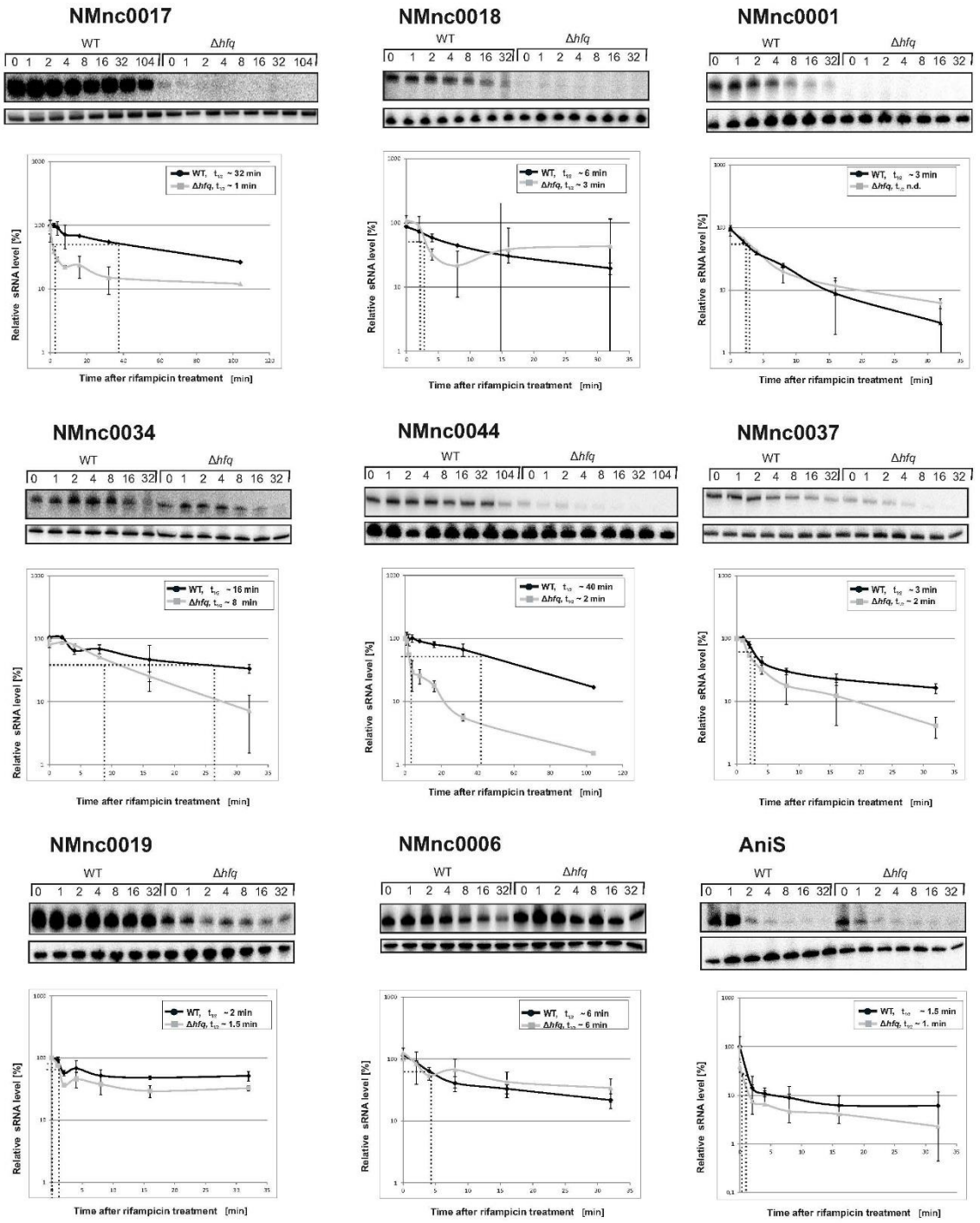

Figure 6-10 RNA half-life determination of Hfq-associated sRNAs

Northern blots of total RNA extracted of the indicated strains (8013 wt and Δ*hfq*) at the indicated time points (0 to 104 minutes) after addition of rifampicin (250 µg/ ml)). For transcript detection, labeled DNA probes complementary to the indicated sRNAs were used which can be found in Table 4-32. The housekeeping 5S rRNAs served as a loading control for each blot. The experiments were performed twice or in triplicate and quantifications for RNA half-lives are summarized below the northern blots. The standard deviation is depicted for each analyzed time point.

6.4. The Hfq-associated sRNAs NMnc0017 and NMnc0018 regulate the putative colonization factor PrpB

6.4.1. Identification of mRNA targets of the highly expressed sRNAs NMnc0017 and NMnc0018

To uncover potential mRNA target and thereby to predict a physiological role for the newly identified Hfq-associated sRNAs, the CopraRNA algorithm (142) was applied using the top ten Hfq binders (Table 6-2) in each RNA class. To minimize the collection of false positive mRNA targets, only mRNAs with 5'UTRs enriched in our Hfq RIP-seq screen were selected for the analysis (Figure 6-9).

Based on these data, a network consisting of Hfq-associated sRNA and their potential mRNA targets could be created which is shown in Figure 6-11. The network consists only of the top nine Hfq-bound sRNAs (Table 6-2), as no putative mRNA targets fulfilling all applied criteria could be predicted for NMnc0030 (Table 6-2). Among all sRNA candidates, Mnc0017 and NMnc0018 were found to be the most enriched sRNAs in the Hfq RIP-seq data (Table 6-2).

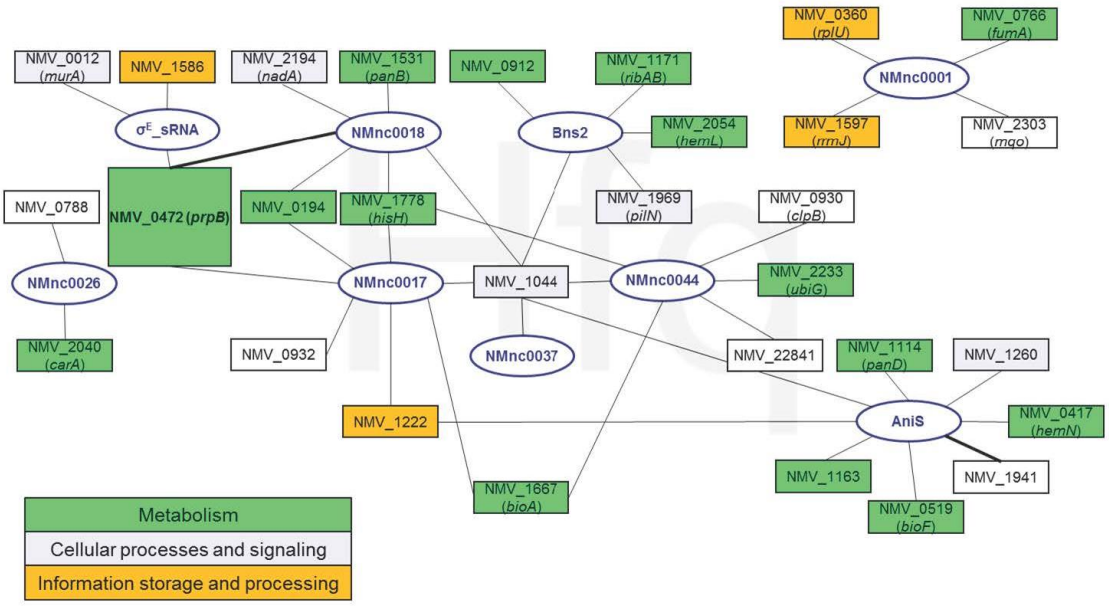

Figure 6-11 Predicted regulatory network consisting of Hfq-associated sRNAs identified by Hfq RIP-seq and their potential mRNA targets

The network represents mRNA targets which were found to be significantly enriched (log_2 f.c. ≥1; cDNA read ≥10) with their 5'UTRs in the Hfq RIP-seq data. Additionally, these mRNAs were predicted as potential mRNA targets of the connected sRNAs in the network by the copra algorithm (142). Only highly enriched sRNAs in the Hfq RIP-seq data were considered in the network. The potential mRNA targets were classified based on the COG classification scheme (123) as indicated by color.

Among the four predicted mRNA targets of the two papralogous sRNAs, *prpB* is the most striking candidate: The predicted RNA interaction between NMnc0017, NMnc0018 and

their target *prpB* contains canonical binding sites overlapping the SD and start codon on the mRNA, indicating sRNA-induced translational inhibition (Figure 6-12).

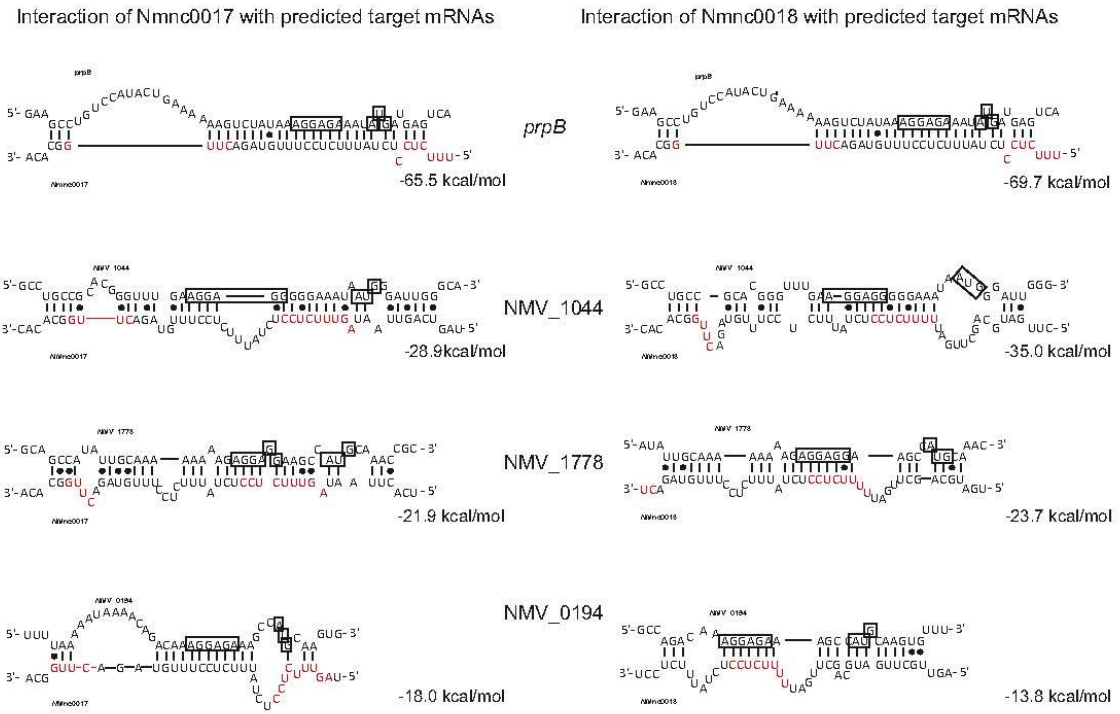

Figure 6-12 Predicted base-pairing interactions of NMnc0017 and NMnc0018 with their potential target mRNAs

The SD sequences and start codons (ATG) of the putative mRNA targets are boxed. Structurally accessible residues are indicated in red. The proposed strength of interaction is denoted below each RNA duplex. Base-pairing interactions were predicted using RNAhybrid (141).

6.4.2. The sRNAs NMnc0017 and NMnc0018 repress the translation of the *prpB* mRNA *in vivo*

To experimentally assess gene expression regulation of *prpB* by the two paralogous sRNAs, deletion mutants of NMnc0017 (Δ*NMnc0017*), NMnc0018 (Δ*NMnc0018*) and a double deletion mutant (ΔΔ*NMnc0017/18*) were generated in the *N. meningitidis* strain 8013 (chapter 5.12.4) (Figure 6-13). As demonstrated by northern blot analysis, *prpB* showed an increased mRNA level in a ΔΔ*NMnc0017*/*18* double deletion mutant and a Δ*hfq* strain, suggesting that both sRNAs are likely to repress *prpB* (Figure 6-13 B). Of note, the *prpB* gene encodes a methyl-citrate lyase and is part of the dicistronic *prpB-prpC* mRNA (Figure 6-13 A). Therefore, the several transcripts detected by northern blot analysis potentially reflect distint processing products of the dicistronic *prpB-prpC* mRNA (Figure 6-14).

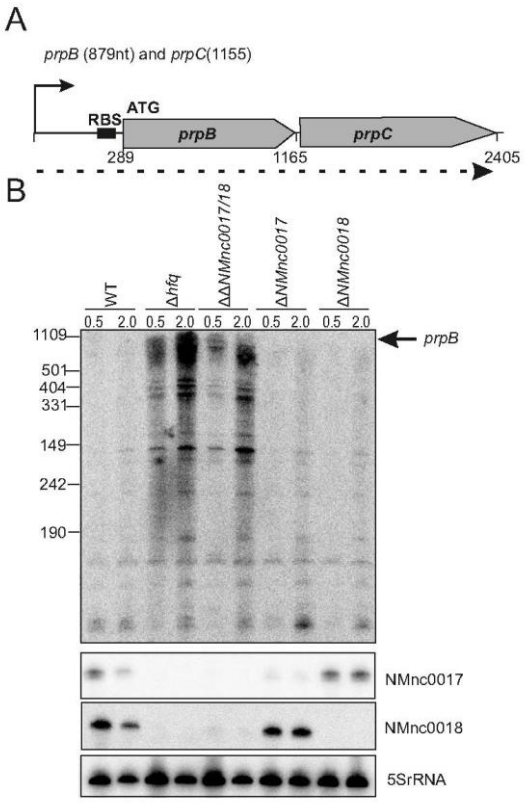

Figure 6-13 Expression analysis of the *prpB* mRNA by northern blot analysis

(Top) Genetic organization of the *prpB* gene locus. The *prpB* transcript is part of the dicistronic operon consisting of the *prpB* gene and the *prpC* gene. The pTSS and RBS are denoted. The distances to the pTSS are indicated by numbers (Bottom) The expression of *prpB*, NMnc0017 and NMnc0018 was analyzed during two growth phases (OD_{600nm} 0.5 and OD_{600nm} 2.0) in *N. meningitidis* 8013 wild-type (wt) strain, Δ*hfq*, ΔΔ*NMnc0017/NMnc0018*, Δ*NMnc0017* and Δ*NMnc0018* deletion mutants by northern blot analysis. For transcript detection, labeled DNA probes complementary to the indicated RNAs were used which can be found in Table 4-32. 5S rRNA served as loading control.

Combining data gained from dRNA-seq and Hfq RIP-seq, a translational reporter system was used to validate sRNA mediated regulation of *prpB* as target for the two paralogous sRNAs *in vivo*. The superfolder GFP (sfgfp) variant, which has been used previously to study sRNA-mediated regulation (114,158), was used as a translational reporter in the chromosome of *N. meningitidis* (Chapter 5.12.6). To reveal if the *prpB* 5'UTR is sufficient for sRNA mediated repression, the endogenous *prpB* promoter was replaced with the unrelated constitutive PLtetO-1 promoter fused to the 5'UTR and the first 15 amino acids of the coding region of *prpB*, upstream of the sf*gfp* reporter gene. This insert was cloned into the pGCC2 vector for homologous recombination into the meningococcal *lctP*/*asp*C locus. A sf*gfp* reporter fusion expressing an unrelated 5'UTR and the first 15 amino acids of the *porA* gene served as a control. Western blot analysis of the PrpB::GFP fusion protein in *N. meningitidis* showed an approximately six- and ten- fold up-regulation upon deletion of both paralogous sRNAs or the *hfq* gene (Figure 6-14). Of note, expression of either one of both sRNAs restored the PrpB::GFP fusion protein level to the wild-type level *in vivo*, indicating that these two sRNAs can complement each other and are largely redundant in this regulation. Of note, the PorA::sfGFP (PorA::GFP) control was not affected by deletion of either both or single RNAs, or by the *hfq* gene. Taken together, the *in vivo* results provide evidence that these paralogous sRNAs are apparently redundant and represses *prpB* at the post- transcriptional level by interacting with its 5'UTR in an Hfq dependent manner.

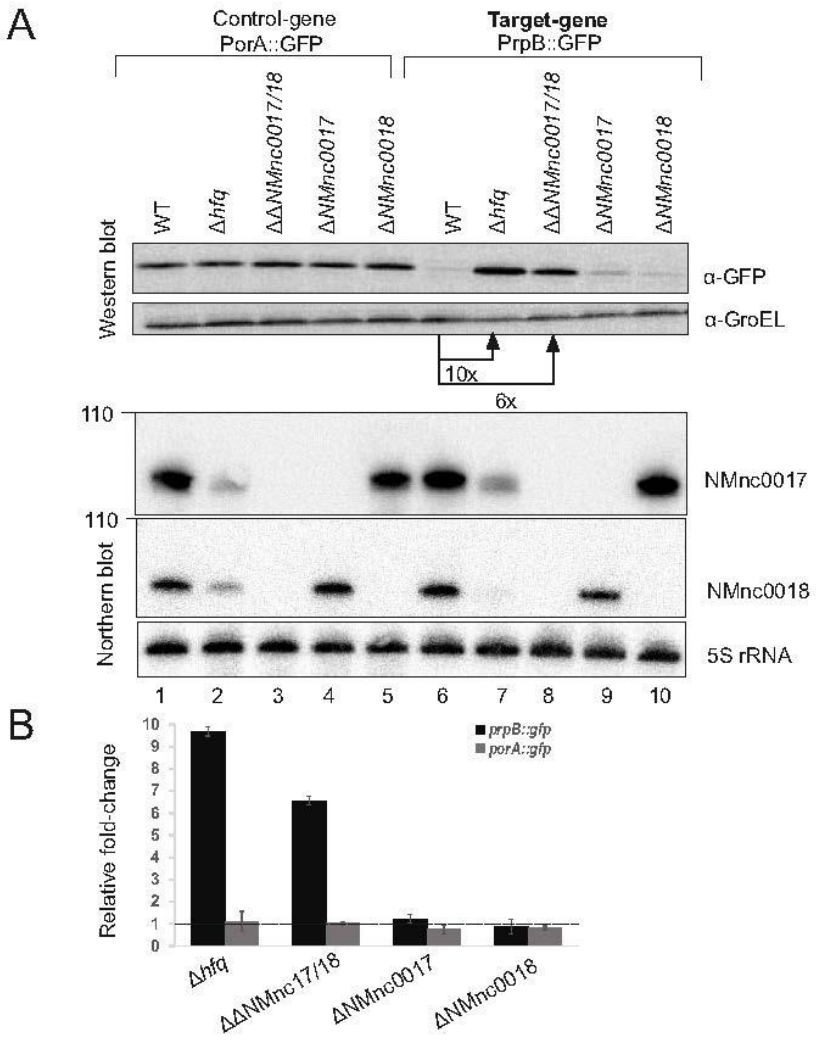

Figure 6-14 *In vivo* verification of *prpB* repression by NMnc0017 and NMnc0018

(A) *N. meningitidis* 8013 wild-type (wt), Δ*hfq*, ΔΔ*NMnc0017/NMnc0018*, Δ*NMnc0017* and Δ*NMnc0018* deletion mutants expressing either the control-*gfp* fusions or *prpB-gfp* fusions were grown to mid logarithmic phase (OD_{600nm} 0.5) in $GCBL^{++}$. Subsequently, protein and RNA samples were taken and analyzed by western blot and northern blot. Whole cell protein fractions were detected with anti-Gfp antiserum. GroEL was used as a loading control. The used oligonucleotides for northern blot analyses are listed in Table 4-32. 5S rRNA served as loading control. (B) Relative fold expression changes of *prpB::gfp* and *porA*::*gfp* (control) fusions upon deletion of *hfq*, both sRNAs NMnc0017 and NMnc0018 or of each sRNA alone analyzed by Western blot analysis for Gfp in comparison with the respective wild-type backgrounds are summarized in the bar diagram. Error bars indicate the standard deviations among three technical replicates.

Next, the paralogous sRNAs and the *prpB* mRNA leader were tested for a direct interaction *in vitro*. Therefore, EMSAs were performed using *in vitro* synthesized RNAs. The sRNAs were radioactively labeled and used at constant concentrations into the EMSAs while the *prpB* 5'end was applied unlabelled and with increasing concentrations. Both NMnc0017 and NMnc0018 revealed concentration-dependent RNA-RNA duplex formation with the *prpB* leader (Figure 6-15). Together, these results confirm the predicted RNA interaction between NMnc0017, NMnc0018 and their target *prpB*.

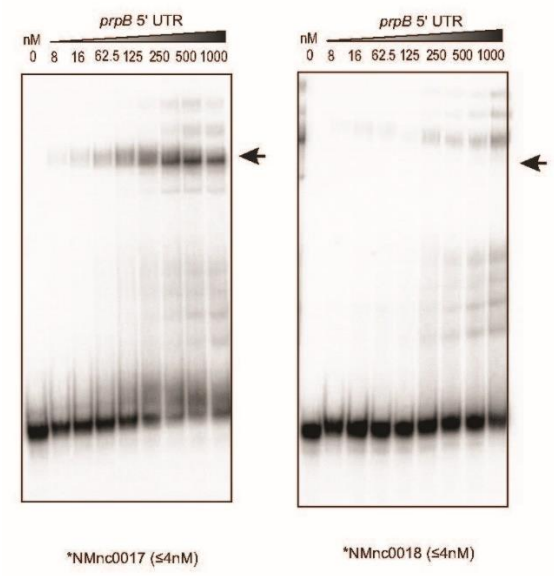

Figure 6-15 EMSAs prove direct interaction between the 5'end of *prpB* and the sRNAs NMnc0017 and NMnc0018 *in vitro*

EMSAs were performed with *in vitro* synthesized sRNAs (NMnc0017/NMnc0018) and the 5'end of the *prpB* mRNA (-289 to +42 relative to the annotated start codon). Approx. 0.04 pmol of ^{32}P-labeled sRNA was incubated with increasing amounts of unlabeled *prpB* 5'UTR (0-1000 nM) for 20 min at 37 °C. Arrows indicate the RNA-hybrid.

The *prpB* target sites of NMnc0017 and NMnc0018 are canonical binding sites overlapping the SD and start codon on the mRNA (Figure 6-12) indicating sRNA-induced translational inhibition as the mechanism of repression. In order to validate this mechanism of repression *in vitro*, the sRNA interaction sides were mapped on nucleotide level. Therefore, an in-line-probing assay was performed with *in vitro* transcribed radioactively-labelled sRNAs in the absence or presence of unlabeled *prpB* leader (Figure 6-16 A). Subsequently, the results of the in-line probing assay were compared to secondary structure predictions of NMnc0017 and NMnc0018 using mfold ((140), chapter 5.33). Both sRNAs were predicted to fold three stem-loops (SL1, SL2, SL3) which are separated by single-stranded regions (Figure 6-16 B). Comparing the *in silico* predicitons to the in-line probing results, the addition of unlabeled *prpB* leader resulted in a clear footprint in the second stem loop region (SL2) of both sRNAs, suggesting that this site is involved in the sRNA–mRNA interaction. Together, the structure probing results support an interaction between the second stem loop of both sRNAs and the SD/AUG sequence in the *prpB* 5'UTR.

.

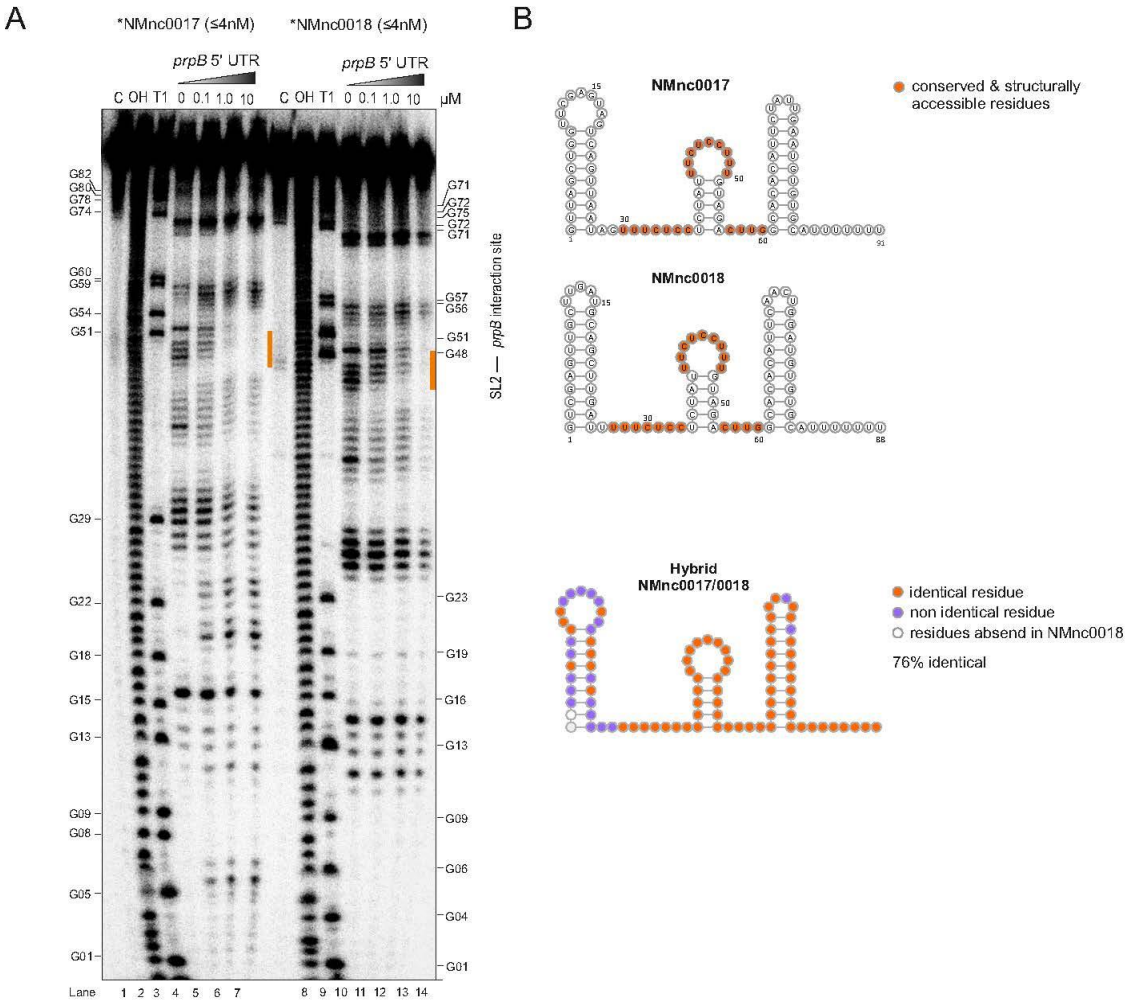

Figure 6-16 In-line probing assay uncovers interaction sites between the sRNAs NMnc0017 and NMnc0018 and the 5'end of *prpB* mRNA

(A) Approx. 0.04pmol of ^{32}P-labeled sRNA were incubated in the absence (0 µM) or presence (0.1, 1, 10 µM) of *prpB* mRNA 5'UTR for 48 hours at room temperature. Untreated RNA (lane C), partially alkali (lane OH) or RNase T1 (lane T1) digested NMnc0017 and NMnc0018 served as nucleotide ladders. (B) Predicted secondary structures of the sRNAs NMnc0017 and NMnc0018 using the program mfold ((140), chapter 5.33). The 5'UTR of the dicistronic *prpB-prpC* mRNA was predicted to interact with three single stranded regions (marked in orange) of both sRNAs investigated. Identical residues and non identical residues (marked in purple) of both sRNAs are represented by the hybrid sRNA structure.

The *prpB* gene is part of the methylcitrate cycle which allows meningococci to catabolize propionic acid to pyruvate and succinate (112). To test the *in vivo* impact of the sRNAs NMnc0017 and NMnc0018 on *prpB* expression and thus propionic acid catabolism, both *N. meningitidis* wild-type and NMnc0017/NMnc0018 deletion strains were grown in CDM (Table 4-10) without any supplements and in CDM supplemented with 5 mM propionic acid (Figure 6-17 A). Although the addition of proprionic acid to the medium affected growth capacities in both the wild-type and double knockout strain, the bacterial growth of both strains was similar to each other under each investigated condition (Figure 6-17 B). In line with that, NMnc0017 and NMnc0018 were not differentially expressed in bacteria

grown in CDM supplemented with 5 mM propionic acid compared to growth in CDM without supplements (Figure 6-17 B). As both *prpB* and *prpC* were expressed for a longer time in CDM supplemented with proprionic acid (ten hours) than in CDM without any supplements (six hours) (Figure 6-17 A), it might be possible that *prpB* and *prpC*, or the whole methylcitrate cycle, is regulated by additional sRNAs or other gene expression regulators.

Thus, the RIP-seq approach with an epitope-tagged Hfq protein not only detected association of sRNAs with Hfq, but also identified mRNA targets of those sRNAs at nucleotide-level resolution, allowing the reliable design of translational reporter systems to validate sRNA mediated regulation of targets *in vivo*. Moreover, gel-shift experiments and in-line probing results verified a direct interaction between the second stem loop of the paralogous sRNAs NMnc0017/18 and the SD/AUG sequence in the *prpB* 5'UTR *in vitro*. Yet, *in vivo* growth curves suggest that further gene expression regulators might tightly control *prpB* expression levels.

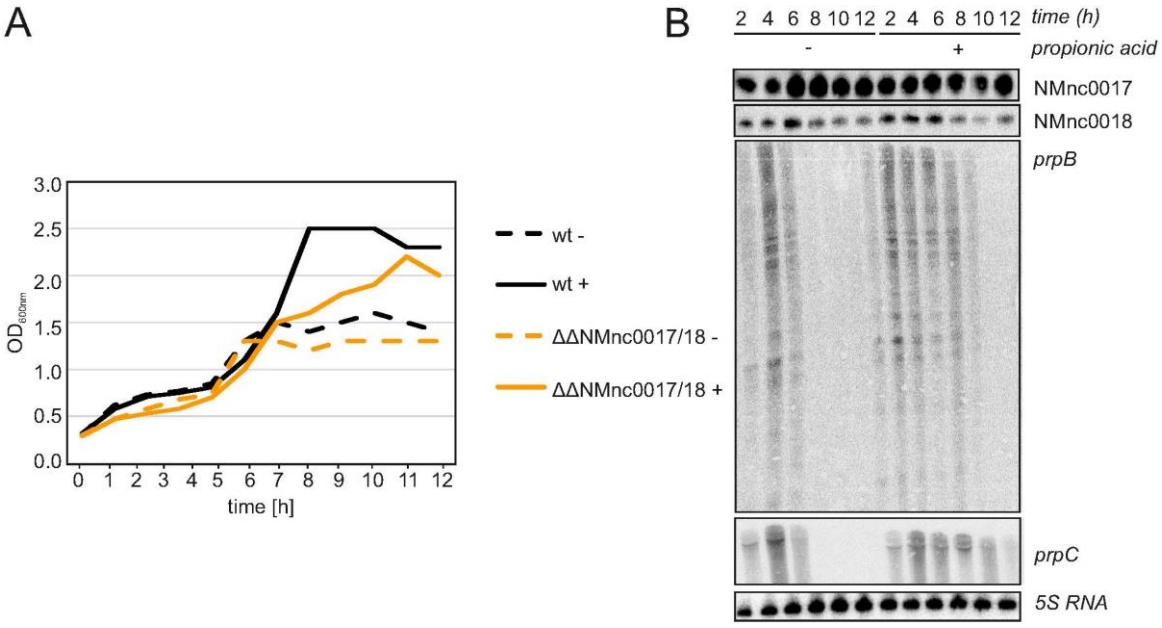

Figure 6-17 Expression analysis of the dicistronic *prpB-prpC* genes and the sRNAs NMnc0017 and NMnc0018 in chemically defined medium with and without treatment with proprionic acid

(A) Growth curves for *N. meningitidis* strains 8013 wild-type and ΔΔNMnc0017/NMnc0018 in liquid CDM medium with (+) and without (-) treatment with proprionic acid, by determining the optical density at 600 nm. One representative of three independent experiments is shown. (B) Total RNA was extracted at distinct time points (h) from *N. meningitidis* 8013 wild-type strain grown in CDM medium (Table 4-10) with and without treatment with 5 mM proprionic acid (+, -) and investigated by northern blot analysis using labeled DNA probes complementary to the indicated genes (Table 4.30). The housekeeping 5S rRNA served as a loading control.

6.5. ProQ is a second global RNA-binding protein in *N. meningitidis*

6.5.1. Genetic organization and expression of meningococcal ProQ

FinO/ProQ domain proteins are a novel class of conserved RBPs which regulate an unusual variation in RNA target number and are required for full virulence in some bacteria (159). As described before, *N. meningitidis* does not encode for CsrA proteins, but expresses Hfq and encodes a minimal ProQ/FinO-domain protein exhibiting RNA chaperone activity *in vitro* (111). Yet, the *in vivo* RNA target suite as well as the physiological role of meningococcal ProQ have been elusive and were therefore analyzed in course of this thesis.

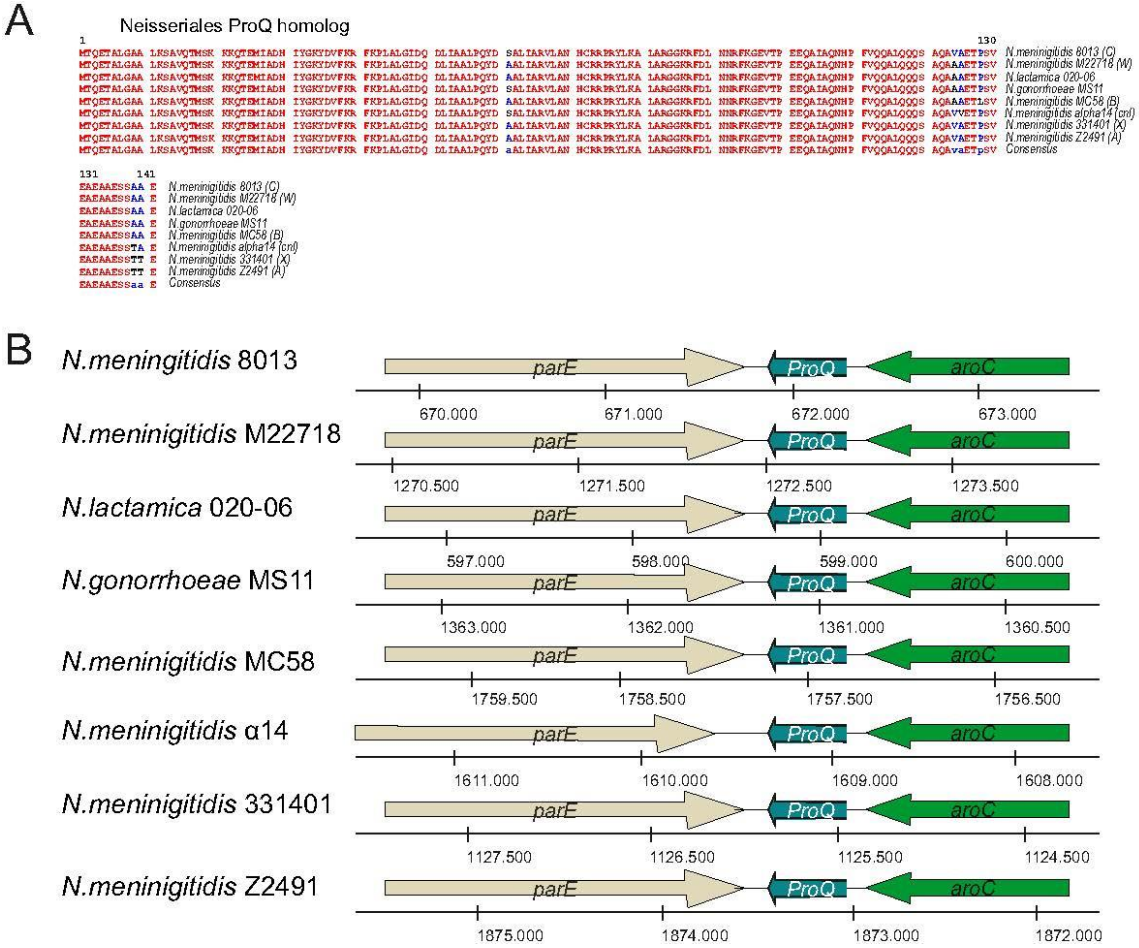

Figure 6-18 Genomic organization of meningococcal ProQ

(A) Amino sequence alignment of the ProQ protein from *N. meningitidis* strains 8013, MC58, Z2491, α14, M22718 and 331401 reflecting distinct meningococcal serogroups, *N. lactamica* strain 020-06 and *N. gonorrhoeae* strain MS11. Serogroups are put in parentheses. The degree of conservation is indicated by the colour of the nucleotides (red: high conservation; blue: little conservation, black: little or no conservation). (B) Schematic illustration of the ProQ locus in the same *N. meningitidis* strains as in panel A. The given nucleotides below indicate genomic positions, gene sizes and distances to flanking genes.

In *N. meningitidis* strain 8013, ProQ is encoded as a single-copy gene at the locus NMV_0689 (Figure 6-18) and orthologous to the previously described ProQ/FinO family

RNA chaperone NMB1681 of strain MC58 (111) (Figure 6-18 A). As indicated by the dRNA-seq data (chapter 6.1)(117), *proQ* is transcribed from its own promotor and located on the minus strand between *parE* encoding for topoisomerase IV subunit B and the chorismate synthase gene *aroC.* Both the nucleotide sequence and genomic localization of ProQ are highly conserved among distinct meningococcal strains as well as in various *Neisseria* species (Figure 6-18 B).

To further investigate the expression profile of ProQ in meningococci during early, mid and late logarithmic growth in GCBL^{++} (chapter 4.4.2), a *N. meningitidis* 8013 strain harboring a chromosomally encoded ProQ-3xFLAG protein (chapter 5.12.5) was used with an anti-FLAG monoclonal antibody. As depicted in Figure 6-19, western blot analysis showed that ProQ is constitutively expressed and nearly as abundant as the highly expressed RNA chaperone Hfq. Together, the gene conservation and expression data suggest an important role of ProQ in the physiology of these β-proteobacteria.

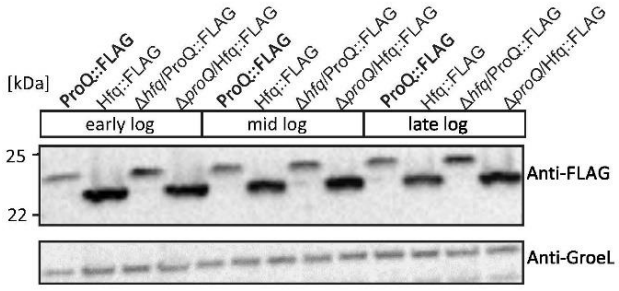

Figure 6-19 Expression profile of ProQ protein

Equal amounts of *N. meninigitids* strain 8013 cells (OD_{600nm} = 0.01) with chromosomally FLAG-tagged Hfq in the wild-type and a Δ*proQ* genetic background and chromosomally FLAG-tagged ProQ in the wild-type and a Δ*hfq* genetic background were analyzed by Western blotting with mouse anti-FLAG antibodies in three growth phases (early logarithmic, mid logarithmic and late logarithmic growth phase). GroEL served as a loading control.

6.5.2. ProQ is not essential in meningococci but affects viability in a *hfq* deletion mutant.

To experimentally assess the biological function of ProQ in *N. meningitidis*, *proQ* deletion mutants (Δ*proQ*) and *proQ* complemented strains (Δ*proQ*-C) were generated in a wild-type and an *hfq* deletion strain (Δ*proQ* Δ*hfq*) in *N. meningitidis* 8013 (chapters 5.12.1, 5.12.2 and 5.12.3). As depicted in Figure 6-20, the deletion of *proQ* did not affect the expression levels of Hfq and *vice versa*. In contrast to the deletion of *hfq*, deletion of *proQ* in the wild-type strain did not affect growth in GCBL^{++} (chapter 4.4.2) as determined by measuring OD_{600nm} (Figure 6-20). However, the deletion of *proQ* resulted in an additive growth defect in a *hfq* deletion mutant (Figure 6-20). In addition, the *proQ* and *hfq* double mutant formed still smaller colonies on solid media when compared to each the *hfq* and the *proQ* single

mutants as well as to the wild-type strain, respectively (data not shown). These data therefore indicate that (i) ProQ is not essential for survival of meningococci in a rich medium and (ii) probably has overlapping functions with Hfq that might allow a (partial) compensation of ProQ function by Hfq in a ProQ deletion mutant but not *vice versa*.

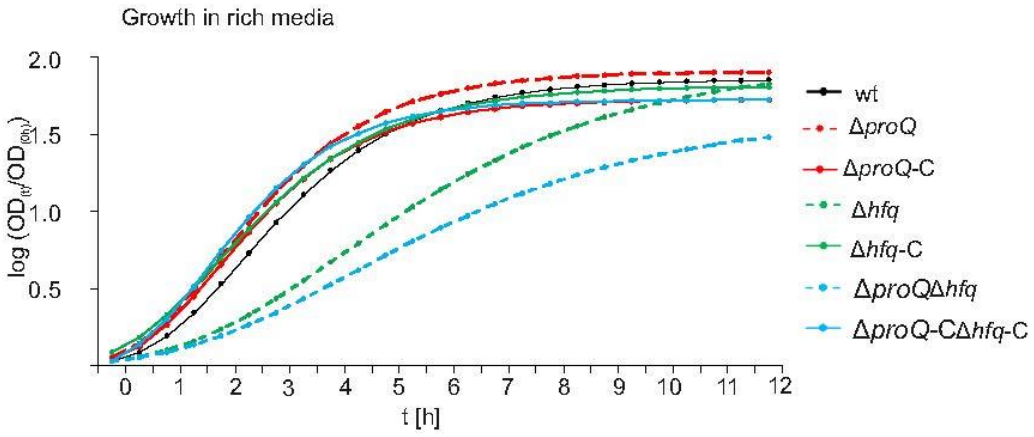

Figure 6-20 ProQ is required for optimal growth of a Δ*hfq* strain

Growth of *N. meningitidis* 8013 wild-type (wt), Δ*proQ*, complemented Δ*proQ*-C, Δ*hfq*, complemented Δ*hfq*-C, Δ*proQ*Δ*hfq* and complemented Δ*proQ*-C Δ*hfq*-C strains in GCBL^{++} medium as determined by measuring the OD_{600nm} in a 96-well TECANplate reader. The data represent mean values of three independent experiments.

6.5.3. ProQ is required for full meningococcal virulence *in vitro* and contributes to oxidative stress and UV irradiation resistance

In order to investigate the influence of ProQ on the different steps required for the transition from meningococcal colonization to invasive infection (4,6,160), an array of established *in vitro* an *ex vivo* virulence assays was employed which aimed to comprehensively model all major steps in the disease process (Figure 6-21). To successfully colonize the mucosa of the human nasopharynx which is the sole ecological niche of *N. meningitidis* the bacteria have to form biofilms on the surface of the mucosal cells (161,162). However, while Hfq mutants were severely impaired in biofilm formation, there was no significant difference between the wild-type and the *proQ* deletion strain in an *in vitro* biofilm assay (Figure 6-21 A). Since meningococci have to frequently face temperature changes depending on the ambient air temperature in the human nasopharynx the impact of *proQ* deletion on temperature-dependent growth was also assessed. Of note, temperature adaption is mediated by mRNA structure regulation (163) and moderate temperature changes were recently shown to affect growth and therefore fitness of meningococci (164). However, as depicted

in Figure 6-21 B, there was also no temperature-dependent difference in the growth phenotype between a wild-type an a *proQ* deletion strain.

To initiate an invasive infection, meningococci have to first cross the epithelial cell barrier lining the nasopharynx and subsequently to survive in the human blood stream (1). As shown in Figure 6-21 C and D, adhesion to and invasion of the human nasopharyngeal epithelial cell line Detroit562 was also not impaired in a *proQ* deletion strain yet.

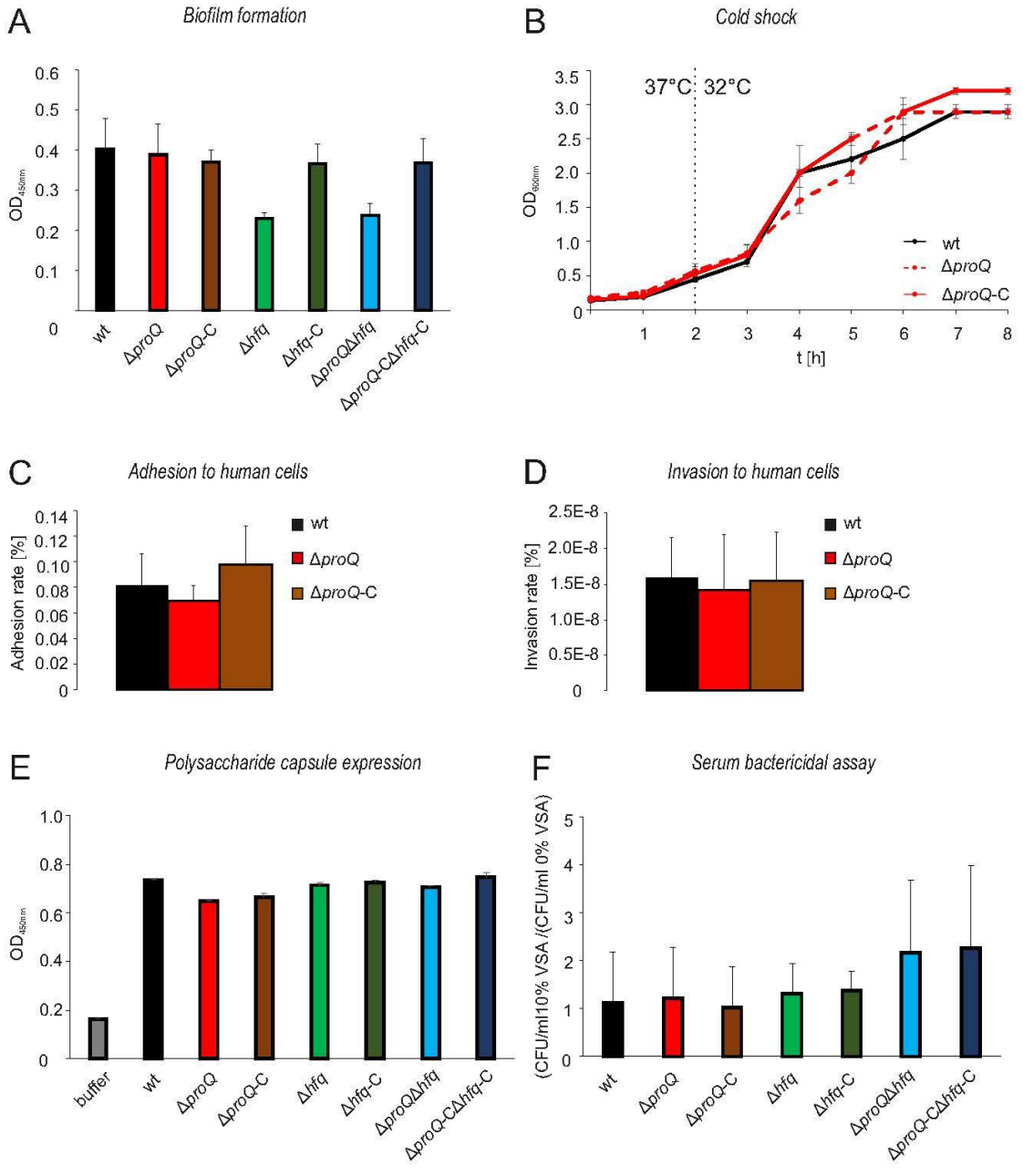

Figure 6-21 ProQ is not required for the interaction with human epithelial cells or for serum resistance

(A) Crystal violet assay of *N. meningitidis* 8013 wild-type (wt), Δ*proQ*, complemented Δ*proQ*-C, Δ*hfq*, complemented Δ*hfq*-C, Δ*proQ*Δ*hfq*, complemented Δ*proQ*-C Δ*hfq*-C strains in GCBL^{++} after 17.5h incubation time. The biofilm on the ground of the 96-well microtiter plate was stained with crystal violet prior to measuring the OD_{450nm} values with an ELISA-plate reader. The diagram shows OD_{450nm} values of the stained

biofilm for each strain minus the blank. Cut off= 3 times blank. (B) Growth curve of *N. meningitidis* 8013 wt, Δ*proQ* and complemented Δ*proQ*-C strains grown at 32 °C in GCBL^{++}as quantified by OD_{600nm} (x-axis) over time in hours (y-axis). The arrow indicates the time point of changing temperature from 37 °C to 32 °C. (C) Adhesion rates of *N. meningitidis* 8013 wild-type (wt), Δ*proQ* and complemented Δ*proQ*-C strains to the human nasopharyngeal epithelial cell line Detroit562. The error bars represent the standard error of the mean of three independent experiments. (D) Invasion rates of *N. meningitidis* 8013 wild-type (wt), Δ*proQ* and complemented Δ*proQ*-C strains to the human nasopharyngeal epithelial cell line Detroit562. For each strain, the adhesion rate was calculated as the number of colony forming units (CFU) recovered after 4 h of infection divided by the seeded CFU defined in parallel. Shown is the average adhesion rate of each mutant strain given on the y- axis from three independent experiments. The error bars represent the standard error of the mean. (E) ELISA of *N. meningitidis* 8013 wild-type (wt), Δ*proQ*, complemented Δ*proQ*-C, Δ*hfq*, complemented Δ*hfq*-C , Δ*proQ*Δ*hfq* and complemented Δ*proQ*-C Δ*hfq*-C strains for determining *N. meningitidis* serogroup C capsule expression. The bar diagram represents the mean of three independent experiments. The error bars represent the standard error of the mean. (F) Bactericidal assay of *N. meningitidis* strains 8013 wild-type (wt), Δ*proQ*, complemented Δ*proQ*-C, Δ*hfq*, complemented Δ*hfq*-C, Δ*proQ*Δ*hfq* and complemented Δ*proQ*-C Δ*hfq*-C. Meningococci (10^5/ml) were incubated in 0% NHS and 10% NHS, and the number of CFU was determined after 60 min of incubation at 37 °C by plating serial dilutions. Shown are the average relative proportions of CFU of each mutant strain given on the y- axis from three independent experiments relative to the wild-type control. The error bars represent the standard error of the mean.

To avoid being killed by professional phagocytes and, crucially, the complement system encountered in the human bloodstream, *N. meningitidis* further employs multiple mechanisms including the expression of a polysaccharide capsule and of numerous DNA damage repair and oxidative stress response genes (165-168). Again, there was no significant difference in the expression of the serogroup C polysaccharide capsule (Figure 6-21 E) and in the survival to 10% human serum (Figure 6-21 F) between the wild-type and the mutant strains. In addition to human serum complement, meningococci also need to cope with oxidative stress exerted by phagocytic cells. In fact, *hfq* as well as p*roQ* deletion strains were significantly more susceptible to the oxidative stress causing agent H_2O_2 compared to the wild-type (Figure 6-22 A). Additionally, *hfq* but not *proQ* deletion strains were significantly more susceptible to the oxidative stress causing agent paraquat compared to the wild-type (Figure 6-22 B). To further investigate the DNA damage repair capacity, which is also central in oxidative stress response, the *N. meningitidis* strains were exposed to different doses of UV light. Again, the *proQ* and *hfq* single deletion strains showed significantly decreased survival rates compared to the wild-type while the knockout of both ProQ and Hfq lead to an additive susceptibility to DNA damage (Figure 6-22 C).

In conclusion, ProQ is not required for the interaction with human cells and serum resistance but for survival after DNA damage induced by exposure to UV light and oxidative stress suggesting a novel role of this class of RNA chaperones in oxidative stress response.

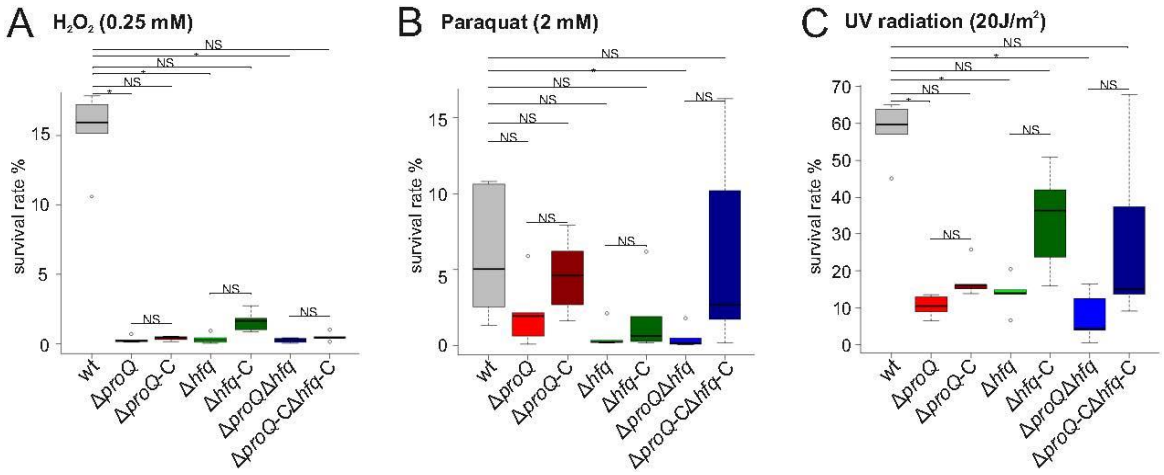

Figure 6-22 ProQ mediates oxidative stress tolerance

(A, B) Sensitivity of. *N. meningitidis* 8013 wild-type (wt), Δ*proQ*, complemented *ΔproQ-C*, Δ*hfq*, complemented *Δhfq-C*, Δ*proQ*Δ*hfq* and complemented *ΔproQ-C Δhfq-C* strains to oxidative stress. Bacterial were grown in GCBL^{++} to OD_{600nm} 0.5 and serial dilutions were incubated at 37 °C with the indicated concentration of H_2O_2 for 15 min and Paraquat for 60min. The number of surviving bacteria was determined by plating serial dilutions. The data are presented as box-and-whisker plots of five independent experiments. P values were determined with the Kruskal-Wallis rank sum test followed by two-sided Dunn's test for multiple comparisons with Bonferroni adjustment (n = 9) of each mutant against the wild-type and the respective complemented strain. *P < 0.05; NS, not significant. (C) Sensitivity of *N. meningitidis* wt, Δ*proQ*, complemented Δ*proQ*-C, Δ*hfq*, complemented Δ*hfq*-C, Δ*proQ*Δ*hfq* and complemented Δ*proQ*-C Δ*hfq*-C strains to DNA damage induced by UV light. Serial dilutions of *N. meningitidis* strains grown overnight on solid media were plated on 5% blood agar plates and exposed to either zero or 20 J/m^2 of UV of 254 nm wavelength and incubated in 5% CO_2 at 37 °C for 20 h. The data are presented as box-and-whisker plots of five independent experiments. P values were determined with the Kruskal-Wallis rank sum test followed by two-sided Dunn's test for multiple comparisons with Bonferroni adjustment (n = 9) of each mutant against the wild-type and the respective complemented strain. *P < 0.05; NS, not significant.

6.5.4. ProQ is a global RBP in *N. meningitidis*

Giving the pleiotropic effects of a *proQ* deletion, the direct RNA binding partners were determined along with the precise binding-sites of ProQ using an established UV-CLIP-seq protocol for purification of cross-linked RNA–protein complexes from bacterial cells which were irradiated with UV light (96,104) (Figure 6-23). The UV-CLIP-seq experiment was performed with *N. meningitidis* strains expressing either 3× FLAG-tagged- (chapter 5.12.5) or wild-type ProQ protein which were grown in GCBL^{++} (chapter 4.4.2) to an OD_{600nm} of 2.0 representing late logarithmic growth phase. The experiment was performed twice and the obtained RNA was converted in cDNA libraries for sequencing. The mapping of the recovered cDNA sequences was done using a genome annotation containing the 5'UTRs, 3'UTRs as well as putative sRNAs detected in the dRNA-seq approach (chapter 6.1).

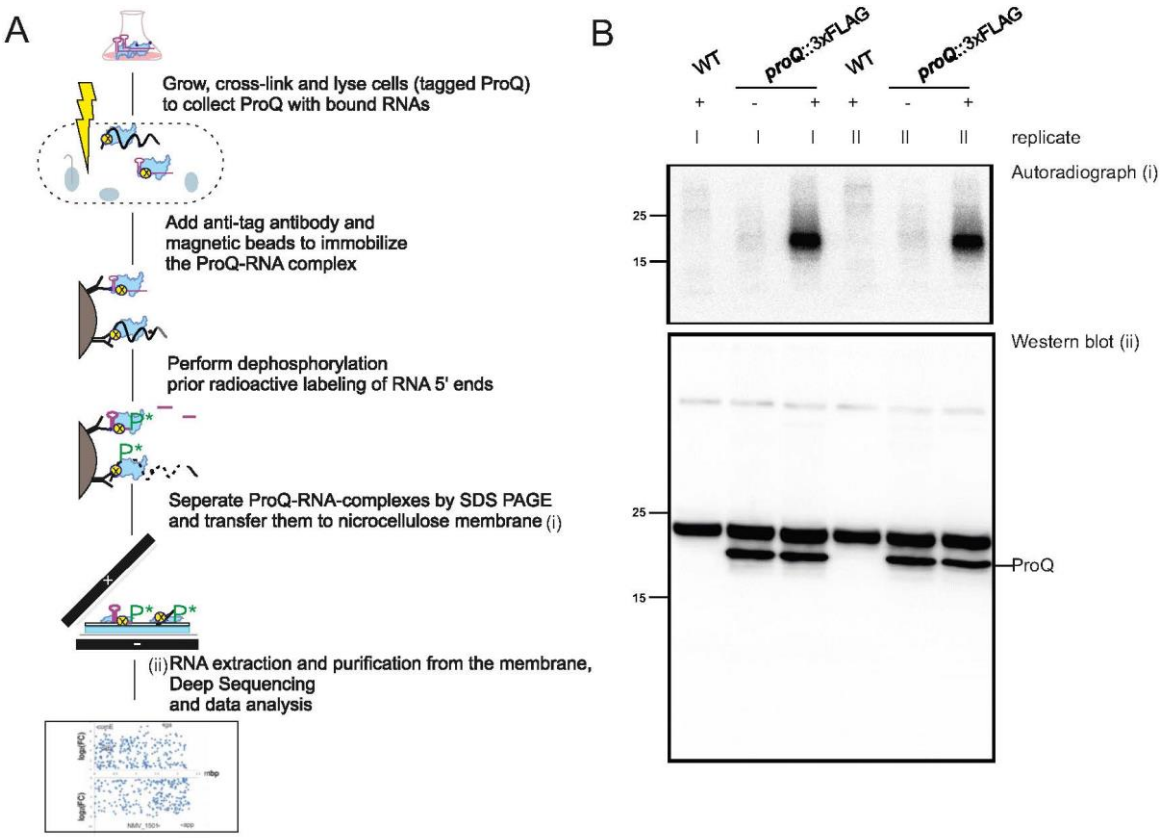

Figure 6-23 Overview of the UV-CLIP approach

(A) Schematic workflow of the UV-CLIP-seq protocol performed with *N. meningitidis* 8013 wild-type and a strain harboring chromosomal 3× FLAG tagged ProQ grown in GCBL^{++} media to late logarithmic growth phase (OD_{600nm} 2.0). (B) (Top panel) Autoradiograph of radioactively labeled RNA–protein complexes after transfer to nitrocellulose membranes. (Bottom panel) Western blot analysis using a mouse anti-FLAG antibody as a control for successful immunoprecipitation. Shown are the obtained signals for the crosslinked wild-type (WT), non-crosslinked 3× FLAG tagged ProQ strain and the cross-linked 3× FLAG tagged ProQ strain in two independent experiments. Crosslinked samples are indicated by (+), non-cross-linked samples by (-) and the two technical replicates by (I, II).

Based on this experimental strategy, 235 genome-wide CLIP-peaks compassing 297 gene associations could be identified with a $\log_2$f.c.>2 and an adjusted p-value<0.05 (Figure 6-24 A). The number of peak mapping exceeds the actual number of peaks as some peaks map to adjacent annotations (e.g. CDSs and 3'UTRs). The ProQ binding sites were evenly distributed over the entire *N. meningitidis* 8013 genome on both strands indicating that ProQ acts as a global RBP (Figure 6-24 A). The identified binding sites were analyzed with regard to different RNA classes. The majority of ProQ binding sites was detected in mRNAs (231 gene associations), followed by 30 intergenic ProQ binding sites and 22 ProQ binding sites in 16 validated sRNAs according to the dRNA-seq data (chapter 6.2, Figure 6-24 B) (117) (117). The 231 mRNA gene associations correspond to 166 distinct mRNAs. Of those, the majority of mRNAs possesses only one ProQ CLIP peak (Figure 6-24 C). Of note, the majority of ProQ binding sites inside mRNAs is situated in the 3' UTRs. While

157 ProQ binding sites were found in 3' UTRs, only 66 binding sites were located inside CDSs and only 8 binding sites inside 5' UTRs (Figure 6-24 A, B). Of note, no significant ProQ binding sites could be detected in rRNAs and only 14 CLIP peaks in tRNAs (Figure 6-24 D).

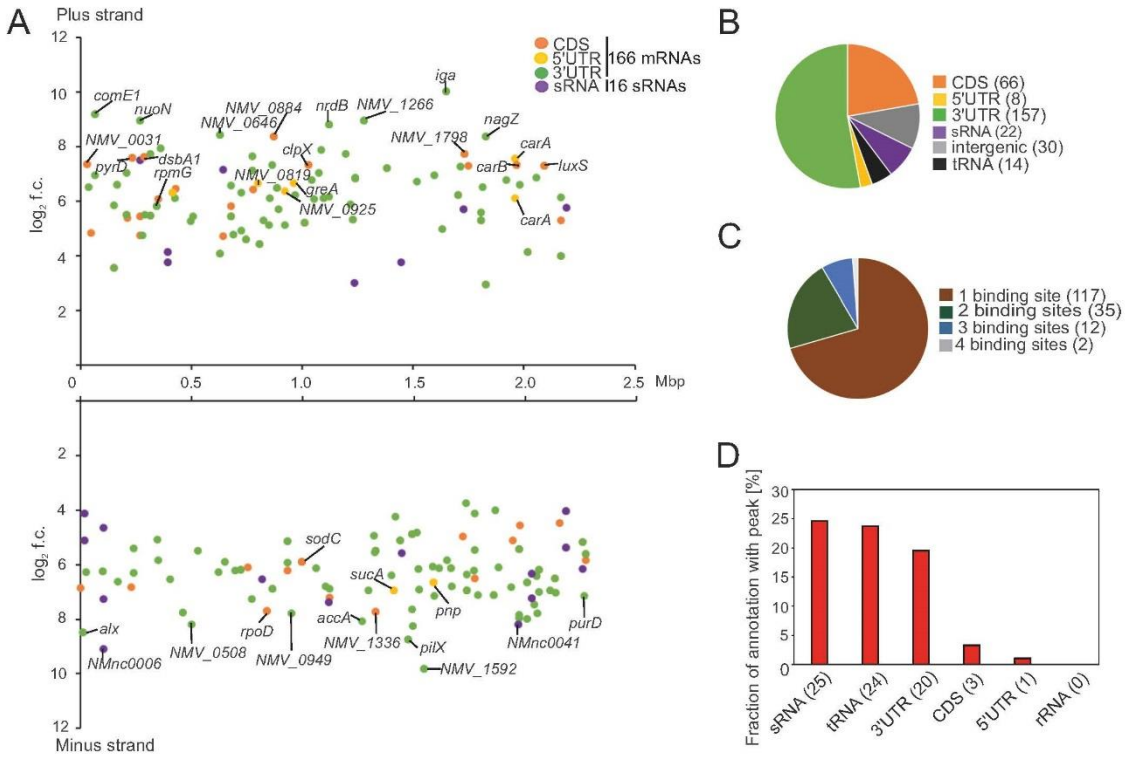

Figure 6-24 Genomic distribution of ProQ binding sites as determined by UV-CLIP-seq

(A) Scatter-plot analysis of UV-CLIP-seq results including 166 mRNAs with their associated RNA features (CDS, 5´ UTR and 3´ UTR) as well as 16 sRNAs that were significantly enriched (log_2 f.c. ≥2; p-value<0.05) in the cross-linked 3× FLAG tagged ProQ strain compared to the non-crosslinked 3xFLAG tagged ProQ strain. The y axis represents the log fold-change between the non-cross-linked 3× FLAG tagged ProQ strain and the cross-linked 3× FLAG tagged ProQ strain while the x-axis axis represents the genomic position of the enriched segments. (B) Pie chart of the ProQ UV-CLIP-seq data showing the relative proportions of ProQ-associated RNA classes. Only significantly enriched RNAs (log_2 f.c. ≥2; p-value<0.05) were included in the analysis. (C) Pie chart showing the distribution of ProQ binding-sites per mRNA based on all features (CDS, 5´ UTR and 3´ UTR) of the 165 mRNAs significantly enriched (log_2 f.c. ≥2; p-value<0.05) in the UV-CLIP-seq data. (D) The percentage of RNA features with a ProQ peak among all features in the indicated RNA class.

The two ProQ binding sites within 5' UTRs with the biggest log_2f.c. between cross-linked samples and non-cross-linked samples were identified for the *pnp* (NMV_1636) gene encoding a polyribonucleotide nucleotidyltransferase and the gene *carA* (NMV_2040) which encodes the small chain of the carbamoyl-phosphate synthase. The CLIP-peaks in 3' UTRs with the biggest log_2f.c. between cross linked samples and non-cross-linked samples belonged to *iga* (NMV_1699) encoding for the IgA-specific serine endopeptidase, the hypothetical protein NMV_1457 and *comE*1 (NMV_0284) encoding for a DNA-binding

competence protein, respectively. The CLIP-peaks inside CDSs with the biggest log_2f.c. between cross linked samples and non-cross-linked samples belonged to the genes NMV_0884 encoding an amino acid ABC transporter permease, the putative ammonium transporter NMV_1798 and the hypothetical protein NMV_1336.

Together, these data indicate that the ProQ targetome comprises over 166 mRNAs and 16 sRNAs and suggests that ProQ constitutes another global RNA chaperone next to Hfq in meningococci.

6.5.5. Meningococcal ProQ binds to DNA uptake sequences and structured RNAs

Additionally, in order to identify sequence motifs recognized by ProQ, the data set of mRNA peaks was divvied into those peaks that mapped to CDSs and those that mapped to 3' UTRs. The significant consensus motif identified by MEME (145) in the whole peak sequences was independent of the location on the mRNA and corresponded to the 12 bp neisserial DNA uptake sequence (DUS) motif ATGCCGTCTGAA (169,170) (Figure 6-25 A). Of note, the genome of *N. meningitidis* strain 8013 contains 1,474 exact copies of the canonical 12 bp DUS and another 682 copies differing only by one base, corresponding to 1,14% of the entire genome. In turn, of the 231 ProQ peak sequences identified in 166 mRNAs 45 were located in DUS (19.48%). However, given the large number of DUS in the meningococcal genome it is difficult to say whether ProQ specifically and selectively binds to DUS or whether the observed DUS binding is just due to chance, given that further 19 DUS sequences identified in the 166 mRNAs were not bound by ProQ.

Cross-link-specific mutations in UV-CLIP peaks identify contact regions of RBPs with their target RNAs at single-nucleotide resolution which can be additionally used as a base for computing RBP binding motifs (171). In the CLIP-seq data, 28% (67/235) of the ProQ peaks contained cDNA mutations. The majority of cDNA mutations were T → C transitions (Figure 6-25 B) contrasting previous CLIP-seq data of ProQ in *Salmonella* most of which were C→ T transitions (104). Further investigation is needed to clarify whether this difference in the number of detected mutations is just due to differences in the protein:RNA interaction compared to *Salmonella* work or has to do with this particular set of libraries. In order to verify if DUS sequences are nucleotide sequence motifs recognized by ProQ, a general RNA binding motif was searched for in a window of 20 nucleotides centered on

the crosslink-specific mutations using the MEME suite (145). Yet, this analysis did also not identify any common ProQ binding motif including the DUS sequence.

Yet, DUS sequences are overrepresented at rho-independent terminators (169) fitting to the enrichment of ProQ binding sites at 3'UTRs of mRNAs (Figure 6-25 C). Likewise, ProQ binding to extensive secondary structures was also observed for sRNAs as well as 5'UTR as illustrated in Figure 6-25. These data suggest that ProQ binds to regions with extensive secondary structures as frequently observed at 3'UTRs and many sRNAs and not to specific sequence motifs at the nucleotide level.

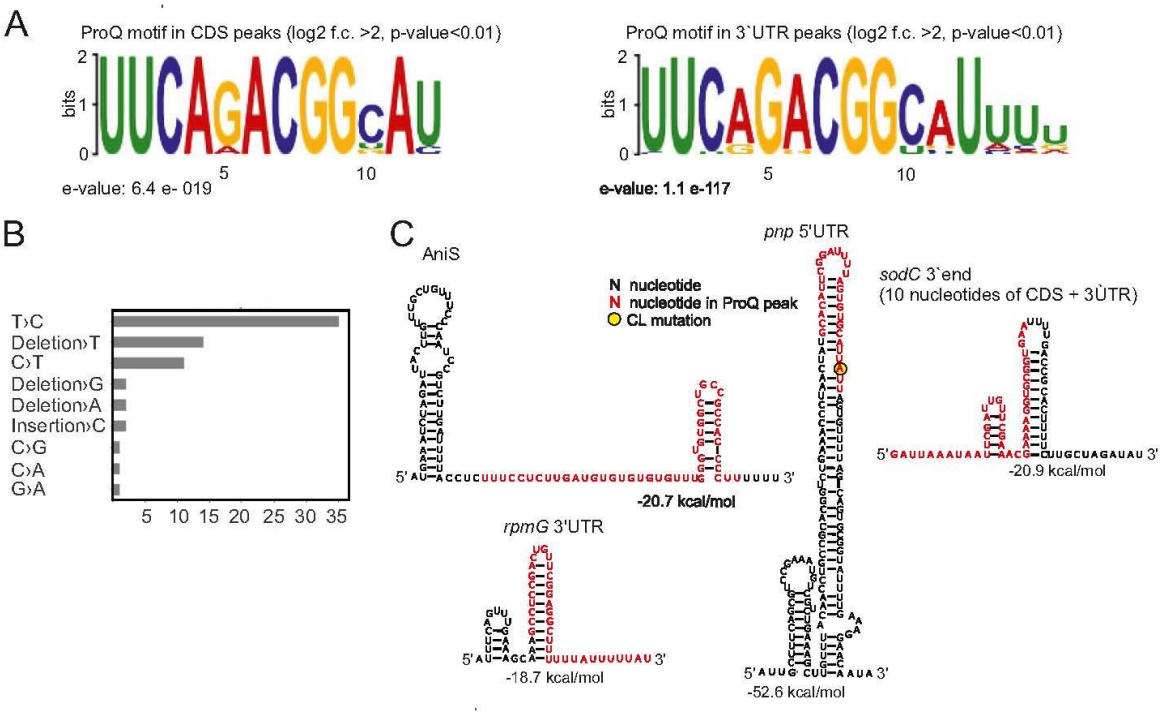

Figure 6-25 RNA binding patterns of ProQ protein

(A) ProQ binding motif identified by applying ProQ CLIP peak sequences in CDSs or 3'UTRs to the MEME program (145). (B) Relative abundance of crosslink -specific read mutations in significantly enriched RNAs (log_2 f.c. ≥2; p-value<0.05) in the UV-CLIP-seq approach. (C) Predicted secondary structures of selected *N. meningitidis* mRNA features (*sodC* 3'end, *rpmG* 3'UTR and *pnp* 5'UTR) and a sRNA (AniS) possessing a significant ProQ CLIP peak (log_2 f.c. ≥2; p-value<0.05) using mfold (172). The ProQ peak sequences are highlighted in color. The predicted folding free energies are indicated below each secondary structure.

6.5.6. ProQ and Hfq bind to overlapping yet distinct targetomes

In order to compare the two major meningococcal RBPs, a cross-comparison of the 166 mRNAs and 16 sRNAs captured by ProQ CLIP-seq (chapter 6.5.4) was performed with 401 mRNAs and 23 sRNAs of the Hfq coIP analysis (chapter 6.3). As depicted in Figure 6-26, ProQ showed significantly different RNA binding preferences compared to Hfq (Pearson's χ^2=10.8, df=3, $p < 0.05$). While Hfq binds significantly more frequently in CDSs (67% vs. 28%) ($p < 0.001$), ProQ binds significantly more frequently in 3'UTRs than Hfq

(62% vs. 13%, $p < 0.001$, 2-sample test for equality of proportions with continuity correction). These differing binding preferences might have mechanistic implications for the expression regulation of the target RNAs by both RNA chaperones.

Figure 6-26 Systematic comparison of the ProQ and Hfq binding preferences in *N. meningitidis*

Comparisons of ProQ-associated RNA features according to UV-CLIP-seq (chapter 6.5.4) with direct Hfq-associated RNA features according to RIP-seq (chapter 6.3) in the *N. meningitidis* strain 8013. In the Venn diagrams, the numbers of ProQ-bound transcripts are indicated in red circles and the numbers of Hfq-bound transcripts are illustrated in green circles.

In line with differing binding preferences, ProQ and Hfq also regulate a significantly different spectrum of biological functions as revealed by COG pathway comparison (Pearson's $\chi^2=205.6$, df=20, $p < 0.001$) (Figure 6-27). Among the 166 mRNAs with significant ProQ CLIP-peaks ($\log_2$ f.c. > 2, p.adj. < 0.05) coding for 194 COG annotated functions, many genes are involved in translation (10%) (COG J) and energy metabolism (10%) (COG C). In contrast, more than 20% of the 401 hfq-associaed mRNAs belonging to 444 COG entries code for proteins of so far unknown function (COG X) including a large proportion of pseudogenes. Together, ProQ and Hfq bind to 526 protein-encoding genes or approximately a quarter of the meningococcal mRNAome. Of note, only 41 mRNAs are directly targeted by both RBPs (Table 6-3) corroborating the view of two distinct RNA classes. Contrary to the general differing binding preferences of both RBPs (Figure 6-26), ProQ and Hfq bind the same RNA features (5'UTR, CDS, 3'UTR) in more than half of these transcripts (26/41) (Table 6-3) indicating that both RBPs might perform redundant regulatory functions on these genes. Interestingly, among this set of 41 transcripts includes the transcriptional regulator Fur known to regulate expression of the sRNA NrrF (chapters 3.2, 3.4.2), virulence-associated tfp genes (*pilX*, *pilE*, *pilC2*, *pilF*) as well as ribosome-associated genes (*rpmG*, *rpmA*, *rpmO*) (Table 6-3).

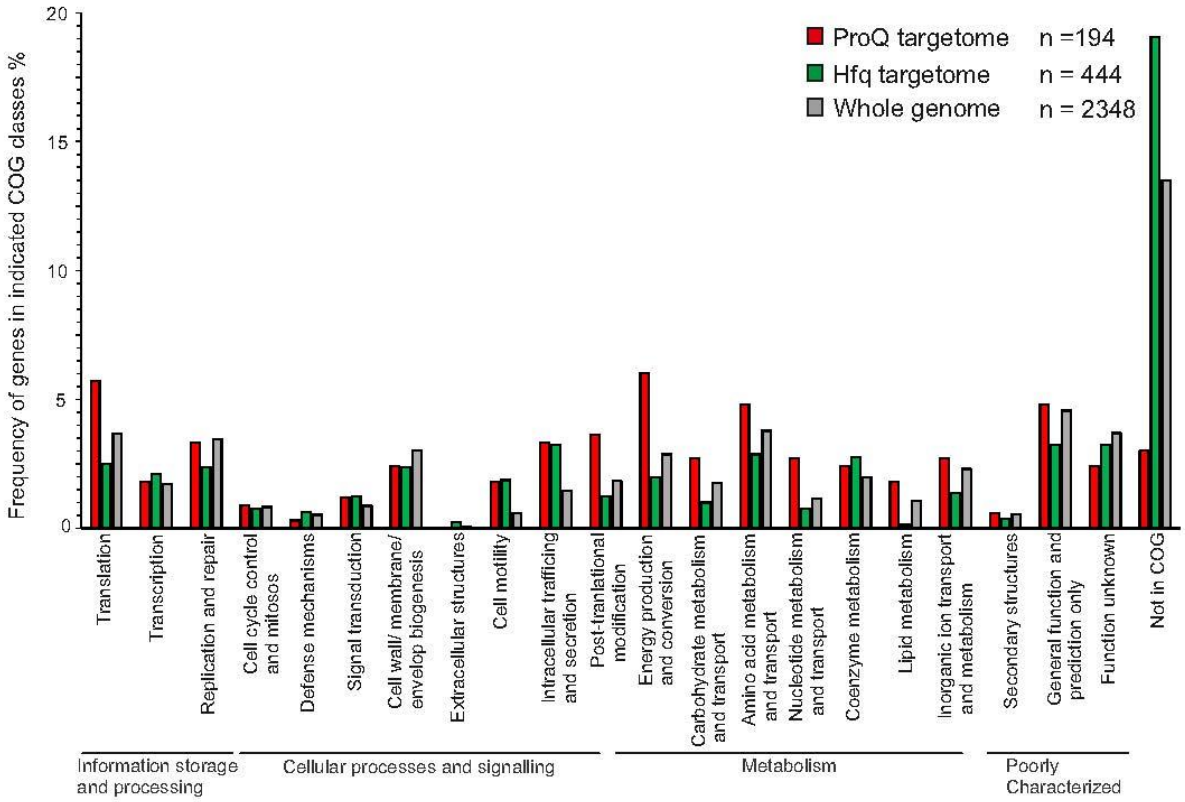

Figure 6-27 Systematic comparison of the ProQ and Hfq targetomes in *N. meningitidis*

The histogram compares the functional profile of all annotated genes with the functional profile of ProQ-associated genes as indicated by UV-CLIP-seq (chapter 6.5.4) and with the functional profile of Hfq-bound genes as determined by RIP-seq (chapter 6.3). The functional classification is based on the COG classification scheme (123).

Table 6-3 Systematic comparison of ProQ-bound mRNA features (5'UTR, CDS, 3'UTR) according to UV-CLIP-seq

Locus_tag	Gene	Product	COG class	Hfq binding region	ProQ binding region
NMV_0442	-	-	-	5`UTR	5`UTR
NMV_0646	-	-	-	CDS	CDS; 3'UTR
NMV_1509	*pilX*	Minor pilin PilX	N	CDS; 3`UTR	3'UTR
NMV_0328	*dsbA2*	Thiol:disulfide interchange lipoprotein DsbA2	C	5`UTR	CDS; 3'UTR
NMV_0019	*pilE*	Major pilin PilE	E	CDS; 3`UTR	3'UTR
NMV_0045	*pilC2*	Type IV pilus-associated protein PilC2	U	CDS	CDS
NMV_0364	*pilF*	Type IV pilus biogenesis protein PilF	U	5`UTR	CDS
NMV_2040	*carA*	Carbamoyl-phosphate synthase small chain	F	5`UTR	5'UTR
NMV_1109	-	Putative ferredoxin-like protein	C	CDS	3'UTR
NMV_1440	*sucA*	2-oxoglutarate dehydrogenase E1 component	C	5`UTR	5'UTR

Locus_tag	Gene	Product	COG class	Hfq binding region	ProQ binding region
NMV_0508	-	Putative spermidine/putrescine-binding lipoprotein	E	CDS	3'UTR
NMV_2195	*glnB*	Nitrogen regulatory protein P-II	E	CDS; 5`UTR	3'UTR
NMV_0692	*tyrB*	Aromatic amino acid aminotransferase	H	3`UTR	3'UTR
NMV_1050	*suhB*	Inositol-1-monophosphatase	G	5`UTR	3'UTR
NMV_2115	-	Putative inositol-1-monophosphatase	K	3`UTR	3'UTR
NMV_1792	*ppsA*	Phosphoenolpyruvate synthase	R	3`UTR	3'UTR
NMV_0356	*rpmG*	50S ribosomal protein L33	J	CDS; 3`UTR	3'UTR
NMV_0359	*rpmA*	50S ribosomal protein L27	J	CDS; 3`UTR	3'UTR
NMV_1803	*rpsO*	30S ribosomal protein S15	J	CDS; 5`UTR; 3`UTR	3'UTR
NMV_2048	*queA*	S-adenosylmethionine:tRNA ribosyltransferase	J	CDS; 3`UTR	3'UTR
NMV_0480	-	Putative HTH-type transcriptional regulator	K	CDS; 5`UTR	3'UTR
NMV_0957	*greA*	Transcription elongation factor GreA	K	5`UTR	5'UTR
NMV_1688	*rpoH*	RNA polymerase sigma factor RpoH	K	5`UTR	3'UTR
NMV_0057	*comE1*	DNA-binding competence protein ComE1	L	CDS; 3`UTR	3'UTR
NMV_1064	*prc*	Carboxy-terminal processing protease	M	CDS; 3`UTR	3'UTR
NMV_2211	-	Hypothetical protein NMV_2211	O	CDS	3'UTR
NMV_0013	*alx*	Alx protein	P	CDS	3'UTR
NMV_0223	*fur*	Ferric uptake HTH-type transcriptional regulator	0	3`UTR	CDS; 3'UTR
NMV_0932	-	Putative dioxygenase	R	5`UTR	CDS; 3'UTR
NMV_1646	*hfq*	Hfq protein	R	CDS;5`UTR; 3`UTR	3'UTR
NMV_1941	-	Putative oxidoreductase	R	5`UTR	3'UTR
NMV_1336	-	Hypothetical protein NMV_1336	P	3`UTR	CDS; 3'UTR
NMV_0640	-	Hypothetical protein NMV_0640	U	3`UTR	3'UTR
NMV_2181	*luxS*	S-ribosylhomocysteine lyase	P	3`UTR	CDS; 3'UTR
NMV_1804	*secF*	Preprotein translocase subunit SecF	J	3`UTR	CDS; 3'UTR
NMV_0541	-	Hypothetical protein NMV_0541	R	3`UTR	3'UTR
NMV_0031	-	Hypothetical protein NMV_0031	-	CDS	CDS
NMV_0299	-	Hypothetical protein NMV_0299	-	CDS	3'UTR
NMV_0441	-	Hypothetical protein NMV_0441	-	3`UTR	3'UTR
NMV_0758	-	Hypothetical protein NMV_0758	-	5`UTR	CDS; 3'UTR
NMV_1295	-	Hypothetical protein NMV_1295	-	CDS	3'UTR

In addition to the different target site spectrum of mRNAs bound by both RBPs, cross-comparison of 33 sRNAs captured by ProQ UV-CLIP-seq (chapter 6.5.4) and the Hfq RIP-seq (chapter 6.3) confirms the view that both RBPs bind to different yet overlapping sRNA subclasses. For instance, the well-studied sRNAs AniS and Bns1 are associated with both ProQ and Hfq, while the paralogous sRNAs NMnc0017/18 are exclusively bound by Hfq (Figure 6-28 A). Additionally, there was a stronger positive relationship between the predicted folding energy of ProQ-associated sRNAs than Hfq-associated sRNAs and sRNA which are associated with both RBPs (Figure 6-28 B). Recently, it was described that polyU-tails of ProQ-associated sRNAs are shorter than the polyU-tails of Hfq-bound sRNAs in *Enterobacteriales* (104). However, the predicted polyU-tails of sRNA bound by meningococcal ProQ were not significantly shorter than the polyU-tails of sRNAs associated with Hfq (Kruskal-Wallis chi-squared test, p-value = 0.3786) (Figure 6-28 C).

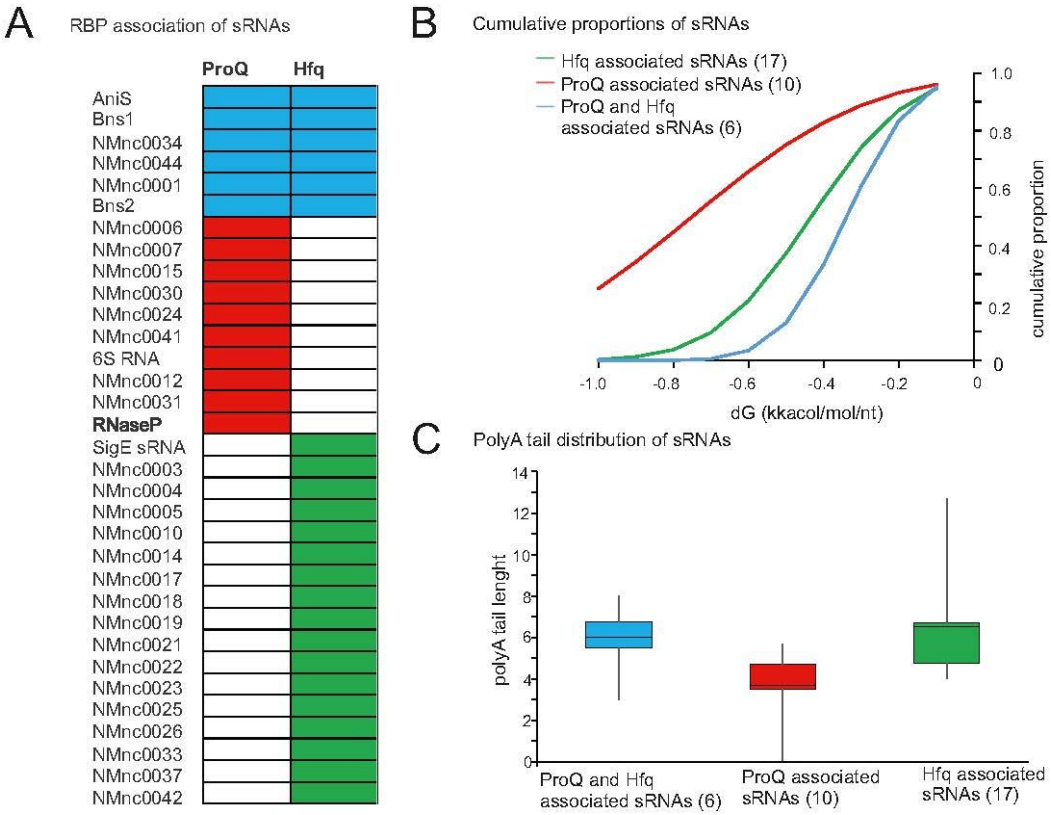

Figure 6-28 Systematic comparison of ProQ- and Hfq-associated sRNAs

(A) Colored boxes indicate sRNA association with Hfq according to RIP-seq (chapter 6.3) and sRNA association with ProQ according to UV-CLIP-seq (chapter 6.5.4). The indicated sRNAs were predicted in a dRNA-seq approach (chapter 6.2). (B) Cumulative distributions of predicted length-normalized thermodynamic ensemble folding free energies for ProQ- and Hfq-associated sRNAs, ProQ-associated sRNAs and Hfq-associated sRNAs. The data analysis bases upon the sRNA compendium shown in panel A. The folding free energies of the sRNAs were predicted with Mfold (chapter 5.33) (C) Boxplots illustrating polyU tail length distribution between ProQ-associated sRNAs, both ProQ- and Hfq-associated sRNAs and Hfq-associated sRNAs. The data analysis bases upon the sRNA compendium shown in panel A.

Taken together, ProQ and Hfq bind to approximately a quarter of the meningococcal mRNAome with differing binding preferences with 41 mRNAs targeted by both RBPs yet. Moreover, these data imply that ProQ-bound sRNAs are characterized by more extensive secondary structures compared to Hfq-bound sRNAs in *N. meningitidis*.

6.5.7. ProQ is a global gene regulator in *N. meningitidis*

Both differentially regulated transcripts and proteins were further analyzed in the *proQ* deletion strain compared to *N. meningitidis* 8013 wild-type at late logarithmic growth phase (OD_{600nm}: 2.0) in $GCBL^{++}$(chapter 4.4.2). As revealed by RNA-seq (chapter 5-24), ProQ deletion globally affects gene expression in *N. meningitidis*, changing the levels of 293 RNA features including 244 mRNAs, 12 sRNAs and one tRNA corresponding to 8.56% of the meningococcal genome (Figure 6-29). ProQ seemed to exert both direct and indirect effects on its ligands as only ~20% of ProQ-associated RNAs according to ProQ UV-CLIP-seq data (chapter 6.5.4) showed significant changes in expression levels. Indirect effects could be mediated by global transcription regulators such as 6S RNA (173), sigmaE sRNA (23) and *nusA*/ *nusB* mRNAs (174) which were differentially expressed in the *proQ* deletion strain (Figure 6-29 A). Of note, the well-studied sRNA Bns1 (37) was found to be the most dow-regulated transcript in the *proQ* deletion strains compared to the isogenic wild-type (Figure 6-29 A).

In a next step, it was tested if differences in the steady-state levels of RNA features between the *proQ* deletion and the wild-type strain were (i) dependent on the type of RNA feature (CDS, 5'UTR, 3'UTR or sRNA) and whether they (ii) were found to be corresponding to ProQ association as denoted in the UV-CLIP data (chapter 1126.5.4).

Thereby, differences in the steady-state levels of RNA features between the *proQ* deletion and the wild-type strain were significantly dependent on the type of RNA feature and whether they were found to bind ProQ in the UV-CLIP data (Kruskal-Wallis rank sum test, χ^2=764, df=7,p = 0.00). While CDSs and 5'UTRs containing ProQ peaks in the UV-CLIP data showed no significant differences in their steady state levels, both RNA features without ProQ-binding peaks were significantly higher expressed in the *proQ* deletion mutant ($p_{Bonferroni} < 0.001$, Wilcoxon signed rank test with Bonferroni adjustment for n = 8 comparisons) (Figure 6-29 B). However, the steady-state levels between CDSs or 5'UTRs with and without ProQ-binding peaks, respectively, were not significantly different (p > 0.05, Dunn's test for multiple comparison with Bonferroni adjustment fo n = 4 comparisons).

RNA features with a significantly lower steady-state expression level in the *proQ* deletion strain (log_2 f.c. < 0) comprise 3'UTRs and sRNAs ($p_{Bonferroni} < 0.001$, Wilcoxon signed rank test with Bonferroni adjustment for n = 8 comparisons), and of the 244 mRNAs with differentially regulated RNA features, 159 mRNAs have down-regulated 3'UTR regions.

Together, these data indicate that ProQ binding in 3'UTRs significantly stabilizes 3'UTR regions of mRNAs while ProQ binding in 5'UTRs, CDS and sRNAs does not, at an average, impact RNA expression levels (Figure 6-29 B). These data suggest that, comparable to *Salmonella* ProQ, also meningococcal ProQ, antagonizes exoribonucleolytic activities at mRNA 3'UTRs (104).

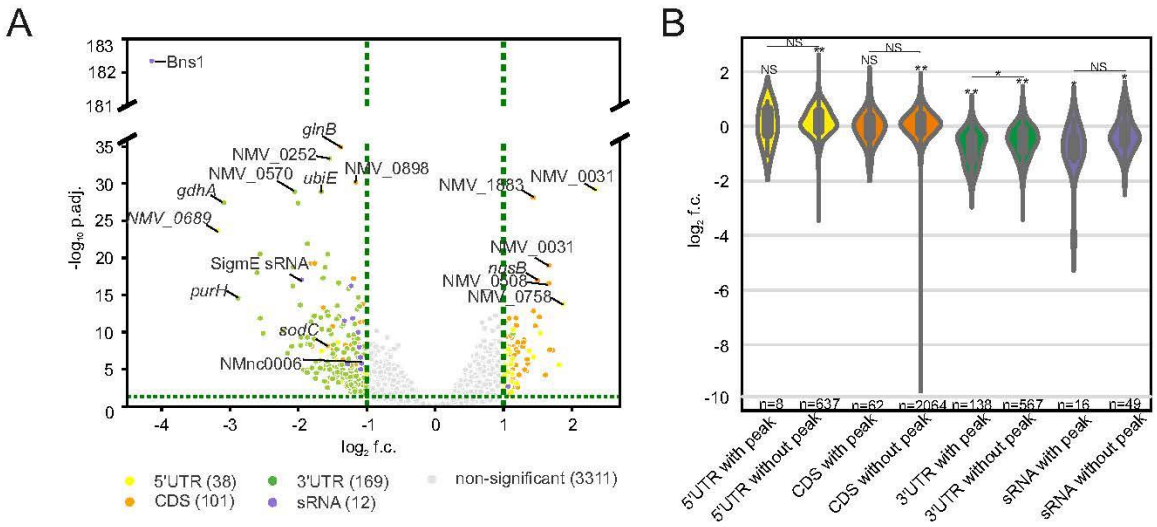

Figure 6-29 ProQ is a global regulator of gene expression

(A) The **v**ulcano plot visualizes RNA-seq results of three technical replicates of *N. meningitidis* 8013 wild-type and ProQ deletion strains grown to OD_{600nm} of 2.0 in $GCBL^{++}$. The volcano plot shows the differential expression changes of 3,631 RNA features (coding sequences, UTRs, sRNAs, tRNAs) plotted against the corresponding adjusted p-values as determined by DEseq2. Features with log_2 f.c. ≥1; p-value<0.05 are consired as significantly enriched RNA features and are therefore highlighted with color. The volcano plot (log_2FoldChange vs. padj) was generated by T. Bischler via a Python 3 script. (B) Violine plot showing the differential expression changes of RNA features (coding sequences, UTRs, sRNAs) determined by RNA-seq harboring a ProQ CLIP peak according to UV CLIP (chapter 6.5.4) or not. Violine plots were generated via a Python 3 script by T. Bischler. The Wilcoxon signed rank test with Bonferroni adjustment was used to compare the log_2 f.c. for each of the n = 8 RNA features individually against log_2 f.c. = 0 in order to test for differences in the RNA steady state levels between the wild-type and the ProQ deletion mutant. A log_2 f.c. = 0 indicates no differences in these RNA steady state levels between the mutant and the wild-type. Dunn`s test for multiple comparison with Bonferroni adjustment was used to compare the steady state levels between RNAs with and without a UV-CLIP peak for the different RNA features 5'UTR, CDS, 3'UTR and sRNA, respectively. *P < 0.05; **P < 0.01, NS, not significant.

In order to understand the impact of ProQ on meningococcal physiology, a gene set enrichment analysis (chapter 5-26) was performed of the differentially regulated transcripts in the RNA-seq data. Although ProQ regulates RNAs of all COG classes, differently expressed mRNAs coding for energy production and conversion (COG C) and amino acid metabolism

and transport (COG E) were significantly overrepresented compared to the wild-type (Figure 6-30) whereat both overrepresented COG classes contain virulence-associated meningococcal genes.

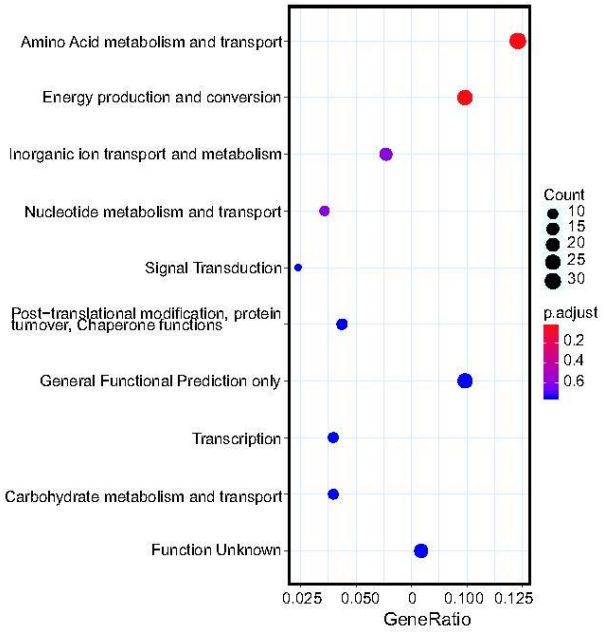

Figure 6-30 Functional enrichment analysis based on the COG classification scheme (65) of the *N. meningitidis* 8013 Δ*proQ* mutant strain compared to the wild-type control

The functional enrichment analysis was based on the fold changes and adjusted p-values of the RNA features in the RNA-seq DEseq2 results. The x-axis gives the enrichment ratios of the top ten enriched functional classes in the Δ*proQ* mutant compared to the wild-type. Significantly enriched COG classes (Padj < 0.05) are indicated by color. The figure was generated by T. Bischler using the "dotplot" function on the "enricher" results object in clusterProfiler (66) v3.10.1.

Among the differentially expressed genes for amino acid metabolism and transport (COG E) are 31 genes such as the virulence-associated NADP-specific glutamate dehydrogenase *gdhA* which plays a major role for nitrogen assimilation (129) (Table 6-4). In a previous study, the highest levels of *gdhA* mRNA were measured in hypervirulent meningococcal strains and *gdhA* was shown to be essential for systemic infection in an infant rat model (175).

Among the differentially expressed genes for energy production and conversion (COG C) are 25 genes such as genes such as *dsbA1* and *dsbA2* coding for the DsbA/DsbB system which catalyses disulfide bond formation in many virulence factors, which are essential for the establishment of infection in many bacterial pathogens (176) (Table 6-5).

Table 6-4 Differently expressed genes for amino acid metabolism and transport (COG E) between *N. meningitidis* strain 8013 wild-type and Δ*proQ*

Locus_tag	Gene	Product	log_2f.c. (5'UTR)	log_2f.c. (CDS)	log_2f.c. (3'UTR)
NMV_0661	*gdhA*	NADP-specific glutamate dehydrogenase (NADP-GDH)	-0,27	-1,6	-3,1
NMV_2195	*glnB*	Nitrogen regulatory protein P-II	-0,46	-1,4	-1,8
NMV_1914	-	Lypothetical protein NMV_1914	-0,14	-0,8	-1,3
NMV_0574	-	Hypothetical protein NMV_0574	-0,13	-0,8	-1,3

Locus_tag	Gene	Product	log_2f.c. (5'UTR)	log_2f.c. (CDS)	log_2f.c. (3'UTR)
NMV_1846	*gcvH*	Gglycine cleavage system H protein	-	-0,8	-1,6
NMV_1325	*proA*	Gamma-glutamyl phosphate reductase	-	-0,7	-1,6
NMV_1631	*cysK*	Cysteine synthase A	-	-0,6	-1,6
NMV_1163	-	Putative transporter	0,47	-0,6	-1,2
NMV_0373	-	Putative branched-chain amino acid aminotransferase	0,03	-0,6	-1,2
NMV_0400	*glnA*	Glutamine synthetase	-0,11	-0,5	-2,0
NMV_0598	*tpsB2*	TpsA2 activation/secretion protein TpsB2	-	-0,5	-1,2
NMV_1036	-	Putative transporter	-	-0,5	-1,6
NMV_0909	*gdhB*	NAD-specific glutamate dehydrogenase (NAD-GDH)	-	-0,5	-1,5
NMV_1808	-	Putative zinc-type alcohol dehydrogenase	0,86	-0,4	-1,6
NMV_1450	*metE*	5-methyltetrahydropteroyltriglutamate--homocysteine methyltransferase	-	-0,3	-2,1
NMV_1887	*aspC*	Aspartate aminotransferase	0,69	-0,3	-1,9
NMV_0193	*dadA*	D-amino acid dehydrogenase small subunit	-	-0,2	-1,1
NMV_0737	-	Putative amino-acid symporter	0,13	-0,2	-1,6
NMV_0443	*putA*	Bifunctional PutA protein	-	-0,1	-1,2
NMV_1027	*argD*	Acetylornithine/succinyldiaminopimelate aminotransferase	-	-0,1	-1,1
NMV_0377	*gloA*	Lactoylglutathione lyase	-	-0,1	-1,2
NMV_0786	-	Putative spermidine/putrescine-binding lipoprotein	0,64	-0,1	-1,2
NMV_1700	*trpB*	Tryptophan synthase beta chain	-	0,1	-1,7
NMV_1145	*aspA*	Aspartate ammonia-lyase (aspartase)	-	0,2	-1,0
NMV_2044	*carB*	Carbamoyl-phosphate synthase large chain	-	0,2	-1,2
NMV_0831	*pepA*	Cytosol aminopeptidase	1,01	0,3	-
NMV_0767	-	Putative amino acid-binding lipoprotein (HBP)	-	0,4	-1,2
NMV_2234	-	Putative aromatic amino acid transporter	1,19	0,8	-0,2
NMV_2235	*gmhB*	D,D-heptose 1,7-bisphosphate phosphatase	1,11	0,9	-
NMV_2348	-	Putative transporter	-	1,1	0,4
NMV_0690	*aroC*	Chorismate synthase	1,02	1,1	-

Significant up-regulation of each RNA feature (5'UTR, CDS, 3'UTR) in the DEseq2 results is indicated in green. Red highlights significant down-regulation (p.adj.<0.05, log_2f.c.</>1).

Comparison with a previously performed study investigating the transcriptome (177) of a *hfq* deletion strain revealed seven mRNAs differentially regulated by both ProQ and Hfq. This set of genes includes *cysK* encoding a cysteine synthase (Table 6-6) which has been

identified from *Brucella abortus* (178) as well as from the meninigococcus (179) as immunoreactive and thus may influence the immune response to septicaemic disease of *N. meningitidis* (179).

Table 6-5 Differently expressed genes for energy production and conversion (COG C) between *N. meningitidis* 8013 wild-type (wt) and Δ*proQ*

Locus_tag	Gene	Product	log f.c. 5'UTR	log f.c. CDS	logf.c. 3'UTR
NMV_0269	*nuoC*	NADH-quinone oxidoreductase chain C	-	1,0	-
NMV_0855	-	H.8 outer-membrane lipoprotein	-	1,1	0,3
NMV_1854	*nqrA*	Na(+)-translocating NADH-quinone reductase subunit A	0,8	1,3	-
NMV_1855	*nqrB*	Na(+)-translocating NADH-quinone reductase subunit B	-	1,2	-
NMV_1856	*nqrC*	Na(+)-translocating NADH-quinone reductase subunit C	-	1,0	-
NMV_1857	*nqrD*	Na(+)-translocating NADH-quinone reductase subunit D	-	1,0	-
NMV_1883	-	Putative L-lactate permease	-	1,4	0,1
NMV_2034	-	Putative membrane-associated thioredoxin	-	1,1	-
NMV_0284	*nuoN*	NADH-quinone oxidoreductase chain N	-	-0,1	-1,1
NMV_0304	*dsbA1*	Thiol:disulfide interchange lipoprotein DsbA1	0,6	0,1	-1,2
NMV_0328	*dsbA2*	Thiol:disulfide interchange lipoprotein DsbA2	-0,2	-0,4	-1,3
NMV_0916	-	Hypothetical protein NMV_0916	0,3	-0,6	-1,7
NMV_1407	*pntB*	NAD(P) transhydrogenase subunit beta	-	-0,2	-1,3
NMV_1476	*icd*	Isocitrate dehydrogenase	0,5	0,1	-1,3
NMV_2164	*aldA*	Aldehyde dehydrogenase A	-	-0,4	-1,4
NMV_1729	-	Putative NADP-dependent malic enzyme (NADP-ME)	0,7	-0,3	-1,2
NMV_1592	-	Putative NAD(P)H nitroreductase	-	-0,3	-1,4
NMV_1434	*sucD*	Succinyl-CoA synthetase alpha chain	-	-0,5	-1,7
NMV_1054	*lpdA1*	Dihydrolipoyl dehydrogenase	-	-0,5	-2,2
NMV_0949	-	Putative ferredoxin-like protein	-	-0,1	-1,0
NMV_0928	*fumC*	Fuumarate hydratase class II (fumarase C)	-	-0,2	-1,6
NMV_0443	*putA*	Bifunctional PutA protein	-	-0,1	-1,1
NMV_0358	-	Putative ubiquinone biosynthesis monooxygenase	0,3	-0,4	-1,4
NMV_0042	*msrAB*	Peptide methionine sulfoxide reductase MsrA/MsrB	0,5	0,1	-1,1
NMV_0685	*ldhA*	D-lactate dehydrogenase	1,1	0,8	-

Significant up-regulation of each RNA feature (5'UTR, CDS, 3'UTR) in the DEseq2 results is indicated in green. Red highlights significant down-regulation (p.adj.<0.05, $\log_2$f.c.</>1).

Table 6-6 Comparison of differentially regulated RNAs with Hfq regulated RNAs as described in (177)

Locus_tag	Name	Product	Base Mean (RNA-seq)	log2 f.c (RNA-seq).	CLIP peak [a]	Microarray (177)
NMV_1883	NMV_1883	Putative L-lactate permease	4111	1,4	3'UTR	-
NMV_1036	NMV_1036	Putative transporter	39	-1,6	/	-
NMV_1631	*cysK*	Cysteine synthase	6052	-1,6	3'UTR	-
NMV_0416	NMV_0416	Putative phosphate permease	1446	1,1	/	-
NMV_1879	NMV_1879	Putative alcohol dehydrogenase	30821	-1,7	CDS, 3'UTR	+
NMV_1784	NMV_1784	Hypothetical protein	1673	-1,4	CDS	+
NMV_1642	NMV_1642	Putative bacterioferritin-associated ferredoxin	588	-1,1	/	+

a indicates ProQ association according to UV-CLIP data as described in Figure 6 25. +: indicates significant up-regulation in the *proQ* deletion strain compared to the wt. -: indicates down-regulation in the *proQ* deletion strain compared to the wt, /: indicates that no ProQ CLIP peak was detected for the depicted gene

On the proteome level (chapter 5.31), *proQ* deletion significantly affects the expression of 80 proteins of which 46 are up-regulated and 34 are down- regulated (Figure 6-32). Notably, PrpC which was shown to be stabilized by the sRNAs Bns1 (37) being the most downregulated sRNA in the Δ*proQ* mutant (Figure 6-30) was the most downregulated protein in the proteomic data ($\log_2$ f.c. < -4). Since it was only moderately regulated at the transcriptional level ($\log_2$ f.c. < 0.5) (Figure 6-31), these data suggest that some of the observed gene expression changes are sRNA mediated at the post-transcriptional level. Overall, the correlation between the protein and the RNA expression differences between the *proQ* mutant and the wild-type as measured by $\log_2$ f.c. was significant but weak (Spearman's rank correlation $\rho = 0.19$, $p < 10^{-8}$) (Figure 6-31).

Comparison with the results of three previously performed studies investigating the proteome (93,94,156) of a *hfq* deletion strain further identified eight proteins such as PrpC which were differentially regulated by both ProQ and Hfq (Table 6-7). Therefore, these findings confirm moderate cross-talk of the two RNA chaperones also on the post-transcriptional level.

Together, these findings indicate that ProQ functions as a second major RNA chaperone and in contrast to Hfq affects predominantly the expression of metabolic genes at the transcriptional as well as post-transcriptional level.

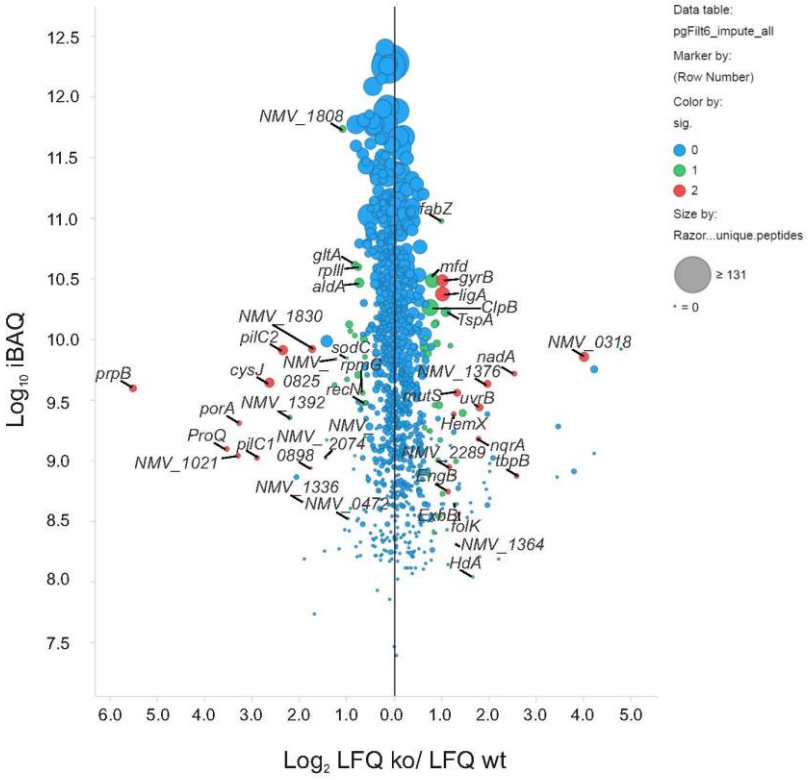

Figure 6-32 Results of quantitative proteomics of the *N. meningitidis* 8013 Δ*proQ* mutant compared to the isogenic wild-type (wt) strain

The plotted log_2- transformed LFQ protein ratios and log_{10} iBAQ values are median values calculated from two technical replicates comparing the deletion mutant to the wt strain. For the analysis, bacterial strains grown to late logarithmic growth phase (OD_{600nm} 2.0) in $GCBL^{++}$ medium were used.

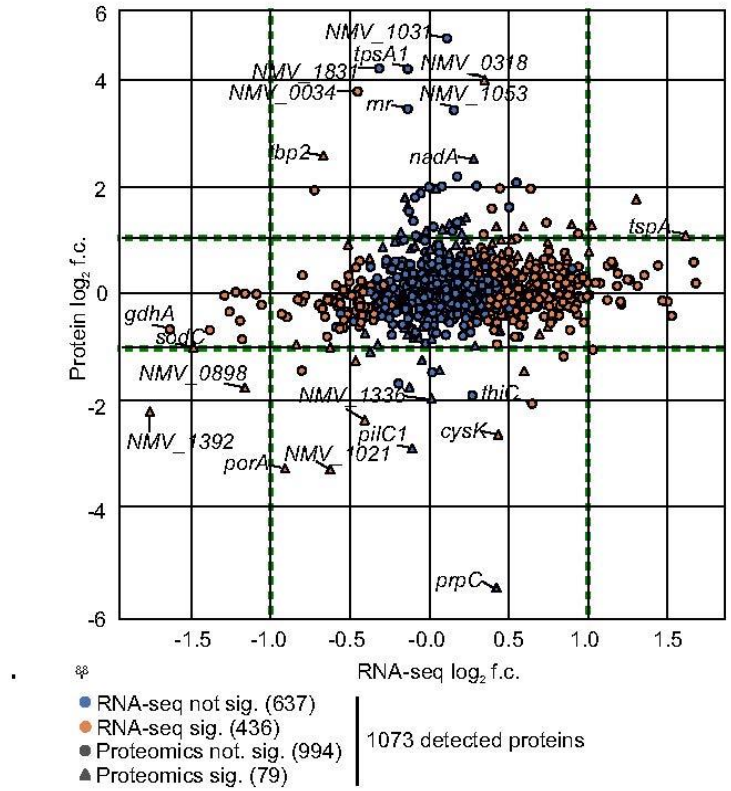

Figure 6-31 Scatter plot matching the CDSs in DESeq2 results to Proteomics data

DESeq2 results were matched to proteomics data based on locus tags and log_2 fold changes in both data sets. The scatter plot was visualized by T. Bischler via a Python 3 script making use of the pandas, matplotlib and seaborn libraries. Statistical significance of log_2 fold changes is displayed via color and shape of data points: for RNA-seq $p_{adj} < 0.05$ was required for significance, while for proteomics data significance class 1 or 2 had to be assigned. The data point representing the ProQ CDS (NMV_0689) was excluded to improve visualization.

Table 6-7 Comparison of differentially regulated ProQ proteins with Hfq regulated proteins as described in literature

Locus_tag	Name	Function	ID	Proteom[d]	CLIP peak[e]	RNA-seq[f]	Hfq a	Hfq b	Hfq c
NMV_1336	-	Hypothetical protein	S	-	CDS	/	+	/	/
NMV_0995	*sodC*	Superoxide dismutase [Cu-Zn]	P	-	3'UTR	-	/	-	/
NMV_1076	*rplI*	50S ribosomal protein L9	J	-	3'UTR	/	/	+	/
NMV_0473	*prpC*	2-methylcitrate synthase	C	-	/	/	+	+	+
NMV_0472	-	Putative methylisocitrate lyase	G	-	/	/	+	+	/
NMV_1441	*gltA*	Citrate synthase	C	-	/	/	+	+	+
NMV_0360	*rplU*	50S ribosomal protein L21	J	+	/	/	+	/	/
NMV_0378	*tspA*	TspA protein	N	+	/	+	/	+	/

a: Hfq regulated proteins as described in (94), b: Hfq regulated proteins as described in (156), c: Hfq regulated proteins as described in (93).e: ProQ association according to UV-CLIP data as described in Figure 6-24. f: ProQ regulation of RNA expression levels according to RNA-seq data described in Figure 6-29. +: indicates significant up-regulation in the proQ deletion strain compared to the wt. -: indicates down-regulation in the proQ deletion strain compared to the wt. /: indicates that no ProQ CLIP peak was detected for the depicted gene

6.5.8. ProQ stabilizes its associated sRNAs

The UV-CLIP-seq approach (chapter 6.5) predicted 16 ProQ-associated sRNAs, including members of the emerging class of sRNAs derived from 3′ mRNA regions (Figure 6-24, Figure 6-28). Five of these sRNAs hold strong expression level changes in the RNA-seq data as well (chapter 6.5.7) and were therefore selected for further experimental validation (Table 6-8).

To experimentally assess the biological impact of ProQ on its associated sRNAs, RNA samples from *proQ* deletion mutants (Δ*proQ*) and *proQ* complemented strains (Δ*proQ*-C) in a *N. meningitidis* 8013 wild-type and an *hfq* deletion strain (Δ*proQ* Δ*hfq*) were subjected to northern blot analysis. All five selected sRNAs showed decreased steady-state levels in the absence of ProQ compared to the wild-type (Figure 6-33). Out of these five sRNAs, NMnc0006 is the only intergenic sRNA which is exclusively associated with ProQ. NMnc0006 is a highly structured sRNA of 188nt length which is transcribed from the intergenic region between the hypothetical protein NMV_0097 and the putative pheromone secretion membrane fusion protein NMV_0099. Of note, NMnc0006 harbors three different ProQ binding sites (Table 6-8) indicating a strong association with ProQ. Although

AniS, Bns1 and NMnc0034 are associated with both ProQ and Hfq, deletion of both RBPs resulted only for AniS in an additive reduction of sRNA steady-state levels compared to the respective single deletion strains Δ*proQ* and Δ*hfq (*Figure 6-33*)*.

To further confirm the interaction between these five sRNAs and ProQ, sRNA half-lives were determined in rifampicin stability assays (Figure 6-34). The half-life of NMnc0006 declined from four minutes in the wild-type strain to about one minute in the Δ*proQ* strain whereas complementation of *proQ* increased the half-life to three minutes. Overall, sRNA stability decreased for all ProQ-bound sRNAs tested in the Δ*proQ* strain to 54% (±11%) of the wild-type level and reached almost wild-type levels in the ProQ complementation strain. Of note, deletion of both ProQ and Hfq did not lead to a further decrease in RNA stability of Bns1, AniS and NMnc0034 compared to the *ΔproQ* or Δ*hfq* strain (Figure 6-35).

To exclude the possibility of secondary effects causing sRNA destabilization in the *ΔproQ* strain, the direct binding of purified ProQ protein to *in vitro* transcribed, radioactively labeled sRNAs was then confirmed in electromobility-shift assays (EMSAs). As depicted in Figure 6-36, each of the ProQ-associated sRNAs shifted in a concentration-dependent manner, suggesting the formation of an sRNA–Protein complex while the ProQ-independent sRNA NMnc0017 used as control did not interact with ProQ under these conditions (Figure 6-36).

In conclusion, these data show that ProQ affects the steady-state levels and the stability of at least five meningococcal sRNAs by direct binding and in addition to the RNA chaperone Hfq.

Table 6-8 Overview of ProQ-associated sRNA selected for validation by northern blot analysis and EMSA

sRNA	Start	Stop	Strand	CLIP peak start	CLIP peak end	RNA-seq logf.c.	RNA-seq p.adj.
AniS	1233477	1233582	+	1233529	1233575	-1,1	2E-06
Bns1	817684	817771	-	817684	817717	-4,1	5E-183
NMnc0006	102550	102732	-	102608	102671	-1,1	1E-08
				102691	102732		
				102554	102580		
NMnc0034	1725963	1726094	+	1726065	1726092	-1,1	1E-10
NMnc0041	1967652	1967827	-	1967658	1967687	-0,9	2E-06

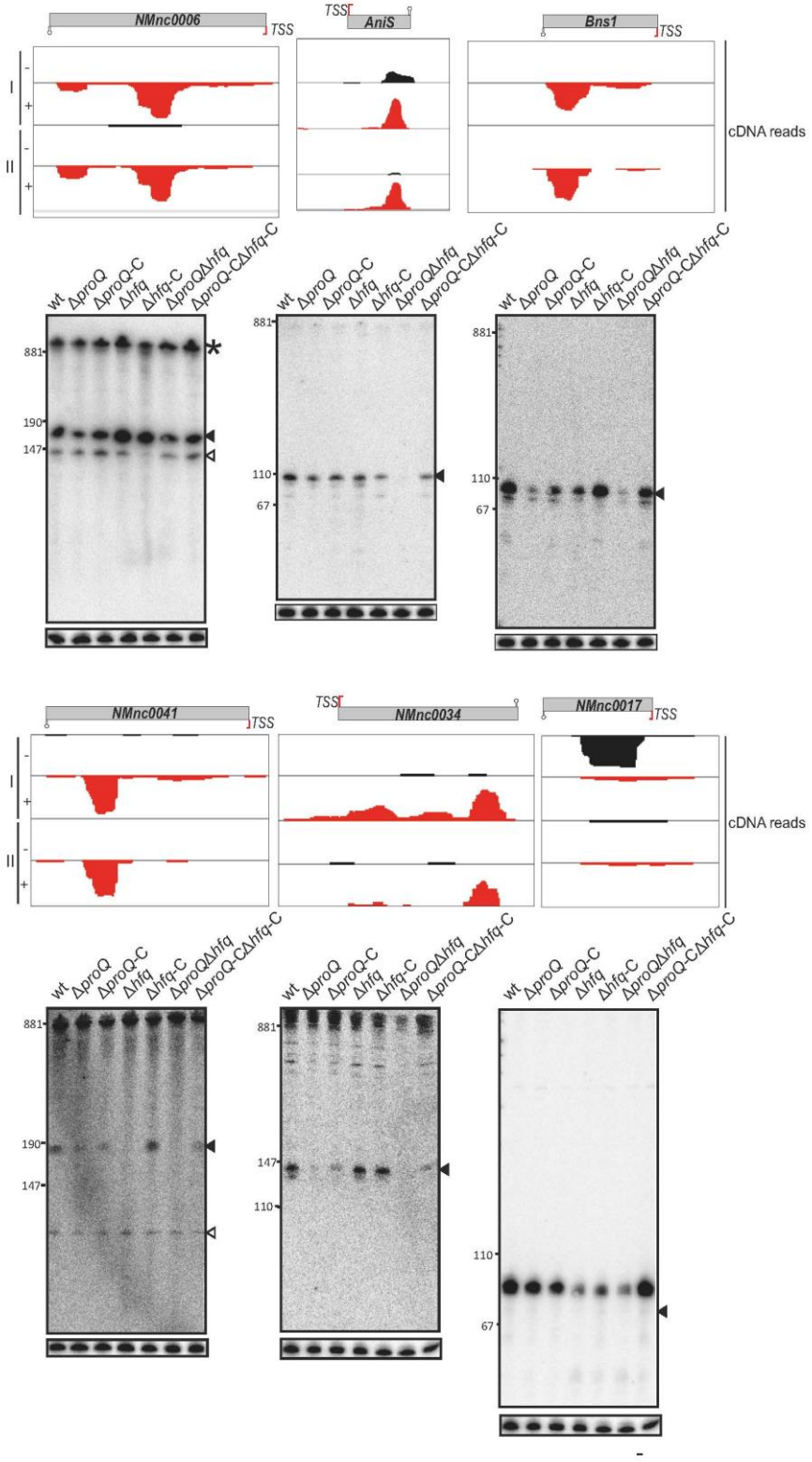

Figure 6-33 Northern blot analysis of ProQ-associated sRNAs as identified by ProQ UV-CLIP

(Top) Screenshots of ProQ UV-CLIP-seq data from late logarithmic growth phase (OD_{600nm} 2.0) at the indicated loci. The data were visualized with the IGB (chapter 5.33). I, II: technical replicates one and two; -: non crosslinked libraries; +: crosslinked libraries (Bottom) Total RNA was extracted at late logarithmic (OD_{600nm} 2.0) growth phase from *N. meningitidis* 8013 wt, Δ*proQ*, Δ*proQ*-C, Δ*hfq*, Δ*hfq*-C, Δ*proQ*Δ*hfq* and Δ*proQ*-C Δ*hfq*-C strains and analyzed by northern blot using labeled DNA probes (Table 4-32). Filled triangles highlight RNAs bands derived from TSS and open triangles highlight bands derived from processing. The housekeeping 5S rRNAs served as a loading control for each blot.

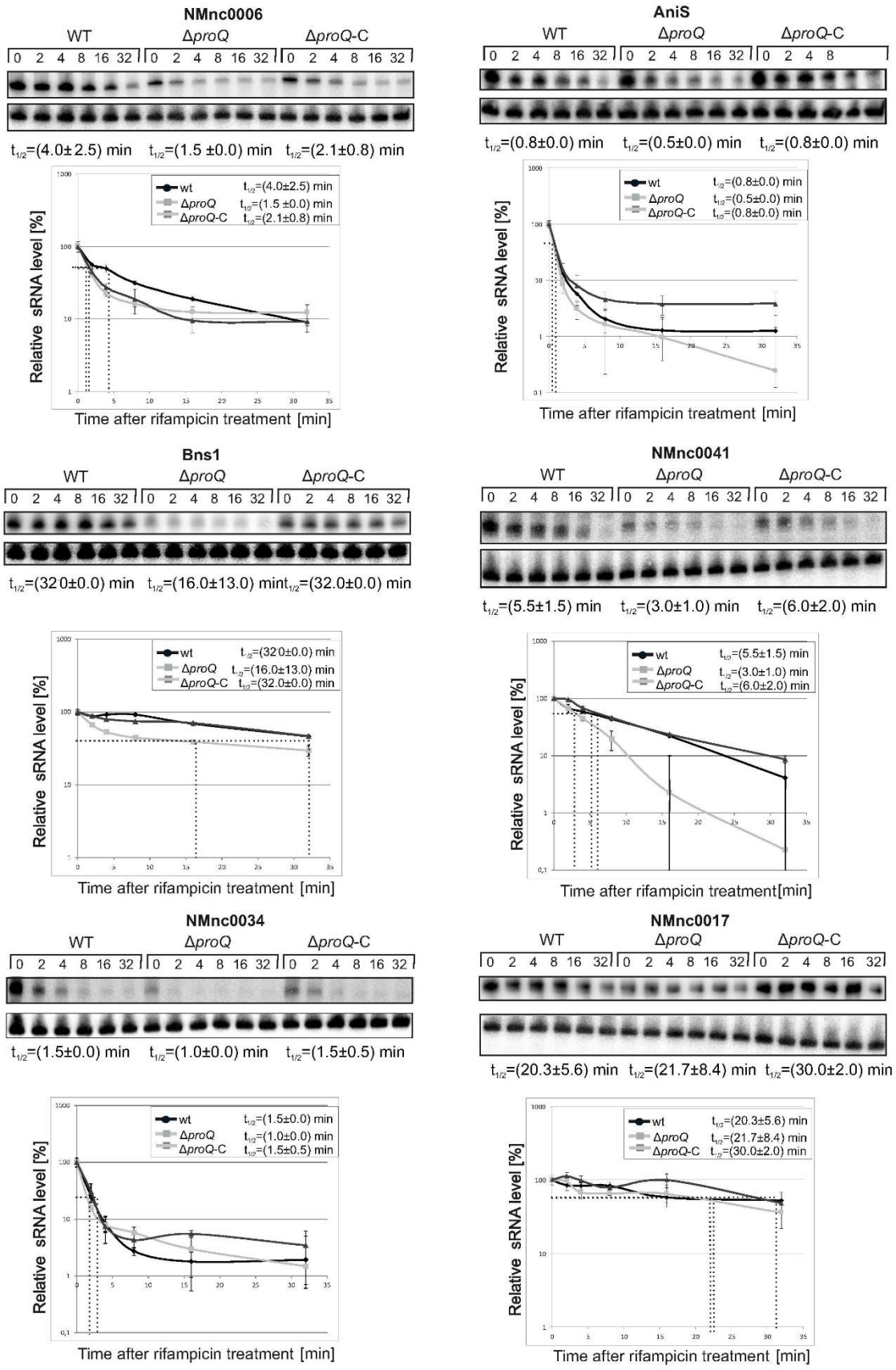

Figure 6-34 RNA half-life determination of ProQ-associated sRNAs

Northern blots of total RNA extracted of the *N. meningitidis* 8013 wt, Δ*proQ* and Δ*proQ*-C strains at the indicated time points (0 to 32 minutes after addition of rifampicin (250 µg/ ml) are shown. For transcript

detection, labeled DNA probes complementary to the indicated sRNAs were used which can be found in Table 4 32. The housekeeping 5S rRNAs served as a loading control for each blot. The experiments were performed in triplicate and quantifications for RNA half-lives are summarized below the northern blots. The standard deviation is indicated for each analyzed time point.

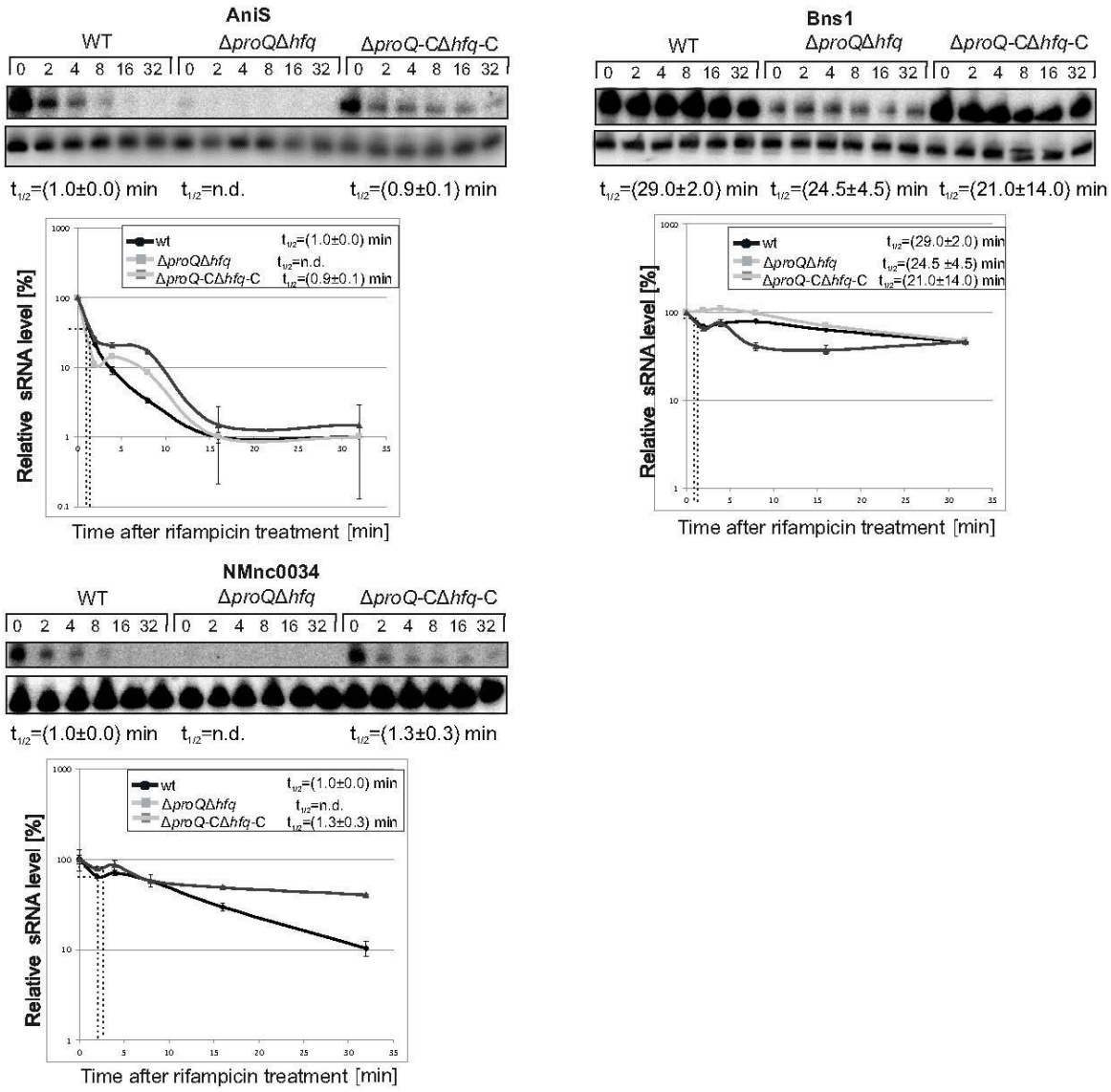

Figure 6-35 RNA half-live determination of ProQ and Hfq-associated sRNAs

Northern blots of total RNA extracted of *N. meningitidis* 8013 wt, Δ*proQ*Δ*hfq*, Δ*proQ*-CΔ*hfq*-C strains at the indicated time points (0 to 32 minutes after addition of rifampicin (250 µg/ ml) are shown. For transcript detection, labeled DNA probes complementary to the indicated sRNAs were used which can be found in Table 4 32. The housekeeping 5S rRNAs served as a loading control for each blot. The experiments were performed in triplicate and quantifications for RNA half-lives are summarized below the northern blots. The standard deviation is indicated for each analyzed time point.

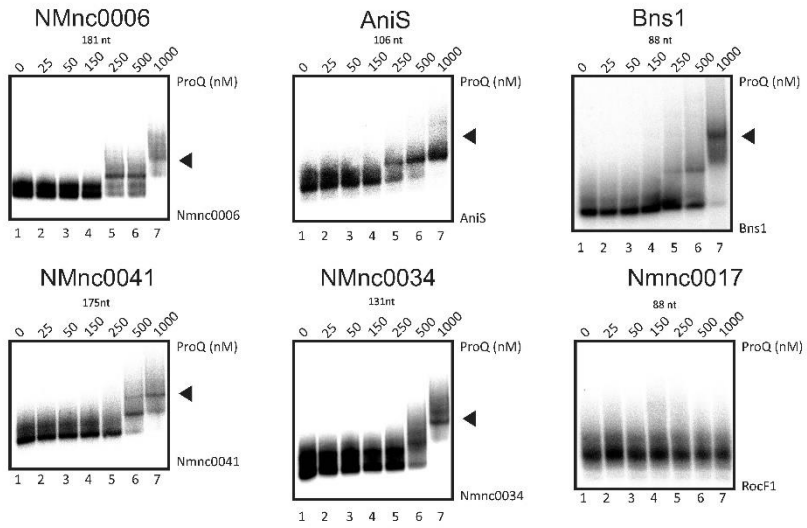

Figure 6-36 ProQ directly interacts with its associated sRNAs *in vitro*

In vitro gel-shift assays (EMSA) of ProQ with its associated sRNAs according to ProQ UV-CLIP data. Migration of 0.04 pmol *in vitro* transcribed and ^{32}P-labeled RNA in a non-denaturating gel after incubation for 20 min with varying concentrations of purified ProQ protein (lane 1–7: 0, 25, 50, 150, 250, 500, 1000 nM). The arrows indicate the RNA-protein complexes. The sRNA NMnc0017, which is associated with Hfq but not ProQ, served as a negative control.

6.5.9. ProQ stabilizes its associated mRNAs

To test whether ProQ stabilizes also cognate mRNAs irrespective of the binding site identified by UV-CLIP, the *pnp* mRNA containing a ProQ CLIP-peak in its 5' UTR, the *rpmG* RNA which harbors a ProQ CLIP-peak in its CDS and *sodC* mRNA with a ProQ-CLIP peak in its 3'UTR were selected for independent validation of mRNA stabilization. All three mRNAs were found to be downregulated in the RNA-seq data (chapter 6.5.7) and *sodC* and *rpmG* were significantly downregulated in the proteome data as well (chapter 6.5.7) (Table 6-9). Of note, *pnp* encodes a polyribonucleotide nucleotidyltransferase, *sodc* encodes a superoxide dismutase and *rpmG* encodes a 50S ribosomal protein.

Table 6-9 Overview of mRNA selected for validation by northern blot analysis and EMSA

Locus_tag	Feature	Start	Stop	Strand	CLIP peak start	CLIP peak stop	RNAseq logf.c.	Proteom Q.norm.log$_2$. (filt.LFQ KO/WT)
NMV_0995 (*sodC*)	3'UTR	996077	996135	-	996103	996142	-2,5	-1,0 (Significance level: 1)
	CDS	996135	996695	-	996103	996142	-1,5	
NMV_0356 (*rpmG*)	3'UTR	341562	341615	+	341580	341615	-0,1	-0,7 (Significance level: 1)
NMV_1636 (*pnp*)	5'UTR	1588859	1588997	-	1588897	1588923	-0,9	-0,8 (Significance level: 0)

All three selected mRNAs showed a decreased steady-state level in the absence of ProQ compared to the wild-type (Figure 6-37) validating the RNA-seq results. While both *sodC* and *pnp* are additionally stabilized by Hfq, *rpmG* is exclusively stabilized by ProQ and holds a 3' end processing product that is destabilized in absence of ProQ (Figure 6-37).

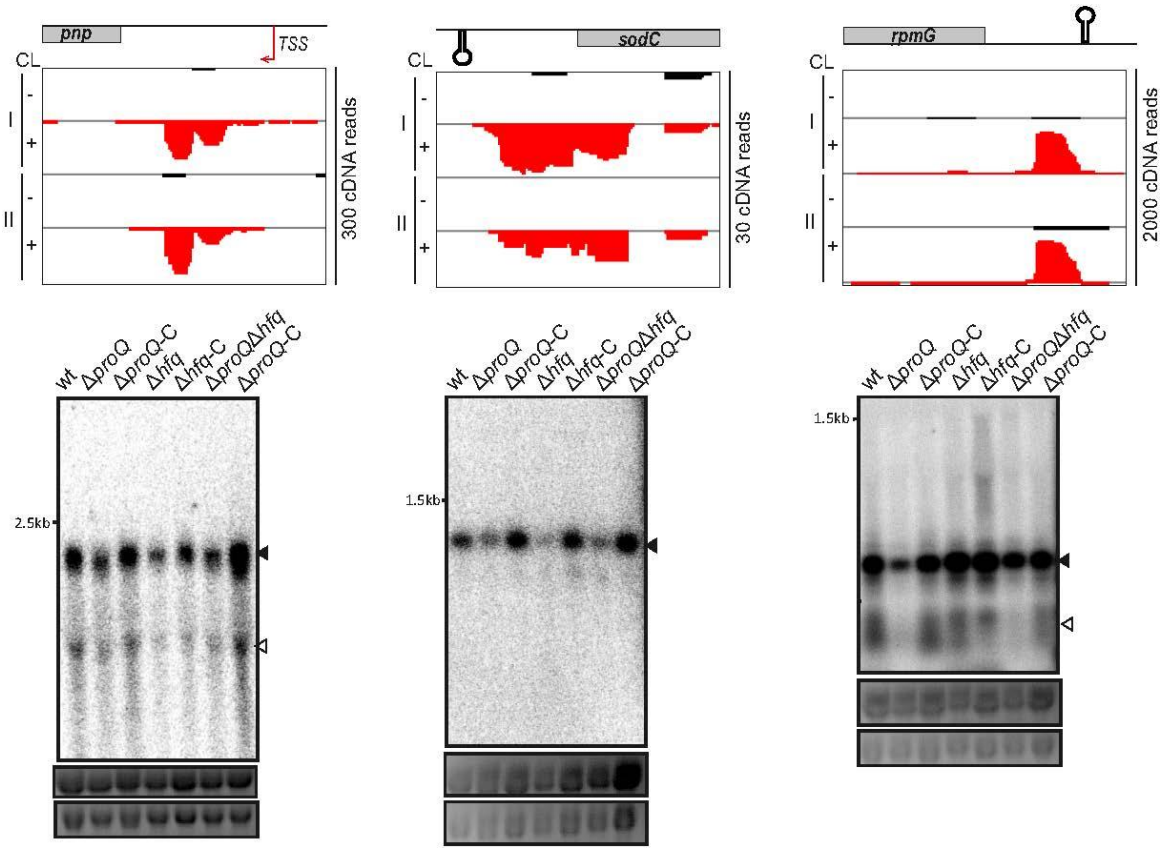

Figure 6-37 Northern blot analysis of ProQ-associated mRNAs as identified by UV-CLIP

(Top) Screenshots of ProQ UV-CLIP-seq data from late logarithmic growth phase (OD_{600nm} 2.0) at the indicated loci. The data were visualized with the IGB (chapter 5.33). I, II: technical replicates one and two; -: non crosslinked libraries; +: crosslinked libraries (Bottom) Total RNA was extracted at late logarithmic (OD_{600nm} 2.0) growth phase from *N. meningitidis* 8013 wt, Δ*proQ*, Δ*proQ*-C, Δ*hfq*, Δ*hfq*-C, Δ*proQ*Δ*hfq* and Δ*proQ*-C Δ*hfq*-C strains and analyzed by northern blot using labeled DNA probes (Table 4-32). Filled triangles highlight RNAs bands derived from TSS and open triangles highlight bands derived from processing. The housekeeping 5S rRNAs served as a loading control for each blot.

To test if ProQ promotes mRNA stability, sRNA half-lives were tested in rifampicin stability assays (Figure 6-38). The half-life of *sodC* declined from 4 min in the wild-type strain to about 2 min in the Δ*proQ* strain whereas complementation of *proQ* increased the half-life back to 4.5 min.

Overall, mRNA half-life in the *proQ* mutants was reduced to 47% (±17%) compared to the wild-type.

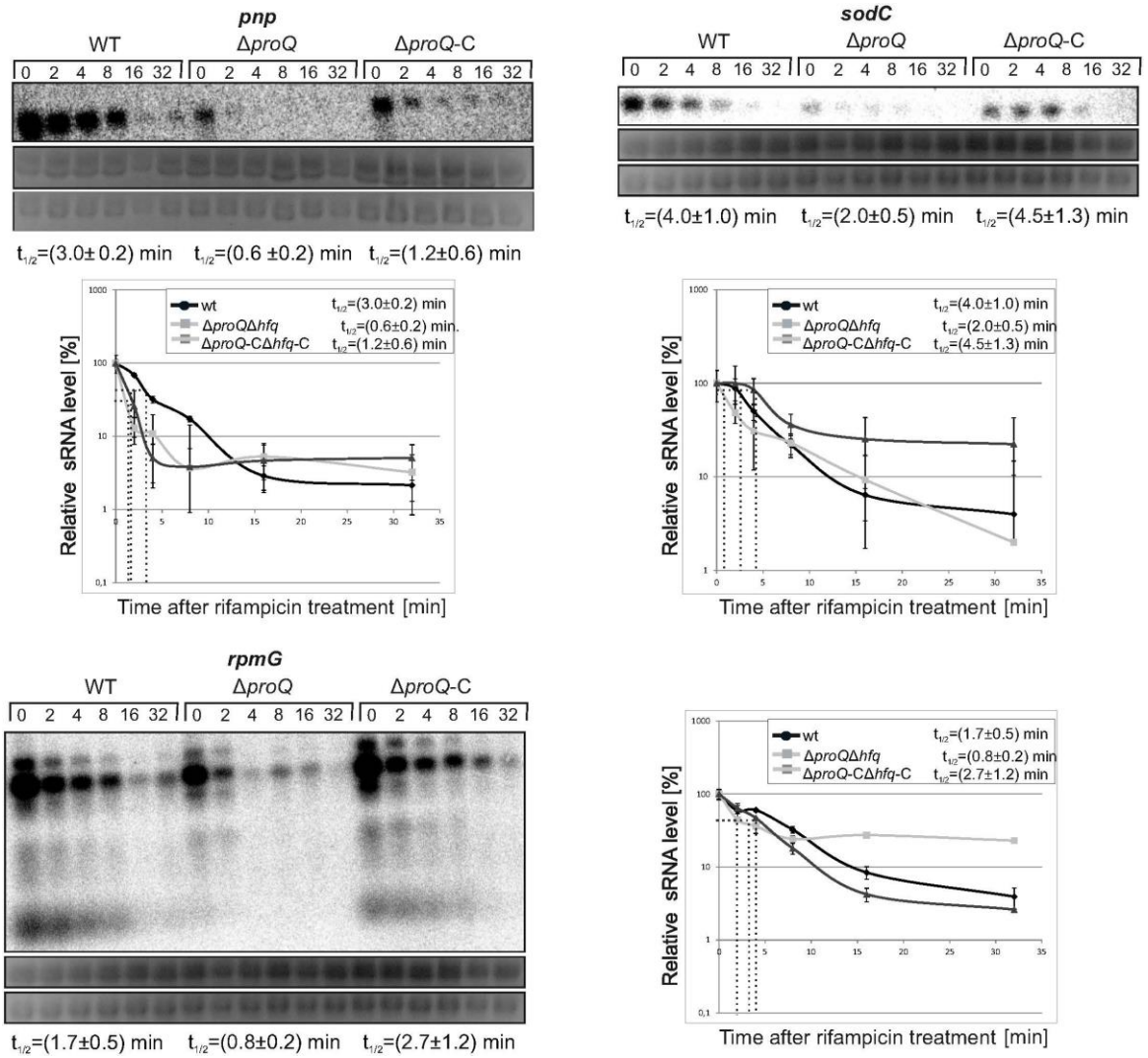

Figure 6-38 Northern blot analysis of ProQ-associated mRNAs

Northern blots of total RNA extracted of *N. meningitidis* 8013 wt, Δ*proQ* and Δ*proQ*-C strains at the indicated time points (0 to 32 minutes after addition of rifampicin (250 µg/ ml) are shown. For transcript detection, labeled DNA probes complementary to the indicated mRNAs were used which can be found in Table 4 32. The housekeeping 16S and 23S rRNAs served as a loading control for each blot. The experiments were performed in triplicate and quantifications for RNA half-lives are summarized next to the northern blots. The standard deviation is indicated for each analyzed time point.

To exclude the possibility of secondary effects causing sRNA destabilization in the *ΔproQ* strain, direct binding of purified ProQ protein to *in vitro* transcribed, radioactively labeled mRNAs was tested in electromobility-shift assays. As shown in Figure 6-39, each of the ProQ-associated mRNAs shifted in a concentration-dependent manner.

Together, these data indicate that in addition to sRNAs ProQ can also stabilize cognate mRNAs irrespective of the binding site.

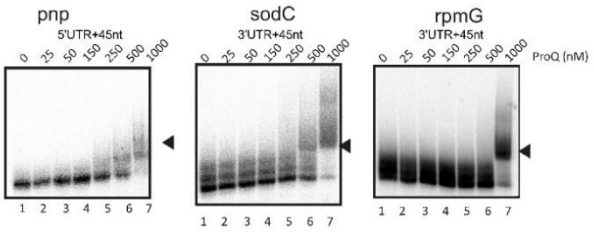

Figure 6-39 ProQ directly interacts with its associated mRNAs *in vitro*

EMSAs of ProQ with its associated mRNAs according to ProQ UV-CLIP data. Migration of 0.04 pmol *in vitro* transcribed and ^{32}P-labeled RNA (lanes 1-7) in a non-denaturating gel after incubation for 20 min with varying concentrations of purified ProQ protein (lane 1–7: 0, 25, 50, 150, 250, 500, 1000 nM). The arrows indicate the RNA-protein complexes.

7. Discussion

Recent studies have shown that riboregulation contributes to bacterial virulence (37,93) in numerous human pathogenic species including *N. meningitidis*. Yet, the work on sRNAs and RNA-binding proteins in *N. meningitidis* is still in its infancy compared to other model organisms such as *E. coli*. Therefore, in this work differential RNA-seq was used to uncover novel meningococcal sRNAs. In addition, a Hfq RIP-seq approach and rifampicin stability assays were used to define the repertoire of Hfq-associated mRNAs and sRNAs in *N. meningitidis*. Combining these data-sets with *in silico* target predictions revealed a regulatory network consisting of Hfq-associated sRNAs and their potential mRNA targets. Some of these interactions could be validated using *in vivo* assays such as northern blot analysis as well as GFP-reporter assays and *in-vitro* assays such as EMSA and in-line probing. In addition, direct meningococcal RNA targets of the recently identified RBP ProQ were identified by applying UV-CLIP-seq. The ProQ regulon could be further analyzed using northern blot analysis, rifampicin stability assays, EMSAs, RNA-seq as well as quantitative proteomics. Finally, an array of established *ex vivo* assays was employed to assess the so far unknown physiological function of the RBP ProQ in *N. meningitidis*.

7.1. An unexpected large repertoire of antisense TSS

The dRNA-seq approach in *N. meningitidis* strain 8013 allows to determine exact boundaries of transcripts and operons as well as to distinguish primary transcripts from processing products (chapter 6.1). Among the total of 1,625 detected transcriptional start-sites was a large amount of antisense transcripts (n = 633 aTSS, 39%) in addition to 706 primary TSSs of annotated genes (Figure 6-2). Thus, roughly one quarter of protein-encoded genes (n = 573) possess at least one aTSS. Antisense RNAs have been ubiquitously reported in bacteria (180) and in line with that a recent study using tiling microarrays detected over 260 antisense transcripts expressed in human blood in *N. meningitidis* strain MC58 (19). However, the functionality of this class of transcript remains debated (180). Llorens-Rico *et al.* 2016 (180) could show that physiological antisense RNA regulatory effects are only observed above certain expression thresholds which are much higher than transcript levels detected in high-throughput-sequencing-approaches. Therefore, the authors speculate that most of the antisense transcripts found in high throughput-sequencing approaches are the consequence of transcriptional noise which arises at spurious promoters throughout the genome. Hitherto, only one functional antisense RNA required for antigenic pili variation has

been described in *N. meningitidis* (148) suggesting that at least some antisense transcripts are expressed at physiological levels in meningococci. Yet, this *cis*-encoded sRNA could not be detected in the dRNA-seq data maybe due to the fact that pilus regulation seems to be a strain-dependent process (Table 6-1, Figure 6-7). Indeed, two other highly-expressed antisense RNAs (NMnc0019, NMnc0024) could be detected by northern blot analysis (Figure 6-5) which indicates that functional antisense RNAs are also likely expressed in *N. meningitidis* strain 8013.

In summary, at least some aTSSs are likely to represent the transcriptional start-sites of functional antisense RNAs in *N. meningitidis*. Further analyses and experiments are required to understand the repertoire and physiological relevance of *cis*-encoded antisense RNAs in *N. meningitidis*.

7.2. Contribution of sRNAs to genetic diversity and virulence of *N. meningitidis*

Bacterial sRNAs are key players in resonding to different cellular and environmental stresses. Of note, pathogenic bacteria have to tightly control gene expression in the course of an invasive infection where they have to respond to various distinct hostile microenvironments. Therefore, many pathogenic bacteria encode hundreds of sRNAs, of which many are upregulated in critical steps of the infection processes (181-183). For example, sRNAs were shown to regulate the adaption to different nutrient availabilities after entering the host body (184) or to orchestrate the adherence to and invasion of host target cells (185).

In line with these previous data, the dRNA-seq data predict 65 sRNAs including 45 novel sRNAs and 20 previously described sRNAs in *N. meningitidis* strain 8013 (Figure 6-6, chapter 6.2). More than one third were sRNAs generated from the 3' ends of mRNAs. These sRNAs were either expressed from mRNA internal-gene promoters or derived from processing products of the parental mRNAs as determined by the specific enrichment of cDNA sequences in the TEX-treated or untreated cDNA libraries. This finding extends to studies in *Salmonella*, where several 3'UTR derived sRNAs have been shown to be functional (186,187).

A representative member of a processed 3'UTR derived sRNA of the dRNA-seq approach, which might be linked to virulence of *N. meningitidis*, is NMnc0001. This sRNA candidate was shown to be an Hfq dependent but not ProQ-associated sRNA (Figure 6-28) and to reveal a strain-dependent expression pattern (Figure 6-7). NMnc0001 is derived from the

transcript encoding *pilE,* the major component of the type IV pilus. The type IV pili of *Neisseria* are important fitness determinants for colonization of humans as they are involved in twitching motility, DNA transformation, and adherence to epithelial cells (188) (chapter 3.1). Therefore, the type IV pili expression status might respond to stress signals and changes in the environment. In *N. meningitidis*, a number of proteins are known to involve pilin regulation upon contact with human cells such as CrgA and NafA (189,190). Additionally, *pilE* expression has been described to be dependent on Hfq in a strain-specific manner. For instance, in MC58 absence of Hfq results in PilE up-regulation (93) while in strain H44/76, loss of Hfq goes along with a down-regulation of PilE (156). Whether these regulations occur in conjunction with NMnc0001 or another small RNA as the previously detected *cis*-encoded antisense RNA of *pilE* (7) in a strain-specific manner awaits further investigation. Yet, expression levels of NMnc0001 are synchronized with *pilE* expression levels (Figure 6-7) indicating a functional link between *pilE* and NMnc0001.

Previous studies have revealed significant divergence between sRNA repertoirs of pathogenic and non-pathogenic bacterial species which might contribute to the differences in pathogenicity (144,191). For instance, Ignatov *et al*. 2013 found two sRNAs which might be key players in the divergent pathogenicity of the facultative pathogenic *Mycobacterium avium* and the highly pathogenic *Mycobacterium tuberculosis* (192). Of the 45 novel sRNAs identified in course of the dRNA-seq analysis (chapter 6.2.187), ten sRNAs were strain specific as determined by BLASTN searches (Table 6-1). Profiling the expression levels of five of those sRNAs among the four meningococcal strains Nm8013, MC58, WUE2594 and Z2491 by northern blot analysis confirmed that the *in silico* approach is not only effective for detecting conserved, but also strain-specific transcripts (Figure 6-6).

The variable sRNA NMnc0031 is absent in serogroup A strains as validated by northern blot analysis (Figure 6-6), because this sRNA is located on the genomic island IHT-E that appears to be derived from a prophage. Of note, it was recently demonstrated that IHT-E is associated with hyperinvasive meningococcal strains (12). Therefore, knowledge of the functional elements of IHT-E helps to understand host pathogen interactions, and the RNA-seq based identification of such island-specific transcripts provides a starting point to study he contribution of sRNAs to virulence in a strain-specific manner.

Another non-conserved sRNA, NMnc0040, is linked to CRISPR-Cas genes, whose expression have been shown to limit natural transformation in menigococci (42) (Figure 6-5).

A recent study in *Francisella novicida* showed that Cas9, but no other protein of the Francisella CRISPR-Cas type II locus, represses the synthesis of a bacterial lipoprotein (BLP) and thereby enables the infecting bacteria to evade the Toll-like receptor 2 -based innate immune response of its host (41). However, *Francisella* Cas9 by itself is not sufficient to provide repression, as it requires tracrRNA as well as a second small CRISPR-associated RNA, the scaRNA. Although neither Cas9 nor tracrRNA affected the expression levels of NMnc0040 (117), it is tempting to speculate that in CRISPR/cas bearing meningococci this sRNA may also be involved in Cas9 mediated regulation of endogenous genes.

Consequently, the dRNA-seq approach helped to identify 3'UTR regions of meningococcal mRNAs as reservoirs of several 3'UTR-derived sRNAs and to identify numerous strain-specific sRNAs which might contribute to meningococcal diversity and virulence.

7.3. Hfq as a major RNA binding protein in *N. meningitidis*

The RIP-seq approach detected 401 mRNAs and additionally 23 sRNAs as putative targets of Hfq, placing Hfq at the center of post-transcriptional regulation in *N. meningitidis* (Chapter 6.3). Many of the identified mRNA targets are involved in cellular processes such as amino acid biosynthesis, cell energetics and metabolism, oxidative stress responses, and pathogenesis. Some Hfq-associated mRNAs previously found to be deregulated in meningococcal cells lacking Hfq could also be detected by proteomic analysis such as *prpB* and *sodB* (93,156) indicating that Hfq binding induces gene expression regulation. A key finding from the RIP-seq analysis is the identification of Hfq binding sites in CDSs as well as at 5'UTRs and 3'UTRs of mRNAs as detected in the previous TSS map analysis (chapter 6.1). Because most sRNAs regulate target mRNAs by operating at transcript boundaries, this finding suggests that many of the Hfq-bound 5'UTRs and 3'UTRs belong to transcripts that are post-transcriptionally regulated by Hfq-associated sRNAs. The strong evidence for Hfq binding to sRNAs and mRNAs presented here agrees with previous reports suggesting a role for Hfq also in both sRNA dependent regulation at mRNA 5' regions and 3' end dependent processes in *N. meningitidis* (66).

Furthermore, comparison of the Hfq-bound 5'UTRs of mRNAs and targets that were predicted for the top nine Hfq binding sRNAs ($(\log_2$ f.c.$) \geq 1$, cDNA read ≥ 100, Q value < 0.1) using the Copra algorithm (Chapter 6.4) identified 26 mRNAs as potential targets for nine meningococcal sRNAs with interaction sites located in the 5'UTR of these mRNAs. Six of the 26 mRNAs are predicted to bind to more than one sRNA, suggesting overlapping modes

of Hfq-mediated sRNA regulation in *N. meningitidis (*Figure 6-11*)*. For instance, NMV_1044 which encodes a putative MarC-family transporter is predicted to be bound by five different sRNAs (AniS, Bns2, NMnc0017, NMnc0018, NMnc0037, NMnc0044). This finding indicates that some mRNAs in *N. meningitidis* might function as post-transcriptional regulatory hubs as described before for the *ompD*, *rpoS* and *csgD* mRNAs (193-196) in *E. coli* and *Salmonella*.

7.4. Functional analysis of the Hfq-associated sRNAs NMnc0017 and NMnc0018

Functional characterization of sRNAs has lagged behind sRNA discovery and hitherto for only three neisserial sRNAs, base-pairing interactions with direct mRNA targets were experimentally confirmed: (i) NrrF, a sRNA involved in maintaining iron metabolism and homeostasis (67,68) (ii) AniS which is up-regulated under anaerobic conditions (36) and (iii) a *cis* acting sRNA that influences antigenic variation of *pilE* in *Neisseriales* (148). In this work, the number of potential mRNA targets of sRNAs was further expanded to include *prpB,* a putative colonization factor, as the target of two novel paralogous sRNAs (NMnc0017, NMnc0018) (Chapter 6.4).

As shown by northern blot analysis the *prpB* mRNA in *N. meningitidis* mutant strains lacking either the two sRNAs or Hfq was stabilized compared to the wild-type (Figure 6-13). This finding most likely results from ribosome-mediated protection against a yet to identify ribonuclease. A potential nuclease candidate is RNase E, which functions in Hfq-mediated regulations in other Gram-negative bacteria (81,197,198). *N. meningitidis* encodes an RNase E homolog (NMV_0215) which has been described to be essential by *in vitro* transposon mutagenesis (146). Yet, the role of meningococcal RNase E in RNA turnover is not known so far.

The regulatory role of these two sRNAs in post-transcriptional control of a *prpB* mRNA was further confirmed by a sfGFP reporter system *in vivo (*Figure 6-14*)*. In-line probing assay surprisingly demonstrated that both sRNAs form short stem-loops in their mRNA base pairing region (Figure 6-16) whereas many well-characterized Hfq-associated sRNAs possess unstructured mRNA base pairing regions (199). Therefore, both sRNAs likely undergo a structural rearrangement as they recognize the *prpB* mRNA, as best visible in the in-line probing experiment.

The *prpB* gene is part of the methylcitrate cycle that is located on the largest genomic island in *N. meningitidis*, an island absent from closely related non-pathogenic *Neisseria* species such as *N. lactamica* (Figure 7-1). The methylcitrate cycle gene cluster allows meningococci to convert propionic acid to pyruvate, supporting growth and limiting the toxicity of propionic acid. The ability to utilize propionic acids is hypothesized to confer an advantage in colonizing the adult nasopharynx, which is rich in propionic-acid generating bacteria mainly present in adults (112). This study together with earlier reports (37,66) indicate that sRNAs play an important role in gene regulation in meningococci. Of note, the data may indicate the existence of another sRNA, σE sRNA (23), that might repress *prpB (*Figure 6-11*).* Interestingly, also the sRNA Bns1 has been predicted, yet not experimentally validated, to positively regulate the *prpB-prpC* operon (37). Therefore, it is likely that genes of the methylcitrate cycle are co-regulated by several sRNAs as described before for some transcripts in *E. coli* and *Salmonella* (195). This hypothesis could also explain why the expression levels of NMnc0017 and NMnc0018 remained unchanged upon proprionic acid supplementation to the growth medium (Figure 6-17).

In the meanwhile, two further studies analyzing the physiological role and *in vivo* targets of these two paralogous sRNAs in *N. meningitidis* (200) and *N. gonorrhoe (201)* have been published. Pannekoek *et al.* 2017 (200) could show that the paralogous sRNAs termed NmsRA (NMnc0018) and NmsRB (NMnc0017) in course of their study regulate switches between cataplerotic and anaplerotic metabolism in *N. meningitidis* (200). Thereby, overexpression of the two sRNAs was tolerated in blood but not in cerebrospinal fluid. In addition, the authors showed down-regulation of six enzymes involved in meningococcal metabolism (*prpB, prpC, gltA, sdhC, sucC, fumC*) by direct interaction with the papralogous sRNAs. Therefore, these results independently validate the interactions of the paralogous sRNAs with methylcitrate cycle genes (*prpB, prpC*) observed in this work. Of note, expression of the sRNAs itself was found to be under the control of the stringent response through the action of RelA (200). In perfect agreement with northern blot analyses (Figure 6-10, Figure 6-14), the authors could show that the relative expression level of NmsRA (NMnc0018) is very low compared to those of NmsRB (NMnc0017) (Figure 6-10 and Figure 6-14). The relatively high expression levels of NmsRB (NMnc0017) might suggest that NmsRA (NMnc0018) acts redundantly in a compensatory manner on the same targets, as has been described for sRNAs of other pathogens (202-204). Yet, the authors described that the action of both sRNAs was found to be more complicated as both paralogous sRNAs were required for growth inhibition of meningococci under nutrient-limiting

conditions. Thus, these observations indicate that the paralogous sRNAs act cumulatively, each contributing in a different degree to meningococcal metabolism and infection biology. Bauer *et al.* 2017 (201) could show that the paralogous sRNAs are encoded at the same genomic location in *N.gonnorrhoe,* that they are abundantly expressed in rich medium and interact with several genes of the tricarboxylic acid cycle (*gltA*, *sdhC*, *sucC* and *fumC*) as well as methylcitrate cycle (*prpB, prpC, ack) (201).* In line with the predicted Hfq-association of the paralogous sRNAs in the Hfq RIP-seq data, four of these validated direct mRNA targets (*ack*, *prpC*, *gltA* and *fumC*) have been previously described to be deregulated in *hfq* deletion mutants in *N. meningitidis* (37). Therefore, the expression pattern as well as the target spectrum of the paralogous sRNAs seem to be highly conserved among distinct *Neisseriales* species.

Interestingly, an enrichment of virulence-associated sRNAs which are associated with metabolic processes has been observed (205). This overrepresentation relates to the dynamic changes of disposable nutrients when bacteria invade their host and therefore face different nutrient sources as hypothezised for *N. meningitidis* as well (129). Therefore, further investigations are required to understand to which extent NMnc0017 and NMnc0018 contribute to meningococcal virulence *via* regulating genes of the methlycitrate cycle as well as the TCA cycle.

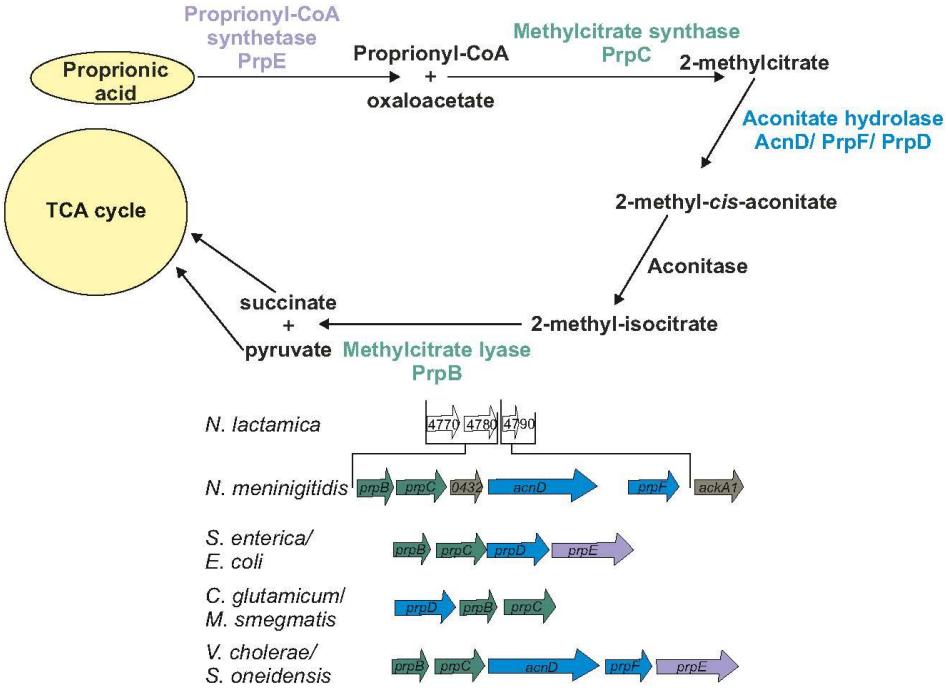

Figure 7-1 Schematic illustration of the methylcitrate cycle and conservation of *prp* clusters from distinct bacteria. The figure was adapted from Catenazzi *et al.* 2014, (112)

7.5. ProQ as a major regulator of bacterial 3'ends

FinO/ProQ domain proteins represent a novel class of conserved RBPs (159) and a recent study indicates that *N. meningitidis* encodes a minimal ProQ/FinO-domain protein that exhibits RNA chaperone activity *in vitro* (111).

To address the major mode of action of meningococcal ProQ, the *in vivo* RNA target suite of the ProQ protein of *N. meningitidis* was determined. An UV-CLIP approach (Figure 6-23) identified *in vivo* 235 significant genome wide RNA target sites in 166 distinct mRNAs and 16 sRNAs, providing the first direct evidence for ProQ being a global RNA binding protein in *N. meningitidis (*Figure 6-24*)*. Consequently, ProQ functions as a global gene regulator in meningococci that alters the expression levels of 293 RNA features including in particular many 3'UTR regions (Figure 6-29). Thus, these data suggest that meningococcal ProQ globally binds and thereby stabilizes 3'UTRs of bacterial mRNAs. For example, both the full-length transcript and a 3' end derived processing product of *rpmG* harbouring a ProQ CLIP peak in its 3'UTR revealed decreased steady-state levels in the *proQ* deletion strain as detected by northern blot analysis (Figure 6-37). These data further suggest a role of ProQ in 3' end-dependent protection from RNA degradation as described before for ProQ in *Salmonella* (4). In *Salmonella*, genetic evidence arised that ProQ can stabilize mRNAs by counteracting decay that is dependent on the 3'→5' exoribonuclease RNase II and endonuclease E by an unknown mechanism that may sterically obstruct access of RNase II to the mRNA (4). In *N. meningitidis*, one RNase E homolog is encoded by NMV_0215 which has been shown to be essential by *in vitro* transposon mutagenesis (146). However, nothing is known so far about what role RNase E may play in RNA turnover in meningococci and NMV_0215 expression was also not affected by ProQ in the UV-CLIP data, RNA-seq analysis and proteomics approach. While 3'→5' exoribonuclease RNase II is not annotated in *N. meningitidis*, the widely conserved 3'→5' exoribonuclease (40,41) *pnp* was found to be associated with ProQ in the UV-CLIP approach in its 5'UTR (Chapter 6.5.4) and consequently stabilized by ProQ (Chapter 6.5.9). Although *pnp* expression levels could only be partially restored in a Δ*proQ* complementation strain and PNPase expression levels were not significantly down-regulated in the *proQ* deletion strain in the proteomics approach, *pnp* is an interesting RNase candidate for investigating RNA degradation in the absence of ProQ in *N. meningitidis*.

Yet, ProQ can also stabilize the whole mRNA transcript by binding either CDS or 5'UTR regions of target mRNAs as illustrated by s*odC* encoding a superoxide dismutase and PNP

(Chapter 6.5.9). In line with the reduced transcript levels of *sodC* in the *proQ* deletion strain (Figure 6-29), SodC protein expression was also impaired in the *proQ* knockout strain (chapter 6.5.9). Yet, further experiments are needed to uncover the interaction mechanisms between ProQ and the CDS and 5'UTR regions, respectively, of target mRNAs resulting in transcript and partially protein stabilization.

7.6. ProQ globally impacts meningococcal gene expression

In order to understand the regulatory behavior of ProQ in *N. meningitidis*, the transcriptome and proteome of *proQ* deletion mutants have been analysed (Chapter 6.5.7). As expected from the large suite of ProQ-bound RNAs (chapter 6.5), *proQ* deletion globally affected both transcript and protein expression in *N. meningitidis*, changing the expression levels of at least 244 mRNAs (Figure 6-29) and 80 proteins (Figure 6-32). Yet, only 34 genes were found to be differentially regulated in both transcriptome and proteome data (Figure 6-31) and thus the majority of regulated transcripts were not differentially expressed on the protein level. Among these 34 genes, only six genes hold a ProQ CLIP peak indicating direct interactions between RNA and ProQ (NMV_0843, *rplI*, *nicB*, NMV_0898, *pilC*2 and *sodC*).

Whereas differences between UV-CLIP-seq data and transcriptome data can be explained by indirect effects mediated by global transcription regulators such as 6S RNA (116), σE sRNA (85) and *nusA*/ *nusB* mRNAs (Figure 6-29), the observed discrepancies between transcriptome data and proteome data are more difficult to reconcile. Apparently, differentially expressed proteins which were not found to be regulated at the mRNA level are likely candidate genes for post-transcriptional regulation by ProQ-associated sRNAs. For instance, PrpC which was shown to be stabilized by the sRNAs Bns1 (87) being the most downregulated sRNA in the Δ*proQ* mutant, was the most down-regulated protein in the proteomic data and only moderately regulated at the transcriptional level. Yet, many sRNAs use RNA decay as a post-transcriptional control of gene expression (206). Thereby, sRNAs regulate mRNA stability either by directly recruiting ribonucleases (RNases) to their targets or indirectly via blocking translation, promoting degradation of ribosome-free mRNAs by RNases as also seen in the course of this study for the interaction between *prpB* mRNA and the paralogous sRNAs (Chapter 6.4.2). Therefore, it is likely that many mRNAs, which are post-transcriptionally regulated by ProQ associated sRNAs, should reveal reduced transcript levels to RNA decay. However, recent studies have shown that the correlation between protein and mRNA expressions data from the same cells under similar conditions

have failed to show a high correlation between both datasets in several studies due to several reasons (207-210):
(i) different translation efficiency, (ii) different half-lives of mRNA and protein, (iii) post transcription machinery, (iiii) post-transcriptional regulation and (iiii) data extraction. To begin with, physical properties of the transcript can influence the translational efficiency. For instance bacterial transcripts that have weak SD sequences are translated less efficiently (211-213). A further physical property influencing translation is the secondary structure of the mRNA. In particular, temperature changes can alter the confirmation of the mRNA and thus also impact translation efficiency (212). Second, mRNAs are in general five times less stable than proteins (214). In addition, the i*n vivo* half-life of a protein depends on its amino-terminal residue (215), the phosphorylation status and the localization of the protein (216). Consequently, the correlation between half-lives of mRNAs and their encoded proteins was found to be low (e.g.unstable mRNA encodes stable protein or *vice versa*) (214). Thirdly, the efficiency of translation can be influenced by the ribosome density in the transcriptional unit. Thus, ribosome-associated mRNA shows better correlation with proteins than other cellular transcripts (217). At last, experimental errors in the type of both sample preparation and data analysis for protein and RNA expression causes extrinsic noise that might impact the dataset correlation.

7.7. Comparison of the ProQ and Hfq regulons

Whereas the target spectrum of Hfq (“targetome”) usually comprises dozens to hundreds of different RNA species in most bacteria investigated so far (58,96,110,117), the targetome of ProQ seems to be more variable (100,104). Phylogenetic profiling further showed that all bacterial families without Hfq also lack FinO-domain proteins (99), suggesting that FinO-domain proteins have functions that are complementary to Hfq rather than substituting for this protein. In addition, while subsets of both sRNAs and mRNAs are bound by both ProQ and Hfq (97), their binding seems to be mutually exclusive (218).

In line with previous results, the extensive association of ProQ with 3’UTRs as indicated by the UV-CLIP-seq data (Figure 6-24) reflects a diverging target site spectrum of meningococcal ProQ compared to meningococcal Hfq (Figure 6-26). Moreover, both RBPs are associated with at least two distinct sRNA regulons as indicated in our Hfq RIP-seq data and UV-CLIP-seq data (Figure 6-28). However, comparing the Hfq and ProQ targetomes in *N. meningitidis* revealed also a shared targetome of 41 directly bound mRNAs (Table

6-3), six directly bound sRNAs (Figure 6-28) and eight differentially regulated proteins (Table 6-7).

Along with the observation that a deletion of ProQ leads to an additive growth phenotype of the *hfq* knockout strain (Figure 6-20) these data suggest only moderate regulatory cross-talk between Hfq and ProQ at the post-transcriptional level. It might be speculated whether the targetome overlaps implies also a functional dependence of the affected RNAs such as AniS and Bns1 on both of these RBPs (Figure 6-28). Of note, AniS expression levels were down-regulated in the double knockout strain compared to the *proQ* deletion strain and *hfq* deletion strain (Figure 6-33), respectively, indicating that these two RBPs have different binding preferences and therefore likely regulatory sites on this sRNA. In contrast to that, Bns1 expression levels were similar in the *hfq* deletion strain, *proQ* deletion strain and the double knockout strain indicating that in this case the two RBPs act redundantly to stabilize and potentially regulate this sRNA (Figure 6-33). In *Salmonell*a the RaiZ sRNA was identified as a Hfq-associated sRNA via a RIP-seq screen (59), but afterwards it was shown that RaiZ depends exclusively on ProQ for both its intracellular stability and for its mRNA target regulation (219). In *E. coli*, in turn the sRNA McaS regulates biofilm formation through both Hfq and the carbon storage regulation chaperone CsrA (220,221). Therefore, further experiments will be necessary to understand the interplay of Hfq and ProQ on meningococcal sRNAs (and mRNAs) and it will be necessary to individually analyse the distinct RNA candidates as different roles of Hfq and ProQ might appear for different RNAs.

These observations raise the question what features distinguish ProQ-associated sRNAs from Hfq-associated sRNAs. Whereas ProQ-bound sRNAs tend to have few single–stranded terminal uridines within their terminators, Hfq-bound sRNAs have longer 3'U-tails as shown for ProQ in *Salmonella* before (104). Although the differences were not significant in meningococci due to the relatively small sample size (Figure 6-28). A different lengths of poly(A) tails have been shown before to affect gene expression levels (222) and therefore might play a functional role as well. A long poly(U)-tail is relevant for Hfq binding to sRNAs (83,223). This finding might explain why Hfq fails to bind ProQ-associated sRNAs harboring a shorter poly(A) tail. On the other hand, it is still unclear in what way a long poly(A) tail might prevent ProQ from binding to this sRNA. Furthermore, ProQ-associated sRNAs tend to have a more complex secondary structure (Figure 6-28) compared to Hfq-associated sRNAs . These findings are in line with Chaulk *et al.* 2010 (111) describing that meningococcal ProQ binds *in vitro* the RNA stem-loop within the short 3′ single-

stranded tail of *FinP* mRNA but not to single stranded and therefore unstructured RNA. Together with the observations that ProQ is associated with many highly structured rho-independent terminators and seems to lack an RNA binding motif at the nucleotide level (Figure 6-25), it is likely that ProQ target selection is structure driven as well. Interestingly, the proximal site of Hfq is known to interact with uridine-rich sequences whereas the distal site mainly binds to ARN or ARNN motifs (R = purine, N = any nucleotide) in several bacteria (26-28). Therefore, Hfq recognizes its RNA targets at least partially by binding RNA motifs on nucleotide level and therefore likely exhibits different selection mechanisms for RNA targets than ProQ.

In summary, these data suggest that the meningococcal RBPs ProQ and Hfq are associated with two distinct, yet partially overlapping, RNA targetomes. ProQ target selection is most likely structure driven while Hfq probably recognizes binding motifs on nucleotide level.

7.8. The physiological role of the ProQ family proteins

In many cases, information about deletion phenotypes provides insights into the physiological roles of genes. For a long time, the only characterized biological function of a FinO-domain protein was F plasmid transfer regulated by the FinO-mediated interaction of FinP antisense RNA with *traJ* mRNA in *E. coli* (224). Recently, the FinO-domain protein RocC in *L. pneumophila* was found to have a role in DNA transactions as well as it regulates bacterial competence *via* one trans-encoded sRNA which translational represses four target genes (100). Of note, there is growing evidence that the chromosome-encoded ProQ protein in *Salmonella* might be involved in the regulation of the maintenance of genomic stability as well as many ProQ-associated antitoxin sRNAs were recently identified (97). Additionally, the chromosome-encoded ProQ protein in *E. coli* was experimentally found to be involved in both oxidative stress response (107,108) and DNA damage repair (225). Therefore, it is likely that the common physiological role of FinO-domain protein-centered networks is to retain genomic integrity.

Indeed, a decreased DNA damage repair capacity and oxidative stress tolerance could also be detected for a *proQ* deletion strain in *N. meningitidis* strain 8013 (Figure 6-22). The observed oxidative stress phenotypes were only partially restored in the complemented strains, suggesting that ProQ levels must be tightly controlled for successful DNA damage and oxidative stress repair as reported before for host invasion control (109) and *rho* mRNA

regulation by ProQ in *Salmonella* (226). Of note, a role of ProQ in meningococcal competence as investigated by transformation assays could not be observed in *N. meningitidis* (227). Together, these findings indicate that maintenance of DNA or genome stability is a broader physiological role of ProQ/FinO-damain proteins. Of note, the role of the meningococcal ProQ in oxidative stress response and DNA damage repair correlates with the known physiological roles of the chromosomal-encoded *E. coli* ProQ which also binds hundreds of target RNAs (104), but not with the *L. pneumophila* chromosome-encoded RocC which is only known to base-pair with five RNAs (100).

In particular, oxidative stress describes intracellular accumulation of reactive oxygen species (ROS) caused by several physiological and pathological conditions (228). For example, bacteria encounter oxidative stress when macrophages and neutrophiles release high concentrations of hypochlorite (HOCl) and hydrogen peroxide (H_2O_2) in order to kill the bacteria and thereby protect the host (229). ROS such as the superoxide (O_2^-) and the hydroxyl radical ($^{\cdot}OH$) can be also generated endogenously from the autooxidation of reduced molecules and from incomplete reduction of molecular oxygen during respiration (230). Oxidative stress is linked to DNA damage when elevated levels of H_2O_2 and O_2^- react with iron to hydroxyl radicals (Fenton reaction) (231,232). Indeed, in comparison to *E. coli*, the meningococcus lacks an SOS response to damaged DNA (233). Yet, *N. meningitidis* possesses a nucleotide excision repair system (NER) to encounter bulky DNA damage induced by e.g. UV light (UvrA, UvrB, UvrC, UvrY, RecN), a base excision repair system (BES) removing oxidative DNA damage (NApe, NExo, Nth, MutM) and a mismatch repair system (MMR) which removes basepair mismatches and insertion/deletion loops (MutS, MutM) (234). Additionally, *N. meningitidis* cells harbor further strong defense mechanisms against ROS constituted by catalases, peroxidases, cytoplasmic superoxide dismutase (SodB), and periplasmic superoxide dismutase (SodC), as well as other components (235).

In particular, a *sodC* deletion mutant was more sensitive to externally generated O_2^- and had decreased virulence in a mouse model (236). It is therefore likely that ProQ regulates oxidative stress response *via* the periplasmic SodC as the *proQ* deletion mutant was not found to be more sensitive to paraquat, which increases solely intracellular production of O_2^-(Figure 6-22) (237). In the course of this study, a *hfq* deletion mutant was more sensitive to both H_2O_2 and paraquat stress (Figure 6-22). In line with that, Hfq has been described to regulate the cytosolic *sodB* gene in *N. meningitidis* (177). Mellin *et al*. 2010 showed that the contribution of Hfq to iron-responsive regulation in *N. meningitidis* was limited to the regulation of only the *sodB* gene and independently of the iron-regulated sRNA NrrF in *N.*

meningitidis strain MC58 (67). In line with a dual specificity of meningococcal Hfq, northern blot analysis showed that *sodC* transcript levels are also down-regulated in a *hfq* deletion strain (Figure 6 36) and SodC has been previously found to be deregulated in a *hfq* deletion strain (94) (Table 6-7).

As *sodC* expression levels don`t differ between the *hfq* deletion strain, *proQ* deletion strain and the double-knockout strain, it might be speculated that these two RBPs act redundantly to regulate *sodC* expression at the post-transcriptional level. These findings indicate that both Hfq and ProQ are likely to regulate superoxide dismutases expression in *N. meningitidis*.

In addition, the direct ProQ target gene *pnp* (Chapter 6.5.9) encoding for a polyribonucleotide nucleotidyltransferase is known to contribute to processing of UV-light induced double-strand breaks in *Bacillus subtilis* and *E. coli* (238,239) and thus might function in *N. meningitidis* in a similar manner. Hitherto, the only described deletion phenotype for PNP in meningococci is hyperaggregation and consequently increased adhesion to human epithelial cells while other cellular functions as well as direct cellular targets have not been reported (240). Therefore, further experiments are required to understand the interplay of meningococcal ProQ and PNP.

In the quantitative proteomics approach, several deregulated proteins in the *proQ* deletion strain involved in meningococcal oxidative stress response such as *recN*, *uvrB* and *mutS* were identified *(*Figure 6-32*)*. Of note, these proteins were not found to be differentially regulated transcripts in the RNA-seq data (Figure 6-29) indicating that ProQ exerts most likely indirect effects on the expression levels of these candidate genes at the post-transcriptional level.

Recently, several proteins were identified that are not damaged by oxidative stress conditions. Instead, these proteins use ROS-mediated thiol modifications to regulate their protein function (241). Reversible oxidation of specific cysteine residues allows these redox-regulated proteins to quickly regulate diverse processes such as protein quality control (Hsp33), gene expression (OxyR) and metabolic fluxes (GapDH) (242-244). Of note, many of these redox-mediated functional changes have been found to significantly contribute to the oxidative stress survival of prokaryotic cells (107). Interestingly, the chromosome-encoded ProQ in *E. coli* has been identified as such a redox-sensitive protein upon both H_2O_2 and NaOCl stress (107,108). Of note, the majority of proteins with NaOCl-sensitive cysteines differed significantly from the proteins with H_2O_2-sensitive cysteines, indicating that the

two physiological oxidants regulate distinct sets of *in vivo* target proteins (107). It might be speculated that the constitutively expressed meningococcal ProQ protein (Figure 6-19) is regulated by ROS-mediated thiol modifications induced by several physiological oxidants thus allowing to quickly regulate global gene expression.

While ProQ in *E. coli* additionally affects biofilm formation and ProQ in *Salmonella* impacts invasion into HeLa cells (109,245), there was no effect of ProQ on one of these phenotypes in meningococci (Figure 6-21). Yet, it needs to be pointed out that the investigated strain 8013 is both a bad biofilm builder and a less-invasive meningococcal strain. Therefore, *N. meningitidis* strain 8013 might not be an appropriate model strain for investigating these latter two phenotypes. Repetition of both assays with a meningococcal *proQ* deletion strain which better forms biofilms and is hyper-invasive such as serogroup B strain MC58 could draw a more informative picture.

Allover, ProQ is involved in oxidative stress response and DNA damage repair in *N. meningitidis*. Thus, the ProQ-centered cellular network likely prevents being killed by professional phagocytes encountered in the human bloodstream by *N. meningitidis*. For a deeper understanding of the interplay of ProQ and its target suite in oxidative stress response and a potential role of the identified ProQ-associated sRNAs, further experiments are required.

7.9. Impact of structures of ProQ/FinO-domain proteins on their targetome and physiological role

The UV-CLIP-seq approach identified the meningococcal ProQ protein lacking any N- and C-terminal extensions (chapter 3.6.3) as a global RBP (Figure 6-18). Recently, it has been shown that the ProQ homologs RocC and FinO harbouring terminal regions regulate few cellular transcripts while the enterobacterial ProQ protein possessing a separate C-terminal domain acts as a global gene regulator (chapter 3.6.3)(99). Therefore, it might be speculated that global activity represents the major mode of action of the central ProQ/FinO-domain while RNA binding selectivity evolves through acquisition of additional terminal regions that constrain target recognition.

Furthermore, it might be speculated that the overall sizes of ProQ proteins correlate with the ecological niche and thus biological role of ProQ proteins in bacteria. Of note, gamma-

proteobacteria such as *Enterobacteriales* harbouring on average biggest ProQ proteins inhabit a number of different ecological niches such as soil, water and intestines of living organisms where they are exposed to a wide range of e.g. temperatures. Interestingly, the *proQ* gene was identified in a screen for genes involved in adaptation of *E. coli* cells to growth at elevated temperature in glucose minimal media (246). In contrast, the beta-proteobacterium *N. meningitidis* harbouring a minimal ProQ protein is host-restricted to the human nasopharynx and therefore to a narrow ecological niche with e.g. little temperature changes. In line with that, we could not observed an impact of *proQ* deletion on temperature changes in *N. meningitidis* in course of our established array of *ex vivo* assays (Figure 6-21).

7.10. Limitations of the study

The current work has some limitations within which the results described in this thesis need to be interpreted carefully.

Hfq RIP-seq has proven its utility in distinct studies in different bacterial organisms (59,171,247,248) althought it suffers from some technical limitations. These include the formation of spurious associations after cell lysis which potentially cause non-specific interactions (249). Moreover, the lengthy RIP-seq protocol can cause degraded mRNAs (250) which are pulled down together with complete transcripts by this protocol. Therefore, the resolution of Hfq RIP-seq is poor and no reliable information on the locations of Hfq binding sites within a messenger transcript can be achieved (251). Thus, downstream analyses as for instance the identification of RBP binding motifs is difficult. To overcome these issues, the recently developed CLIP-seq approach was employed for the identification of ProQ-associated RNAs (chapter 6.5.4). Thereby, UV cross-linking of RNA binding partners to ProQ allowed both the use of several stringent washes and a transfer step of ProQ-RNA complexes to nitrocellulose membrane reducing unspecific interactions. In addition, RNase treatment increased the resolution of CLIP-seq compared to RIP-seq and thus allowed the identification of RBP binding motifs for ProQ. Although CLIP-seq has proven its functionality in distinct recent studies (96,104), it also suffers from some technical limitations. Of note, not all RBP:RNA interactions are cross-linked with the same efficiency and therefore some physiological interactions will certainly be missed by this method. Yet the factors which influence these biases are still elusive (252).

Therefore, comparisons of Hfq-bound RNAs identified by Hfq RIP-seq to RNAs associated with ProQ according to ProQ CLIP-seq (chapter 6.5.6) might be subjected to bias as the applied methodologies differ from each other.

Furthermore, many sRNAs have a short half-live and are only expressed under specific growth conditions (59) and thus may be highly abundant in one experimental set-up while being undetected in another experiment. Since both Hfq RIP-seq (chapter 6.3) and ProQ CLIP-seq (chapter 6.5.4) were only performed in one *in vitro* growth condition, it is likely that not the complete cellular repertoire of RBP binding partners could be detected. Due to the large amount of high-quality RNA required for both RIP-seq and CLIP-seq protocols, it was in particular not possible to select an *ex vivo* stress condition of importance in *N. meningitidis* infection biology e.g. exposition to human saliva, blood or liquor. Yet, stationary growth phase is known to expose the bacterial cells to several environmental stresses such as nutritional stresses (129). Therefore, performing ProQ CLIP-seq at stationary growth-phase is a suitable *in vitro* condition for mimicking to some extent meningococcal infection conditions. Unfortunately, Hfq RIP-seq was performed at mid logarithmic growth phase only although genome-wide sRNA identification *via* dRNA-seq (chapter 6.2) was performed in both growth condidtions (mid logarithmic, late logarithmic) and did not reveal large differences in sRNA and mRNA expression between both growth phases.

As described in chapter 6.2.2, roughly one quarter of the identified sRNAs of *N. meningitidis* strain 8013 are expressed in a strain-specific manner. In accordance with these findings, previous comparative transcriptomics studies have revealed significant differences between pathogenic and non-pathogenic *Listeria* species (191) and between different *Campylobacter jejuni* strains (144) in a subset of non-coding RNAs, respectively. These variable sRNAs possibly contribute to the differences in pathogenicity between the investigated strains. Therefore, performing RBP pull-down experiments as well as dRNA-seq approaches with different strains from hyperinvasive and carriage lineages in *N. meningitidis* might increase our knowledge of the repertoire of RBP-RNA complexes which might contribute to phenotypic diversity by regulating strain-specific gene expression.

7.11. Conclusion and outlook

The capability of *N. meningitidis* to adapt quickly to highly selective and dynamic environments is of key importance for survival within the human host. Regulation of gene expression through sRNAs mediated by RNA chaperones has been shown to serve as a

repository of possible phenotypes, which allows fast adaptation and survival in unpredictable and challenging environments. In summary, novel transcriptional start sites of annotated genes and identified novel transcripts comprising new sRNAs and antisense RNAs were identified in this work on a global scale using dRNA-seq. In addition, an Hfq interactome map of the whole transcript complement was generated using Hfq RIP-seq that enabled the identification of a putative colonization factor as target for two new paralogous sRNAs. Further, a translational reporter assay accurately confirmed target regulation *in vivo* which might help to improve target validation for sRNAs in other *N. meningitidis* strains. These findings together with earlier reports (37,66) indicate that sRNAs play an important role in gene regulation in meningococci.

By applying ProQ UV-CLIP-seq, the existence of a second global, yet minor, RNA-binding protein in *N. meningitidis* could be demonstrated besides the Hfq protein (Figure 7-2). By phenotypic screening of a ProQ deletion strain, for the first time a physiological function of this hitherto uncharacterized hypothetical protein in *N. meningitidis (*Figure 7-2*)* could be described. In addition, the meningococcal ProQ was found to be a global gene regulator. Yet, the physiological role and mode of action of the discovered ProQ-associated sRNA is so far unknown. Further experiments such as MS2 affinity purification coupled with RNA sequencing (MAPS) (253) could help to identify sRNA-centered regulons which could serve as a foundation for investigating the molecular base pairing mechanisms of ProQ-associated sRNAs with their target genes. In contrast to Hfq, ProQ seems to govern its network of mRNAs and sRNAs by reading RNA secondary structure (Figure 7-2). As structural analysis of ProQ proteins is in its infancy, the data provided in this work might help to understand the structural recognition code and resulting target selectivity of FinO-like RBPs in future analyses. Together, these data provide further insights into homogeneity patterns and diversity of FinO domain containing RBPs conserved among proteobacteria. Comparing the ProQ targetome to the Hfq regulon in *N. meningitidis*, (Figure 7-2) suggests a regulatory cross-talk between Hfq and ProQ at the post-transcriptional level. Therefore, the recently-developed RIL-seq approach (RNA Interaction by Ligation and sequencing) could help to uncover the individual contribution of ProQ and Hfq protein associated with the same RNAs (254). Understanding how both RNA chaperons work together and in isolation remains a challenging task but it is becoming clear that Hfq is not the only RNA chaperone in *N. meningitidis* globally affecting gene expression. Of note, roughly half of the identified sRNA candidates were not found to be associated with either Hfq or ProQ protein. Taking advantage of the recently developed gradient profiling by sequencing

(Grad-seq) approach could help to identify so far uncharacterized additional RBPs in *N. meningitidis (97)* and to uncover their role in meningococcal riboregulation.

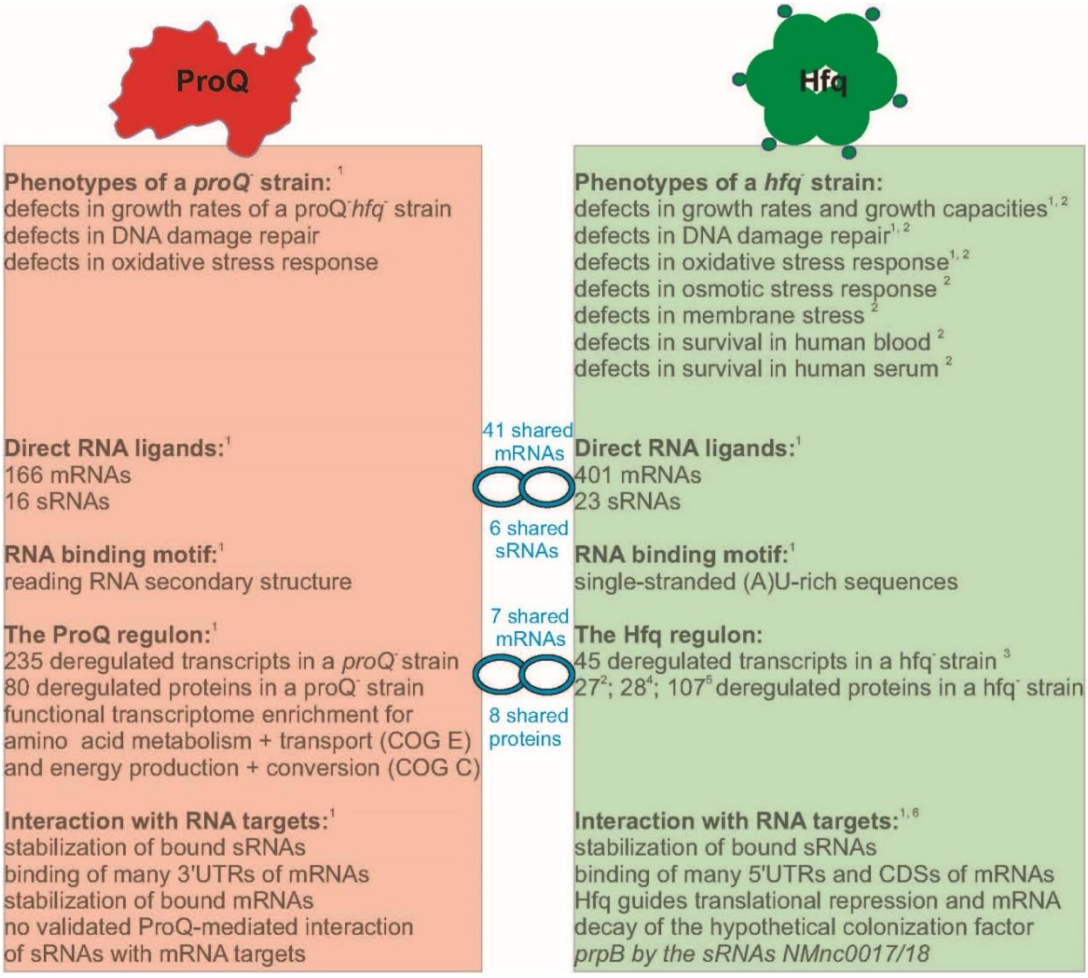

Figure 7-2 Characterization of the two RBPs ProQ and Hfq in *N. meningitidis*

(1) as delineated in this study, (2) as delineated in Fantappie *et al*., 2009 (93), (3) as delineated in Mellin *et al.*, 2010 (177), (4) as delineated in Pannekoek *et al*., 2009 (156), (5) as delineated in Huis *et al*., 2017 (94), (6) as delineated in Bauer *et al*., 2017 (201).

8. References

1. Caugant, D.A. and Maiden, M.C. (2009) Meningococcal carriage and disease--population biology and evolution. *Vaccine*, **27 Suppl 2**, B64-70.
2. Yazdankhah, S.P. and Caugant, D.A. (2004) Neisseria meningitidis: an overview of the carriage state. *Journal of medical microbiology*, **53**, 821-832.
3. Claus, H., Maiden, M.C., Wilson, D.J., McCarthy, N.D., Jolley, K.A., Urwin, R., Hessler, F., Frosch, M. and Vogel, U. (2005) Genetic analysis of meningococci carried by children and young adults. *The Journal of infectious diseases*, **191**, 1263-1271.
4. Stephens, D.S., Greenwood, B. and Brandtzaeg, P. (2007) Epidemic meningitis, meningococcaemia, and Neisseria meningitidis. *Lancet (London, England)*, **369**, 2196-2210.
5. Coureuil, M., Join-Lambert, O., Lecuyer, H., Bourdoulous, S., Marullo, S. and Nassif, X. (2013) Pathogenesis of meningococcemia. *Cold Spring Harbor perspectives in medicine*, **3**.
6. Rosenstein, N.E., Perkins, B.A., Stephens, D.S., Popovic, T. and Hughes, J.M. (2001) Meningococcal disease. *The New England journal of medicine*, **344**, 1378-1388.
7. Tan, F.Y., Wormann, M.E., Loh, E., Tang, C.M. and Exley, R.M. (2015) Characterization of a novel antisense RNA in the major pilin locus of Neisseria meningitidis influencing antigenic variation. *Journal of bacteriology*, **197**, 1757-1768.
8. Wormann, M.E., Horien, C.L., Bennett, J.S., Jolley, K.A., Maiden, M.C., Tang, C.M., Aho, E.L. and Exley, R.M. (2014) Sequence, distribution and chromosomal context of class I and class II pilin genes of Neisseria meningitidis identified in whole genome sequences. *BMC genomics*, **15**, 253.
9. Koomey, M. (1998) Competence for natural transformation in Neisseria gonorrhoeae: a model system for studies of horizontal gene transfer. *APMIS. Supplementum*, **84**, 56-61.
10. Halperin, S.A., Bettinger, J.A., Greenwood, B., Harrison, L.H., Jelfs, J., Ladhani, S.N., McIntyre, P., Ramsay, M.E. and Safadi, M.A. (2012) The changing and dynamic epidemiology of meningococcal disease. *Vaccine*, **30 Suppl 2**, B26-36.
11. Tan, L.K., Carlone, G.M. and Borrow, R. (2010) Advances in the development of vaccines against Neisseria meningitidis. *The New England journal of medicine*, **362**, 1511-1520.
12. Joseph, B., Schwarz, R.F., Linke, B., Blom, J., Becker, A., Claus, H., Goesmann, A., Frosch, M., Muller, T., Vogel, U. *et al.* (2011) Virulence evolution of the human pathogen Neisseria meningitidis by recombination in the core and accessory genome. *PloS one*, **6**, e18441.
13. Schoen, C., Blom, J., Claus, H., Schramm-Glück, A., Brandt, P., Müller, T., Goesmann, A., Joseph, B., Konietzny, S., Kurzai, O. *et al.* (2008) Whole-genome comparison of disease and carriage strains provides insights into virulence evolution in Neisseria meningitidis. *Proceedings of the National Academy of Sciences of the United States of America*, **105**, 3473-3478.

14. Buckee, C.O., Jolley, K.A., Recker, M., Penman, B., Kriz, P., Gupta, S. and Maiden, M.C. (2008) Role of selection in the emergence of lineages and the evolution of virulence in Neisseria meningitidis. *Proceedings of the National Academy of Sciences of the United States of America*, **105**, 15082-15087.

15. Ampattu, B.J., Hagmann, L., Liang, C., Dittrich, M., Schluter, A., Blom, J., Krol, E., Goesmann, A., Becker, A., Dandekar, T. *et al.* (2017) Transcriptomic buffering of cryptic genetic variation contributes to meningococcal virulence. *BMC genomics*, **18**, 282.

16. Joseph, B., Schneiker-Bekel, S., Schramm-Gluck, A., Blom, J., Claus, H., Linke, B., Schwarz, R.F., Becker, A., Goesmann, A., Frosch, M. *et al.* (2010) Comparative genome biology of a serogroup B carriage and disease strain supports a polygenic nature of meningococcal virulence. *Journal of bacteriology*, **192**, 5363-5377.

17. Bervoets, I. and Charlier, D. (2019) Diversity, versatility and complexity of bacterial gene regulation mechanisms: opportunities and drawbacks for applications in synthetic biology. *FEMS microbiology reviews*, **43**, 304-339.

18. Dietrich, G., Kurz, S., Hubner, C., Aepinus, C., Theiss, S., Guckenberger, M., Panzner, U., Weber, J. and Frosch, M. (2003) Transcriptome analysis of Neisseria meningitidis during infection. *Journal of bacteriology*, **185**, 155-164.

19. Gruber, T.M. and Gross, C.A. (2003) Multiple sigma subunits and the partitioning of bacterial transcription space. *Annual review of microbiology*, **57**, 441-466.

20. Sharma, U.K. and Chatterji, D. (2010) Transcriptional switching in Escherichia coli during stress and starvation by modulation of sigma activity. *FEMS microbiology reviews*, **34**, 646-657.

21. Gunesekere, I.C., Kahler, C.M., Ryan, C.S., Snyder, L.A., Saunders, N.J., Rood, J.I. and Davies, J.K. (2006) Ecf, an alternative sigma factor from Neisseria gonorrhoeae, controls expression of msrAB, which encodes methionine sulfoxide reductase. *Journal of bacteriology*, **188**, 3463-3469.

22. Hopman, C.T., Speijer, D., van der Ende, A. and Pannekoek, Y. (2010) Identification of a novel anti-sigmaE factor in Neisseria meningitidis. *BMC microbiology*, **10**, 164.

23. Huis in 't Veld, R.A., Willemsen, A.M., van Kampen, A.H., Bradley, E.J., Baas, F., Pannekoek, Y. and van der Ende, A. (2011) Deep sequencing whole transcriptome exploration of the sigmaE regulon in Neisseria meningitidis. *PloS one*, **6**, e29002.

24. Palonen, E., Lindstrom, M., Somervuo, P. and Korkeala, H. (2013) Alternative sigma factor sigmaE has an important role in stress tolerance of Yersinia pseudotuberculosis IP32953. *Applied and environmental microbiology*, **79**, 5970-5977.

25. Haines-Menges, B., Whitaker, W.B. and Boyd, E.F. (2014) Alternative sigma factor RpoE is important for Vibrio parahaemolyticus cell envelope stress response and intestinal colonization. *Infection and immunity*, **82**, 3667-3677.

26. Stock, J.B., Ninfa, A.J. and Stock, A.M. (1989) Protein phosphorylation and regulation of adaptive responses in bacteria. *Microbiological reviews*, **53**, 450-490.

27. Oshima, T., Aiba, H., Masuda, Y., Kanaya, S., Sugiura, M., Wanner, B.L., Mori, H. and Mizuno, T. (2002) Transcriptome analysis of all two-component regulatory system mutants of Escherichia coli K-12. *Molecular microbiology*, **46**, 281-291.

28. Yamamoto, K., Hirao, K., Oshima, T., Aiba, H., Utsumi, R. and Ishihama, A. (2005) Functional characterization in vitro of all two-component signal transduction systems from Escherichia coli. *The Journal of biological chemistry*, **280**, 1448-1456.

29. Jamet, A., Rousseau, C., Monfort, J.B., Frapy, E., Nassif, X. and Martin, P. (2009) A two-component system is required for colonization of host cells by meningococcus. *Microbiology (Reading, England)*, **155**, 2288-2295.

30. Tzeng, Y.L., Zhou, X., Bao, S., Zhao, S., Noble, C. and Stephens, D.S. (2006) Autoregulation of the MisR/MisS two-component signal transduction system in Neisseria meningitidis. *Journal of bacteriology*, **188**, 5055-5065.

31. Newcombe, J., Jeynes, J.C., Mendoza, E., Hinds, J., Marsden, G.L., Stabler, R.A., Marti, M. and McFadden, J.J. (2005) Phenotypic and transcriptional characterization of the meningococcal PhoPQ system, a magnesium-sensing two-component regulatory system that controls genes involved in remodeling the meningococcal cell surface. *Journal of bacteriology*, **187**, 4967-4975.

32. Tzeng, Y.L., Kahler, C.M., Zhang, X. and Stephens, D.S. (2008) MisR/MisS two-component regulon in Neisseria meningitidis. *Infection and immunity*, **76**, 704-716.

33. Vallenet, D., Belda, E., Calteau, A., Cruveiller, S., Engelen, S., Lajus, A., Le Fevre, F., Longin, C., Mornico, D., Roche, D. *et al.* (2013) MicroScope--an integrated microbial resource for the curation and comparative analysis of genomic and metabolic data. *Nucleic acids research*, **41**, D636-647.

34. Madan Babu, M. and Teichmann, S.A. (2003) Evolution of transcription factors and the gene regulatory network in Escherichia coli. *Nucleic acids research*, **31**, 1234-1244.

35. Delany, I., Rappuoli, R. and Scarlato, V. (2004) Fur functions as an activator and as a repressor of putative virulence genes in Neisseria meningitidis. *Molecular microbiology*, **52**, 1081-1090.

36. Fantappie, L., Oriente, F., Muzzi, A., Serruto, D., Scarlato, V. and Delany, I. (2011) A novel Hfq-dependent sRNA that is under FNR control and is synthesized in oxygen limitation in Neisseria meningitidis. *Molecular microbiology*, **80**, 507-523.

37. Fagnocchi, L., Bottini, S., Golfieri, G., Fantappie, L., Ferlicca, F., Antunes, A., Guadagnuolo, S., Del Tordello, E., Siena, E., Serruto, D. *et al.* (2015) Global transcriptome analysis reveals small RNAs affecting Neisseria meningitidis bacteremia. *PloS one*, **10**, e0126325.

38. Fuli, X., Wenlong, Z., Xiao, W., Jing, Z., Baohai, H., Zhengzheng, Z., Bin-Guang, M. and Youguo, L. (2017) A genome-wide prediction and identification of intergenic small RNAs by comparative analysis in Mesorhizobium huakuii 7653R. *Frontiers in microbiology*, **8**, 1730.

39. Westhof, E. (2010) The amazing world of bacterial structured RNAs. *Genome biology*, **11**, 108.

40. Waters, L.S. and Storz, G. (2009) Regulatory RNAs in bacteria. *Cell*, **136**, 615-628.

41. Sampson, T.R., Saroj, S.D., Llewellyn, A.C., Tzeng, Y.L. and Weiss, D.S. (2013) A CRISPR/Cas system mediates bacterial innate immune evasion and virulence. *Nature*, **497**, 254-257.

42. Zhang, Y., Heidrich, N., Ampattu, B.J., Gunderson, C.W., Seifert, H.S., Schoen, C., Vogel, J. and Sontheimer, E.J. (2013) Processing-independent CRISPR RNAs limit natural transformation in Neisseria meningitidis. *Molecular cell*, **50**, 488-503.

43. Heidrich, N., Hagmann, A., Bauriedl, S., Vogel, J. and Schoen, C. (2019) The CRISPR/Cas system in Neisseria meningitidis affects bacterial adhesion to human nasopharyngeal epithelial cells. *RNA biology*, **16**, 390-396.

44. Grundy, F.J. and Henkin, T.M. (2004) Regulation of gene expression by effectors that bind to RNA. *Current opinion in microbiology*, **7**, 126-131.

45. Kortmann, J. and Narberhaus, F. (2012) Bacterial RNA thermometers: molecular zippers and switches. *Nature reviews. Microbiology*, **10**, 255-265.

46. Barnwal, R.P., Loh, E., Godin, K.S., Yip, J., Lavender, H., Tang, C.M. and Varani, G. (2016) Structure and mechanism of a molecular rheostat, an RNA thermometer that modulates immune evasion by Neisseria meningitidis. *Nucleic acids research*, **44**, 9426-9437.

47. Loh, E., Lavender, H., Tan, F., Tracy, A. and Tang, C.M. (2016) Thermoregulation of meningococcal fHbp, an important virulence factor and vaccine antigen, is mediated by anti-ribosomal binding site sequences in the open reading frame. *PLoS pathogens*, **12**, e1005794.

48. Loh, E., Kugelberg, E., Tracy, A., Zhang, Q., Gollan, B., Ewles, H., Chalmers, R., Pelicic, V. and Tang, C.M. (2013) Temperature triggers immune evasion by Neisseria meningitidis. *Nature*, **502**, 237-240.

49. Georg, J. and Hess, W.R. (2011) cis-antisense RNA, another level of gene regulation in bacteria. *Microbiology and molecular biology reviews : MMBR*, **75**, 286-300.

50. Brantl, S. (2007) Regulatory mechanisms employed by cis-encoded antisense RNAs. *Current opinion in microbiology*, **10**, 102-109.

51. Belzer, C., van Schendel, B.A., Kuipers, E.J., Kusters, J.G. and van Vliet, A.H. (2007) Iron-responsive repression of urease expression in Helicobacter hepaticus is mediated by the transcriptional regulator Fur. *Infection and immunity*, **75**, 745-752.

52. Wen, Y., Feng, J., Scott, D.R., Marcus, E.A. and Sachs, G. (2011) A cis-encoded antisense small RNA regulated by the HP0165-HP0166 two-component system controls expression of ureB in Helicobacter pylori. *Journal of bacteriology*, **193**, 40-51.

53. Grundling, A., Burrack, L.S., Bouwer, H.G. and Higgins, D.E. (2004) Listeria monocytogenes regulates flagellar motility gene expression through MogR, a transcriptional repressor required for virulence. *Proceedings of the National Academy of Sciences of the United States of America*, **101**, 12318-12323.

54. Liu, Z., Trevino, J., Ramirez-Pena, E. and Sumby, P. (2012) The small regulatory RNA FasX controls pilus expression and adherence in the human bacterial pathogen group A Streptococcus. *Molecular microbiology*, **86**, 140-154.

55. Storz, G., Vogel, J. and Wassarman, K.M. (2011) Regulation by small RNAs in bacteria: expanding frontiers. *Molecular cell*, **43**, 880-891.

56. Papenfort, K. and Vogel, J. (2010) Regulatory RNA in bacterial pathogens. *Cell Host Microbe*, **8**, 116-127.

57. Frohlich, K.S. and Vogel, J. (2009) Activation of gene expression by small RNA. *Current opinion in microbiology*, **12**, 674-682.

58. Vogel, J. and Luisi, B.F. (2011) Hfq and its constellation of RNA. *Nature reviews. Microbiology*, **9**, 578-589.

59. Chao, Y., Papenfort, K., Reinhardt, R., Sharma, C.M. and Vogel, J. (2012) An atlas of Hfq-bound transcripts reveals 3' UTRs as a genomic reservoir of regulatory small RNAs. *The EMBO journal*, **31**, 4005-4019.

60. Ellis, M.J., Trussler, R.S., Charles, O. and Haniford, D.B. (2017) A transposon-derived small RNA regulates gene expression in Salmonella Typhimurium. *Nucleic acids research*, **45**, 5470-5486.

61. Loh, E., Dussurget, O., Gripenland, J., Vaitkevicius, K., Tiensuu, T., Mandin, P., Repoila, F., Buchrieser, C., Cossart, P. and Johansson, J. (2009) A trans-acting riboswitch controls expression of the virulence regulator PrfA in Listeria monocytogenes. *Cell*, **139**, 770-779.

62. Sharma, C.M., Papenfort, K., Pernitzsch, S.R., Mollenkopf, H.J., Hinton, J.C. and Vogel, J. (2011) Pervasive post-transcriptional control of genes involved in amino acid metabolism by the Hfq-dependent GcvB small RNA. *Mol Microbiol*, **81**, 1144-1165.

63. Sharma, C.M., Darfeuille, F., Plantinga, T.H. and Vogel, J. (2007) A small RNA regulates multiple ABC transporter mRNAs by targeting C/A-rich elements inside and upstream of ribosome-binding sites. *Genes & development*, **21**, 2804-2817.

64. Prevost, K., Salvail, H., Desnoyers, G., Jacques, J.F., Phaneuf, E. and Masse, E. (2007) The small RNA RyhB activates the translation of shiA mRNA encoding a permease of shikimate, a compound involved in siderophore synthesis. *Mol Microbiol*, **64**, 1260-1273.

65. Masse, E. and Gottesman, S. (2002) A small RNA regulates the expression of genes involved in iron metabolism in Escherichia coli. *Proceedings of the National Academy of Sciences of the United States of America*, **99**, 4620-4625.

66. Del Tordello, E., Bottini, S., Muzzi, A. and Serruto, D. (2012) Analysis of the regulated transcriptome of Neisseria meningitidis in human blood using a tiling array. *Journal of bacteriology*, **194**, 6217-6232.

67. Mellin, J.R., Goswami, S., Grogan, S., Tjaden, B. and Genco, C.A. (2007) A novel fur- and iron-regulated small RNA, NrrF, is required for indirect fur-mediated regulation of the sdhA and sdhC genes in Neisseria meningitidis. *Journal of bacteriology*, **189**, 3686-3694.

68. Metruccio, M.M., Fantappie, L., Serruto, D., Muzzi, A., Roncarati, D., Donati, C., Scarlato, V. and Delany, I. (2009) The Hfq-dependent small noncoding RNA NrrF directly mediates Fur-dependent positive regulation of succinate dehydrogenase in Neisseria meningitidis. *Journal of bacteriology*, **191**, 1330-1342.

69. Jackson, L.A., Pan, J.C., Day, M.W. and Dyer, D.W. (2013) Control of RNA stability by NrrF, an iron-regulated small RNA in Neisseria gonorrhoeae. *Journal of bacteriology*, **195**, 5166-5173.

70. Romeo, T., Vakulskas, C.A. and Babitzke, P. (2013) Post-transcriptional regulation on a global scale: form and function of Csr/Rsm systems. *Environ Microbiol*, **15**, 313-324.

71. Dugar, G., Svensson, S.L., Bischler, T., Waldchen, S., Reinhardt, R., Sauer, M. and Sharma, C.M. (2016) The CsrA-FliW network controls polar localization of the dual-function flagellin mRNA in Campylobacter jejuni. *Nature communications*, **7**, 11667.

72. Vakulskas, C.A., Potts, A.H., Babitzke, P., Ahmer, B.M. and Romeo, T. (2015) Regulation of bacterial virulence by Csr (Rsm) systems. *Microbiology and molecular biology reviews : MMBR*, **79**, 193-224.

73. Barrick, J.E., Sudarsan, N., Weinberg, Z., Ruzzo, W.L. and Breaker, R.R. (2005) 6S RNA is a widespread regulator of eubacterial RNA polymerase that resembles an open promoter. *RNA (New York, N.Y.)*, **11**, 774-784.

74. Fox, G.E. (2010) Origin and evolution of the ribosome. *Cold Spring Harbor perspectives in biology*, **2**, a003483.

75. Ray-Soni, A., Bellecourt, M.J. and Landick, R. (2016) Mechanisms of bacterial transcription termination: All good things must end. *Annual review of biochemistry*, **85**, 319-347.

76. Holmqvist, E. and Vogel, J. (2018) RNA-binding proteins in bacteria. *Nature reviews. Microbiology*, **16**, 601-615.

77. Franze de Fernandez, M.T., Eoyang, L. and August, J.T. (1968) Factor fraction required for the synthesis of bacteriophage Qbeta-RNA. *Nature*, **219**, 588-590.

78. Wilusz, C.J. and Wilusz, J. (2005) Eukaryotic Lsm proteins: lessons from bacteria. *Nature structural & molecular biology*, **12**, 1031-1036.

79. Sauer, E., Schmidt, S. and Weichenrieder, O. (2012) Small RNA binding to the lateral surface of Hfq hexamers and structural rearrangements upon mRNA target recognition. *Proceedings of the National Academy of Sciences of the United States of America*, **109**, 9396-9401.

80. Brennan, R.G. and Link, T.M. (2007) Hfq structure, function and ligand binding. *Current opinion in microbiology*, **10**, 125-133.

81. Aiba, H. (2007) Mechanism of RNA silencing by Hfq-binding small RNAs. *Current opinion in microbiology*, **10**, 134-139.

82. Schumacher, M.A., Pearson, R.F., Moller, T., Valentin-Hansen, P. and Brennan, R.G. (2002) Structures of the pleiotropic translational regulator Hfq and an Hfq-RNA complex: a bacterial Sm-like protein. *The EMBO journal*, **21**, 3546-3556.

83. Sauer, E. and Weichenrieder, O. (2011) Structural basis for RNA 3'-end recognition by Hfq. *Proceedings of the National Academy of Sciences of the United States of America*, **108**, 13065-13070.

84. Link, T.M., Valentin-Hansen, P. and Brennan, R.G. (2009) Structure of Escherichia coli Hfq bound to polyriboadenylate RNA. *Proceedings of the National Academy of Sciences of the United States of America*, **106**, 19292-19297.

85. Schu, D.J., Zhang, A., Gottesman, S. and Storz, G. (2015) Alternative Hfq-sRNA interaction modes dictate alternative mRNA recognition. *The EMBO journal*, **34**, 2557-2573.

86. Olsen, A.S., Moller-Jensen, J., Brennan, R.G. and Valentin-Hansen, P. (2010) C-terminally truncated derivatives of Escherichia coli Hfq are proficient in riboregulation. *Journal of molecular biology*, **404**, 173-182.

87. Vecerek, B., Rajkowitsch, L., Sonnleitner, E., Schroeder, R. and Blasi, U. (2008) The C-terminal domain of Escherichia coli Hfq is required for regulation. *Nucleic acids research*, **36**, 133-143.

88. Santiago-Frangos, A., Kavita, K., Schu, D.J., Gottesman, S. and Woodson, S.A. (2016) C-terminal domain of the RNA chaperone Hfq drives sRNA competition and release of target RNA. *Proceedings of the National Academy of Sciences of the United States of America*, **113**, E6089-e6096.

89. Vytvytska, O., Moll, I., Kaberdin, V.R., von Gabain, A. and Blasi, U. (2000) Hfq (HF1) stimulates ompA mRNA decay by interfering with ribosome binding. *Genes & development*, **14**, 1109-1118.

90. Mohanty, B.K., Maples, V.F. and Kushner, S.R. (2004) The Sm-like protein Hfq regulates polyadenylation dependent mRNA decay in Escherichia coli. *Mol Microbiol*, **54**, 905-920.

91. Chen, J. and Gottesman, S. (2017) Hfq links translation repression to stress-induced mutagenesis in E. coli. *Genes & development*, **31**, 1382-1395.

92. Chao, Y. and Vogel, J. (2010) The role of Hfq in bacterial pathogens. *Current opinion in microbiology*, **13**, 24-33.

93. Fantappie, L., Metruccio, M.M., Seib, K.L., Oriente, F., Cartocci, E., Ferlicca, F., Giuliani, M.M., Scarlato, V. and Delany, I. (2009) The RNA chaperone Hfq is involved in stress response and virulence in Neisseria meningitidis and is a pleiotropic regulator of protein expression. *Infection and immunity*, **77**, 1842-1853.

94. Huis In 't Veld, R.A.G., Kramer, G., van der Ende, A., Speijer, D. and Pannekoek, Y. (2017) The Hfq regulon of Neisseria meningitidis. *FEBS Open Bio*, **7**, 777-788.

95. Sittka, A., Sharma, C.M., Rolle, K. and Vogel, J. (2009) Deep sequencing of Salmonella RNA associated with heterologous Hfq proteins in vivo reveals small RNAs as a major target class and identifies RNA processing phenotypes. *RNA biology*, **6**, 266-275.

96. Holmqvist, E., Wright, P.R., Li, L., Bischler, T., Barquist, L., Reinhardt, R., Backofen, R. and Vogel, J. (2016) Global RNA recognition patterns of post-transcriptional regulators Hfq and CsrA revealed by UV crosslinking in vivo. *The EMBO journal*, **35**, 991-1011.

97. Smirnov, A., Forstner, K.U., Holmqvist, E., Otto, A., Gunster, R., Becher, D., Reinhardt, R. and Vogel, J. (2016) Grad-seq guides the discovery of ProQ as a major small RNA-binding protein. *Proceedings of the National Academy of Sciences of the United States of America*, **113**, 11591-11596.

98. Durand, S., Tomasini, A., Braun, F., Condon, C. and Romby, P. (2015) sRNA and mRNA turnover in Gram-positive bacteria. *FEMS microbiology reviews*, **39**, 316-330.

99. Olejniczak, M. and Storz, G. (2017) ProQ/FinO-domain proteins: another ubiquitous family of RNA matchmakers? *Molecular microbiology*, **104**, 905-915.

100. Attaiech, L., Boughammoura, A., Brochier-Armanet, C., Allatif, O., Peillard-Fiorente, F., Edwards, R.A., Omar, A.R., MacMillan, A.M., Glover, M. and Charpentier, X. (2016) Silencing of natural transformation by an RNA chaperone and a multitarget small RNA. *Proceedings of the National Academy of Sciences of the United States of America*, **113**, 8813-8818.

101. Arthur, D.C., Ghetu, A.F., Gubbins, M.J., Edwards, R.A., Frost, L.S. and Glover, J.N. (2003) FinO is an RNA chaperone that facilitates sense-antisense RNA interactions. *The EMBO journal*, **22**, 6346-6355.

102. Kunte, H.J., Crane, R.A., Culham, D.E., Richmond, D. and Wood, J.M. (1999) Protein ProQ influences osmotic activation of compatible solute transporter ProP in Escherichia coli K-12. *Journal of bacteriology*, **181**, 1537-1543.

103. Smirnov, A., Wang, C., Drewry, L.L. and Vogel, J. (2017) Molecular mechanism of mRNA repression in trans by a ProQ-dependent small RNA. *The EMBO journal*, **36**, 1029-1045.

104. Holmqvist, E., Li, L., Bischler, T., Barquist, L. and Vogel, J. (2018) Global maps of ProQ binding in vivo reveal target recognition via RNA structure and stability control at mRNA 3' Ends. *Molecular cell*, **70**, 971-982.e976.

105. Smirnov, A. and Forstner, K.U. (2016) Grad-seq guides the discovery of ProQ as a major small RNA-binding protein. **113**, 11591-11596.

106. Sheidy, D.T. and Zielke, R.A. (2013) Analysis and expansion of the role of the Escherichia coli protein ProQ. *PloS one*, **8**, e79656.

107. Leichert, L.I., Gehrke, F., Gudiseva, H.V., Blackwell, T., Ilbert, M., Walker, A.K., Strahler, J.R., Andrews, P.C. and Jakob, U. (2008) Quantifying changes in the thiol redox proteome upon oxidative stress in vivo. *Proceedings of the National Academy of Sciences of the United States of America*, **105**, 8197-8202.

108. Xie, K., Bunse, C., Marcus, K. and Leichert, L.I. (2019) Quantifying changes in the bacterial thiol redox proteome during host-pathogen interaction. *Redox biology*, **21**, 101087.

109. Westermann, A.J., Venturini, E., Sellin, M.E., Forstner, K.U., Hardt, W.D. and Vogel, J. (2019) The major RNA-binding protein ProQ impacts virulence gene expression in Salmonella enterica Serovar Typhimurium. *mBio*, **10**.

110. Updegrove, T.B., Zhang, A. and Storz, G. (2016) Hfq: the flexible RNA matchmaker. *Current opinion in microbiology*, **30**, 133-138.

111. Chaulk, S., Lu, J., Tan, K., Arthur, D.C., Edwards, R.A., Frost, L.S., Joachimiak, A. and Glover, J.N. (2010) N. meningitidis 1681 is a member of the FinO family of RNA chaperones. *RNA biology*, **7**, 812-819.

112. Catenazzi, M.C., Jones, H., Wallace, I., Clifton, J., Chong, J.P., Jackson, M.A., Macdonald, S., Edwards, J. and Moir, J.W. (2014) A large genomic island allows Neisseria meningitidis to utilize propionic acid, with implications for colonization of the human nasopharynx. *Molecular microbiology*, **93**, 346-355.

113. Freese, N.H., Norris, D.C. and Loraine, A.E. (2016) Integrated genome browser: visual analytics platform for genomics. *Bioinformatics (Oxford, England)*, **32**, 2089-2095.

114. Corcoran, C.P., Podkaminski, D., Papenfort, K., Urban, J.H., Hinton, J.C. and Vogel, J. (2012) Superfolder GFP reporters validate diverse new mRNA targets of the classic porin regulator, MicF RNA. *Molecular microbiology*, **84**, 428-445.

115. Chomczynski, P. and Sacchi, N. (2006) The single-step method of RNA isolation by acid guanidinium thiocyanate-phenol-chloroform extraction: twenty-something years on. *Nature protocols*, **1**, 581-585.

116. Berezikov, E., Thuemmler, F., van Laake, L.W., Kondova, I., Bontrop, R., Cuppen, E. and Plasterk, R.H. (2006) Diversity of microRNAs in human and chimpanzee brain. *Nature genetics*, **38**, 1375-1377.

117. Heidrich, N., Bauriedl, S., Barquist, L., Li, L., Schoen, C. and Vogel, J. (2017) The primary transcriptome of Neisseria meningitidis and its interaction with the RNA chaperone Hfq. *Nucleic acids research*, **45**, 6147-6167.

118. Gardner, P.P., Barquist, L., Bateman, A., Nawrocki, E.P. and Weinberg, Z. (2011) RNIE: genome-wide prediction of bacterial intrinsic terminators. *Nucleic acids research*, **39**, 5845-5852.

119. Hoffmann, S., Otto, C., Kurtz, S., Sharma, C.M., Khaitovich, P., Vogel, J., Stadler, P.F. and Hackermuller, J. (2009) Fast mapping of short sequences with mismatches, insertions and deletions using index structures. *PLoS computational biology*, **5**, e1000502.

120. Martin, M. (2011) Cutadapt removes adapter sequences from high-throughput sequencing reads. *EMB.net*, **17**, 3.

121. Love, M.I., Huber, W. and Anders, S. (2014) Moderated estimation of fold change and dispersion for RNA-seq data with DESeq2. *Genome biology*, **15**, 550.

122. Galperin, M.Y., Makarova, K.S., Wolf, Y.I. and Koonin, E.V. (2015) Expanded microbial genome coverage and improved protein family annotation in the COG database. *Nucleic acids research*, **43**, D261-269.

123. Tatusov, R.L., Natale, D.A., Garkavtsev, I.V., Tatusova, T.A., Shankavaram, U.T., Rao, B.S., Kiryutin, B., Galperin, M.Y., Fedorova, N.D. and Koonin, E.V. (2001) The COG database: new developments in phylogenetic classification of proteins from complete genomes. *Nucleic acids research*, **29**, 22-28.

124. Yu, G., Wang, L.G., Han, Y. and He, Q.Y. (2012) clusterProfiler: an R package for comparing biological themes among gene clusters. *Omics : a journal of integrative biology*, **16**, 284-287.

125. Regulski, E.E. and Breaker, R.R. (2008) In-line probing analysis of riboswitches. *Methods in molecular biology (Clifton, N.J.)*, **419**, 53-67.

126. Pernitzsch, S.R., Tirier, S.M., Beier, D. and Sharma, C.M. (2014) A variable homopolymeric G-repeat defines small RNA-mediated posttranscriptional regulation of a chemotaxis receptor in Helicobacter pylori. *Proceedings of the National Academy of Sciences of the United States of America*, **111**, E501-510.

127. Cox, J. and Mann, M. (2008) MaxQuant enables high peptide identification rates, individualized p.p.b.-range mass accuracies and proteome-wide protein quantification. *Nature biotechnology*, **26**, 1367-1372.

128. Cox, J., Hein, M.Y., Luber, C.A., Paron, I., Nagaraj, N. and Mann, M. (2014) Accurate proteome-wide label-free quantification by delayed normalization and maximal peptide ratio extraction, termed MaxLFQ. *Molecular & cellular proteomics : MCP*, **13**, 2513-2526.

129. Schoen, C., Kischkies, L., Elias, J. and Ampattu, B.J. (2014) Metabolism and virulence in Neisseria meningitidis. *Frontiers in cellular and infection microbiology*, **4**, 114.

130. Takahashi, H., Watanabe, H., Kim, K.S., Yokoyama, S. and Yanagisawa, T. (2018) The meningococcal cysteine transport System plays a crucial role in Neisseria meningitidis survival in human brain microvascular endothelial cells. *mBio*, **9**.

131. Davidsen, T., Tuven, H.K., Bjoras, M., Rodland, E.A. and Tonjum, T. (2007) Genetic interactions of DNA repair pathways in the pathogen Neisseria meningitidis. *Journal of bacteriology*, **189**, 5728-5737.

132. Claus, H., Frosch, M. and Vogel, U. (1998) Identification of a hotspot for transformation of Neisseria meningitidis by shuttle mutagenesis using signature-tagged transposons. *Mol Gen Genet*, **259**, 363-371.

133. Vogel, U., Morelli, G., Zurth, K., Claus, H., Kriener, E., Achtman, M. and Frosch, M. (1998) Necessity of molecular techniques to distinguish between Neisseria meningitidis strains isolated from patients with meningococcal disease and from their healthy contacts. *Journal of clinical microbiology*, **36**, 2465-2470.

134. Schneider, C.A., Rasband, W.S. and Eliceiri, K.W. (2012) NIH Image to ImageJ: 25 years of image analysis. *Nature methods*, **9**, 671-675.

135. Altschul, S.F., Gish, W., Miller, W., Myers, E.W. and Lipman, D.J. (1990) Basic local alignment search tool. *Journal of molecular biology*, **215**, 403-410.

136. Edgar, R., Domrachev, M. and Lash, A.E. (2002) Gene Expression Omnibus: NCBI gene expression and hybridization array data repository. *Nucleic acids research*, **30**, 207-210.

137. Mao, X., Ma, Q., Zhou, C., Chen, X., Zhang, H., Yang, J., Mao, F., Lai, W. and Xu, Y. (2014) DOOR 2.0: presenting operons and their functions through dynamic and integrated views. *Nucleic acids research*, **42**, D654-659.

138. Nawrocki, E.P., Burge, S.W., Bateman, A., Daub, J., Eberhardt, R.Y., Eddy, S.R., Floden, E.W., Gardner, P.P., Jones, T.A., Tate, J. *et al.* (2015) Rfam 12.0: updates to the RNA families database. *Nucleic acids research*, **43**, D130-137.

139. R Development Core Team, R. (2006) A language and environment for statistical computing. *Computing*, **1**.

140. Zuker, M. (2003) Mfold web server for nucleic acid folding and hybridization prediction. *Nucleic acids research*, **31**, 3406-3415.

141. Rehmsmeier, M., Steffen, P., Hochsmann, M. and Giegerich, R. (2004) Fast and effective prediction of microRNA/target duplexes. *RNA (New York, N.Y.)*, **10**, 1507-1517.

142. Wright, P.R., Georg, J., Mann, M., Sorescu, D.A., Richter, A.S., Lott, S., Kleinkauf, R., Hess, W.R. and Backofen, R. (2014) CopraRNA and IntaRNA: predicting small RNA targets, networks and interaction domains. *Nucleic acids research*, **42**, W119-123.

143. Corpet, F. (1988) Multiple sequence alignment with hierarchical clustering. *Nucleic acids research*, **16**, 10881-10890.

144. Dugar, G., Herbig, A., Forstner, K.U., Heidrich, N., Reinhardt, R., Nieselt, K. and Sharma, C.M. (2013) High-resolution transcriptome maps reveal strain-specific regulatory features of multiple Campylobacter jejuni isolates. *PLoS genetics*, **9**, e1003495.

145. Bailey, T.L., Johnson, J., Grant, C.E. and Noble, W.S. (2015) The MEME Suite. *Nucleic acids research*, **43**, W39-49.

146. Rusniok, C., Vallenet, D., Floquet, S., Ewles, H., Mouze-Soulama, C., Brown, D., Lajus, A., Buchrieser, C., Medigue, C., Glaser, P. *et al.* (2009) NeMeSys: a biological resource for narrowing the gap between sequence and function in the human pathogen Neisseria meningitidis. *Genome biology*, **10**, R110.

147. Delany, I., Ieva, R., Alaimo, C., Rappuoli, R. and Scarlato, V. (2003) The iron-responsive regulator fur is transcriptionally autoregulated and not essential in Neisseria meningitidis. *Journal of bacteriology*, **185**, 6032-6041.

148. Cahoon, L.A. and Seifert, H.S. (2013) Transcription of a cis-acting, noncoding, small RNA is required for pilin antigenic variation in Neisseria gonorrhoeae. *PLoS pathogens*, **9**, e1003074.

149. Mandal, M., Lee, M., Barrick, J.E., Weinberg, Z., Emilsson, G.M., Ruzzo, W.L. and Breaker, R.R. (2004) A glycine-dependent riboswitch that uses cooperative binding to control gene expression. *Science (New York, N.Y.)*, **306**, 275-279.

150. Labrie, S.J., Samson, J.E. and Moineau, S. (2010) Bacteriophage resistance mechanisms. *Nature reviews. Microbiology*, **8**, 317-327.

151. Gordia, S. and Gutierrez, C. (1996) Growth-phase-dependent expression of the osmotically inducible gene osmC of Escherichia coli K-12. *Molecular microbiology*, **19**, 729-736.

152. Lindgreen, S., Umu, S.U., Lai, A.S., Eldai, H., Liu, W., McGimpsey, S., Wheeler, N.E., Biggs, P.J., Thomson, N.R., Barquist, L. *et al.* (2014) Robust identification of noncoding RNA from transcriptomes requires phylogenetically-informed sampling. *PLoS computational biology*, **10**, e1003907.

153. Dunning Hotopp, J.C., Grifantini, R., Kumar, N., Tzeng, Y.L., Fouts, D., Frigimelica, E., Draghi, M., Giuliani, M.M., Rappuoli, R., Stephens, D.S. *et al.* (2006) Comparative genomics of Neisseria meningitidis: core genome, islands of horizontal transfer and pathogen-specific genes. *Microbiology (Reading, England)*, **152**, 3733-3749.

154. Sharma, C.M. and Vogel, J. (2009) Experimental approaches for the discovery and characterization of regulatory small RNA. *Current opinion in microbiology*, **12**, 536-546.

155. Bauriedl, S. (2014) The repertoire of Hfq regulated small non-coding RNAs in Neisseria meningitidis. . *Master thesis*.

156. Pannekoek, Y., Huis in 't Veld, R., Hopman, C.T., Langerak, A.A., Speijer, D. and van der Ende, A. (2009) Molecular characterization and identification of proteins regulated by Hfq in Neisseria meningitidis. *FEMS Microbiol Lett*, **294**, 216-224.

157. Heidrich, N., Bauriedl, S. and Schoen, C. (2019) Investigating RNA-protein interactions in Neisseria meningitidis by RIP-Seq analysis. *Methods in molecular biology (Clifton, N.J.)*, **1969**, 33-49.

158. Urban, J.H. and Vogel, J. (2007) Translational control and target recognition by Escherichia coli small RNAs in vivo. *Nucleic acids research*, **35**, 1018-1037.

159. Attaiech, L., Glover, J.N.M. and Charpentier, X. (2017) RNA chaperones step out of Hfq's shadow. *Trends in microbiology*, **25**, 247-249.

160. Rouphael, N.G. and Stephens, D.S. (2012) Neisseria meningitidis: biology, microbiology, and epidemiology. *Methods in molecular biology (Clifton, N.J.)*, **799**, 1-20.

161. Lappann, M. and Vogel, U. (2010) Biofilm formation by the human pathogen Neisseria meningitidis. *Med Microbiol Immunol*, **199**, 173-183.

162. Bowen, W.H., Burne, R.A., Wu, H. and Koo, H. (2018) Oral biofilms: Pathogens, matrix, and polymicrobial interactions in microenvironments. *Trends in microbiology*, **26**, 229-242.

163. Zhang, Y., Burkhardt, D.H., Rouskin, S., Li, G.W., Weissman, J.S. and Gross, C.A. (2018) A stress response that monitors and regulates mRNA structure is central to cold shock adaptation. *Molecular cell*, **70**, 274-286.e277.

164. Lappann, M., Otto, A., Brauer, M., Becher, D., Vogel, U. and Johswich, K. (2016) Impact of moderate temperature changes on Neisseria meningitidis adhesion phenotypes and proteome. *Infection and immunity*, **84**, 3484-3495.

165. Criss, A.K. and Seifert, H.S. (2012) A bacterial siren song: intimate interactions between Neisseria and neutrophils. *Nature reviews. Microbiology*, **10**, 178-190.

166. Lo, H., Tang, C.M. and Exley, R.M. (2009) Mechanisms of avoidance of host immunity by Neisseria meningitidis and its effect on vaccine development. *Lancet Infect Dis*, **9**, 418-427.

167. Schneider, M.C., Exley, R.M., Ram, S., Sim, R.B. and Tang, C.M. (2007) Interactions between Neisseria meningitidis and the complement system. *Trends in microbiology*, **15**, 233-240.

168. van der Veen, S. and Tang, C.M. (2015) The BER necessities: the repair of DNA damage in human-adapted bacterial pathogens. *Nature reviews. Microbiology*, **13**, 83-94.

169. Ambur, O.H., Frye, S.A. and Tonjum, T. (2007) New functional identity for the DNA uptake sequence in transformation and its presence in transcriptional terminators. *Journal of bacteriology*, **189**, 2077-2085.

170. Treangen, T.J., Ambur, O.H., Tonjum, T. and Rocha, E.P. (2008) The impact of the neisserial DNA uptake sequences on genome evolution and stability. *Genome biology*, **9**, R60.

171. Zhang, C. and Darnell, R.B. (2011) Mapping in vivo protein-RNA interactions at single-nucleotide resolution from HITS-CLIP data. *Nature biotechnology*, **29**, 607-614.

172. Lorenz, R., Bernhart, S.H., Honer Zu Siederdissen, C., Tafer, H., Flamm, C., Stadler, P.F. and Hofacker, I.L. (2011) ViennaRNA Package 2.0. *Algorithms Mol Biol*, **6**, 26.

173. Wassarman, K.M. (2007) 6S RNA: a small RNA regulator of transcription. *Current opinion in microbiology*, **10**, 164-168.

174. Kamarthapu, V. and Nudler, E. (2015) Rethinking transcription coupled DNA repair. *Current opinion in microbiology*, **24**, 15-20.

175. Pagliarulo, C., Salvatore, P., De Vitis, L.R., Colicchio, R., Monaco, C., Tredici, M., Tala, A., Bardaro, M., Lavitola, A., Bruni, C.B. *et al.* (2004) Regulation and differential expression of gdhA encoding NADP-specific glutamate dehydrogenase in Neisseria meningitidis clinical isolates. *Molecular microbiology*, **51**, 1757-1772.

176. Smith, R.P., Paxman, J.J., Scanlon, M.J. and Heras, B. (2016) Targeting bacterial Dsb proteins for the development of anti-virulence agents. *Molecules (Basel, Switzerland)*, **21**.

177. Mellin, J.R., McClure, R., Lopez, D., Green, O., Reinhard, B. and Genco, C. (2010) Role of Hfq in iron-dependent and -independent gene regulation in Neisseria meningitidis. *Microbiology (Reading, England)*, **156**, 2316-2326.

178. Connolly, J.P., Comerci, D., Alefantis, T.G., Walz, A., Quan, M., Chafin, R., Grewal, P., Mujer, C.V., Ugalde, R.A. and DelVecchio, V.G. (2006) Proteomic analysis of Brucella abortus cell envelope and identification of immunogenic candidate proteins for vaccine development. *Proteomics*, **6**, 3767-3780.

179. Mendum, T.A., Newcombe, J., McNeilly, C.L. and McFadden, J. (2009) Towards the immunoproteome of Neisseria meningitidis. *PloS one*, **4**, e5940.

180. Llorens-Rico, V., Cano, J., Kamminga, T., Gil, R., Latorre, A., Chen, W.H., Bork, P., Glass, J.I., Serrano, L. and Lluch-Senar, M. (2016) Bacterial antisense RNAs are mainly the product of transcriptional noise. *Science advances*, **2**, e1501363.

181. Toledo-Arana, A., Dussurget, O., Nikitas, G., Sesto, N., Guet-Revillet, H., Balestrino, D., Loh, E., Gripenland, J., Tiensuu, T., Vaitkevicius, K. *et al.* (2009) The Listeria transcriptional landscape from saprophytism to virulence. *Nature*, **459**, 950-956.

182. Albrecht, M., Sharma, C.M., Dittrich, M.T., Muller, T., Reinhardt, R., Vogel, J. and Rudel, T. (2011) The transcriptional landscape of Chlamydia pneumoniae. *Genome biology*, **12**, R98.

183. Haning, K., Cho, S.H. and Contreras, L.M. (2014) Small RNAs in mycobacteria: an unfolding story. *Frontiers in cellular and infection microbiology*, **4**, 96.

184. Lee, E.J., Choi, J. and Groisman, E.A. (2014) Control of a Salmonella virulence operon by proline-charged tRNA(Pro). *Proceedings of the National Academy of Sciences of the United States of America*, **111**, 3140-3145.

185. Srikumar, S., Kroger, C., Hebrard, M., Colgan, A., Owen, S.V., Sivasankaran, S.K., Cameron, A.D., Hokamp, K. and Hinton, J.C. (2015) RNA-seq brings new insights to the intra-macrophage transcriptome of Salmonella Typhimurium. *PLoS pathogens*, **11**, e1005262.

186. Chao, Y. and Vogel, J. (2016) A 3' UTR-derived small RNA provides the regulatory noncoding arm of the inner membrane stress response. *Molecular cell*, **61**, 352-363.

187. Miyakoshi, M., Chao, Y. and Vogel, J. (2015) Cross talk between ABC transporter mRNAs via a target mRNA-derived sponge of the GcvB small RNA. *The EMBO journal*, **34**, 1478-1492.

188. Obergfell, K.P. and Seifert, H.S. (2015) Mobile DNA in the pathogenic Neisseria. *Microbiology spectrum*, **3**, 15-26.

189. Kuwae, A., Sjolinder, H., Eriksson, J., Eriksson, S., Chen, Y. and Jonsson, A.B. (2011) NafA negatively controls Neisseria meningitidis piliation. *PloS one*, **6**, e21749.

190. Deghmane, A.E., Giorgini, D., Larribe, M., Alonso, J.M. and Taha, M.K. (2002) Down-regulation of pili and capsule of Neisseria meningitidis upon contact with epithelial cells is mediated by CrgA regulatory protein. *Molecular microbiology*, **43**, 1555-1564.

191. Wurtzel, O., Sesto, N., Mellin, J.R., Karunker, I., Edelheit, S., Becavin, C., Archambaud, C., Cossart, P. and Sorek, R. (2012) Comparative transcriptomics of pathogenic and non-pathogenic Listeria species. *Molecular systems biology*, **8**, 583.

192. Ignatov, D., Malakho, S., Majorov, K., Skvortsov, T., Apt, A. and Azhikina, T. (2013) RNA-Seq analysis of Mycobacterium avium non-coding transcriptome. *PloS one*, **8**, e74209.

193. Frohlich, K.S., Papenfort, K., Berger, A.A. and Vogel, J. (2012) A conserved RpoS-dependent small RNA controls the synthesis of major porin OmpD. *Nucleic acids research*, **40**, 3623-3640.

194. Serra, D.O., Mika, F., Richter, A.M. and Hengge, R. (2016) The green tea polyphenol EGCG inhibits E. coli biofilm formation by impairing amyloid curli fibre assembly and downregulating the biofilm regulator CsgD via the sigma(E) -dependent sRNA RybB. *Molecular microbiology*, **101**, 136-151.

195. Holmqvist, E., Reimegard, J., Sterk, M., Grantcharova, N., Romling, U. and Wagner, E.G. (2010) Two antisense RNAs target the transcriptional regulator CsgD to inhibit curli synthesis. *The EMBO journal*, **29**, 1840-1850.

196. Repoila, F., Majdalani, N. and Gottesman, S. (2003) Small non-coding RNAs, co-ordinators of adaptation processes in Escherichia coli: the RpoS paradigm. *Molecular microbiology*, **48**, 855-861.

197. Lalaouna, D., Simoneau-Roy, M., Lafontaine, D. and Masse, E. (2013) Regulatory RNAs and target mRNA decay in prokaryotes. *Biochimica et biophysica acta*, **1829**, 742-747.

198. Chao, Y., Li, L., Girodat, D., Forstner, K.U., Said, N., Corcoran, C., Smiga, M., Papenfort, K., Reinhardt, R., Wieden, H.J. *et al.* (2017) In vivo cleavage map illuminates the central role of RNase E in coding and non-coding RNA pathways. *Molecular cell*, **65**, 39-51.

199. Papenfort, K., Bouvier, M., Mika, F., Sharma, C.M. and Vogel, J. (2010) Evidence for an autonomous 5' target recognition domain in an Hfq-associated small RNA. *Proceedings of the National Academy of Sciences of the United States of America*, **107**, 20435-20440.

200. Pannekoek, Y., Huis In 't Veld, R.A., Schipper, K., Bovenkerk, S., Kramer, G., Brouwer, M.C., van de Beek, D., Speijer, D. and van der Ende, A. (2017) Neisseria meningitidis uses sibling small regulatory RNAs to switch from cataplerotic to anaplerotic metabolism. *mBio*, **8**.

201. Bauer, S., Helmreich, J., Zachary, M., Kaethner, M., Heinrichs, E., Rudel, T. and Beier, D. (2017) The sibling sRNAs NgncR_162 and NgncR_163 of Neisseria gonorrhoeae participate in the expression control of metabolic, transport and regulatory proteins. *Microbiology (Reading, England)*, **163**, 1720-1734.

202. Gottesman, S. and Storz, G. (2011) Bacterial small RNA regulators: versatile roles and rapidly evolving variations. *Cold Spring Harbor perspectives in biology*, **3**.

203. Lenz, D.H., Mok, K.C., Lilley, B.N., Kulkarni, R.V., Wingreen, N.S. and Bassler, B.L. (2004) The small RNA chaperone Hfq and multiple small RNAs control quorum sensing in Vibrio harveyi and Vibrio cholerae. *Cell*, **118**, 69-82.

204. Svenningsen, S.L., Tu, K.C. and Bassler, B.L. (2009) Gene dosage compensation calibrates four regulatory RNAs to control Vibrio cholerae quorum sensing. *The EMBO journal*, **28**, 429-439.

205. Choi, E., Han, Y., Cho, Y.J., Nam, D. and Lee, E.J. (2017) A trans-acting leader RNA from a Salmonella virulence gene. *Proceedings of the National Academy of Sciences of the United States of America*, **114**, 10232-10237.

206. Laalami, S., Zig, L. and Putzer, H. (2014) Initiation of mRNA decay in bacteria. *Cellular and molecular life sciences : CMLS*, **71**, 1799-1828.

207. Chen, G., Gharib, T.G., Huang, C.C., Taylor, J.M., Misek, D.E., Kardia, S.L., Giordano, T.J., Iannettoni, M.D., Orringer, M.B., Hanash, S.M. *et al.* (2002) Discordant protein and mRNA expression in lung adenocarcinomas. *Molecular & cellular proteomics : MCP*, **1**, 304-313.

208. Pascal, L.E., True, L.D., Campbell, D.S., Deutsch, E.W., Risk, M., Coleman, I.M., Eichner, L.J., Nelson, P.S. and Liu, A.Y. (2008) Correlation of mRNA and protein levels: cell type-specific gene expression of cluster designation antigens in the prostate. *BMC genomics*, **9**, 246.

209. Gygi, S.P., Rochon, Y., Franza, B.R. and Aebersold, R. (1999) Correlation between protein and mRNA abundance in yeast. *Molecular and cellular biology*, **19**, 1720-1730.

210. Yeung, E.S. (2011) Genome-wide correlation between mRNA and protein in a single cell. *Angewandte Chemie (International ed. in English)*, **50**, 583-585.

211. Shine, J. and Dalgarno, L. (1975) Determinant of cistron specificity in bacterial ribosomes. *Nature*, **254**, 34-38.

212. Grossman, A.D., Zhou, Y.N., Gross, C., Heilig, J., Christie, G.E. and Calendar, R. (1985) Mutations in the rpoH (htpR) gene of Escherichia coli K-12 phenotypically suppress a temperature-sensitive mutant defective in the sigma 70 subunit of RNA polymerase. *Journal of bacteriology*, **161**, 939-943.

213. Bingham, A.H., Ponnambalam, S., Chan, B. and Busby, S. (1986) Mutations that reduce expression from the P2 promoter of the Escherichia coli galactose operon. *Gene*, **41**, 67-74.

214. Schwanhausser, B., Busse, D., Li, N., Dittmar, G., Schuchhardt, J., Wolf, J., Chen, W. and Selbach, M. (2011) Global quantification of mammalian gene expression control. *Nature*, **473**, 337-342.

215. Bachmair, A., Finley, D. and Varshavsky, A. (1986) In vivo half-life of a protein is a function of its amino-terminal residue. *Science (New York, N.Y.)*, **234**, 179-186.

216. Maier, T., Guell, M. and Serrano, L. (2009) Correlation of mRNA and protein in complex biological samples. *FEBS letters*, **583**, 3966-3973.

217. Ingolia, N.T., Ghaemmaghami, S., Newman, J.R. and Weissman, J.S. (2009) Genome-wide analysis in vivo of translation with nucleotide resolution using ribosome profiling. *Science (New York, N.Y.)*, **324**, 218-223.

218. Gonzalez, G.M., Hardwick, S.W., Maslen, S.L., Skehel, J.M., Holmqvist, E., Vogel, J., Bateman, A., Luisi, B.F. and Broadhurst, R.W. (2017) Structure of the Escherichia coli ProQ RNA-binding protein. *RNA (New York, N.Y.)*, **23**, 696-711.

219. Smirnov, A., Wang, C., Drewry, L.L. and Vogel, J. (2017) Molecular mechanism of mRNA repression in trans by a ProQ-dependent small RNA. **36**, 1029-1045.

220. Holmqvist, E. and Vogel, J. (2013) A small RNA serving both the Hfq and CsrA regulons. *Genes & development*, **27**, 1073-1078.

221. Jorgensen, M.G., Thomason, M.K., Havelund, J., Valentin-Hansen, P. and Storz, G. (2013) Dual function of the McaS small RNA in controlling biofilm formation. *Genes & development*, **27**, 1132-1145.

222. Lima, S.A., Chipman, L.B. and Nicholson, A.L. (2017) Short poly(A) tails are a conserved feature of highly expressed genes. **24**, 1057-1063.

223. Otaka, H., Ishikawa, H., Morita, T. and Aiba, H. (2011) PolyU tail of rho-independent terminator of bacterial small RNAs is essential for Hfq action. *Proceedings of the National Academy of Sciences of the United States of America*, **108**, 13059-13064.

224. van Biesen, T. and Frost, L.S. (1994) The FinO protein of IncF plasmids binds FinP antisense RNA and its target, traJ mRNA, and promotes duplex formation. *Molecular microbiology*, **14**, 427-436.

225. Skunca, N., Bosnjak, M., Krisko, A., Panov, P., Dzeroski, S., Smuc, T. and Supek, F. (2013) Phyletic profiling with cliques of orthologs is enhanced by signatures of paralogy relationships. *PLoS computational biology*, **9**, e1002852.

226. Silva, I.J., Barahona, S., Eyraud, A., Lalaouna, D., Figueroa-Bossi, N., Masse, E. and Arraiano, C.M. (2019) SraL sRNA interaction regulates the terminator by preventing premature transcription termination of rho mRNA. *Proceedings of the National Academy of Sciences of the United States of America*, **116**, 3042-3051.

227. Mehling, H. (2017) Influences on natural transformation in Neisseria meningitdis by the RNA-chaperons Hfq and ProQ. *Bachelor thesis*.

228. Stadtman, E.R. (2001) Protein oxidation in aging and age-related diseases. *Annals of the New York Academy of Sciences*, **928**, 22-38.

229. Storz, G. and Imlay, J.A. (1999) Oxidative stress. *Current opinion in microbiology*, **2**, 188-194.

230. Imlay, J.A. (2003) Pathways of oxidative damage. *Annual review of microbiology*, **57**, 395-418.

231. Koppenol, W.H. (1993) The centennial of the Fenton reaction. *Free radical biology & medicine*, **15**, 645-651.

232. Imlay, J.A., Chin, S.M. and Linn, S. (1988) Toxic DNA damage by hydrogen peroxide through the Fenton reaction in vivo and in vitro. *Science (New York, N.Y.)*, **240**, 640-642.

233. Davidsen, T. and Tonjum, T. (2006) Meningococcal genome dynamics. *Nature reviews. Microbiology*, **4**, 11-22.

234. Nagorska, K., Silhan, J., Li, Y., Pelicic, V., Freemont, P.S., Baldwin, G.S. and Tang, C.M. (2012) A network of enzymes involved in repair of oxidative DNA damage in Neisseria meningitidis. *Molecular microbiology*, **83**, 1064-1079.

235. Seib, K.L., Tseng, H.J., McEwan, A.G., Apicella, M.A. and Jennings, M.P. (2004) Defenses against oxidative stress in Neisseria gonorrhoeae and Neisseria meningitidis: distinctive systems for different lifestyles. *The Journal of infectious diseases*, **190**, 136-147.

236. Wilks, K.E., Dunn, K.L., Farrant, J.L., Reddin, K.M., Gorringe, A.R., Langford, P.R. and Kroll, J.S. (1998) Periplasmic superoxide dismutase in meningococcal pathogenicity. *Infection and immunity*, **66**, 213-217.

237. Hassan, H.M. and Fridovich, I. (1978) Superoxide radical and the oxygen enhancement of the toxicity of paraquat in Escherichia coli. *The Journal of biological chemistry*, **253**, 8143-8148.

238. Cardenas, P.P., Carzaniga, T., Zangrossi, S., Briani, F., Garcia-Tirado, E., Deho, G. and Alonso, J.C. (2011) Polynucleotide phosphorylase exonuclease and polymerase activities on single-stranded DNA ends are modulated by RecN, SsbA and RecA proteins. *Nucleic acids research*, **39**, 9250-9261.

239. Rath, D., Mangoli, S.H., Pagedar, A.R. and Jawali, N. (2012) Involvement of pnp in survival of UV radiation in Escherichia coli K-12. *Microbiology (Reading, England)*, **158**, 1196-1205.

240. Engman, J., Negrea, A., Sigurlasdottir, S., Georg, M., Eriksson, J., Eriksson, O.S., Kuwae, A., Sjolinder, H. and Jonsson, A.B. (2016) Neisseria meningitidis polynucleotide phosphorylase affects aggregation, adhesion, and virulence. *Infection and immunity*, **84**, 1501-1513.

241. Kiley, P.J. and Storz, G. (2004) Exploiting thiol modifications. *PLoS biology*, **2**, e400.

242. Jakob, U., Muse, W., Eser, M. and Bardwell, J.C. (1999) Chaperone activity with a redox switch. *Cell*, **96**, 341-352.

243. Zheng, M., Aslund, F. and Storz, G. (1998) Activation of the OxyR transcription factor by reversible disulfide bond formation. *Science (New York, N.Y.)*, **279**, 1718-1721.

244. Leslie, N.R., Bennett, D., Lindsay, Y.E., Stewart, H., Gray, A. and Downes, C.P. (2003) Redox regulation of PI 3-kinase signalling via inactivation of PTEN. *The EMBO journal*, **22**, 5501-5510.

245. Chaulk, S.G., Smith Frieday, M.N., Arthur, D.C., Culham, D.E., Edwards, R.A., Soo, P., Frost, L.S., Keates, R.A., Glover, J.N. and Wood, J.M. (2011) ProQ is an RNA chaperone that controls ProP levels in Escherichia coli. *Biochemistry*, **50**, 3095-3106.

246. Sandberg, T.E., Pedersen, M., LaCroix, R.A., Ebrahim, A., Bonde, M., Herrgard, M.J., Palsson, B.O., Sommer, M. and Feist, A.M. (2014) Evolution of Escherichia coli to 42 degrees C and subsequent genetic engineering reveals adaptive mechanisms and novel mutations. *Molecular biology and evolution*, **31**, 2647-2662.

247. Sittka, A., Lucchini, S., Papenfort, K., Sharma, C.M., Rolle, K., Binnewies, T.T., Hinton, J.C. and Vogel, J. (2008) Deep sequencing analysis of small noncoding RNA and mRNA targets of the global post-transcriptional regulator, Hfq. *PLoS genetics*, **4**, e1000163.

248. Christiansen, J.K., Nielsen, J.S., Ebersbach, T., Valentin-Hansen, P., Sogaard-Andersen, L. and Kallipolitis, B.H. (2006) Identification of small Hfq-binding RNAs in Listeria monocytogenes. *RNA (New York, N.Y.)*, **12**, 1383-1396.

249. Mili, S. and Steitz, J.A. (2004) Evidence for reassociation of RNA-binding proteins after cell lysis: implications for the interpretation of immunoprecipitation analyses. *RNA (New York, N.Y.)*, **10**, 1692-1694.

250. Faner, M.A. and Feig, A.L. (2013) Identifying and characterizing Hfq-RNA interactions. *Methods (San Diego, Calif.)*, **63**, 144-159.

251. Barquist, L. and Vogel, J. (2015) Accelerating discovery and functional analysis of small RNAs with new technologies. *Annual review of genetics*, **49**, 367-394.

252. McHugh, C.A., Russell, P. and Guttman, M. (2014) Methods for comprehensive experimental identification of RNA-protein interactions. *Genome biology*, **15**, 203.

253. Lalaouna, D., Prevost, K., Eyraud, A. and Masse, E. (2017) Identification of unknown RNA partners using MAPS. *Methods (San Diego, Calif.)*, **117**, 28-34.

254. Melamed, S., Peer, A., Faigenbaum-Romm, R., Gatt, Y.E., Reiss, N., Bar, A., Altuvia, Y., Argaman, L. and Margalit, H. (2016) Global mapping of small RNA-target interactions in bacteria. *Molecular cell*, **63**, 884-897.

9. Annex

9.1. Abbreviation index

% (v/v)	% (volume/volume)
% (w/v)	% (weight/volume)
aa	amino acid
APS	ammonium persulfate
ATP	adenosine triphosphate
aTSS	antisense transcriptional start site
AUG	start codon
bp	base pairs
BSA	bovine serum albumin
Cas	CRISPR-associated
cc	clonal complex
CD	cluster of differentiation
CDM	chemically defined medium
cDNA	complementary desoxyribonucleic acid
CDS	coding sequence
CI	confidence interval
CIP	calf intestinal phosphatase
CLIP-seq	*In vivo* UV-cross-linking with RNA-deep sequencing
Cm	chlorampheicol
CFU	colony forming units
CRISPR	clustered regularly interspaced short palindromic repeats
CO_2	carbon dioxide
COG	cluster of orthologous genes
COS	Columbia agar plates
coIP	co-immunoprecipitation
ddNTP	didesoxyribonucleotide
DEPC	diethylpyrocarbonate
dH_2O	distilled water
DIG	digoxigenin
DMSO	dimethylsulfoxide
DNA	desoxyribonucleic acid
dNTP	desoxyribonucleotide
dRNA-seq	differential RNA-sequencing
ds	double stranded
DTT	dithiothreitol
DUS	DNA uptake sequence
ECL	enhanced chemiluminescence
EDTA	ethylendiamin tetraacetate
EL	earlylog phase
ELISA	enzyme-linked immunosorbent assay
EmEm	MEM eagle medium
EMSA	electromobility shift assay
Ery	erythromycin
EtOH	ethanol
FCS	Fetal calf serum
Fig.	figure
gDNA	genomic DNA
GEO	gene expression omnibus
GFP	green fluorescent protein

H_2O	water
HRP	horseradish peroxidase
iBAC	intensity-based absolute quantification
IGR	intergenetic region
IMD	invasive meningococcal disease
iTSS	Internal transcriptional start site
IPTG	isopropyl β-D-1-thiogalactopyranoside
Km	kanamycin
Kb	kilo base pair
kDa	kilo Dalton
LB	Luria-Bertani (broth)
LFQ	label-free quantification
LL	latelog phase
LLL	stationary phase
log_2c.p.m.	base 2 logarithm count per million
log_2f.c.	base 2 logarithm fold change
LPS	lipopolysaccharides
LSM	sm-like proteins
M	mol per liter
ML	midlog phase
MLST	multilocus sequence typing
MOI	multiplicity of infection
MOPS	3-propanesulfonic acid
mRNA	messenger ribonucleic acid
mw	molecular weight
NEAA	non-essential amino acids
ncRNA	non-coding ribonucleic acid
nt	nucleotide
NHS	Normal human serum
NTP	nucleoside triphosphate
OD	optical density
OD_{600nm}	optical density at 600 nm
OMP	outer membrane protein
ORF	open reading frame
oTSS	orphan transcriptional start site
PAA	polyacrylamide
PAGE	polyacrylamide gel electrophoresis
PBS	phosphate buffered saline
PCI	Phenol/ chloroform/ isomylalcohol
PCR	polymerase chain reaction
PBST	phosphate buffered saline with Tween 20
pilP	pilus assembly protein
PK	proteinase K
PMFS	phenylmethylsulfonyl fluoride
PNK	T_4 polynucleotide kinase
pTSS	Primary transcriptional start site
RBP	RNA-binding protein
RBS	ribosome binding site
RIP-seq	RNA immunoprecipitation coupled RNA-sequencing
RNA	ribonucleic acid
RNAP	RNA polymerase P
RNA-seq	RNA-sequencing
RNase	ribonuclease
RNP	ribonucleoprotein particle

rpm	revolutions per minute
RPMI	Roswell Park Memorial Institute developed medium
rRNA	Ribosomal RNA
RT	room temperature
RT primer	reverse transcription primer
Salmonella	*Salmonella enterica*
SD	Shine-dalgarno
SDS	sodium dodecyl sulfat
sfGFP	superfolder green fluorescent protein
ST	sequence type
Sn	supernatant
SOD	superoxide dismutase
sRNA	small regulatory ribonucleic acid
ss	single-stranded
SSC	saline-sodium citrate
SRP	signal recognition particle
sTSS	secondary transcriptional start site
TAE	tris-acetate EDTA
TBE	tris/Borate/EDTA
TCA cycle	tricarboxylic acid cycle
TCS	two-component system
TEMED	N,N,N',N'-Tetramethylethylenediamine
TEX	terminator exonuclease
Tfp	type IV pili
Tris	tris-(hydroxymethyl)-aminomethan
tRNA	transfer ribonucleic acid
tmRNA	transfer-messenger RNA
tracrRNA	*trans*-acting crRNA
TSS	transcription start site
UTR	untranslated region
UV	ultraviolet
V	Volt
VBS	veronal buffered saline
WT	wild-type

9.2. List of figures and tables

9.2.1. Figures

9.2.2. Tables

10. Curriculum vitae

11. List of publications

Research papers

Heidrich N, Hagmann A, Bauriedl S, Vogel J, Schoen C (2018)
The CRISPR/Cas system in *Neisseria meningitidis* affects bacterial adhesion to human nasopharyngeal epithelial cells.
RNA Biol 30:1-7

Heidrich N, Bauriedl S, Barquist L, Li L, Schoen C, Vogel J (2017)
The primary transcriptome of *Neisseria meningitidis* and its interaction with the RNA chaperone Hfq.
Nucleic Acids Res 45(10):6147-6167

The following manuscript related to the PhD work is submitted

Bauriedl S, Bischler T., Gerovac M, Heidrich N, Barquist L, Vogel J, Schoen C (2019)
The minimal ProQ protein of *Neisseria meningitidis* reveals an intrinsic capacity for structure-based global RNA recognition by the FinO domain.

Book chapter

Heidrich N, Bauriedl S, Schoen C (2019)
Investigating RNA-protein interactions in *N. meningitidis* by RIP-seq analysis.
Neisseria meningitidis. Eds. Kate L. Seib and Ian R. Peak.
Methods Molecular Biology, Vol. 1969:33-49

Presentations

Bauriedl S, Barquist L, Heidrich N, Schoen C, Vogel J
The RNA chaperone ProQ as a global gene regulator in *Neisseria meningitidis.*
70. Jahrestagung der Deutschen Gesellschaft für Hygiene und Mikrobiologie (DGHM), Bochum, Deutschland, 19.-21.02.2018

Bauriedl S, Heidrich N, Schoen C, Vogel J
Combination of dRNA-seq and RIP-seq identifies two novel Hfq-dependent sRNAs in *Neisseria meningitidis* regulating the expression of a putative colonization factor.
Microbiology and Infection, Würzburg, Deutschland, 05.-08.03.2017

Bauriedl S, Heidrich N, Schoen C, Vogel J
Identification of a hypothetical colonization factor as target of two new sRNAs in *N. meningitidis*
Eureka! 11th International GSLS Student Symposium, 12.-13. 10. 2016

Bauriedl S, Heidrich N, Barquist L, Li L,Vogel J, Schoen C
The primary transcriptome of the human commensal pathogen *Neisseria meningitidis* and its interaction with the RNA chaperone Hfq.
68. Jahrestagung der Deutschen Gesellschaft für Hygiene und Mikrobiologie (DGHM), Ulm, Deutschland, 11.-14.09.2016

Heidrich N, Bauriedl S, Barquist L, Li L, Schoen C, Vogel J
The primary transcriptome of the human commensal pathogen *Neisseria meningitidis* and its interaction with the RNA chaperone Hfq.
Workshop on Sensory and Regulatory RNAs in Prokaryotes, Young Scholars program of the Bavarian Academy of Sciences and Humanities (BadW) München, Deutschland, 18.-19.07.2016

Bauriedl S, Heidrich N, Schoen C, Vogel J
Identification of a hypothetical colonization factor as target of two new sRNAs in *N. meningitidis*
Eureka! 11th International GSLS Student Symposium, 12.-13. 10. 2016

Bauriedl S, Heidrich N, Schoen C, Vogel J
The sRNA regulon of *Neisseria meningitidis.*
13. Kongress für Infektionskrankheiten und Tropenmedizin, Würzburg, Deutschland, 15.-18.06.2016

Bauriedl S, Heidrich N, Schoen C, Vogel J
The sRNA regulon of *Neisseria meningitidis*
Eureka! 10th International GSLS Student Symposium, 14.-15. 10. 2015

12. Contribution by others

The work described in this dissertation was conducted under the supervision of Prof. Dr. Dr. Christoph Schoen at the Institute for Hygiene and Microbiology (IHM) and Prof. Dr. Jörg Vogel from the Institute for Molecular Infection Biology (IMIB) at the University of Würzburg in Germany. Yet, several parts of the work delineated in this doctoral thesis have been contributed by others as indicated below:

- Mapping and Processing of dRNA-seq data were performed by Dr. rer. nat. **Lei Li**. Mapping and processing of Hfq coIP data and ProQ UV CLIP data were done by Prof. Dr. rer. nat. **Lars Barquist**. Mapping, figure generation and COG pathway analysis of RNA-seq data were performed by Dr. rer. nat. **Thorsten Bischler**.
- Quantitative proteomics of ProQ was performed in collaboration with the group of Prof. Dr. rer. nat. **Andreas Schlosser** (RVZ Würzburg).
- Purification of the ProQ protein was done by Dr. rer. nat. **Maren Bleckmann**.
- Wet lab experiments (mutant construction, dRNA-seq, Hfq coIP and ProQ UV CLIP) were conducted with the help of Dr. rer. nat. **Nadja Heidrich** who contributed to the whole work both intellectually and experimentally.
- Statistical analyses of RNA-seq DESeq2 results as well as oxidative stress assays were carried out by Prof. Dr. rer. nat. Dr. med. **Christoph Schoen**.
- The Hfq coIP experiment was performed during my master thesis at the Institute for Hygiene and Microbiology, Würzburg, Germany. Yet, the precise data analysis and data validation was performed by myself during my PhD.
- Wet lab experiments (mutant construction, oxidative stress assays) were conducted with the technical assistance of **Barbara Conrad** and B.sc. **Helene Mehling**.
- cDNA libraries were constructed and partially sequenced by the **vertis Biotechnologie AG** in Freising, Weihenstephan, Germany (http://www.vertis-biotech.com).
- High-throughput sequencing was partially performed by the **Sequencing core unit** at the Institute for Molecular Infection Biology (IMIB), Würzburg, Germany.

13. Acknowledgements

Thank you!